TWO DIMENSIONAL ENERGY INTERCEPTION AND WATER BALANCE MODEL FOR HEDGEGROW TREE CROPS

JG Annandale · NZ Jovanovic ·
NS Mpandeli · P Lobit · N du Sautoy

WRC Report No. 945/1/02

Water Research Commission

TWO-DIMENSIONAL ENERGY INTERCEPTION AND WATER BALANCE MODEL FOR HEDGEROW TREE CROPS

Report to the

Water Research Commission

by

J.G. Annandale, N.Z. Jovanovic, N.S. Mpandeli and P. Lobit

Department of Plant Production and Soil Science
University of Pretoria, Hatfield 0001

N. du Sautoy

Department of Soil Science
University of the North, P. B. X1106, Sovenga 0727

and

N. Benadé

NB Systems, P.B. 15102, Sinoville 0129

WRC Report: 945/1/02
ISBN No. : 1 86845 8695

Disclaimer

This report emanates from a project financed by the Water Research Commission (WRC) and is approved for publication. Approval does not signify that the contents necessarily reflect the views and policies of the WRC or the members of the project steering committee, nor does mention of trade names or commercial products constitute endorsement or recommendation for use.

TABLE OF CONTENTS

EXECUTIVE SUMMARY

Introduction

The interest in crop modelling started since the introduction and popularisation of computer technology, which facilitated the dynamic simulation of complex natural systems. In particular, crop growth and soil water balance models for irrigation scheduling are popular at locations where water is a limiting factor for crop production.

In a previous Water Research Commission project, a simple, but mechanistic, generic crop growth and soil water balance model (SWB) for irrigation scheduling under full and deficit irrigation was made available. The SWB model was primarily developed for predicting real-time soil water deficit of field crops with a one-dimensional canopy light interception and water redistribution procedure.

Hedgerow tree crops are planted in widely spaced rows to allow access between trees to carry out necessary management practices (e.g. pest control and harvesting). Distribution of energy is not uniform in widely spaced crops. In addition, localised under-tree irrigation is often used for tree crops to reduce system installation costs. This irrigation (micro- or drip) only wets a limited area under the canopy of the trees so that evaporation from the soil surface is also not uniform. One can expect root density to vary with depth as well as with distance between the rows so water uptake for transpiration will also vary in two dimensions. It is also essential to take into account the limited volume of soil wetted under micro-irrigation or its capacity will easily be exceeded with a standard one-dimensional approach, leading to undesirable over-irrigation in the wetted zone, and possibly crop stress due to too long an irrigation interval. In order to accurately estimate canopy growth, water balance and yield, it is therefore essential to model canopy radiant interception and soil water balance of hedgerow tree crops in two dimensions and on an hourly time step, based on sound physical principles.

Lack of suitable user-friendly tools to mechanistically describe the two-dimensional energy and soil water balance of tree crops was identified. Due to the importance of fruit crops, on the export as well as local markets, it was decided to improve the SWB model by incorporating a two-dimensional system for use in hedgerow plantings.

Objectives

The objectives of this project were:

i) To develop a two-dimensional fruit tree water balance model, which takes into account the unique fractional interception of solar radiation associated with hedgerow orchards as opposed to the horizontal planar interception encountered in agronomic crops.

ii) To verify the model for deciduous fruit trees using peaches as an example.

iii) To verify the model for evergreen fruit trees using citrus as an example.

iv) To develop a core of irrigation expertise, within the University of the North, Faculty of Agriculture, to be of service, in collaboration with the National Community Water and Sanitation Training Institute, to agriculture in the Northern Province.

v) Over time, to equip a centre at the University of the North to have the capacity to conduct irrigation research and train students in the use of these techniques.

Approach

The two-dimensional energy interception and soil water balance model was developed and validated using data from two field trials. The first trial was established in a peach orchard on the lysimeter facilities at Pretoria University's experimental farm, Hatfield. The second trial was established in a citrus orchard at the Syferkuil experimental farm of the University of the North. During the course of the project and for the purpose of validating the energy interception model for different conditions (tree size and shape, row orientation etc.), an additional field trial was carried out on Leucaena fodder trees at Hatfield. Contact was also made with private farming enterprises and two field trials were carried out in Brits on citrus farms.

Although the validation was done only for some orchards, the model could be applicable to other orchards and conditions provided that correct input parameters are used.

Model development

Two types of model, both predicting crop water requirements on a daily time step, were developed for hedgerow tree crops during the course of this project and included in SWB:

i) A mechanistic two-dimensional energy interception and finite difference, Richards' equation based soil water balance model; and

ii) An FAO-based crop factor model, with a quasi-2D cascading soil water balance model.

The two dimensional model for hedgerow crops calculates the two-dimensional energy interception, based on solar and row orientation, tree size and shape, as well as leaf area density. The two-dimensional soil water redistribution is calculated with a finite difference solution. The two-dimensional energy and soil water balance model was developed during the visit of the project leader to Washington State University.

The two-dimensional energy interception model assumes leaves to be uniformly distributed within an ellipsoid truncated at its base, and radiation penetrating the canopy is attenuated according to Beer's law. This geometry is very versatile as many different shapes can be generated. In order to determine the spatial distribution of soil irradiance across the tree row, the canopy path length through which the radiation must travel to reach a certain point on the soil surface is calculated. Radiation can penetrate neighbouring rows, so two rows on either side of the simulated row are considered.

Beam or direct radiation and diffuse radiation for the PAR (photosynthetically active radiation) and NIR (near-infrared radiation) wavebands are calculated separately, as they interact differently with the canopy. The ratio of actual measured to potential radiation is used to estimate the proportion of direct and diffuse radiation in these two spectral bands. The attenuation of beam radiation by the canopy is strongly dependent on zenith angle, and, for crops planted in rows, azimuth angle and row orientation will also be crucial. Elevation and azimuth angles are calculated from latitude, solar declination that depends on day of year and hour of day integrated for a daily time step. Before the length of canopy through which radiation penetrates can be calculated, azimuth angle needs to be adjusted to take row orientation into account.

Input data required to run the two-dimensional canopy interception model are: day of year, latitude, standard meridian, longitude, daily solar radiation, row width and orientation, canopy height and width, skirting height, extinction coefficient, absorptivity and leaf area density.

In order to simulate two-dimensional water movement in the soil, a grid of nodes had to be established. This divides the soil up into a number of elements. The distances between nodes are selected so that model output can easily be compared to field measured values. Each element has its own physical properties, so this scheme allows variation in soil properties in two dimensions. Symmetry planes are assumed to occur mid-way between two

rows on either side of the hedgerow and no water flux is allowed across these planes. The model redistributes water in the soil in two-dimensions using a finite difference solution to Richards' continuity equation for water flow. The aim is to find the matric potentials, which will cause the mass balance error to be negligible. This is done using the Newton-Raphson procedure. Two lower boundary conditions can be chosen in the model: i) gravity drainage for well-drained soils, and ii) zero-flux lower boundary to simulate an impermeable layer.

A precipitation or irrigation in mm is converted to a flux in kg m^{-1} s^{-1} by dividing the time step and multiplying by the horizontal distance over which the water is distributed. The infiltration does not have to be uniform over the surface. Non-uniform infiltration is especially important in very coarse soils where lateral redistribution is likely to be limited, or in the case of micro-irrigation. As with the infiltration flux, evaporation is multiplied by the horizontal distance over which it occurs in order to get an evaporative flux in kg m^{-1} s^{-1}. Potential evapotranspiration (PET) is calculated from weather data using the Penman-Monteith equation and the maximum crop factor after rainfall occurs. PET is then partitioned at the soil surface into potential evaporation and potential transpiration depending on solar orientation, row direction and canopy size, shape and leaf area density. Crop water uptake (transpiration) can either be limited by atmospheric demand or soil-root water supply. Root densities at different soil depths are accounted for in the calculation of root water uptake. The user can specify root depth and the fraction of roots in the wetted volume of soil.

Required inputs for the two-dimensional soil water balance model are: starting and planting dates, altitude, rainfall and irrigation water amounts, as well as maximum and minimum daily temperature. Two points on the water retention function (usually field capacity and permanent wilting point), initial volumetric soil water content and bulk density are required for each soil layer. Soil saturated hydraulic conductivity can also be entered as input for each soil layer, or calculated by the model using the water retention curve. Row distance, wetted diameter of micro-jets or drippers, fraction of roots in the wetted volume of soil as well as distance of the nodes from the tree row are also required as input.

The FAO-based crop factor model is simpler and was developed to enable users to predict crop water requirements with limited input data. This model includes a semi-empirical approach for partitioning of above-ground energy, a cascading soil water redistribution that separates the wetted and non-wetted portion of the ground, as well as prediction of crop yields. The FAO-based crop factor procedure was combined with the mechanistic SWB model, thereby still allowing evaporation and transpiration to be modelled separately as supply and demand limited processes. The crop factor model does not grow the canopy mechanistically and therefore the effect of water stress on canopy size is not simulated. The simpler crop factor model should, however, still perform satisfactorily if the estimated canopy cover closely resembles that found in the field.

The following input parameters are required to run the FAO-type crop factor model: planting date, latitude, altitude, maximum and minimum daily air temperatures, FAO crop factors and duration of crop stages. The input data required to run the two-dimensional cascading model are rainfall and irrigation amounts, volumetric soil water content at field capacity and permanent wilting point, as well as initial volumetric soil water content for each soil layer. Row spacing, wetted diameter, distance between micro-irrigators or drippers and the fraction of roots in the wetted volume of soil are also required. Required input data for yield prediction with the FAO model are FAO stress factors for growing stages and potential yield.

Field trials

Validation of the SWB model was carried out for a wide range of conditions (row orientation, growth stage and canopy density). For this purpose, two main field trials were set up. The first trial was established in a peach (*Prunus persica* cv Transvaalia) orchard on the lysimeter facilities at Hatfield (Pretoria University experimental farm). This provided a site

where detailed observations could be easily recorded to validate the SWB model for a deciduous tree species. The second trial was established in a clementine (*Citrus reticulata* cv. Blanco) orchard at the Syferkuil experimental farm of the University of the North. This was the site where measured data were collected to validate the SWB model for an evergreen tree species.

In both field trials, the following field measurements were carried out and used to validate the two-dimensional energy interception and soil water balance model:

i) Weather measurements (temperature and relative humidity, wind speed, solar radiation and rainfall).

ii) Soil texture, bulk density, penetrometer resistance as well as saturated and unsaturated hydraulic conductivity.

iii) Volumetric soil water content with neutron water meter and time domain reflectometry (TDR).

iv) Soil matric potential with heat dissipation sensors.

v) Root distribution by taking soil core samples and washing out roots to determine root length.

vi) Soil irradiance at different distances from the tree row with tube solarimeters.

vii) Leaf area index and density with a LAI-2000 plant canopy analyzer.

viii) Canopy size and row orientation.

In addition, load cell lysimeters were used in the peach orchard at Hatfield in order to measure crop water use. Measurements of soil evaporation with micro-lysimeters were also carried out at Hatfield in order to validate the soil evaporation subroutine of the model. In the peach trial at Hatfield, soil matric potential was also measured with tensiometers.

Additional field trials were carried out in order to test the two-dimensional radiant interception model for different environmental conditions (tree size and shape as well as row orientation). One trial was at the Hatfield experimental station on Leucaena (*Leucaena leucocephela*) fodder trees. Two other trials were carried out on two commercial orchards at Brits in Empress mandarin (*Citrus reticulata* cv. Blanco) and Delta Valencia (*Citrus sinensis* [L.] cv. Osbeck) orchards. In these field trials, weather data were recorded, as were leaf area index and density, canopy size and row orientation. Soil irradiance across the row was measured with tube solarimeters.

Results

The SWB model evaluation consisted of checking internal consistency and units used in the computer program, comparison of model output with independent data sets of real-life observations and sensitivity analyses.

Verification of the model was performed by inspection of the internal consistency of the model and its software implementation. In particular, the following actions were taken: analysis of dimensions and units; on-line checks of mass conservation; detection of violation of natural ranges of parameters and variables; inspection of qualitative behaviour of the model and its implementation by checking whether the response of model output to changing values of a parameter conforms to theoretical insights.

The simple, quasi two-dimensional, cascading soil water balance model was calibrated using data from the peach trial at the Hatfield experimental station. In the process, FAO basal crop coefficients (Kcb) were determined for first and second leaf peach trees. The daily crop factor (Kc) was calculated using evapotranspiration measurements from the lysimeters and the grass reference evapotranspiration calculated from weather data. The Kcb values for the

various growth stages were determined by fitting an appropriate line through the lower values of Kc, which were taken to reflect the condition where the soil surface was dry (negligible evaporation), subsoil drainage was negligible and there was sufficient water not to restrict transpiration. There was good agreement between predicted and measured daily soil water deficit for water stressed and non-stressed treatments. This was expected since the calibration data came from the trial.

Field measurements in Hatfield also indicated that in hedgerow plantings the whole area across the row must be borne in mind when assessing soil water content. The practice of using single or restricted locality measurements, as utilised in agronomic crops, can be misleading in orchards. The reason for this is the effect of the irrigation distribution and rain interception by the canopy, the variation in radiation interception by the canopy across the row, the irradiance reaching the soil surface as the season progresses, the presence of a grass sod or bare soil in the inter-row region and the root density across the row. In both field trials at Hatfield and Syferkuil, it was found that there are significant amounts of roots in the inter-row region and thus this portion of the rooting volume must not be disregarded when assessing the water balance.

The two-dimensional energy interception and soil evaporation components were validated separately. The crucial interactions between the model components were integrated in the validation of the two-dimensional soil water balance model, which uses the energy interception and soil evaporation sub-models to split evaporation and transpiration.

The radiant interception model predictions and the tube solarimeter measured soil irradiance generally gave very good agreement at different distances from the tree row and in different orchards. However, some discrepancies between measurements and model predictions occurred. This was attributed to the presence of trunks and branches shading the tube solarimeters at low values of leaf area density, irregularities in the shape of the hedgerow, non-uniform distribution of leaves within the canopy and inaccuracies in the calculation of direct and diffuse radiation.

The soil evaporation sub-model was tested in the peach orchard at Hatfield using soil irradiance measured with tube solarimeters and soil evaporation measured with micro-lysimeters. A linear correlation between accumulated energy interception and daily evaporation was found for the first two days of the experiment. After the second day, the correlation between energy interception and evaporation was lost, which means that during these days, evaporation began to be limited by soil water supply and was no longer directly correlated to energy interception. Evaporation measured in the grass-covered area was lower than that measured at corresponding positions in the bare soil area (in particular in zones of low evaporation). This may be due to the fact that part of the grass was dead at the time of the experiment, so that it did not transpire water but prevented the solar radiation reaching the surface of the soil and increase resistance to water movement. Measurements of soil evaporation were compared to model simulations. The best agreement between measurements and simulations was obtained assuming 30% air humidity in the orchard for the soil evaporation model.

The output obtained with the two-dimensional soil water balance model was compared to independent field measurements in order to validate the full SWB two-dimensional model. Volumetric soil water content data collected with the TDR system in the peach and citrus orchards were compared to SWB simulations. Results of model simulations done during drying cycles showed that the surface layer predictions were generally very good. However, discrepancies between measurements and simulations were observed in particular for deeper soil layers. This could have been due to spatial variability of soil properties, as well as soil disturbance during the installation of TDR probes. It is clear that TDR probes can be used in irrigation scheduling to determine crop water use over certain periods. Caution

should, however, be exercised in the interpretation of absolute values of volumetric soil water content obtained from the probes.

Scenario modelling and sensitivity analyses were carried out varying some input parameters and observing variations in certain output variables. The aim was to identify the most suitable management practice in order to maximise water use efficiency. Two case studies were considered for two imaginary orchards located at different latitudes and in different climates (Kakamas in the Northern Cape and Stellenbosch in the Western Cape). The results of the scenario simulations indicated that the orchards should be planted in a N-S row orientation, a wetted diameter of 0.5 m should be applied as well as pruning to reduce the canopy width to 2 m, in order to maximise canopy light interception and minimise water losses through evaporation.

A sensitivity analysis was also carried out for both case studies varying the fraction of roots in the wetted volume of soil, and observing variations in the output results of evaporation and transpiration. The contribution to crop water uptake from the inter-row volume of soil can be high, in particular under high atmospheric evaporative demand, and this needs to be accounted for in irrigation management in order to maximise rainfall use efficiency.

The finite difference and the cascading soil water balance models were compared for the two case studies. The aim was to determine if the simpler cascading model yields similar results to the more complex finite difference model. The simulation results indicated that the cascading model predicted smaller transpiration values than the finite difference model at small canopy widths. Transpiration values simulated with the two models were close at large canopy widths. The cascading model underestimated soil evaporation at small canopy widths, but it overestimated it at large widths. The main reason for this disagreement is the different algorithm of water redistribution used in the two models.

Conclusions and recommendations

A two-dimensional energy interception and soil water balance model was developed (objective 1). The model was fully validated for deciduous trees (objective 2) using data obtained in field trials on peaches and Leucaena fodder trees (Hatfield experimental station, University of Pretoria). For model validation in evergreen citrus orchards (objective 3), data obtained in field trials set up at the Syferkuil experimental station (University of the North) and on two commercial farms in Brits were used. The development of a core of irrigation expertise at the University of the North (objective 4) and the supply of equipment to the University of the North for research and training (objective 5) were also achieved.

The two-dimensional energy interception and soil water balance model was developed by the research team and included in the Soil Water Balance irrigation scheduling model. A simpler model, based on the FAO crop factor approach and a cascading soil water balance, was also developed to enable users to predict crop water requirements with a limited set of input data. The SWB model is written in Delphi v. 5.0 (Inprise Corp.), and is available for use with Windows 95 on an IBM-PC or compatible computer. The minimum requirement is 16 Mb RAM and a CD-ROM drive.

The FAO-based model and the cascading soil water balance were calibrated for first leaf and second leaf peaches at Hatfield.

The two-dimensional model was fully validated for deciduous orchards using data obtained in Hatfield. For model validation in evergreen citrus orchards, data obtained in field trials set up at Syferkuil and Brits were used.

Irregular trunks and branches could cause inaccuracies in predictions of the energy balance. At low values of leaf area density, the shade from trunks and branches is not accounted for in the SWB model. The subroutine splitting total solar radiation into diffuse and direct radiation should be tested further. The relative importance of non-symmetric canopy shape

as opposed to non-uniform leaf distribution should also be investigated. It would also be interesting to test the model for conditions where the canopy has a shape of an ellipse with the bottom part cut off, or with canopies that do not have an elliptical shape at all.

Concerning evaporation, model predictions matched the measurements made with micro-lysimeters less accurately. This may be due to errors in both the micro-lysimeter measurements of evaporation and in the model predictions. It appeared important to measure air relative humidity in orchards and use it as input in order to predict soil evaporation accurately.

The major difficulties encountered in the validation of the soil water balance were due to spatial variability of soil properties and disturbance of the soil when the water status monitoring sensors were installed. Careful installation is therefore recommended for sensors that give localised measurements like those used in this study (heat dissipation sensors and TDR probes).

The successful validation of the two-dimensional energy interception and soil water balance model opens the opportunity to develop a useful yield predictor and productivity efficiency measure if one knows the canopy to fruit ratio.

As demonstrated with data from the peach trial at Hatfield, soil or cover crops between rows can also have a large effect on the efficient use of rainfall, and this could be further investigated.

Although not common, it is practiced on certain commercial farms to irrigate orchards with drip irrigation systems several times during the day. This implies the need for an hourly time step model in order to accurately predict the soil water balance.

The two-dimensional energy and soil water balance model is primarily meant to be a real-time, irrigation scheduling tool for commercial orchards. Results from this study should guide irrigation scheduling consultants, extension officers and farmers to more efficiently use scarce water resources on high value tree crops. The two-dimensional model, however, can also be used for planning purposes as demonstrated in the scenario simulations. The mechanistic canopy radiation interception routine which has been shown to be very accurate will make it possible to evaluate the effect of row orientation and spacing as well as the effect of wetted diameter and pruning practices on water use.

The biggest contribution of this model is likely to be the quantification of the contribution that rainfall can make to crop water use by taking the non-irrigated inter-row soil reservoir into account. It is recommended to accurately estimate the root fraction in the wetted and non-wetted volume of soil by digging a trench across the row, taking core soil samples and determining root densities.

The two-dimensional energy interception and finite difference soil water balance model is expected to be more accurate than the cascading soil water balance, due to the sound physical principles on which it is based. The mechanistic detailed approach could give guidance with respect to the magnitude of errors made by using simpler, more empirical approaches. However, the two-dimensional model will also require more input parameters compared to the simpler cascading model. In particular, the most difficult parameters to determine will be the leaf area density for the radiant energy interception part due to the cost of the instrumentation, and the hydraulic conductivity for the soil part due to the specialised knowledge and scientific equipment required. On the other hand, the cascading model requires calibrated FAO crop factors in order to reasonably partition evaporation and transpiration. It would be interesting to compare the cascading and the two-dimensional soil water balance models against field measurements in order to determine the level of accuracy in predictions.

During this project, two user-friendly tools have also been developed, the ETo and HDS calculator. The ETo calculator was developed as a stand-alone tool for the calculation and database storage of the Penman-Monteith reference evapotranspiration (ETo). It can also be used to check what weather measurements can be omitted without experiencing large errors in the estimation of ETo at a particular site. This should facilitate the application of SWB in combination with a weather station, and improve the accuracy of model predictions. The HDS calculator was indispensable for processing data obtained from heat dissipation sensors, which were used to estimate soil matric potential in the field trials. The HDS calculator was used for individual calibration and temperature correction of sensor readings.

Capacity building and technology transfer

This project had a strong capacity building and technology transfer component.

Mr N Du Sautoy, Senior Lecturer from the Faculty of Agriculture (University of the North, UNIN), completed his capacity building component. Within the Department of Soil Science at UNIN, a course on irrigation scheduling based on the principles included in the SWB model is now presented. The Department of Soil Science (UNIN) also organized a workshop on irrigation scheduling based on the principles included in the SWB model, where the participants were mainly students from the Northern Province. During the installation of the equipment at the Syferkuil experimental farm (UNIN), a large group of students from the University of the North was trained in the theory and application of the techniques used. The Faculty of Agriculture (UNIN) has been equipped with instrumentation of the total value of about R 185,000.

Mr NS Mpandeli, an M. Inst. Agrar. student at the Dept. Plant Production and Soil Science (University of Pretoria), was trained and employed as Research Assistant on this project. He attended courses, workshops and conferences, and visited the Oklahoma Climatology Survey Institute (USA) for a training period of 28 days.

Results from this project should guide irrigation scheduling consultants, extension officers and farmers (commercial concerns and emerging commercial black farmers) in the more efficient use of scarce water resources on high value tree crops. The SWB model was presented and demonstrated to OTK and the South African Irrigation Institute. Cooperation was established with Infruitec (Stellenbosch) and the University of Stellenbosch. Several conference presentations and papers emanated or will emanate from this project.

ACKNOWLEDGEMENTS

The research in this report emanated from a project funded by the Water Research Commission, entitled:

"Two-Dimensional Energy Interception and Water Balance Model for Hedgerow Tree Crops".

The Steering Committee responsible for this project, consisted of the following persons:

Dr SS Mkhize	Water Research Commission
Dr GR Backeberg	Water Research Commission
Dr PJ Dye	CSIR
Dr JE Hoffman	Dept. of Soil Science, University of Stellenbosch
Dr SA Lorentz	School of Bioresources Engineering and Environmental Hydrology, University of Natal
Dr EW Pavel	Dept. Plant Production and Soil Science, University of Pretoria
Ms T Volschenk	Agricultural Research Council – Infruitec, Stellenbosch

The financing of the project by the Water Research Commission and the contribution of the members of the Steering Committee is gratefully acknowledged.

This project was only possible with the co-operation of many individuals and institutions. The authors therefore wish to record their sincere thanks to the following:

Dr T Fyfield (Agricultural Research Council – Institute for Soil, Climate and Water, Pretoria) for performing penetrometer resistance and root density measurements in the field trial at the Hatfield experimental farm.

Mr Karl Monnik for co-ordinating the overseas Mbeki-Gore capacity building trip of Mr NS Mpandeli.

Mr Mbangiseni Nepfumbada and Dr Simon Lorentz for assistance with the determination of soil hydraulic properties.

LIST OF TABLES

LIST OF FIGURES

LIST OF ACRONYMS AND SYMBOLS

List of acronyms

CROPWAT - CROP WATer requirements model (FAO, Rome, Italy)
FAO - Food and Agriculture Organization of the United Nations (Rome, Italy)
HDS - Heat dissipation sensor
SWB - Soil Water Balance model (University of Pretoria, South Africa)
PEST–ASP - Model-Independent Parameter ESTimation (Watermark Numerical Computing, Australia)

List of symbols

a	Half the width of the tree canopy (m)
Acb	Canopy base unit area (m^2 ground)
b	Half the depth of the tree canopy (m)
c	Half the height of the tree canopy (m)
D	Index of agreement of Willmott (1982)
DOY	Day of year
E	Evaporation (mm)
ETo	Penman-Monteith grass reference evapotranspiration (mm)
Fl_{evap}	Canopy cover fraction
Fl_{irrig}	Irrigated surface fraction
g	Gravitation constant (9.8 m s^{-2})
h_c	Canopy humidity
Hc	Crop height (m)
Hc_{max}	Maximum crop height (m)
h_s	Soil surface humidity
i	Vertical position of a node
j	Horizontal position of a node
k	Extinction coefficient
K	Hydraulic conductivity (kg s m^{-3})
Kc	Daily crop coefficient
Kcb	FAO basal crop coefficients
Kc_{max}	Maximum value for Kc following rain or irrigation
K_{PAR}	Canopy extinction coefficient for PAR
K_s	Saturated hydraulic conductivity (kg s m^{-3})
Ky	Stress factor
l	Leaf area index (m^2 leaves m^{-2} ground)
LAb	Leaf area (m^2 leaves)
LAD	Leaf area density (m^2 leaves m^{-3} canopy volume)
M	Molar mass of water (0.018 kg mol^{-1})
MAE	Mean absolute error
MBE	Mass balance error
N	Number of observations
NIR	Near-infrared radiation (range 0.7-3 μm)
NWM	Neutron water meter
PAR	Photosynthetically active radiation (range 0.4-0.7 μm)
PE	Potential evaporation (mm)

PET	Potential evapotranspiration (mm)
PT	Potential crop transpiration (mm)
R	Gas constant (8.314 J K^{-1} mol^{-1})
RD	Root depth (m)
RH	Relative humidity
RH_{min}	Daily minimum relative humidity
RMSE	Root mean square error
Rn	Net radiation (W m^{-2})
r^2	Coefficient of determination
S	Path length of radiation through the canopy (m)
SI	Stress index
SVP	Saturation vapour pressure (kPa)
SWC	Soil water content (m water m^{-1} soil)
SWD	Soil water deficit (mm)
t	Time (s)
T	Kelvin temperature (K); Actual crop transpiration (mm)
TDR	Time domain reflectometry
T_{max}	Maximum transpiration rate (mm d^{-1})
U	Wind speed (m s^{-1})
U_2	Mean daily wind speed at 2 m height (m s^{-1})
Vc	Canopy unit volume (m^{-3})
VP	Vapour pressure (kPa)
VPD	Vapour pressure deficit (kPa)
Y	Estimated yield (Mg ha^{-1})
Y_{pot}	Potential yield (Mg ha^{-1})
Y_{red}	Percentage yield reduction (%)
$Y_{rel(Init)}$	Relative yield for initial stage
$Y_{rel(Dev)}$	Relative yield for development stage
$Y_{rel(Mid)}$	Relative yield for mid-season stage
$Y_{rel(Late)}$	Relative yield for late-season stage
z_o	Distance between the soil surface and the centre of the canopy (m)
z_b	Height at which the base of the canopy is cut off (skirting height) (m)

α	Leaf absorptivity for total solar radiation
α_p	Leaf absorptivity for photosynthetically active radiation
α_s	Leaf absorptivity for total solar radiation
θ	Volumetric soil water content (m water m^{-1} soil)
θ_{ea}	Elevation angle (°)
θ_{fc}	Volumetric soil water content at field capacity (m water m^{-1} soil)
θ_{pwp}	Volumetric soil water content at permanent wilting point (m water m^{-1} soil)
θ_s	Saturated volumetric water content (m water m^{-1} soil)
ρ_b	Bulk density (Mg m^{-3})
ρ_f	Foliage density (m^2 leaf m^{-3} canopy)
ρ_s	Particle density (Mg m^{-3})
ρ_w	Density of water (1000 kg m^{-3})
τ	Fractional transmission of radiation
τ_d	Daily diffuse transmission coefficient
N	Azimuth angle (°)
Φ	Matric flux potential (kg m^{-1} s^{-1})

ψ Solar zenith angle (°)
Ψ Soil water potential (J kg^{-1})
Ψ_e Air entry potential (J kg^{-1})
Ψ_{fc} Soil matric potential at field capacity (J kg^{-1})
Ψ_{lm} Leaf water potential at maximum transpiration, generally occurring in the early afternoon hours (J kg^{-1})
Ψ_m Soil matric potential (J kg^{-1})
Ψ_{pwp} Soil matric potential at permanent wilting point (J kg^{-1})

CHAPTER 1

INTRODUCTION

Problem

The interest in crop modelling started after the introduction and popularisation of computer technology, which facilitated the dynamic simulation of complex natural systems (Sinclair and Seligman, 1996). Several crop models were described in the Agronomy Monograph No. 31 (Hanks and Ritchie, 1991). Advantages and disadvantages as well as research needs were discussed in this publication. Crop models have been developed with different levels of complexity depending on the specific requirements (Whisler et al., 1986). The most common applications are in irrigation management and planning, fertilisation and herbicide recommendations, pollution prevention, soil erosion impact and control, pests and disease forecasting, as well as yield prediction and risk management. In particular, crop growth and soil water balance models for irrigation scheduling are popular at locations where water is a limiting factor for crop production (Bennie et al., 1988; Smith, 1992a; Crosby, 1996; Annandale et al., 2000). For irrigation scheduling purposes, models should simulate growth and development of the crop well. Several mechanistic irrigation scheduling models are available (Campbell and Stockle, 1993; Singels and de Jager, 1991a, b and c; Hodges and Ritchie, 1991). Mechanistic crop growth models require, however, specific crop growth input parameters, which are not readily available in particular for trees.

In simulating crop growth and the field soil water balance, many models use canopy radiant interception for two purposes: a) to determine the photosynthetic rate and dry matter production from the amount of energy intercepted by the crop canopy (Monteith, 1977), and b) to estimate soil water evaporation and crop transpiration from the amount of energy available for these two processes (Ritchie, 1972). Canopy radiant interception represents the fraction of solar radiation available to the crops. In the horizontal planar interception encountered in agronomic, vegetable and pasture crops, which cover the whole surface area uniformly, this can be quantified in one dimension as the fraction of ground covered by the canopy (canopy cover).

Tree hedgerow crops are planted in widely spaced rows to allow access between trees to carry out necessary management practices (e.g. pest control and harvesting). Distribution of energy is not uniform in widely spaced crops. The one-dimensional assumption could therefore lead to serious inaccuracies caused by adjacent row shading, which depends on solar and row orientation, tree size and shape, as well as slope and land aspect. The amount and spatial distribution of intercepted solar radiation will influence evaporation and transpiration, which must be quantified.

In addition, localised irrigation is often used for tree crops to reduce system installation costs. Localised irrigation (micro- or drip) used in orchards only wets a limited area under the canopy of the trees so evaporation from the surface is not uniform. This must be taken into account in modelling the water balance by simulating shading of the wetted portion of the ground. The lack of radiant energy in the shaded portion of the row may limit evaporation, whilst dry soil may limit the process between the rows. Interception of rain by trees is also channelled down the stem and drips from the edge of the canopy so rain is also not evenly distributed at the surface. Root density varies with depth and with distance between the rows so water uptake for transpiration will also vary in two dimensions. It is important to quantify water uptake between rows in order to estimate the effectiveness of rain and the competition for water from cover crops or weeds growing between rows. It is also essential to take into account the limited volume of soil wetted under micro-irrigation or its capacity will easily be exceeded with a standard one-dimensional approach, leading to undesirable over irrigation in the wetted zone, and possibly crop stress due to too long an irrigation interval.

In order to accurately estimate canopy growth, water balance and yield, it is therefore essential to model canopy radiant interception and soil water balance of hedgerow tree crops in two dimensions and on an hourly time step, based on sound physical principles.

Background

Campbell and Diaz (1988) published a simple soil water balance model to predict crop water use. Two outstanding features of this model were:

i) Keeping the model simple with minimal soil, plant, and atmospheric data requirements; and

ii) Developing the model on sound physical and physiological principles (referred to as mechanistic) as opposed to an empirical approach.

Annandale et al. (2000) tested the model on green peas. Based on the results, it was decided to:

i) Further develop the program's user friendliness and practicality; and

ii) Determine the necessary crop parameters for other irrigated crops in South Africa.

This materialised in the development of a simple, but mechanistic, generic crop growth and soil water balance model (SWB) for irrigation scheduling under full and deficit irrigation (Annandale et al., 1999). The SWB model was mainly developed for predicting real-time soil water deficit of field crops with a one-dimensional canopy light interception and water redistribution procedure.

There is lack of suitable tools to mechanistically describe the energy and soil water balance of tree crops. Due to the importance of fruit crops, on the export as well as local markets, it was decided to improve the SWB model by incorporating a two-dimensional system for use in hedgerow plantings.

Objectives

The objectives of this project were:

i) To develop a two-dimensional fruit tree water balance model that takes into account the unique fractional interception of solar radiation associated with hedgerow orchards as opposed to the horizontal planar interception encountered in agronomic crops.

ii) To verify the model for deciduous fruit trees using peaches as an example.

iii) To verify the model for evergreen fruit trees using citrus as an example.

iv) To develop a core of irrigation expertise, within the University of the North, Faculty of Agriculture, to be of service, in collaboration with the National Community Water and Sanitation Training Institute, to agriculture in the Northern Province.

v) Over time, to equip a centre at the University of the North to have the capacity to conduct irrigation research and train students in the use of these techniques.

Approach

An extensive literature search was carried out on two-dimensional energy and water balance models. In this report, no separate Chapter on literature review is included. References are, however, presented in the various Sections as applicable.

The two-dimensional energy and soil water balance model was developed during the visit of the study leader to Washington State University. Verification of the model comprised the

inspection of the internal consistency of the model and its software implementation (CAMASE, 1995).

According to the guidelines of CAMASE (1995), the usefulness and relevance of a model needs to be established for the specific purpose for which it was developed. Also, validation should be representative of the situations in which the model is to be used. Validation of the model presented in this study was therefore carried out for a wide range of conditions (row orientation, period of the year and canopy density), and for both deciduous and evergreen tree crops.

For this purpose, two field trials were set up. The first trial was established in a peach orchard on the lysimeter facilities at Pretoria University's experimental farm. This would provide a site where detailed observations could be easily recorded to validate the SWB model for deciduous trees. The second trial was established in a citrus orchard at the Syferkuil experimental farm of the University of the North. This was the site where measured data were collected to validate the SWB model for evergreen trees. During the course of the project and for the purpose of validating the energy interception model for different conditions (tree size and shape, row orientation etc.), an additional trial was carried out on Leucaena fodder trees in Hatfield. Contact was also made with private farming enterprises and two field trials were carried out in Brits on citrus farms.

Although the validation was done only for some orchards, the model could be applicable to other orchards and conditions provided that correct input parameters are used.

CAMASE (1995) also suggested that, if the subject of the model is too large for regular validation, the model is to be divided into sub-models that are separately validated. For this reason, the two-dimensional energy interception and soil evaporation components were validated separately. The crucial interactions between the model components were integrated in the validation of the two-dimensional soil water balance model, which uses the energy interception and soil evaporation sub-models to split evaporation and transpiration.

This report firstly presents the theoretical description of the two-dimensional energy interception and soil water balance model for hedgerow tree crops, developed to achieve objective i) (Chapter 2). A simple, quasi two-dimensional cascading soil water balance model based on the FAO crop factor approach is also presented.

Chapter 3 describes material and methods of the field trials used to validate the model. Chapter 4 presents the validation of the two-dimensional energy interception and soil water balance model for deciduous and evergreen trees (objectives ii) and iii)), as well as the calibration of the simple FAO-based cascading model for peaches, including the most relevant field observations.

Scenario simulations were then carried out to perform logical sensitivity analyses. According to the definition of CAMASE (1995), logical sensitivity analysis is the effort to establish by inspection of results whether the model is sensitive to changes in input.

The capacity building and technology transfer actions carried out in order to achieve objectives iv) and v), are presented in Chapter 7.

CHAPTER 2

MODEL DESCRIPTION

Two types of model were developed for hedgerow tree crops during the course of this project and included in SWB:

i) A two-dimensional energy interception and soil water balance model; and

ii) An FAO-based *crop factor model*.

The first model calculates the two-dimensional energy interception for hedgerow tree crops, based on solar and row orientation, tree size and shape, as well as leaf area density. A two-dimensional soil water redistribution is also calculated with a finite difference solution. This model is based on sound physical principles, but it requires certain input parameters that are not always easy to obtain (e.g. leaf area density and soil saturated hydraulic conductivities).

A second simpler model, based on the FAO crop factor approach, was therefore developed to enable users to predict crop water requirements with limited input data. This model includes a semi-empirical approach for partitioning above-ground energy, a cascading soil water redistribution that separates the wetted and non-wetted portion of the ground, as well as prediction of crop yields according to the CROPWAT model developed by the FAO (Smith, 1992a).

In this chapter of the report, the theoretical description is presented for both models.

2.1. Two-dimensional model for hedgerow tree crops (SWB-2D)

2.1.1. Two-dimensional energy interception model

The radiation interception model described here is based on the work of Charles-Edwards and Thornley (1973) and Charles-Edwards and Thorpe (1976). The model assumes leaves to be uniformly distributed within an ellipsoid, and radiation penetrating the canopy is attenuated according to Beer's law. Fractional transmission of radiation (τ) through a canopy can be described as follows:

$$\tau = e^{-kl} \qquad (2.1.1)$$

where k is the extinction coefficient that represents the horizontal projection of leaves relative to one sided leaf area as defined by Campbell and Norman (1998), and l is the leaf area index. The transmission of radiation to a certain point on the ground will clearly depend on the distance (S) within the canopy through which the beam travels. Norman and Welles (1983) showed that:

$$\rho_f S = \frac{l}{\cos\Psi} \qquad (2.1.2)$$

where ρ_f is foliage density (m^2 leaves m^{-3} canopy), S in metres is the path length of radiation through the canopy, and ψ is the solar zenith angle. Campbell and Norman (1998) derived the extinction coefficient for leaves with a spherical leaf angle distribution, which is a good approximation for most canopies:

$$k = \frac{1}{2\cos\Psi} \qquad (2.1.3)$$

The transmissivity calculated in Eq. (2.1.1) now becomes:

$$\tau = e^{(-0.5\rho_f S\sqrt{\alpha})} \qquad (2.1.4)$$

where the absorptivity of leaves for solar radiation (α) equals 0.5, and this term takes radiation scattering (transmission and reflection) within the canopy into account. The same Eq. (2.1.4) can be used for photosynthetically active radiation (PAR, 0.4-0.7 μm) by setting α to 0.8 and to 0.2 for the near infrared range (NIR, 0.7-3 μm).

In order, therefore, to determine the spatial distribution of soil irradiance, the canopy path length through which the radiation must travel to reach a certain point on the soil surface must be calculated. A method to calculate this path length, based on Charles-Edwards and Thornley (1973), describes an ellipsoidal tree canopy surface as follows:

$$\frac{x^2}{a^2} + \frac{y^2}{b^2} + \frac{z^2}{c^2} = 1 \qquad (2.1.5)$$

where x, y and z are the Cartesian co-ordinate axes, and a is half the width, b half the depth and c half the height of the tree canopy. An ellipsoid is very versatile as many different shapes can be generated by adjusting a, b and c. For a hedgerow canopy, however, the dimension b can be made very large so the y^2/b^2 term tends to zero and can therefore be neglected. Also, in order to lift the ellipsoid above the ground surface the vertical axis needs to be offset and Eq. (2.1.5) becomes:

$$\frac{x^2}{a^2} + \frac{(z - z_o)^2}{c^2} = 1 \qquad (2.1.6)$$

with z_o the distance between the soil surface and the centre of the canopy. This is illustrated in Figure 2.1.

In order to determine the diffuse transmission coefficient, S needs to be evaluated for all azimuth (ϕ) and elevation angles (θ_{ea}). If Q (x_q, y_q, z_q) denotes the position where the ray penetrates the canopy, and P (x_p, y_p, z_p) the point where the ray is intercepted on the soil surface, then:

$$\frac{x_q - x_p}{\sin\theta_{ea}\cos\phi} = \frac{z_q}{\cos\theta_{ea}} \qquad (2.1.7)$$

If N (x_n, y_n, z_n) denotes the lower surface of the canopy where the ray exits, then the path length S through which the beam travels and along which it can be attenuated is given by:

$$S = \frac{z_q - z_n}{\cos\theta_{ea}} \qquad (2.1.8)$$

This is schematically presented in Figure 2.2. z_q and z_n can be determined by rearranging Eq. (2.1.7) to give an expression for x_q, which can be used to eliminate this term by substitution in Eq. (2.1.6). This results in a quadratic equation in z_q of the form:

$$uz_q^2 + vz_q + w = 0 \qquad (2.1.9)$$

where the coefficients are:

$$u = c^2\sin^2\theta\cos^2\phi + a^2\cos^2\theta \qquad (2.1.10)$$

$$v = 2\left[c^2\sin\theta\cos\theta\cos\phi x_p - a^2\cos^2\theta z_o\right] \qquad (2.1.11)$$

$$w = c^2 \cos^2\theta\left[xp^2 + a^2(z_0^2/c^2 - 1)\right] \qquad (2.1.12)$$

If a ray from a particular direction penetrates a row, the height of entry into the canopy z_q and that at which it exits the canopy z_n are given by the roots r_1 and r_2 ($r_1 \geq r_2$) of Eq. (2.1.9). If the ray misses the canopy the roots will be imaginary.

The model also makes provision for elliptical shapes with the base pruned (Figure 2.2). If the base of the canopy is cut off at a height z_b, an additional condition is added to describe the canopy shape:

$$z \geq z_b \qquad (2.1.13)$$

Three cases can then be distinguished:

- Case 1: $r_1 \geq z_b$ and $r_2 \geq z_b$. Both roots belong to the canopy: $z_q=r_1$ and $z_n=r_2$
- Case 2: $r_1 \geq z_b$ and $r_2 < z_b$. Root r_1 belongs to the surface of the canopy but r_2 is below the cut base: $z_q=r_1$, $z_n=z_b$
- Case 3: $r_1 < z_b$ (and therefore $r_2 < z_b$). The ray misses the canopy.

Radiation can penetrate neighbouring rows so more than one row needs to be considered. In this model, two rows on either side of the simulated row were considered (Charles-Edwards and Thorpe, 1976). Eq. (2.1.6) then becomes:

$$\frac{(x-nh)^2}{a^2} + \frac{(z-z_o)^2}{c^2} = 1 \qquad (2.1.14)$$

with n the row number from 0 to 4, and h the row spacing. This is illustrated in Figure 2.3, and the soil surface over which radiant transmittance is calculated is also shown. If a ray penetrates more than one row then S will be the sum of the individual path lengths through each canopy.

It is essential that beam or direct radiation and diffuse radiation be treated separately, as they will interact differently with the canopy. Weiss and Norman (1985) gave an example for a canopy with a leaf area index of 2 that would typically have a diffuse transmittance of 0.25 but direct beam transmittance could vary from near zero to 0.4 depending on solar zenith angle. A daily diffuse transmission coefficient (τ_d) is calculated by determining the path lengths of radiation penetration through the canopy for all azimuth and zenith angles. τ_d is therefore dependent only on tree size and canopy density. Diffuse and beam radiation are not usually measured separately so it is necessary to estimate the relative contributions of these two components from measured global radiation. The method of Weiss and Norman (1985) has been followed, where diffuse and direct beam radiation for the PAR and NIR wavebands are estimated from total incoming solar radiation. They developed relationships for potential values of direct and diffuse PAR and NIR from clear day experiments. The ratio of actual measured to potential measured radiation is then used to estimate the proportion of direct and diffuse radiation in these two spectral bands.

As illustrated earlier, the attenuation of beam radiation by the canopy is strongly dependent on zenith angle, and for crops planted in rows, azimuth angle and row orientation will also be crucial. Elevation and azimuth angles can be calculated from latitude, solar declination that depends on day of year, and time of day (Campbell and Norman, 1998). Before the length of canopy through which radiation penetrates can be calculated, azimuth angle needs to be adjusted to take row orientation into account. Azimuth angle is calculated in degrees clockwise from N, so E is 90°, S is 180° and W is 270°. The X-axis must always be oriented perpendicular to the row direction for these simulations.

Required inputs

Input data required to run the two-dimensional canopy interception model are: latitude, standard meridian, longitude, daily solar radiation, row width and orientation, canopy height and width, stem height and distance to the bottom of the canopy, extinction coefficient, absorptivity and leaf area density. Extinction coefficient can be assumed to be 0.5 for leaves with a spherical leaf angle distribution. Absorptivity of leaves for total solar radiation can also be assumed to be 0.5. The most difficult input parameter to estimate is the leaf area density. During the course of this project, a method for the estimation of leaf area density was developed using the LAI-2000 plant canopy analyzer (Li-Cor, Lincoln, Nebraska).

A flow diagram of the two-dimensional energy interception model for hedgerow tree crops is shown in Figure 2.4. The source code of the energy interception model written in Delphi is given in Appendix A.

2.1.2. Spatial distribution of soil evaporation

The model calculates the spatial distribution of evaporation at the soil surface in two steps:

i) Potential evaporation at each node (PE_j) is estimated by applying the Penmann-Monteith equation (Allen et al., 1998), using radiation estimated locally as input.

ii) Evaporation from the soil surface at each node (E_j) is calculated as a function of potential evaporation, air humidity h_c, and humidity of the soil surface h_j (given by the two-dimensional model of soil water redistribution, explained in Section 2.1.3), according to Campbell (1985):

$$E_j = PE_j \frac{(h_j - h_c)}{(1 - h_c)} \qquad (2.1.15)$$

where h_c and h_j are the canopy humidity and the humidity of the soil surface at node j respectively.

The surface humidity depends on the soil water potential Ψ_j (J kg^{-1}) at the surface and is calculated after Campbell (1977) as:

$$h_j = \exp\left(\frac{M\Psi}{RT}\right) \qquad (2.1.16)$$

with M the molar mass of water (0.018 kg mol^{-1}), R the gas constant (8.314 J K^{-1} mol^{-1}) and T the Kelvin temperature.

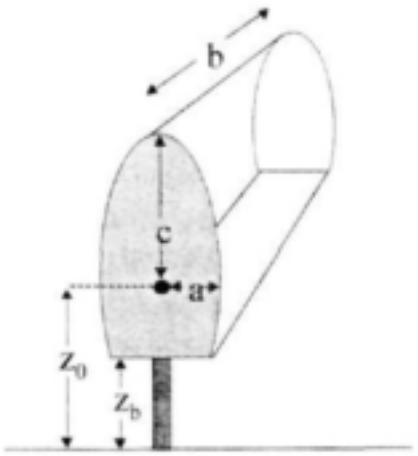

Figure 2.1. Three-dimensional representation of a tree. c is half the height, a half the width and b half the depth of the canopy. z_0 is the height from the ground to the centre of the canopy, and z_b the height of the base of the canopy.

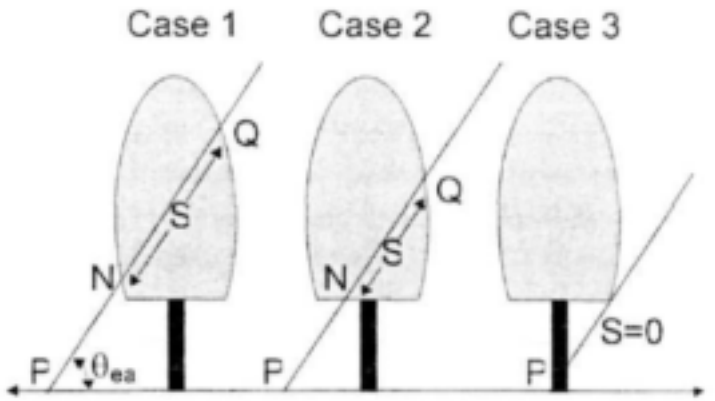

Figure 2.2. Schematic representation of ray passing through the tree canopy. S is the path length, θ_{ea} is the elevation angle, Q is the position where the ray enters the canopy, N where it exits and P where it is intercepted on the soil surface. Three cases are shown: (1) both Q and N are on the ellipsoidal part of the canopy, (2) N is at the base of the canopy, (3) the ray does not intercept the canopy.

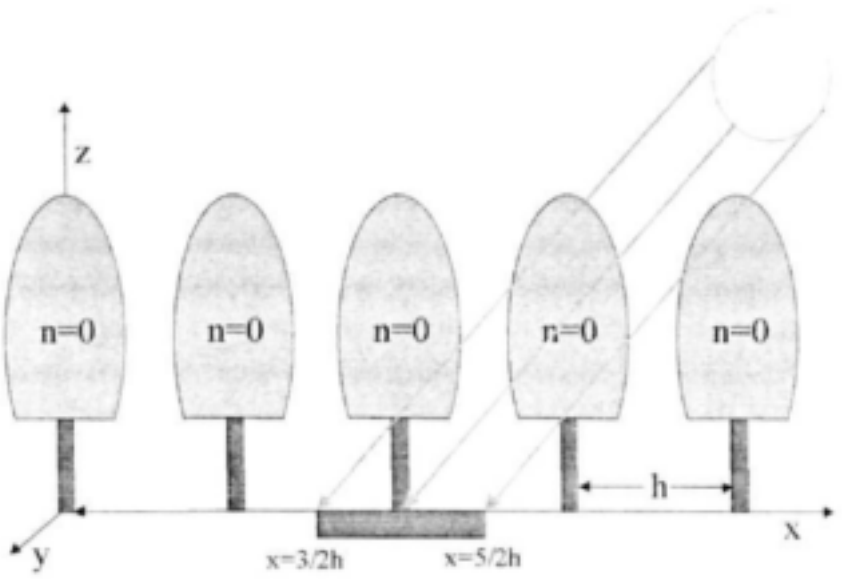

Figure 2.3. Schematic illustration of the system simulated; n is the tree row number, h is the row spacing, x, y and z the cartesian axes, and the soil surface over which radiant transmittance is estimated is between 3/2h and 5/2h.

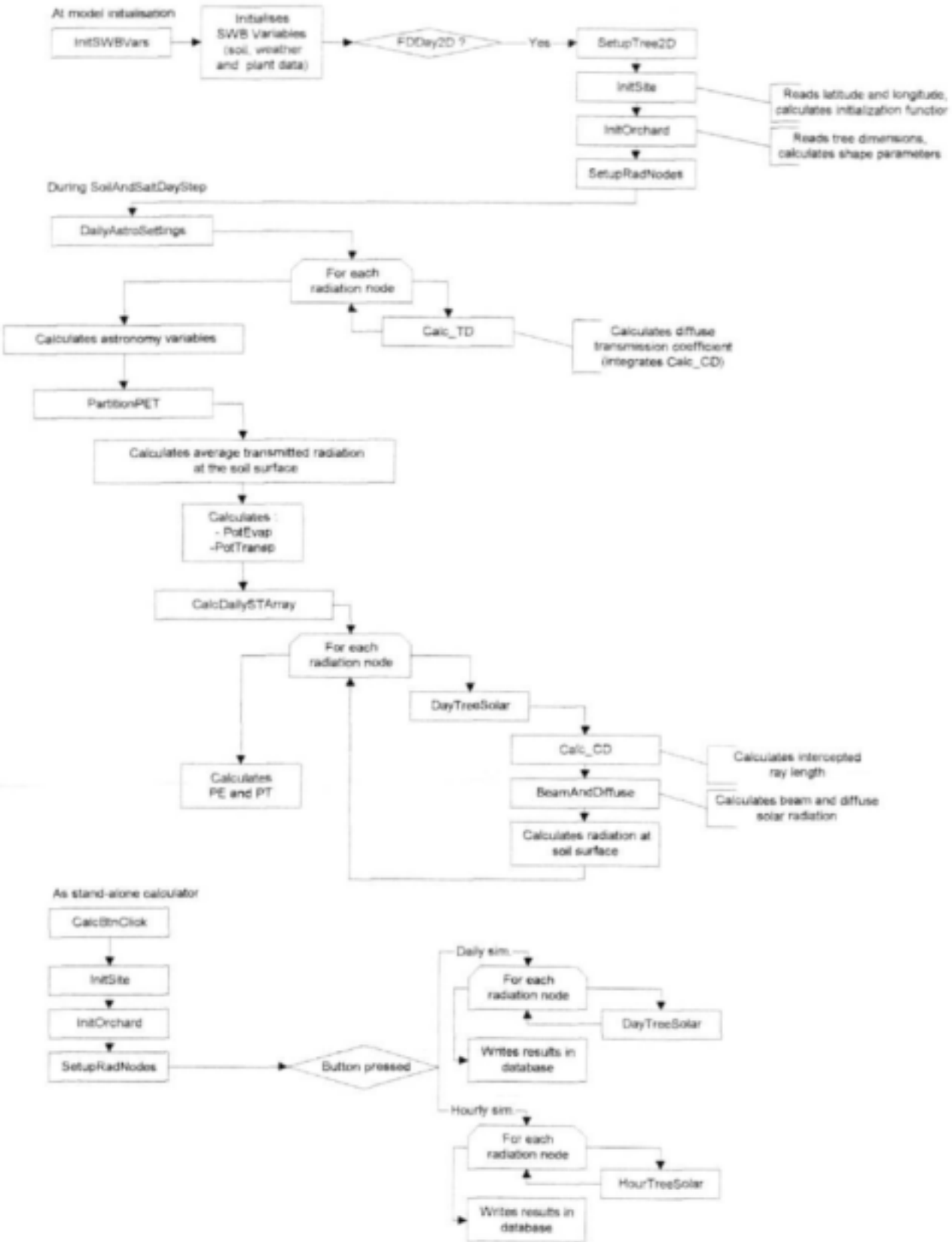

Figure 2.4. Flow diagram of the two-dimensional energy interception model for hedgerow tree crops.

2.1.3. *Two-dimensional finite difference soil water balance model*

2.1.3.1 *The soil profile*

In order to simulate two-dimensional water movement in the soil, a grid of nodes had to be established. This nodal system is set up like the one in Campbell (1985) with i representing the vertical position of a node and j the horizontal position. This divides the soil into a number of elements. Each element is referenced by the node reference of the upper left corner of the element. This is illustrated in Figure 2.5.

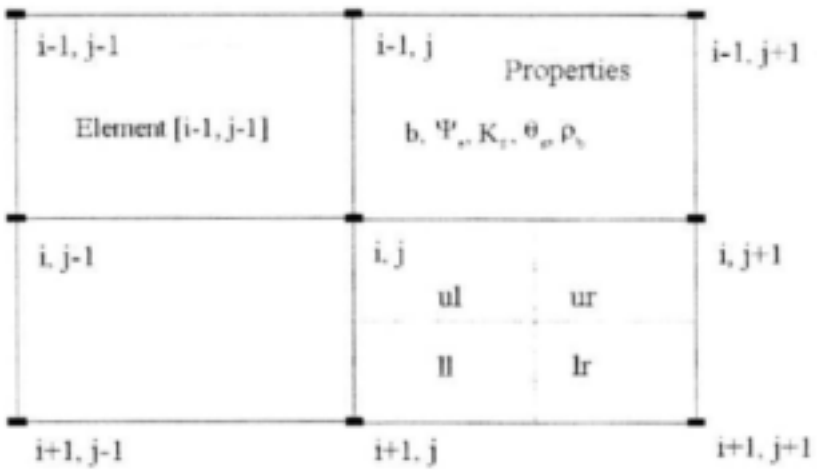

Figure 2.5. The two-dimensional nodal system. Element [i,j] has been divided into quarters: ul (upper left); ur (upper right); ll (lower left) and lr (lower right). Element [i-1, j] shows the soil properties which are fixed for a particular element: b is the slope of a log-log water retention function; Ψ_e the air entry potential; K_s the saturated hydraulic conductivity; ρ_b is bulk density and θ_s the saturated volumetric water content.

The distances between nodes are selected so that model output can easily be compared to field measured values. Each element has its own physical properties, so this scheme allows variation in soil properties in two dimensions. The properties referred to are bulk density (ρ_b), the Campbell 'b' value or slope of a log-log water retention function, the air entry potential (Ψ_e), saturated hydraulic conductivity (K_s) and the saturated water content (θ_s). A fixed set of properties for element [i –1, j] can be seen in Figure 2.5, as can the division of element [i, j] into quarters labelled ul (upper left), ur (upper right), ll (lower left) and lr (lower right). The reason for this division will be explained in the next section.

The soil bulk density values used in this model were based on field measurements. These values were used to estimate saturated volumetric water contents using Eq. (2.1.17):

$$\theta_s = 1 - \frac{\rho_b}{\rho_s} \qquad (2.1.17)$$

where ρ_s is particle density, assumed to be 2.65 Mg m $^{-3}$.

The Campbell 'b' value, air entry potential (Ψ_e) and the saturated hydraulic conductivity (Ks) are determined from water release curves (Campbell, 1985):

$$b = \frac{\ln(\Psi_{pwp} / \Psi_{fc})}{\ln(\theta_{fc} / \theta_{pwp})} \qquad (2.1.18)$$

$$\Psi_e = \Psi_{fc} \left(\frac{\theta_{fc}}{\theta_s} \right)^b \qquad (2.1.19)$$

$$K_s = \frac{0.001}{\Psi_e^{\,2}} \qquad (2.1.20)$$

The soil matric potential at field capacity (Ψ_{fc}) and permanent wilting point (Ψ_{pwp}), as well as the volumetric soil water content at field capacity (θ_{fc}) and permanent wilting point (θ_{pwp}) are model inputs.

The complete grid system used in this model can be seen in Figure 2.6. The soil profile is enclosed by the heavy solid line and all nodes falling outside the profile are there merely to generalise the flux equations. Symmetry planes are assumed to occur mid way between two rows on either side of the hedgerow and no water flux is allowed across these planes. The distances between nodes should be selected so that model output can easily be compared to measured data.

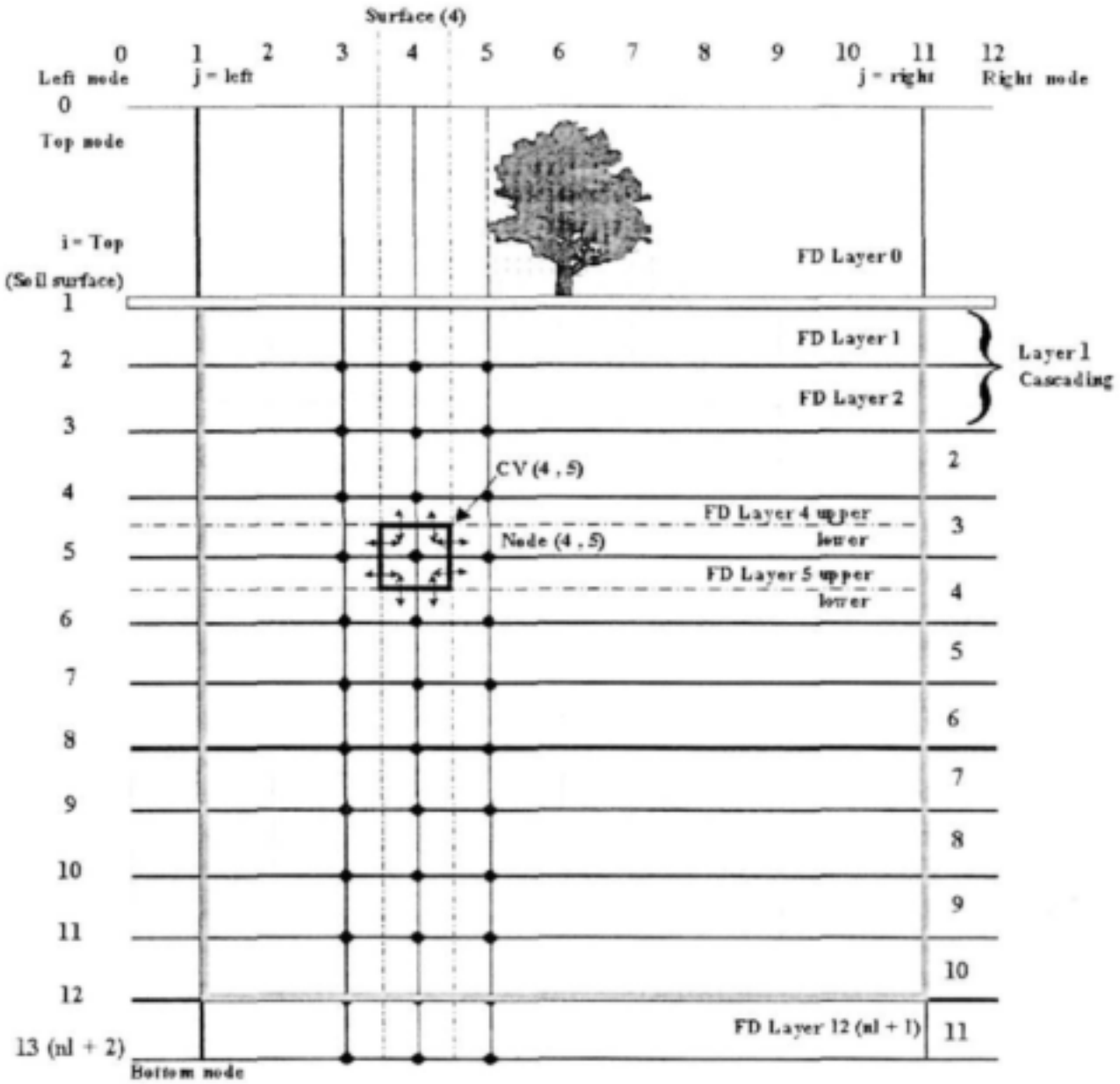

Figure 2.6. Nodal grid system showing symmetry planes and hedgerow. The soil layers for the cascading model are also represented.

2.1.3.2 Two-dimensional water flow

The model redistributes water in the soil in two-dimensions using a finite difference solution to Richards' continuity equation for water flow. The two-dimensional differential equation for water flow is:

$$\rho_w \frac{\partial \theta}{\partial t} = \frac{\partial}{\partial x}\left(k \frac{\partial \Psi}{\partial x}\right) + \frac{\partial}{\partial z}\left(k \frac{\partial \Psi}{\partial z}\right) - g \frac{\partial k}{\partial z} + S \qquad (2.1.21)$$

The left hand side of the equation represents the change in water storage with time, and for mass conservation this must equal the difference between the influx and outflux of water, plus any changes in storage due to a sink term. The density of water ρ_w is 1000 kg m^{-3}, θ is volumetric water content, and t is time in seconds. The horizontal coordinate x is parallel to the soil surface and perpendicular to the row direction (y), and z is the vertical coordinate. The hydraulic conductivity K (kg s m^{-3}), is a function of matric potential Ψ (J kg^{-1}) and is expressed by Campbell (1985) as

$$K = Ks\left(\frac{\Psi}{\Psi_e}\right)^{-n} \qquad \Psi < \Psi_e \qquad (2.1.22)$$

$$K = Ks \qquad \Psi \geq \Psi_e \qquad (2.1.23)$$

with n an empirical constant related to the slope of the water retention curve

$$n = 2 + \frac{3}{b} \qquad (2.1.24)$$

The flux of water due to gravity g (9.8 m s^{-2}) is taken into account in the term -g(δK/δz). The sink-source term S includes evaporation, infiltration and crop water uptake. Some of the non-linearity of Eq (2.1.21) can be reduced by using the Kirchhoff transform, which defines a new variable Φ, the matrix flux potential. Campbell (1985) defined this variable as

$$\Phi = \int_{-\infty}^{\Psi} K(\Psi)\delta\Psi \qquad (2.1.25)$$

Substituting Eqs. (2.1.22) or (2.1.23) and integrating gives

$$\Phi = \frac{K\Psi}{1-n} \qquad \Psi < \Psi_e \qquad (2.1.26)$$

$$\Phi = Ks\left(\frac{\Psi_e}{1-n} + \Psi - \Psi_e\right) \qquad \Psi \geq \Psi_e \qquad (2.1.27)$$

with Φ in kg m^{-1} s^{-1}.

The two-dimensional continuity equation expressed in terms of matrix flux potential is

$$\rho_w \frac{\partial\theta}{\partial t} = \frac{\partial^2\Phi}{\partial x^2} + \frac{\partial^2\Phi}{\partial z^2} - g\frac{\partial k}{\partial z} + S \qquad (2.1.28)$$

In difference form

$$\frac{\rho_w\left(\theta_{i,j}^{t+\Delta t} - \theta_{i,j}^{t}\right)}{\Delta t} = \frac{\left(\frac{\Phi_{i,j+1} - \Phi_{i,j}}{x_{j+1} - x_j} - \frac{\Phi_{i,j} - \Phi_{i,j-1}}{x_j - x_{j-1}}\right)}{\left(\frac{x_{j+1} - x_{j-1}}{2}\right)} + \frac{\left(\frac{\Phi_{i+1,j} - \Phi_{i,j}}{z_{j+1} - z_i} - \frac{\Phi_{i,j} - \Phi_{i-1,j}}{z_i - z_{j-1}} - g\left(K_{i,j} - K_{i-1,j}\right)\right)}{\left(\frac{z_{j+1} - z_{j-1}}{2}\right)} + S$$

(2.1.29)

The volumetric water contents at the beginning and end of the time step are θ^t and $\theta^{t+\Delta t}$ respectively. Campbell (1985) related volumetric water content to water potential as follows:

$$\theta = \theta_s \left(\frac{\Psi}{\Psi_e} \right)^{-1/b} \qquad \Psi < \Psi_e \qquad (2.1.30)$$

The time averaged matrix flux potential Φ is given by

$$\theta = \theta_s \qquad \Psi \geq \Psi_e \qquad (2.1.31)$$

$$\Phi = \eta \Phi^{t+\Delta t} + (1-\eta)\Phi^t \qquad 1 \geq \eta \geq 0 \qquad (2.1.32)$$

Redinger et al. (1984) report that with non-linear flow problems, a backward differencing scheme gives the best results; i.e. $\eta = 1$.

The difference equation derived is similar to the one used by Redinger et al. (1984). This form of equation can be used if the soil profile to be modelled is isotropic. If, however, soil variation is to be taken into account, an approach like that of Ross and Bristow (1990) needs to be taken because matrix flux potential, like water content, is not continuous across textural discontinuities. In the one-dimensional model of Ross and Bristow (1990) nodes were placed at textural discontinuities and two matrix flux potentials were calculated for each node. The matrix flux potential, and also volumetric water content and hydraulic conductivity would depend on the soil properties of the element and the potential at the node. This is illustrated in Figure 2.7 for element [i, j].

The four-quarter elements surrounding a node can be seen as a control volume to which the continuity equation is applied. Taking two-dimensional soil variation into account results in eight flux equations, which are illustrated in Figure 2.8.

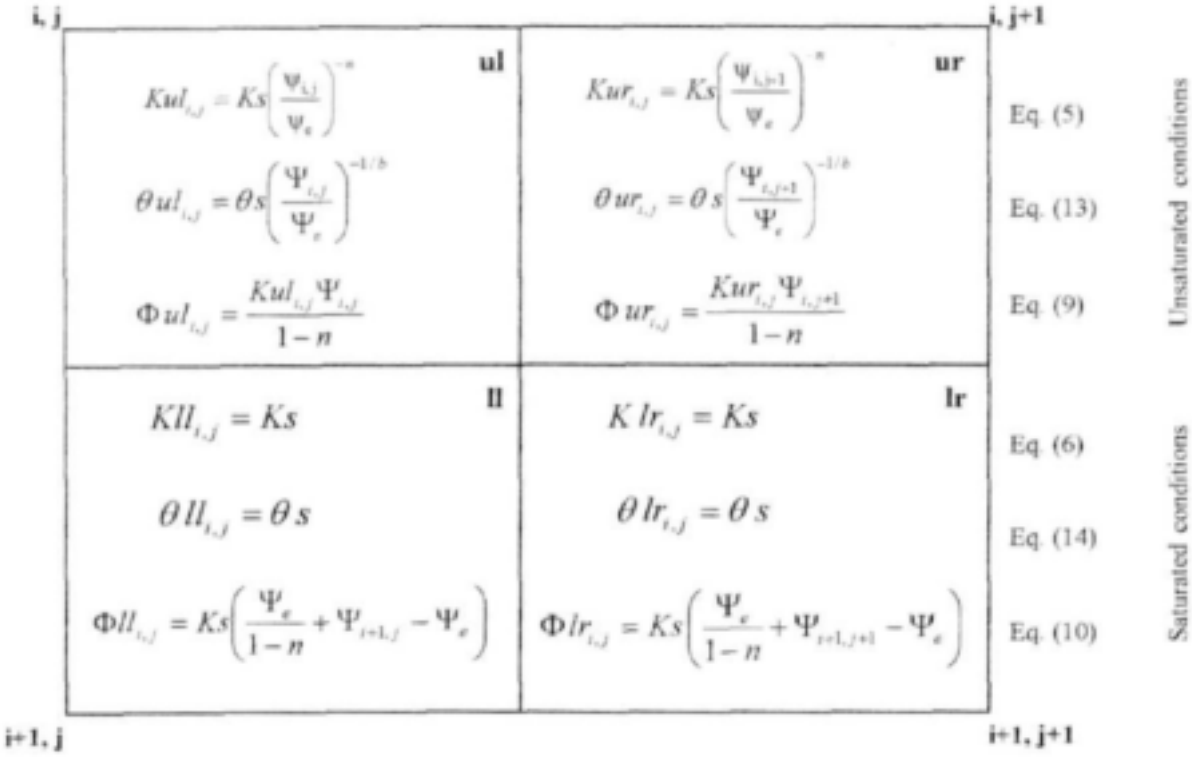

Figure 2.7. Detail of element [i ,j] (see Figure 2.5), with K, θ and Φ calculated for each quarter (ul, ur, ll and ul). For demonstration purposes, nodes [i,j] and [i,j+1] are below Ψ_e whilst nodes [i+1,j] and [i+1,j+1] are above Ψ_e.

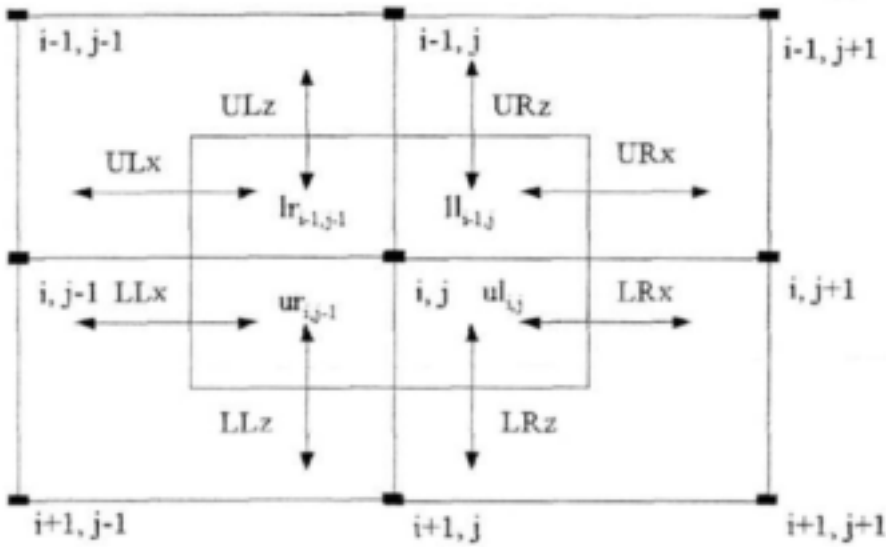

Figure 2.8. Control volume [i, j] illustrating the eight water fluxes.

The fluxes have been named upper right (UR) x and z, upper left (UL) x and z, lower right (LR) x and z and lower left (LL) x and z. The difference form of these equations follows with positive values representing fluxes into the control volume.

$$URx = \frac{(\Phi lr_{i-1,j} - \Phi ll_{i-1,j})(Z_i - Z_{i-1})}{2(X_{j+1} - X_j)} \qquad (2.1.33)$$

$$LRx = \frac{(\Phi ur_{i,j} - \Phi ul_{i,j})(Z_{i+1} - Z_i)}{2(X_{j+1} - X_j)} \qquad (2.1.34)$$

$$ULx = \frac{(\Phi ll_{i-1,j-1} - \Phi lr_{i-1,j-1})(Z_i - Z_{i-1})}{2(X_j - X_{j-1})} \qquad (2.1.35)$$

$$LLx = \frac{(\Phi ul_{i,j-1} - \Phi ur_{i,j-1})(Z_{i+1} - Z_i)}{2(X_j - X_{j-1})} \qquad (2.1.36)$$

$$URz = \frac{(\Phi ul_{i-1,j} - \Phi ll_{i-1,j})(X_{j+1} - X_j)}{2(Z_i - Z_{i-1})} + \frac{g\ Kul_{i-1,j}(X_{j+1} - X_j)}{2} \qquad (2.1.37)$$

$$LRz = \frac{(\Phi ll_{i,j} - \Phi ul_{i,j})(X_{j+1} - X_j)}{2(Z_{i+1} - Z_i)} - \frac{g\ Kul_{i,j}(X_{j+1} - X_j)}{2} \qquad (2.1.38)$$

$$ULz = \frac{(\Phi ur_{i-1,j-1} - \Phi lr_{i-1,j-1})(X_j - X_{j-1})}{2(Z_i - Z_{i-1})} + \frac{g\ Kur_{i-1,j-1}(X_j - X_{j-1})}{2} \qquad (2.1.39)$$

$$LLz = \frac{(\Phi lr_{i,j-1} - \Phi ur_{i,j-1})(X_j - X_{j-1})}{2(Z_{i+1} - Z_i)} - \frac{g\ Kur_{i,j-1}(X_j - X_{j-1})}{2} \qquad (2.1.40)$$

$$\Delta S = \frac{\rho_w(\theta_{i,j}^{t+\Delta t} - \theta_{i,j}^{t})(X_{j+1} - X_{j-1})(Z_{i+1} - Z_{i-1})}{4\Delta t} \qquad (2.1.41)$$

Note that the vertical fluxes include gravitational components. The change in storage ΔS, is given in difference form since the volumetric water content, $\theta_{i,j}$, is the weighted average water content for the control volume [i, j]:

$$\theta_{i,j} = \frac{\left(\theta lr_{i-1,j-1}\frac{(X_j - X_{j-1})(Z_i - Z_{i-1})}{4} + \theta ll_{i-1,j}\frac{(X_{j+1} - X_j)(Z_i - Z_{i-1})}{4} + \theta ur_{i,j-1}\frac{(X_j - X_{j-1})(Z_{i+1} - Z_i)}{4} + \theta ul_{i,j}\frac{(X_{j+1} - X_j)(Z_{i+1} - Z_i)}{4}\right)}{\left(\frac{(X_{j+1} - X_{j-1})(Z_{i+1} - Z_{i-1})}{4}\right)} \qquad (2.1.42)$$

The mass balance error MBE is given by:

$$MBE = URx + LRx + ULx + LLx + URz + LRz + ULz + LLz - \Delta S + Infiltration - Evaporation - Plant\ uptake \qquad (2.1.43)$$

Infiltration and evaporation will be discussed later. Plant water uptake (i.e. transpiration) depends on canopy radiation interception, atmospheric evaporative demand, and root weighted matric potential. The mechanistic, supply- or demand-limited approach is explained in detail by Annandale et al. (2000). The aim is to find the matric potentials that will cause the mass balance error to be negligible. This is done using the Newton-Raphson procedure as described in Campbell (1985). This requires taking the derivatives of all the terms in Eq. (2.1.43) with respect to matric potential. These derivatives follow:

$$\frac{\partial URx}{\partial \Psi_{i,j}} = \frac{-Kll_{i-1,j}(Z_i - Z_{i-1})}{2(X_{j+1} - X_j)} \qquad (2.1.44)$$

$$\frac{\partial LRx}{\partial \Psi_{i,j}} = \frac{-Kul_{i,j}(Z_{i+1} - Z_i)}{2(X_{j+1} - X_j)} \qquad (2.1.45)$$

$$\frac{\partial ULx}{\partial \Psi_{i,j}} = \frac{-Klr_{i-1,j-1}(Z_i - Z_{i-1})}{2(X_j - X_{j-1})} \qquad (2.1.46)$$

$$\frac{\partial LLx}{\partial \Psi_{i,j}} = \frac{-Kur_{i,j-1}(Z_{i+1} - Z_i)}{2(X_j - X_{j-1})} \qquad (2.1.47)$$

$$\frac{\partial URz}{\partial \Psi_{i,j}} = \frac{-Kll_{i-1,j}(X_{j+1} - X_j)}{2(Z_i - Z_{i-1})} \qquad (2.1.48)$$

$$\frac{\partial LRz}{\partial \Psi_{i,j}} = \frac{-Kul_{i,j}(X_{j+1} - X_j)}{2(Z_{i+1} - Z_i)} - \frac{g(X_{j+1} - X_j)}{2} \frac{\partial Kul_{i,j}}{\partial \Psi_{i,j}} \qquad (2.1.49)$$

$$\frac{\partial ULz}{\partial \Psi_{i,j}} = \frac{-Klr_{i-1,j-1}(X_j - X_{j-1})}{2(Z_i - Z_{i-1})} \qquad (2.1.50)$$

$$\frac{\partial LLz}{\partial \Psi_{i,j}} = \frac{-Kur_{i,j-1}(X_j - X_{j-1})}{2(Z_{i+1} - Z_i)} - \frac{g(X_j - X_{j-1})}{2} \frac{\partial Kur_{i,j-1}}{\partial \Psi_{i,j}} \qquad (2.1.51)$$

$$\frac{\partial S}{\partial \Psi_{i,j}} = \rho_w \frac{\partial \Theta_{i,j}^{t+\Delta t}}{\partial \Psi_{i,j}} \left(\frac{(X_{j+1} - X_{j-1})(Z_{i+1} - Z_{i-1})}{4\Delta t} \right) \qquad (2.1.52)$$

The derivative of the hydraulic conductivity is:

$$\frac{\partial K}{\partial \Psi} = \frac{-nK}{\Psi} \qquad \Psi < \Psi_e \qquad (2.1.53)$$

$$\frac{\partial K}{\partial \Psi} = 0 \qquad \Psi \geq \Psi_e \qquad (2.1.54)$$

While the differential water capacity is:

$$\frac{\partial \theta}{\partial \Psi} = \frac{-\theta}{b\Psi} \qquad \Psi < \Psi_e \qquad (2.1.55)$$

$$\frac{\partial \theta}{\partial \Psi} = 0 \qquad \Psi \geq \Psi_e \qquad (2.1.56)$$

The control volume differential water capacity is also calculated as a weighted average. The derivatives of the sink terms will be discussed later. The sum of all the derivatives at node i, j is $\partial MBE_{i,j}/\partial \Psi_{i,j}$ and this is used to improve the estimate of $\Psi_{i,j}$ in the Newton-Raphson procedure using:

$$\Delta \Psi_{i,j} = \frac{MBE_{i,j}}{\partial MBE_{i,j} / \partial \Psi_{i,j}} \qquad (2.1.57)$$

with $\Delta\Psi$ to be subtracted from $\Psi_{i,j}$. Ross and Bristow (1990) found the slopes $\partial MBE_{i,j}/\partial \Psi$ far from the solution so gave poor estimates of the changes in potential actually needed. They suggest restricting the value of $\Delta\Psi$ to 0.8 $\Psi_{i,j}$ for values of $\Psi_{i,j}$ below an arbitrary cut off value of -0.1 J kg^{-1}. The cut off value is necessary to avoid the limit for change approaching zero as $\Psi_{i,j}$ approaches zero. The cut off value was set to -0.01 J kg^{-1} in this model.

2.1.3.3 Upper boundary condition

The soil surface loses water to the atmosphere by evaporation and gains water by infiltration.

Infiltration

A precipitation or irrigation in mm is converted to a flux in kg m^{-1} s^{-1} by dividing by the time step and multiplying by the horizontal distance, x, over which the water fell. The infiltration does not have to be uniform over the surface.

Non-uniform infiltration is especially important in very coarse soils where lateral redistribution is likely to be limited, or in the case of micro-irrigation.

Evaporation

As with the infiltration flux, it is necessary to multiply the evaporation by the horizontal distance over which it occurs (*Surface*) in order to get an evaporative flux in kg m^{-1} s^{-1}:

$$E = PE \frac{(h_s - h_c)}{(1 - h_c)} Surface \qquad (2.1.58)$$

where h_s is the soil surface humidity and h_c is the canopy humidity. The two-dimensional radiation interception model enables the distribution of energy at the surface.

The derivative of this flux with respect to water potential $\partial E/\partial \Psi$ is needed for the Newton Raphson solution and is calculated as

$$\frac{\partial E}{\partial \Psi} = PE \frac{Mh_s/(RT)}{(1 - h_c)} Surface \qquad (2.1.59)$$

2.1.3.4 Lower boundary condition

Two lower boundary conditions can be chosen in the model:

i) A gravity drainage lower profile condition is created by setting the lower matrix flux potentials of the bottom elements equal to the upper matrix flux potentials. The only driving force for downward movement of water is then gravity. This condition is typical for well-drained soil.

ii) A zero-flux lower boundary can be established by setting the upper conductivities (Kur and Kul) of the bottom element to zero. This would simulate an impermeable layer.

These two boundary conditions can be used to test the model. Infiltration and evaporation can be excluded and redistribution of water in a wet profile simulated. The no-flow lower boundary condition should result in water collecting at the bottom of the profile and a unit gradient in matric potential Ψ_m developing (i.e. 0.1 J kg^{-1} decrease in potential per cm increase in height above the bottom). The gravity drainage lower boundary condition should result in a fairly uniform matric potential with depth, with Ψ_m decreasing over time. The horizontal fluxes can be tested by wetting one side of the profile and monitoring redistribution with gravity set to zero. A uniform wetting front should be seen to be moving across the profile with no vertical movement of water.

2.1.3.5 Model stability

In the calculation of soil water redistribution, the aim is to solve the Richards' equation (Eq. 2.1.21) with the Newton-Raphson iterative procedure for each control volume, and assign new values of equilibrated soil water potentials to each node in the grid. The acceptable solution to Richards' equation is the one which causes the mass balance error of the soil water balance to be negligible (Eq. 2.1.43). In SWB-2D, equilibrium in soil water potentials is assumed to occur when MBE # 0.0000003. However, conditions may occur when equilibrium in soil water potentials cannot be achieved. The simulation is then interrupted and a warning message appears, which indicates that the maximum number of iterations has been reached. The maximum number of iterations is 20000. The simulation can be resumed by the operator, but this may cause considerable mass balance errors.

Two specific causes of non-convergence can be singled out:

i) The horizontal (∂x) or vertical (∂z) distances between nodes are too big. This may cause large differences in soil water potential at adjacent nodes and equilibrium conditions may not be reached, in particular if nodes have different soil water retention and hydraulic characteristics. The model calculates unsaturated hydraulic conductivity as a function of soil matric potential (Eq. 2.1.22), and uses the arithmetic average hydraulic conductivity between two adjacent nodes to calculate the soil water flux between the two nodes (Eq. 2.1.25). Due to the non-linearity of Eq. 2.1.22, the use of average conductivity could cause large errors if the distances between nodes and the differences in nodal water potentials are large, in which case a weighted average unsaturated hydraulic conductivity would be more suitable. This problem can be overcome if the operator selects smaller distances between nodes.

ii) The time step (∂t) is too big. Large upper boundary fluxes (infiltration or evaporation) could cause large differences in soil water potential at adjacent nodes and equilibrium conditions may not be reached. This problem cannot be overcome by the operator. The model could be improved by including an hourly time step, where smaller upper boundary fluxes over shorter time periods could be used as input.

It would be interesting to carry out a sensitivity analysis to determine the effect of ∂x, ∂z and ∂t on soil water redistribution. It would also be interesting to assess the effect of assuming the arithmetic mean hydraulic conductivity between two adjacent nodes. The model could be made more user-friendly by including a warning system to indicate to the operator the cause of non-convergence (node distance ∂x and ∂z, or time step ∂t).

2.1.4. Link between the two-dimensional radiation and soil water balance model

SWB-2D simulates canopy radiation interception across the row, as well as the two-dimensional soil water balance in widely spaced, micro-irrigated row crops on a daily time step.

Potential transpiration from the trees is calculated as follows. Potential evapotranspiration (PET) is partitioned between potential evaporation (from the soil) and potential transpiration (from the canopy). PET is calculated from weather data using the Penman-Monteith equation (Allen et al., 1998) and the maximum crop factor after rainfall occurs (Jovanovic and Annandale, 1999), as described in Section 2.2.1. Local potential evaporation calculated at each radiation node (PE_j, calculation described in Section 2.1.2) are weighted by the surface the node represents and accumulated over the whole soil surface to calculate overall potential evaporation (PE). Potential transpiration is taken as the difference between PET and PE. Crop water uptake (transpiration) can either be limited by atmospheric demand or soil-root water supply (Annandale et al., 2000). Root densities at different soil depths are accounted for in the calculation of root water uptake using the approach of Campbell and Diaz (1988). Root depth and the root fraction in the wetted and non-wetted volume of soil can also be entered by the user.

Required inputs

Required inputs for the two-dimensional soil water balance model are: starting and planting dates, altitude, rainfall and irrigation water amounts, as well as maximum and minimum daily temperature. For seasonal simulations, the "planting date" is generally taken at bud burst for deciduous trees and at some arbitrarily chosen date after harvest and before flowering for evergreen trees, which should correspond to the beginning of the initial stage of the FAO growth curve (Doorenbos and Pruitt, 1977). For convenience, the starting date of the simulation is selected to coincide with the planting date, unless soil water measurements prior to "planting date" are made and used as initial water contents.

Two points on the water retention function, namely field capacity and permanent wilting point, initial volumetric soil water content and bulk density are required for each soil layer. The field capacity corresponds to the drained upper limit, whilst permanent wilting point is the lower limit of crop water uptake. The principles and methods for the determination of the upper and lower limits of crop water uptake were discussed by Hillel (1998). Soil saturated hydraulic conductivities can also be entered as input for each soil layer. If these are not available, the model calculates them using the water retention curve according to the procedure described by Campbell (1985) (Eq. 2.1.20). Row distance, wetted diameter of micro-jets or drippers, fraction of roots in the wetted volume of soil as well as distance of the nodes from the tree row are also required as input.

A flow diagram of the two-dimensional soil water balance model for hedgerow tree crops is shown in Figure 2.9. The source code of the finite difference soil water balance model written in Delphi is given in Appendix B.

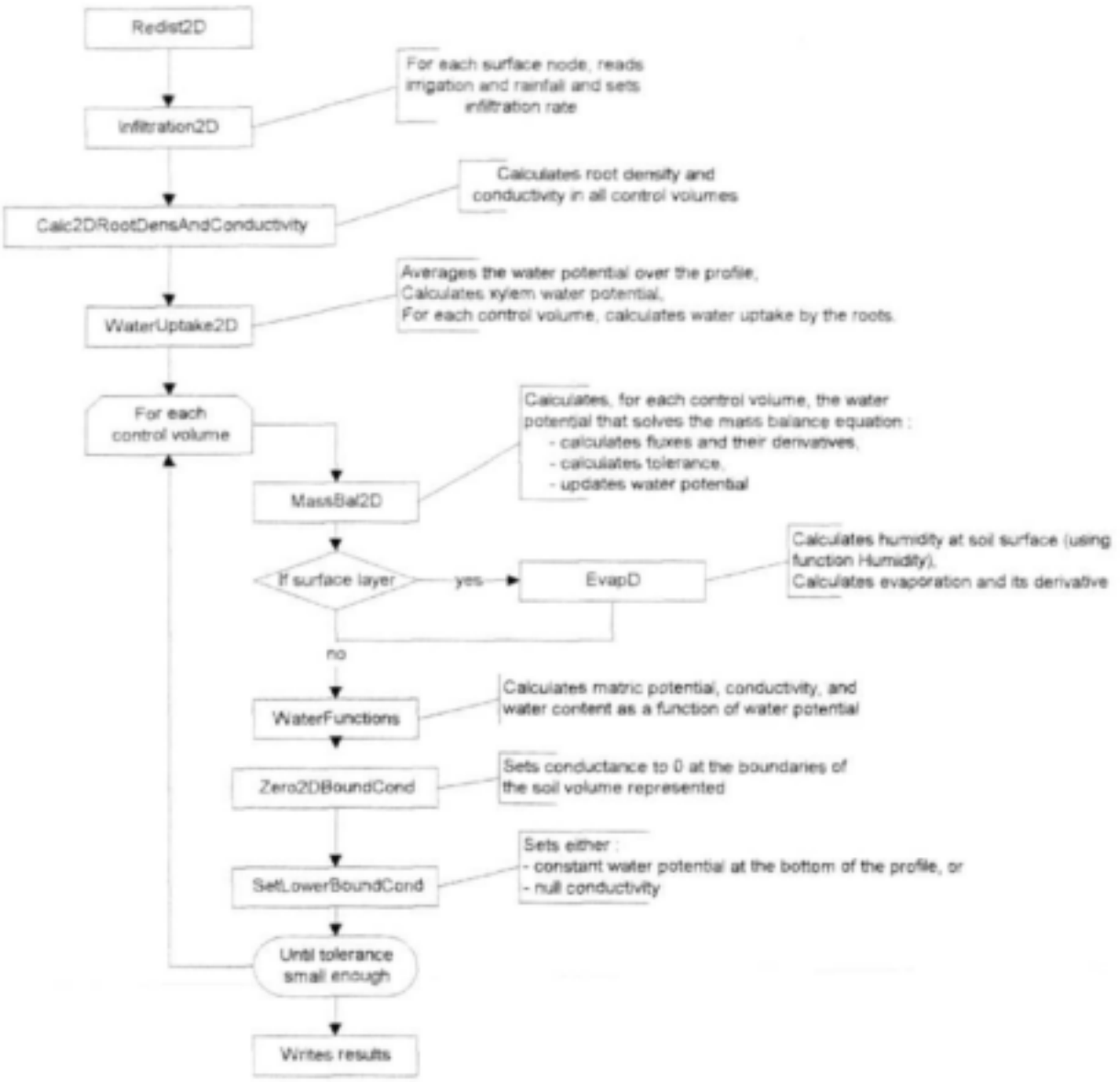

Figure 2.9. Flow diagram of the two-dimensional soil water balance model for hedgerow tree crops.

2.2. *FAO-based crop factor model*

The Food and Agriculture Organization (FAO) of the United Nations recommended a semi-empirical approach for calculating crop water requirements, based on the fact that crop yield depends on climatic conditions, genetic potential of the crop and irrigation water management (Doorenbos and Pruitt, 1977). The FAO approach was used to develop the crop water requirement models CROPWAT (Smith, 1992a) and, in South Africa, SAPWAT (Crosby, 1996). Doorenbos and Pruitt (1977) gave a comprehensive database of FAO crop coefficients (Kc) for different climatic conditions and phenological stages (initial, mid-season and late-season stages). They also stressed the need to collect local data on growing season and rate of crop development of irrigated crops. Green (1985a and b) reviewed Kc values empirically related to pan evaporation and growth periods for crops grown in South Africa.

The Kc's published by the FAO represent mean values for a given irrigation cycle and strongly depend on wetting frequency, wetted area and soil type. Allen et al. (1996) defined Kc as the sum of the basal crop coefficient (Kcb) and the time-averaged effects of evaporation from the soil surface layer. They also reported Kcb values and maximum crop height (Hc_{max}) for a wide range of species.

Due to the very limited number of specific crop growth parameters for trees available in literature for the purpose of mechanistic modelling, the authors decided to make use of the already published FAO database of Kcb's and growth periods.

An FAO-based crop factor procedure has therefore been developed and combined with the mechanistic SWB model, thereby still allowing evaporation and transpiration to be modelled separately as supply and demand limited processes. The crop factor model does not grow the canopy mechanistically and therefore the effect of water stress on canopy size is not simulated. The simpler crop factor model should, however, still perform satisfactorily if the estimated canopy cover closely resembles that found in the field.

In the following Sections of this report, the FAO-based crop factor model that was built in SWB is described. In particular, the following improvements to SWB are presented:

i) FAO-type crop factor modification;
ii) Soil water balance with localised (micro- or drip) irrigation; and
iii) Yield predictions with the FAO model.

2.2.1. FAO-type crop factor modification

SWB calculates the grass reference evapotranspiration (ETo) using the revised FAO Penman-Monteith methodology (Smith et al., 1996). Potential evapotranspiration is calculated as follows:

$$PET = ETo\ Kc_{max} \qquad (2.2.1)$$

Kc_{max} represents the maximum value for Kc following rain or irrigation. It is selected as the maximum of the following two expressions (Allen et al., 1996):

$$Kc_{max} = 1.2 + [0.04\ (U2 - 2) - 0.004\ (RHmin - 45)]\ (Hc/3)0.3 \qquad (2.2.2)$$

$$Kc_{max} = Kcb + 0.05 \qquad (2.2.3)$$

where

U_2 - Mean daily wind speed at 2 m height (m s^{-1})
RH_{min} - Daily minimum relative humidity (%)
Hc - Crop height (m)

The upper limit of Kc_{max} is set at 1.45.

SWB partitions PET into potential crop transpiration (PT) and potential evaporation (PE), and estimates FI_{transp} using the following equations:

$$PT = Kcb\ ETo \qquad (2.2.4)$$

(Allen et al., 1996)

$$FI_{transp} = PT/PET \qquad (2.2.5)$$

$$PE = (1 - FI_{transp})\ PET \qquad (2.2.6)$$

SWB assumes Kcb, Hc and root depth (RD) are equal to the initial values during the initial stage. During the crop development stage, they increase linearly from the end of the initial stage until the beginning of the mid-stage, when they attain maximum values. They remain constant at this maximum during the mid-stage. During the late stage, Kcb decreases

linearly until harvest when it reaches the value for the late stage, whilst RD and Hc remain constant at their maximum value. The following crop parameters need therefore to be known: Kcb for the initial, mid- and late stages, crop growth periods in days for initial, development, mid- and late stages, initial and maximum RD, as well as initial Hc and Hc_{max}.

The following input parameters are required to run the FAO-type crop factor model: planting date, latitude, altitude, as well as maximum and minimum daily air temperatures. In the absence of measured data, SWB estimates solar radiation, vapour pressure and wind speed according to the FAO recommendations (Smith, 1992b; Smith et al., 1996). It is, however, recommended that these be measured.

A stand-alone computer program, the ETo calculator, was developed for the calculation of long series of ETo and for the estimation of errors that can occur if solar radiation, wind and vapour pressure data are not available and have to be estimated. The ETo calculator is described in detail in Appendix C of this report.

Caution should be exercised against blind acceptance of the FAO parameters taken from literature, as local conditions, management and cultivars are likely to influence crop growth periods and Kcb's. A simple methodology used to generate a database of Kcb values from limited available data, has therefore been developed. Daily Kcb can be calculated from FI_{transp}, Hc and weather data using the following equation:

$$Kcb = FI_{transp}\, PET/ETo \qquad (2.2.7)$$

ETo is calculated from weather data. Weather data and crop height are used to calculate crop PET, whilst FI_{transp} can be easily measured in the field. The procedure can be easily and cheaply applied to determine FAO-type crop factors for any species. Validation of the model with independent data sets is always recommended.

A flow diagram of the FAO-type crop factor model included in SWB is shown in Figure 2.10.

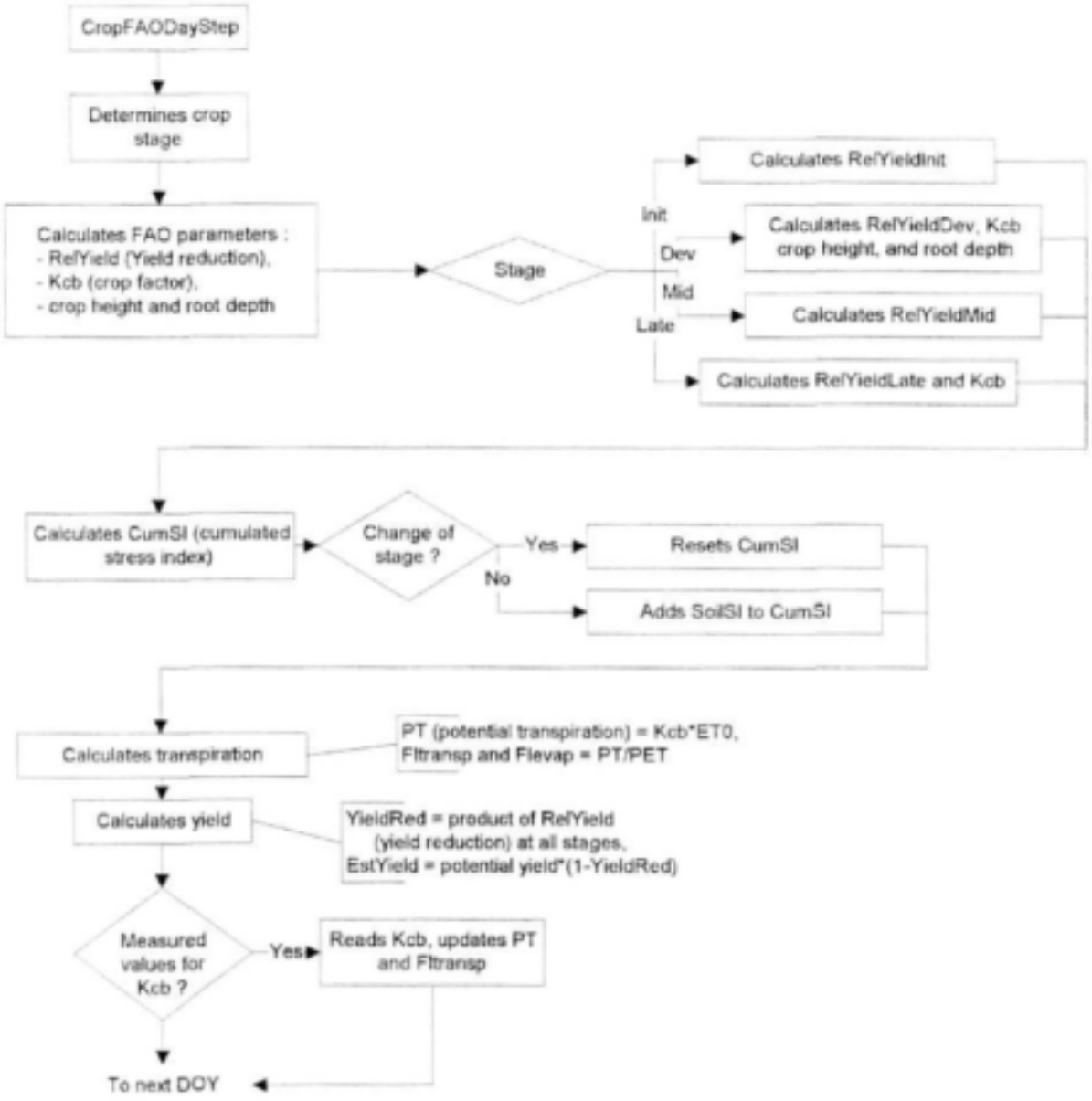

Figure 2.10. Flow diagram of the FAO-type crop factor model.

2.2.2. *Soil water balance with localised irrigation*

An option for the calculation of the soil water balance under localised irrigation was included in SWB (drip or micro-irrigation). When this option is selected, the model uses a simplified procedure for the calculation of non-uniform wetting of the soil surface, evaporation and transpiration.

In this quasi two-dimensional procedure, a cascading water balance is calculated for both the wetted and non-wetted portion of the profile. Daily soil water contents per soil layer are calculated for both the wetted and non-wetted volumes of soil. The output of soil water deficit is based on the soil water contents in the wetted volume of soil only, as this is the part of the profile managed by the irrigator.

Water redistribution

Interception of water by the crop canopy is calculated only when rainfall occurs, as the canopy is not wet by micro-jets or drippers. Micro- or drip irrigation, commonly used in orchards, only wets a limited area under the canopy of the trees.

Runoff, infiltration and drainage are then calculated like in the one-dimensional cascading model (Annandale et al., 1999), but for both the irrigated and non-irrigated portions of the soil. Runoff and drainage for the irrigated and non-irrigated portions of the soil are weighted by the fraction of the surface irrigated (FI_{irrig}). Total runoff and drainage are calculated as the sum of the components from the irrigated and non-irrigated portions.

Evaporation

Evaporation from the soil surface is also not uniform under micro- or drip irrigation. Two possible cases are simulated when drip/micro irrigations are performed:

i) If the canopy cover fraction is larger than the irrigated surface fraction ($FI_{transp} \exists FI_{irrig}$), evaporation is simulated only from the non-irrigated portion of the ground.

ii) If ($FI_{transp} < FI_{irrig}$), evaporation from the non-irrigated surface fraction ($1-FI_{irrig}$) and from the non-shaded area ($FI_{irrig} - FI_{transp}$) are calculated separately and added to calculate total evaporation.

The procedure used to calculate water loss by evaporation in the cascading model was described in Annandale et al. (1999).

Transpiration

No root water uptake is calculated for the uppermost soil layer. SWB assumes layer water uptake is weighted by root density when soil water potential is uniform (Campbell and Diaz, 1988). Water loss by crop transpiration is calculated as a function of maximum transpiration rate (T_{max}) and leaf water potential at T_{max} (Ψ_{lm}) (Campbell, 1985; Annandale et al., 2000). It represents the lesser of root water uptake or maximum loss rate. T_{max} and Ψ_{lm} are input parameters that can be easily estimated from crop expert's experience. Ψ_{lm} is the minimum leaf water potential occurring generally in the early afternoon under no water constraints, when the transpiration rate is at its peak. In this way, a mechanistic supply and demand limited water uptake calculation was linked to an FAO crop factor approach with a minimal addition of crop input parameters required.

The user can input the fraction of roots in the wetted volume of soil. Daily transpiration is then calculated as the sum of water losses from the wetted and non-wetted volumes of soil, weighted for root fraction and matric potential.

The input data required to run the two-dimensional cascading model are rainfall and irrigation amounts, volumetric soil water content at field capacity and permanent wilting point, as well as initial volumetric soil water content for each soil layer. Row spacing, wetted diameter, distance between micro-jets or drippers, and the fraction of roots in the wetted volume of soil are also required.

A flow diagram of the cascading soil water balance for tree crops under localised irrigation is shown in Figure 2.11.

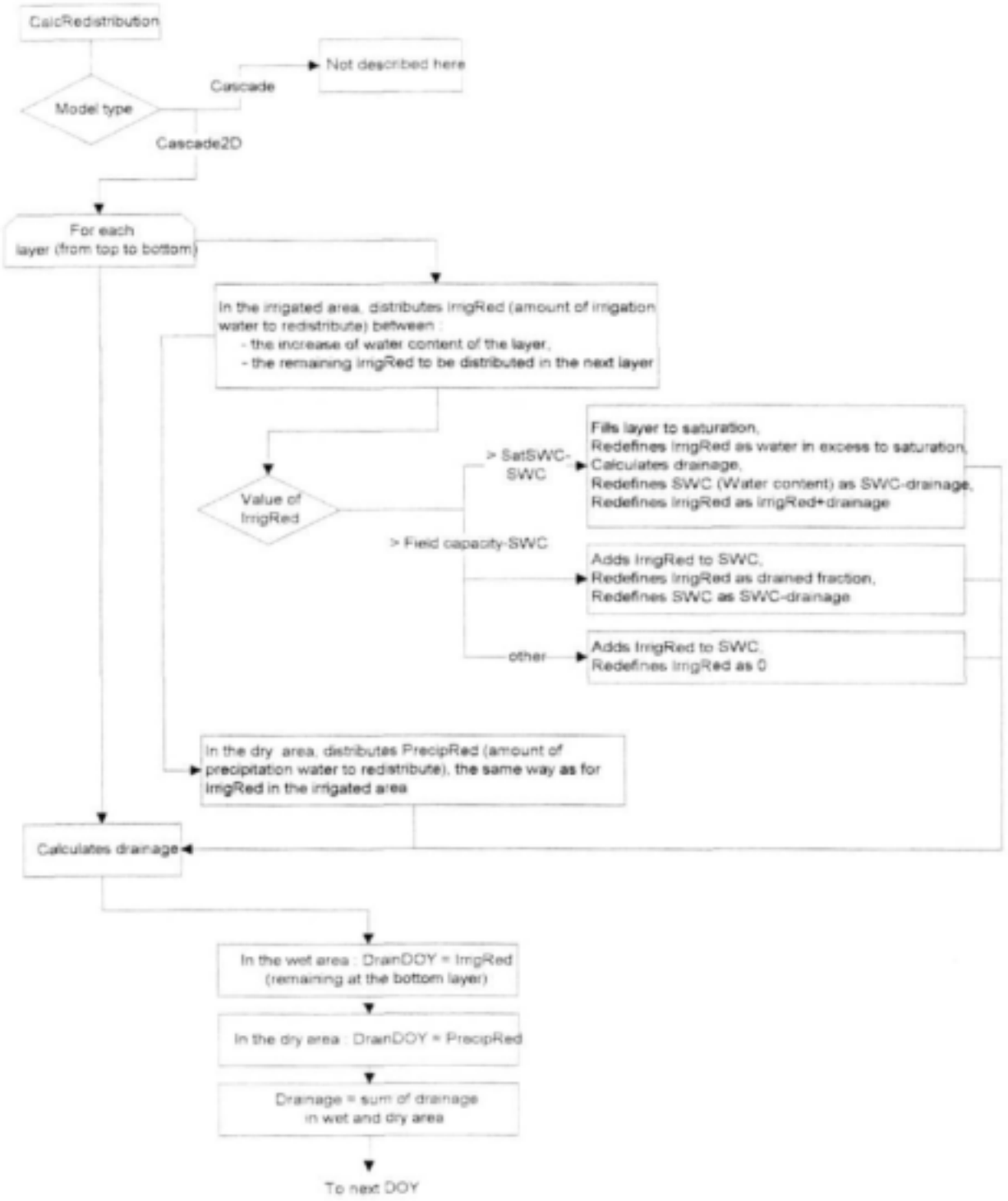

Figure 2.11. Flow diagram of the cascading soil water balance for tree crops under localised irrigation.

2.2.3. Yield predictions with the FAO model

A subroutine for the estimation of yield with the FAO model under conditions of water stress, was included in SWB. The procedure recommended by the FAO was used to compile this procedure (Smith, 1992a). The estimated yield (Y, in Mg ha^{-1}) is calculated as follows:

$$Y = Y_{pot} (1 - Y_{red}) \quad (2.2.8)$$

where

Y_{pot} - Potential yield (Mg ha^{-1})
Y_{red} - Fractional yield reduction (%)

Y_{pot} is a specific crop input parameter. Y_{red} is calculated as follows:

$$Y_{red} = (1 - Y_{rel(Init)}\ Y_{rel(Dev)}\ Y_{rel(Mid)}\ Y_{rel(Late)}) \quad (2.2.9)$$

where

$Y_{rel(Init)}$ - Fractional yield for initial stage
$Y_{rel(Dev)}$ - Fractional yield for development stage
$Y_{rel(Mid)}$ - Fractional yield for mid-season stage
$Y_{rel(Late)}$ - Fractional yield for late-season stage

Relative yield for each stage (Y_{rel}) is calculated as a function of the stress factor (Ky) for that particular stage and a stress index (SI):

$$Y_{rel} = 1 - \frac{Ky}{N} \sum_{d=1}^{d=N} (1 - SI_d) \quad (2.2.10)$$

Ky for each stage and the duration of the stage in days (N) are crop specific input parameters. d indicates the day of the stage.

SWB calculates SI on a daily basis as follows:

$$SI_d = T / (FI_{evap}\ PET) \quad (2.2.11)$$

where

T - Actual crop transpiration (mm)

SI therefore represents the relative transpiration of the crop (ratio of actual and potential crop transpiration). The CROPWAT model of the FAO (Smith, 1992a) uses the ratio of actual and potential evapotranspiration instead of SI, as it does not calculate soil water supply limited root uptake.

SWB calculates and outputs estimated yield (Y) and Y_{red} on a daily basis, assuming that no water stress (SI = 1) will occur from that particular day until the end of the growing season.

Required input data for yield prediction with the FAO model are: FAO stress factors for growth stages (initial, development, mid-season and late-season stage) and potential yield.

CHAPTER 3

MATERIALS AND METHODS

In order to validate the SWB model, field measurements had to be collected and compared to model simulations. For this purpose, two field trials were set up. The first trial was established in a peach orchard (deciduous trees) on the lysimeter facilities of Pretoria University's experimental farm. The second trial was established in a citrus orchard (evergreen trees) at the Syferkuil experimental farm of the University of the North. Field data were also collected in Brits from commercial citrus farms and from rows of Leucaena fodder trees on the Hatfield experimental farm.

The sites at the Hatfield and Syferkuil experimental farms were selected because suitable facilities were available. These sites were used to collect data for the validation of the model for deciduous and evergreen fruit trees as examples. The data collected in the field trials in Brits and on Leucaena rows in Hatfield were used to support the validation of the energy interception subroutine of the model. Although these data are not representative for other orchards, the model should still give a reasonable prediction of energy and soil water balance for a wide range of orchards and conditions, provided that correct input parameters are used. In this Chapter, materials and methods used for data collection in the field trials are described.

3.1. Experimental set-up at the University of Pretoria

3.1.1. Location and environmental characteristics

The field trial at the Hatfield experimental farm (University of Pretoria) was located 120 m West of RSA weather station No. 513465 (25°45'S, 28°16'E, alt. 1372 m). This is a summer rainfall region with an average of *ca* 670 mm a^{-1} (October - March). The rainfall occurs as high intensity short duration events with sunny periods between rains. The monthly average maximum temperature is 30 °C (January), with a monthly minimum average of 1.5 °C (July). Frost occurs during the winter. Even though the frost severity is less than experienced in typical highveld climates, it is sufficient for the low chilling requirement deciduous fruit cultivars commercially propagated in Gauteng and the Northern Province.

The soil in the trial site is a sandy loam (28% clay, 10% silt and 62% sand) Hutton (Soil classification working group, 1991) or Ferralsol (FAO, 1998). Soil depth is generally in excess of 1.2 m (a small portion having scattered hard plinthic formations at 1.1 m). Soil analysis revealed adequate P (120 mg kg^{-1}), pH(H_2O) being 6.4 and sufficient Ca, Mg and K (580, 140 and 160 mg kg^{-1} respectively).

3.1.2. Orchard lay-out, irrigation and cultivation practices

Since it was expedient to develop a reasonable tree canopy as soon as possible, an early maturing vigorous deciduous tree was used in this trial. Young grafted peach trees (*Prunus persica* cv Transvaalia) were planted on 6 September 1996 (DOY 250) in a high density 4.5 x 1 m hedgerow pattern. The tree row orientation was in an E-SE to W-NW axis (110° - 290°). At planting the trees were cut back to 250 mm above the soil surface. As the trees developed during the growing period, steps were taken to promote the central leader growth pattern and develop lower horizontal branches. During winter of 1997 (2 to 15 July) the trees were cut back to a height of 2 m and pruned to a central leader system. By 7 August 1997 (DOY 219) trees were at 80% blossom and reached full bloom on 12 August 1997 (224). From this date the canopy developed throughout the summer. The fruitlets were counted on 15 September 1997 (DOY 258) to establish the extent of fruit removal, which was done on 25 September 1997 (DOY 268). The first fruit was harvested on 17 and 18 November 1997 (DOY 321 and 322).

During the establishment period (first 3 weeks) the trees were basin irrigated manually with a hosepipe daily (first week), and subsequently reducing the irrigation frequency to once per week by the third week. On 2 October 1996 (DOY 276) a low pressure irrigation system (DT-Rotator micro sprayer; Vetsak) capable of delivering 40 l h^{-1} $tree^{-1}$ in a 1.2 m wide band in the tree row was installed. Initially this system worked very well but as the trees developed and created an environment favourable for insects, spiders set up homestead in the rotators and rendered them useless. The rotators were replaced during January 1997 by micro-jets (DT-Spreader 360°/12 stream) having the same delivery rate but covering a slightly larger area (1.3 m band) under the trees. This reduced the insect blocking problem but did not eliminate it. From 8 October 1997 (DOY 281) the irrigation pressure was increased to 3 bar, which increased the wetting area to a 2 m band under the tree canopy. Irrigation amounts were measured with flowmeters.

At planting, 57 g super phosphate (10.5% P) per tree was incorporated in the planting hole. Nitrogen was supplied monthly at a rate of 20, 30, 40 and 50 g LAN (28% N) $tree^{-1}$ during October, November, December 1996 and January 1997 with irrigation. Trees were monitored for visual signs of trace element deficiencies (Zn and Mn). Foliar sprays containing ZnO, $MnSO_4$ and spray urea were applied when necessary.

3.1.3. Lysimeter characteristics

The pair of lysimeters was installed in the 70's as mechanical weighing lysimeters. The surface dimensions are 2 x 2 m. The depth is 0.9 m. Each lysimeter has two trees.

At some stage, load cells coupled to a Campbell Scientific CR10 data logger, were attached within the lever mechanism to automate recording weight changes. Before planting, tests with trial masses (sand bags of known mass) revealed that there was tremendous variability in the readings and it was necessary to use long measuring periods (one to two hours) to determine average weights for a specific period. By moving the load cell attachment locations to the recording arm of the weighing mechanism, and removing the counter balance weights, it was possible to damp the oscillations (*"see-saw effect"*) and thus reduce variability in the readings.

Each load cell was supplied with an independent constant voltage source. This voltage was supplied through a transformer which converts 220 V AC to 16 V DC, which was used to charge a 12 V, 6.5 AH lead acid motorcycle battery as an emergency supply should there be a power failure. From the 12 V DC battery the power passed through an electronic voltage stabilising circuit designed and fabricated by personnel of the UP Engineering Faculty electronics workshop. As a precaution, the voltage supplied to each load cell was monitored hourly by a data logger.

Once the best location for the load cell attachment had been identified, and the trees planted, the lysimeters were calibrated with sandbags of known mass. The best input voltage to the load cell of the eastern lysimeter was 9.34 ± 0.03 V while a voltage of 9.21 ± 0.03 V gave the best readings for the western lysimeter. Voltage output from each load cell was recorded as an equivalent depth of water on the basis that one litre (i.e. 1 kg) per m^2 is equivalent to 1 mm. One set of calibration curves for both lysimeters are presented in Figure 3.1. This calibration was done on 27 August 1996. It is seen that the lysimeters gave a linear response to changes in weight and that the standard error of the recorded mm value was 0.14 mm for the eastern lysimeter (LyEast) and 0.138 mm for the western lysimeter (LyWest).

Free drainage of excess water from the lysimeters was ensured. Drainage was measured with tipping bucket gauges connected to a Campbell Scientific CR10 data logger, by collecting excess water from the bottom of the lysimeters with a pipe.

3.1.4. Calculation of evapotranspiration and crop coefficient from lysimeter data

The data logger was programmed to read at 10 s intervals and average these values every 15 min. At a specific time of the day e.g. 0h15 (day i +1) the 15 min average was taken as the lysimeters water status ($Ly_{(i)}$) for the previous day, i.e. day i. This was done for both lysimeters (LyEast and LyWest). The water loss for each lysimeter for day i (in mm) was then taken as:

$$\Delta LyEast_{(i)} = LyEast_{(i)} - LyEast_{(i+1)} \qquad (3.1.1)$$

$$\Delta LyWest_{(i)} = LyWest_{(i)} - LyWest_{(i+1)} \qquad (3.1.2)$$

In the event of there being large unexplainable differences between $LyEast_{(i)}$ and $LyWest_{(i)}$ the values for that day were discarded.

The average of these values was used to reflect daily water loss:

$$\Delta Ly_{(i)} = (\Delta LyEast_{(i)} + \Delta LyWest_{(i)}) / 2 \qquad (3.1.3)$$

Gross evapotranspiration of the lysimeter for the day was determined by including rain, irrigation and drainage values as follows:

$$ET_{Lys} = \Delta Ly_{(i)} + Rain + Irrig - Drainage \qquad (3.1.4)$$

On the infrequent occasion of ET_{Lys} being negative or inexplicably large for a particular day, the value was disregarded.

It must be remembered that the lysimeters only covered 2 m of the 4.5 m row spacing and thus did not account for 2.5 m of the inter-row, which is normally dry and thus has low evaporative losses. Thus to make a valid comparison with the grass reference evapotranspiration, ETo, which reflects the total area (4.5 m wide rows), the following correction, which assumed no contribution to evaporation from the area outside the lysimeters, was applied:

$$ET = ET_{Lys} * 2/4.5 = ET_{Lys} * 0.444 \qquad (3.1.5)$$

The daily crop coefficient, Kc, was then determined by:

$$Kc = ET/ETo \qquad (3.1.6)$$

To determine transpiration rates, the lysimeters were irrigated to "an equivalent field capacity" overnight and then the surface of the lysimeters was covered with a heavy duty plastic early the next morning. During these measurements, the drainage taps were closed to eliminate any drainage loss being considered. After these measurement periods, the lysimeters were uncovered and allowed to dry out so that the profile could be aerated. This was done to counteract the negative effects of any anaerobic conditions, which could develop while the lysimeters were at a high water content and with the surface sealed.

3.1.5. Weather monitoring

An automatic weather station was installed in the Hatfield weather station enclosure on 24 September 1996 (DOY 268) to give comprehensive weather data from DOY 269. The following weather data was monitored and recorded hourly by a CR10 data logger:

- Temperature and relative humidity (RH) with an HMP35C sensor;
- Wind speed with an R.M. Young cup anemometer;
- Solar radiation with an LI 200X pyranometer; and
- Rainfall with a Rimco R/TBR tipping bucket rain gauge.

The data-logger was programmed to automatically calculate hourly average saturation vapour pressure (SVP), vapour pressure (VP) and vapour pressure deficit (VPD).

The logged daily data was regularly downloaded using a laptop computer to calculate hourly and daily short grass reference evapotranspiration (ETo).

3.1.6. Soil measurements

During winter 1998, two cross-sectional trenches were dug across the rows between two trees to install soil water intensive monitoring sites. Time-domain reflectometry (TDR) probes and heat dissipation sensors (HDS) were installed, on both sides of the row, at depths of 0.06, 0.26, 0.56 and 0.86 m, at distances of 2, 1 and 0 m from the tree trunk, to form a vertical grid across the row as depicted in Figure 3.2. This was done for two tree rows, the one on bare soil, the other with grass sod. During this process, profile characterisation samples were collected, soil hydraulic properties were measured with tension and double ring infiltrometers, and penetrometer resistance measurements were taken at corresponding sites.

A complete description of soil measurements performed during the course of the trial follow.

3.1.6.1 Soil physical and hydraulic properties

Profile description

The soil profile is characterised as having a uniform red colour and apedal structure typical of a Hutton profile. The orthic A horizon can be taken as being 15 cm deep and having a gradual transition into the Red Apedal B horizon which reaches a depth of 1 m.

Texture

There is very little variation in soil texture across the tree row (Figure 3.3) with the silt, clay and sand percentages being 16, 30 and 54 % respectively. This classifies the soil as a clay loam. With depth (Figure 3.4), the clay content increases from 24 to 35 % with a corresponding decrease from 62 to 48 % in the sand fraction. The silt content shows only a slight increase from 14 to 18 % with depth.

Bulk density

Between the depths of 20 and 80 cm, the bulk density of the soil was 1.41 ± 0.11 (CV 8%) for the southern tree row and 1.37 ± 0.08 (CV 6 %) for the northern tree row. One could not identify any consistent trends in bulk density either across the rows or down the profile.

Penetrometer resistance

Penetrometer resistance was measured by Dr T Fyfield (Agricultural Research Council - Institute of Soil, Climate and Water, Pretoria) using a Bush Recording Soil Penetrometer. This instrument records cone resistance at 35 mm depth intervals to a maximum depth of penetration of 525 mm. With a 12.9 mm diameter 30° cone fitted, the maximum recordable force is 50 kg x g or 3.81 MPa. A mean value was determined from three measurements made at each position. As can be seen in Figure 3.5, there is negligible difference in resistance to penetration between the two rows (southern row having grass sod inter-row and the northern row being clean cultivated). The apparent higher resistance nearer to the soil surface is due to the soil being dryer than the subsoil. The influence of soil water content on penetration resistance is depicted in Figure 3.6.

Hydraulic properties

The hydraulic conductivity (K(h)) under a suction head (h) of 0.1 to 15 cm water was determined using tension infiltrometers at random sites across the tree rows and at different depths. Once these measurements had been made, double ring infiltrometers were placed on the same sites to determine the saturated hydraulic conductivity. Typical variations in K

as influenced by h are presented in Figures 3.7 and 3.8. Except for one surface measurement (North row site 9; 10 cm depth; Figure 3.7), all the measurements followed similar trends.

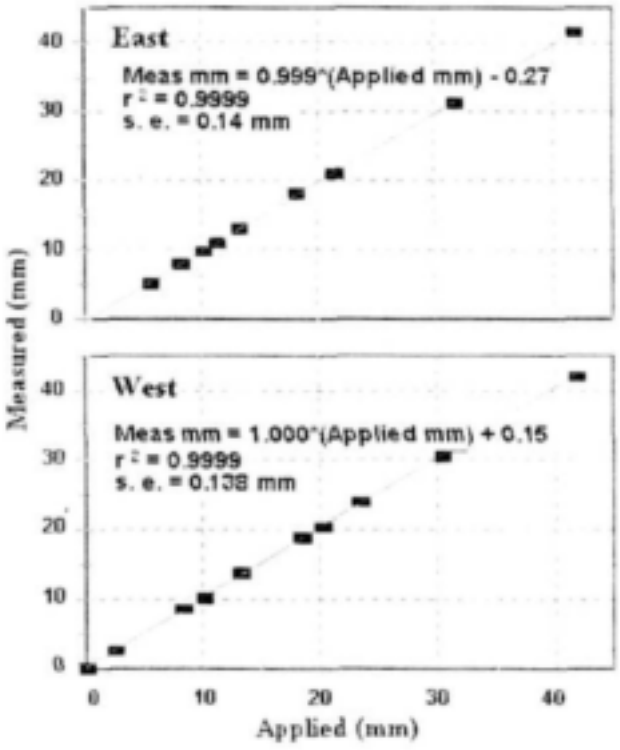

Figure 3.1. Calibration curves of the lysimeters (East and West).

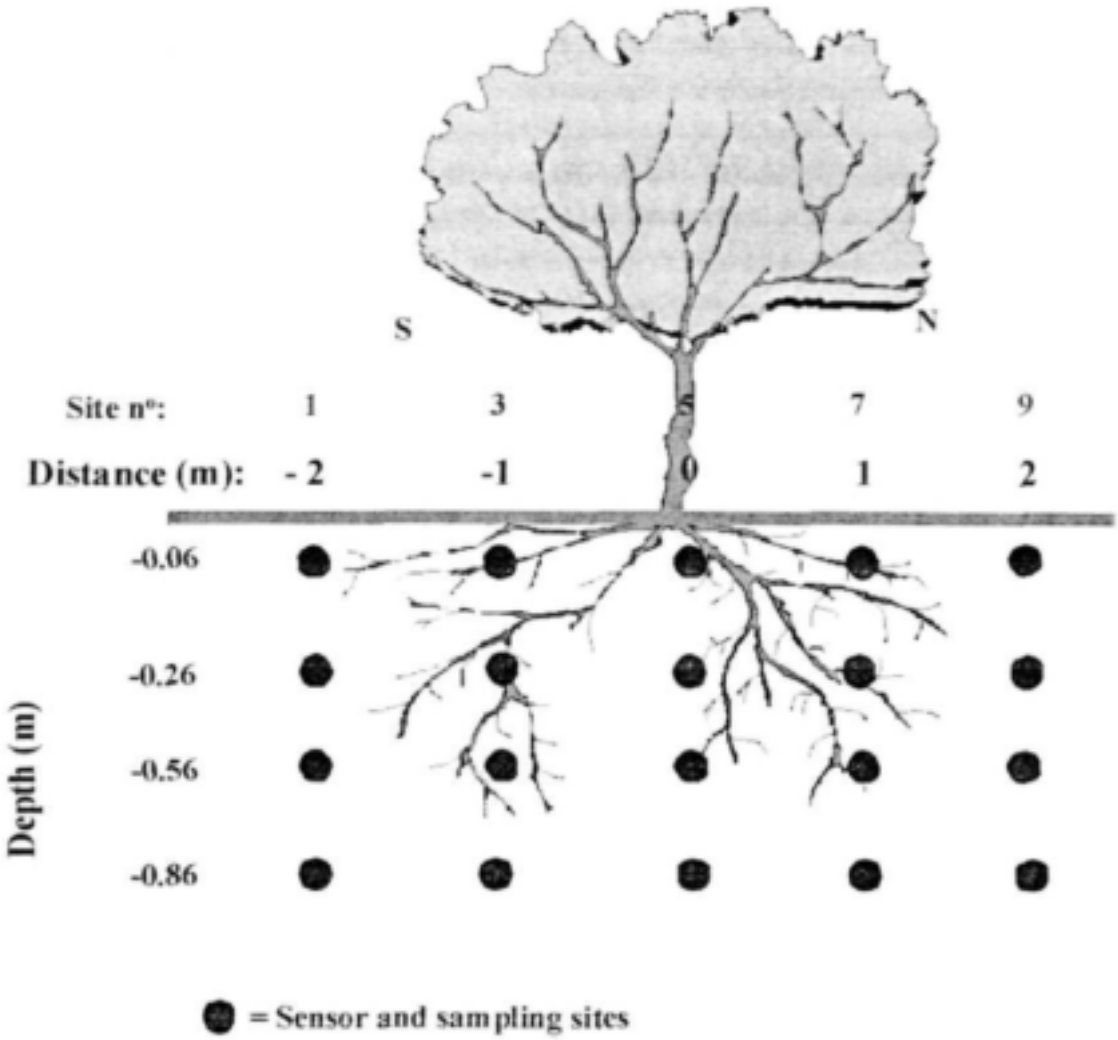

Figure 3.2. Diagrammatic grid indicating monitoring and soil sampling locations in the soil profile for the Hatfield and Syferkuil hedgerow system.

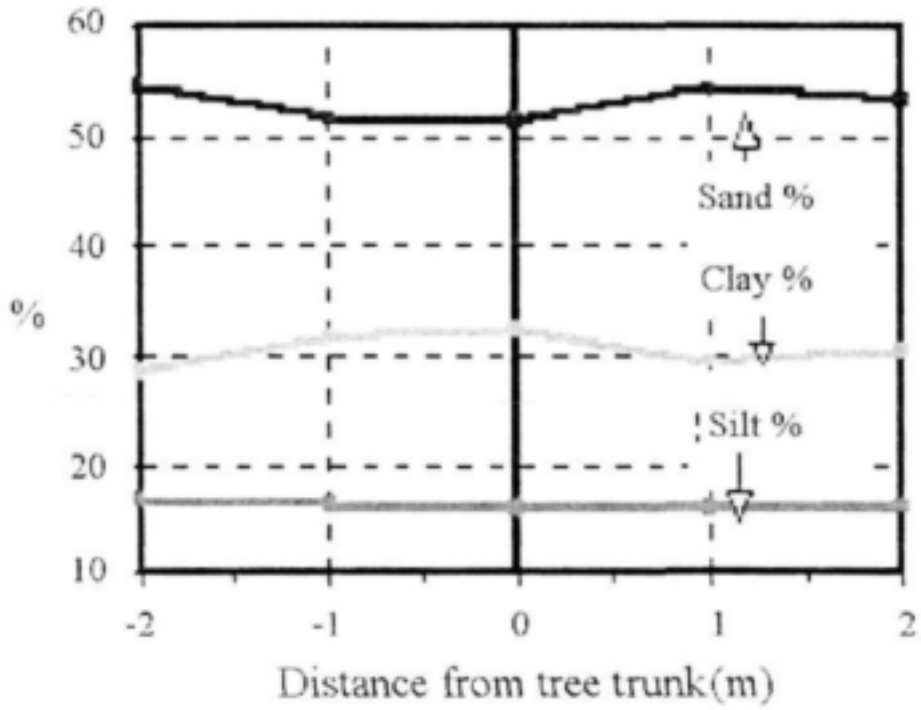

Figure 3.3. Variation of soil texture across tree row.

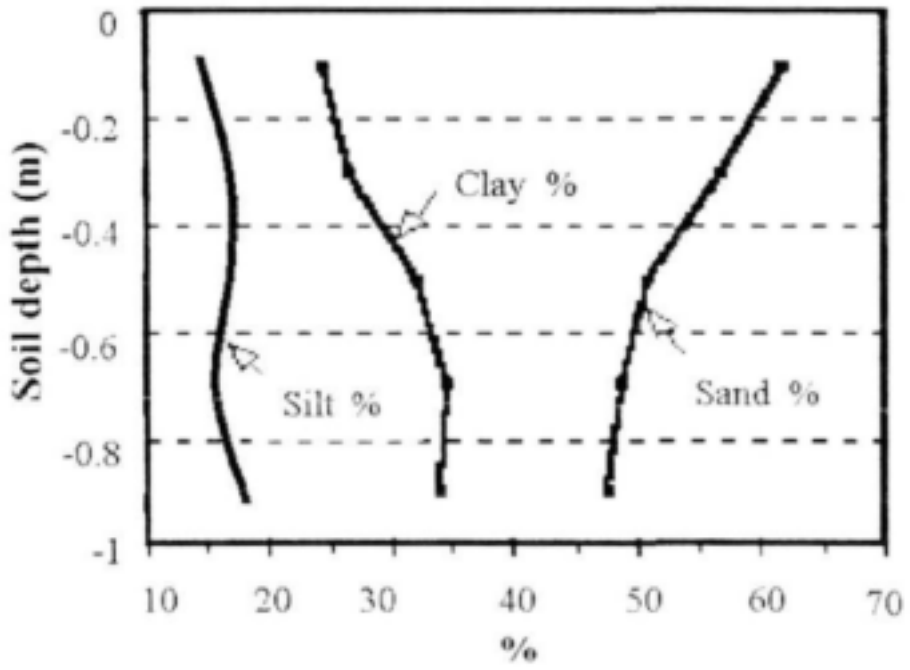

Figure 3.4. Variation of soil texture with depth.

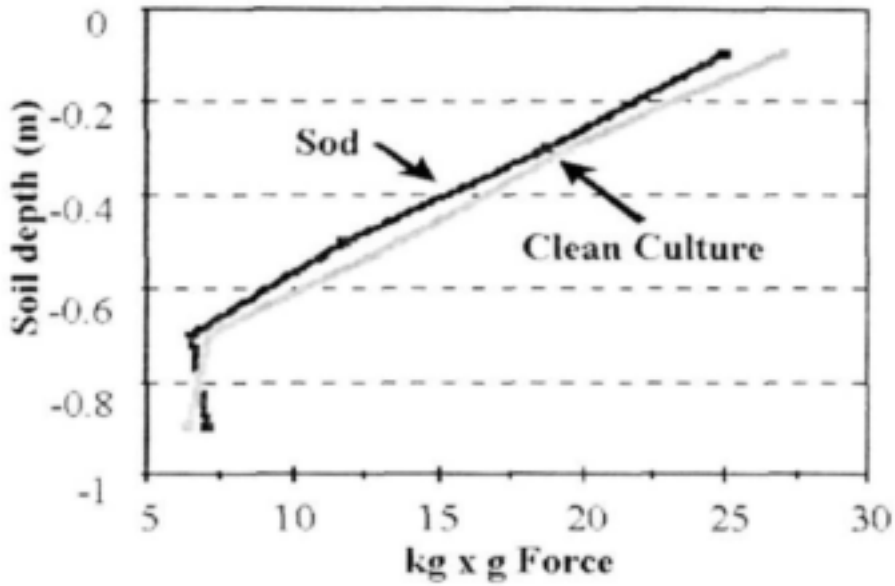

Figure 3.5. Variation of soil penetration resistance with depth.

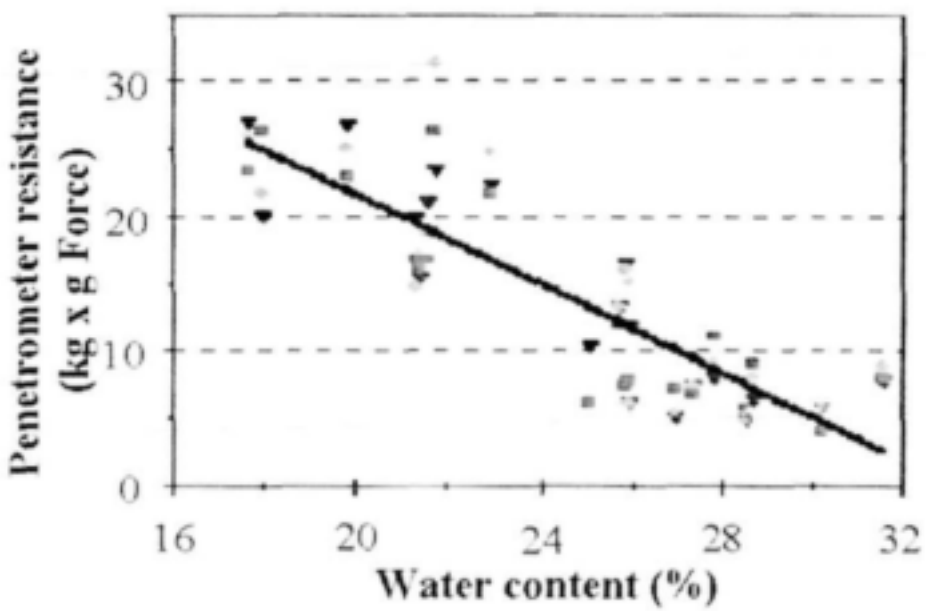

Figure 3.6. Effect of soil water content on soil penetration resistance.

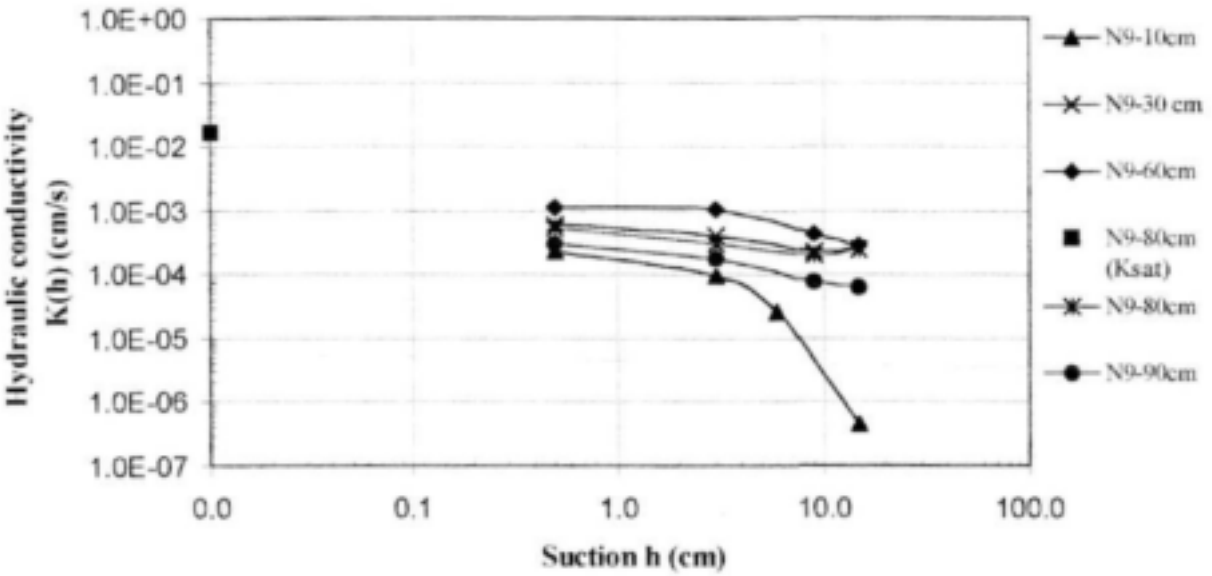

Figure 3.7. Variation of hydraulic conductivity (K) with suction (h) at site North 9 (N9).

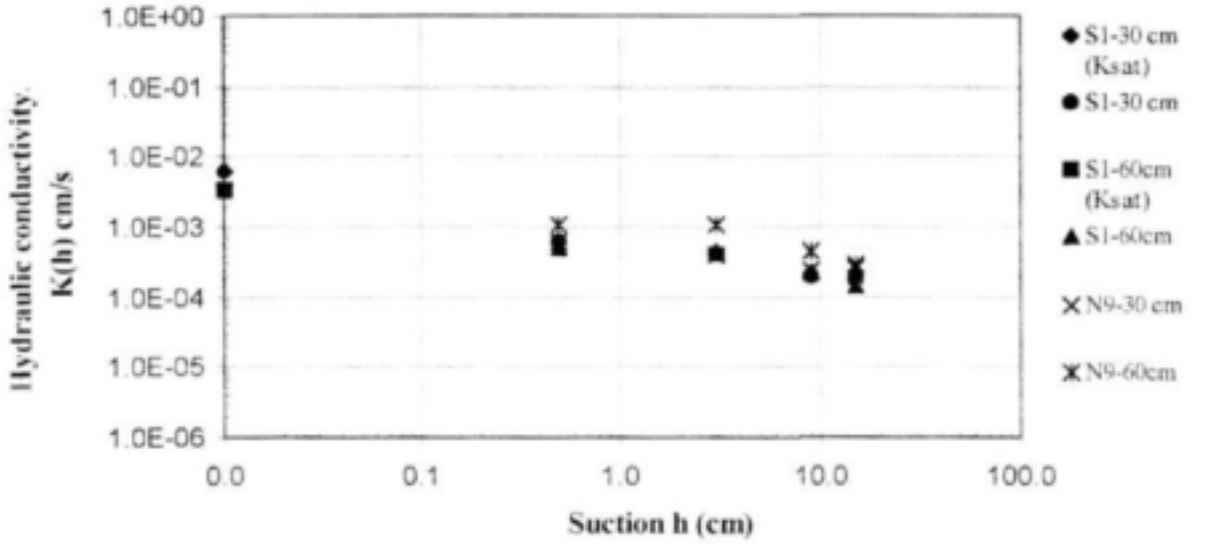

Figure 3.8. Variation of hydraulic conductivity (K) with suction (h) for site South 1 (S1) and North 9 (N9).

3.1.6.2 Soil matric potential

Tensiometers

On 24 October 1996 (DOY 298), tensiometers were installed at 30 and 60 cm depth for each tree in the lysimeters. A week later, after a good rain when the soil profile was soft, it was possible to install 2 sets of 30 and 60 cm tensiometers in the tree rows. A pair of tensiometers (30 and 60 cm depths) was installed at the centre of the tree row (between two trees) and the second pair of the set was placed 1 m from the row centre on the southern side of the row.

Heat dissipation sensors

Soil matric potential (ψ_m) was measured with CS 229 heat dissipation sensors (HDS). Heat dissipation sensors rely on the effect of the water content of a porous block in equilibrium with soil water, on thermal conductivity and heat capacity. Heat dissipation is determined by applying a heat pulse to a heater within the soil sensor and monitoring the temperature at the centre of the block before and during heating. The temperature rise is a function of the thermal diffusivity, and therefore of the water content of the block. Transient heat-pulse theory was discussed by Jackson and Taylor (1986), and Campbell et al. (1991). The heat dissipation technique for the estimation of ψ_m was also described in the literature by Campbell and Gee (1986), Bristow et al. (1993), and Jovanovic and Annandale (1997).

The system used in the peach field trial, consisted of the following components:

i) Two Campbell Scientific data loggers for controlling the system, as well as recording and storing data.

ii) Two AM416 relay multiplexers, used to increase the number of input channels for the differential measurement of temperature.

iii) Five CE8 eight-channel current excitation modules, used to increase the number of excitation channels.

iv) Forty CS 229 heat dissipation sensors, used to determine soil matric potential.

A scheme of the heat dissipation sensor system is shown in Figure 3.9.

Each data logger was powered by a 12 V battery. The site of each sensor is shown schematically in Figure 3.2. Soil temperature was recorded. A 20 s heat pulse was then applied to the sensors and the difference in block temperature 20 s and 1 s after heating commenced (ΔT) was recorded. The output readings were processed using the normalisation procedure of Campbell et al. (2001), which simplifies calibration of individual sensors using the dimensionless temperature rise and corrects the reading for soil temperature to the value it would have at 20°C. For this purpose, a user-friendly Delphi program (HDS calculator) was developed. This is described in detail in Appendix D.

The interval between subsequent heat dissipation measurements should be long enough to permit the heat pulse to dissipate without affecting the following reading. A minimum of 3 min was recommended between readings in order to permit block temperature to re-equilibrate (Jovanovic and Annandale, 1997). In the peach field trial, sample readings were taken every hour.

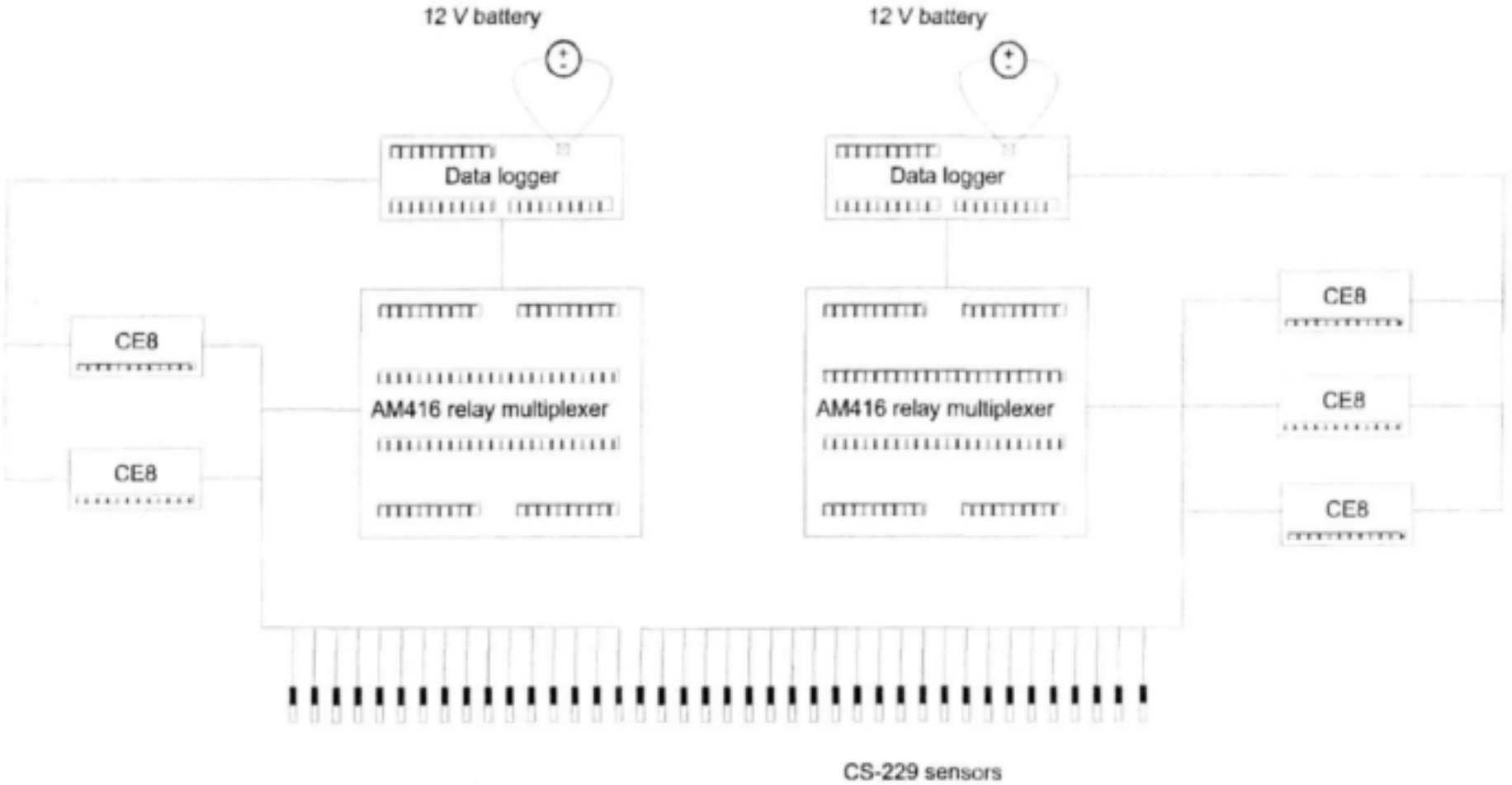

Figure 3.9. Heat dissipation sensor system used in the field trial.

3.1.6.3 Soil water content

Neutron water meter

On 18 October 1996, black PVC access tubes for neutron water meter (NWM) measurements were installed in the lysimeters. In two sites in the portion of the orchard surrounding the lysimeters, sets of 12 similar access tubes were installed in a row at right angles to the tree row in such a manner that the soil water content (SWC) across the whole area could be monitored. During winter 1997 a further two sets of 12 tubes were installed. Thus it was possible to monitor the SWC across the tree rows in four sites surrounding the lysimeters.

Soil water content was measured with a NWM, model 503DR CPN Hydroprobe, which had been calibrated for the site. Initially, readings were taken daily when a series of other measurements were made to monitor the water status of the trees. From February 1997, the SWC was monitored twice weekly.

Soil water content was also measured at two locations outside the experimental plot. One neutron probe access tube was set up about 10 m on the North side, the other about 10 m on the South side outside the plot. This was done to monitor possible lateral movement of water from and towards the experimental plot.

Time-domain reflectometry

Volumetric soil water content in two dimensions was also measured with a time-domain reflectometry system (Topp et al., 1980). This is a relatively new technique that has been successfully employed in similar applications. Initially, the system set up at the Hatfield experimental farm, consisted of the following components:

i) The Tektronix 1502C metallic cable tester is a reflectometer used as a source to send very short time-rise electromagnetic pulses to the probes, and to collect a signal (waveform), which is a reflection of the applied pulse.

ii) Six SDMX50 eight to one, 50 ohm, coax multiplexers with BNC connectors. These multiplexers are used to connect additional multiplexers or probes to the 1502C cable tester.

iii) Forty 30 cm three-rod (unbalanced design) CS605 soil probes. A BNC connector on the RG-58 coax cable of the probe attaches directly to the SDMX50.

iv) TDR 50 ohm RG-8 coax cables with BNC connectors. These cables are used for connecting cable tester and multiplexers.

v) WinTDR 98 v. 4.0 software for controlling the measurement sequence, applying algorithms for calculating water content and storing the resulting data.

vi) A computer with the software WinTDR 98 v. 4.0 used for controlling the system, analysing waveforms and storing data.

A scheme of the TDR system used is shown in Figure 3.10.

The cable tester, multiplexers and computer require a power supply. The 1502C and computer with software were housed together in an enclosure, and supplied with 220 V AC through an extension cable. Each SDMX50 multiplexer had its own enclosure. The multiplexers were powered with a 12 V battery serially.

The 1502C was connected to, and controlled by the computer with a 25 to 9 pin cable. The computer software was the WinTDR 98 v. 4.0. This is a Windows 3.1x / Windows 95 based program used to measure the volumetric water content and electrical conductivity of soils by controlling the Tektronix 1502B or 1502C time-domain reflectometry cable tester, and multiplexers if present. Minimum requirements for the computer are 66 Mhz 486 processor,

VGA display, 5 Mb of hard disk space, and a Windows environment. The software was developed by Or et al. (1998), and it was downloaded from the Utah State University web site (USU Soil Physics Group) along with the user's guide.

The SDMX50 multiplexers include eight multiplexed coaxial connections and one common. The eight multiplexed connections were used to connect additional higher level multiplexers or probes, whilst the common connection was used to connect to the 1502C or to lower level multiplexers. The SDMX50 multiplexers are Synchronous Devices for Measurement (SDM). The computer communicates with these devices via a parallel port. Addresses set in the multiplexers allowed the 1502C-computer system to communicate with the correct device. The allocation of the correct address was done by positioning jumpers (hardware switches) on the circuit board. There are two jumpers for each multiplexer. The jumpers are labelled MSD for Most Significant Digit and LSD for Least Significant Digit. Each jumper has four pair of pins. Depending which pair of pins is connected to the jumper, the digit can have the value of 0, 1, 2, or 3. A summary of the SDMX50 address allocation for the system used, is given in Figure 3.10. The 1502C and the computer are labelled level 0. The multiplexer with its input connected to the coax cable from the 1502C is level 1, and level 2 multiplexers (five of them) are connected to the level 1 multiplexer. The computer is connected to the control ports of the level 1 multiplexer with a communication cable carrying address and data information. The other multiplexers are wired serially. The communication cable is linked according to the set-up given by Or et al. (1998) (Figure 3.10). Particular attention should be paid to this set-up, as multiplexers and computer parallel ports could be damaged due to incorrect wiring.

The pulse generated by the 1502C and its reflection are subject to distortion during travel between the 1502C and TDR probe. Connectors, coax cables and multiplexers connecting the probes to the reflectometer have a characteristic impedance resulting in both resistive and reactive losses. Distortion of the waveform caused by this impedance can introduce error into the water content determination. The TDR system used in this trial was designed to ensure correct probe impedance giving robust reflections. This was done by minimising cable length and by using low attenuation RG-8 coax cable. The SDMX50 multiplexers and CS605 probes are designed to minimise signal attenuation, interference and delay in order to optimise accuracy of measurement. An RG-8 coax cable connected the 1502C and the common connection of the level 1 SDMX50 multiplexer. Five RG-8 coax cables were used to connect the level 1 SDMX50 to the five level 2 SDMX50 multiplexers (Figure 3.10).

The CS605 probes are the sensors of the system. They are made of a block of epoxy, which holds three rods rigidly spaced. The probes act as a wave guide extension on the end of coaxial cable and provide a reflection that is related to the change in impedance. The impedance value is related to the geometrical configuration of the probe (size and spacing of rods), and also inversely related to the dielectric constant of the surrounding material. A change in volumetric water content of the medium surrounding the probe causes a change in the dielectric constant. This is seen as a change in probe impedance, which affects the shape of the reflection. The shape of the reflection contains information used to determine water content with WinTDR 98 v. 4.0. The probes were labelled, and pressed into the soil with the rods at the same depth. The site of each probe is shown schematically in Figure 3.2. The BNC connector of the 50 ohm RG-58 coax cable of the probes connected directly to the level 2 SDMX50 multiplexers (Figure 3.10).

Measurements were taken twice weekly. The output included dielectric constant of the medium and the volumetric soil water content obtained by analysing the waveform of each probe with WinTDR 98 v. 4.0. As surface waves propagate along TDR probes buried in soil, the signal energy is attenuated in proportion to the electrical conductivity along the travel path. This proportional reduction in signal voltage serves as a basis for the measurement of bulk soil electrical conductivity. A laboratory calibration for impedance is, however, required for each probe separately in order to accurately estimate the electrical conductivity of the soil solution. The probes were not calibrated for impedance before being installed in the soil, as

the irrigation water was not saline and the measurement of electrical conductivity was not essential for the purpose of this project.

From September 2000, the TDR system was changed. Volumetric soil water content data were recorded at four hourly intervals by making use of a CR10X data logger (Campbell Scientific Inc., Utah, Logan, USA), a Tektronix 1502C cable tester and SDMX50 multiplexers.

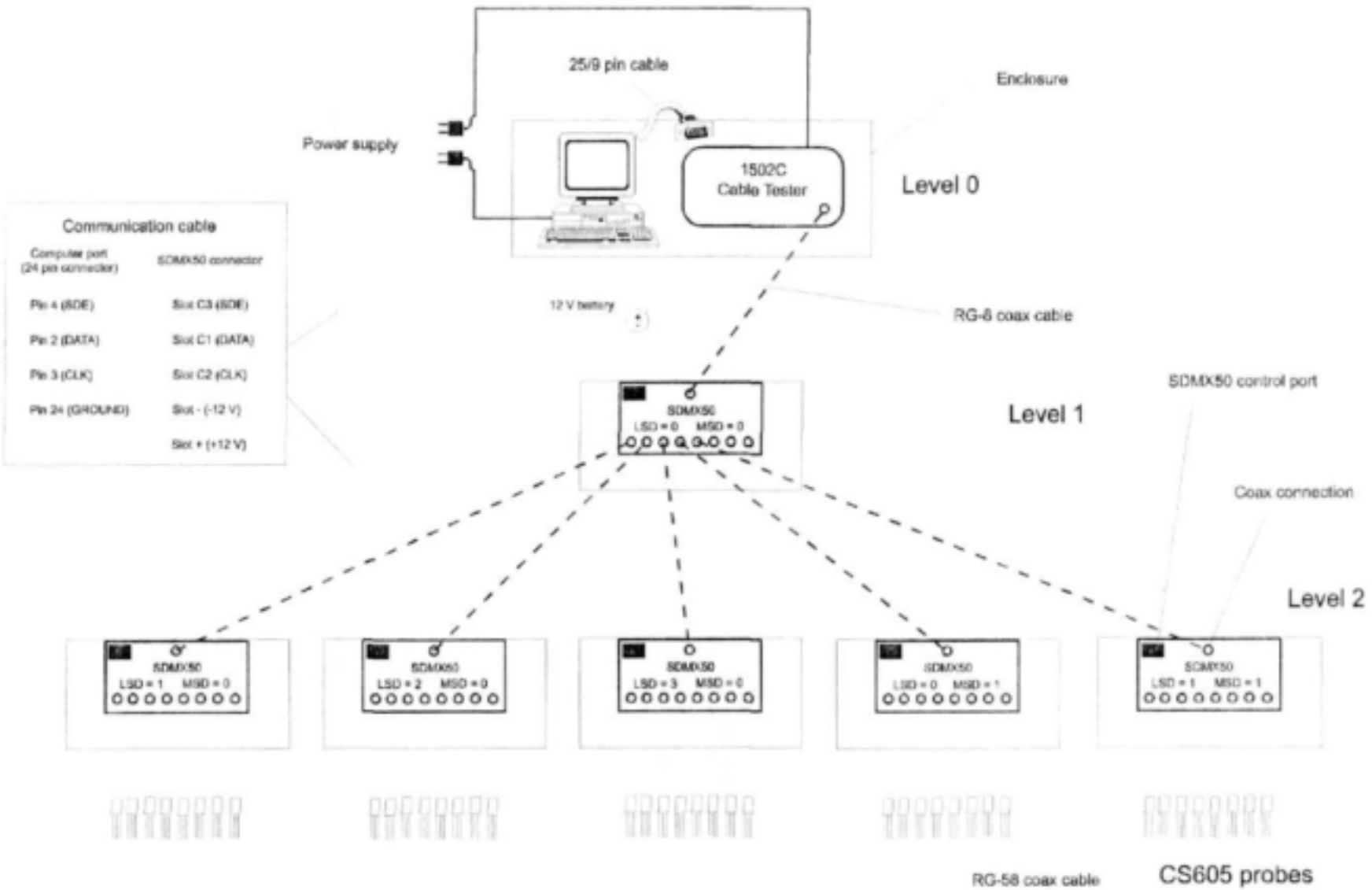

Figure 3.10. Time domain reflectometry system used in the field trial.

3.1.6.4 Soil evaporation

Evaporation from the soil surface was measured using the micro-lysimeter method (Boast and Robertson, 1982). Micro-lysimeters are containers filled with soil, and placed at given positions at the soil surface. Evaporation is determined by measuring the loss of mass of the micro-lysimeter. In this experiment, the micro-lysimeters were made of PVC pipes of 300 mm length with 110 mm internal diameter and 3.5 mm wall thickness. The micro-lysimeters were made as follows: PVC tubes were hammered into the soil in a portion of the orchard where the soil had been irrigated: in this way, tubes filled with an undisturbed core of soil were obtained. The tubes were then carefully twisted and pulled out of the soil, leaving the soil core inside intact. The base of the tubes was then closed with a plastic cap. Holes were made in the orchard at the positions where the lysimeters had to be installed, and the tubes were inserted in the holes to a depth at which the upper rim was aligned with the soil surface, so as not to alter the wind regime above the soil surface.

The main experiment with micro-lysimeters consisted of measurements of evaporation in the orchard. Nineteen micro-lysimeters were installed across the rows of the orchard, at distances ranging from 0 to 2.5 m from the row. Eleven of them were installed in a row where the soil was kept bare, and 8 others in a grass-covered area. After an initial irrigation of 20 mm, applied with sprinklers, soil water evaporation was measured for six days (05-12/03/2001, DOY 64 to 71). Another test experiment was conducted to validate the micro-lysimeter technique. It consisted of measurements of soil water evaporation in an open field located close to the weather station, after irrigation with the same sprinkler system as for the peach orchard. These measurements went on for seven days after the initial irrigation.

Evaporation measurements were made by weighing the micro-lysimeters daily. Measurements were taken at 10h00 and 12h00 with an electronic balance, and the average value was retained (in a few cases, discrepancies between these consecutive measurements led to discard one of them). The daily evaporation (mm) was calculated as the difference of mass between two consecutive days, divided by the product of the density of water and the area of the tube.

3.1.7. Plant measurements

The following plant measurements were carried out:

- Root distribution by taking soil core samples and washing out roots to determine root length;
- Canopy interception with tube solarimeters;
- Leaf area index and density; and
- Canopy size and row orientation.

3.1.7.1 Root distribution

During the winter dormant period, when the soil water measurement instrumentation was installed, core samples were taken at regular intervals across the tree row / inter-row and at specific depths for root length density determinations. These samples were analysed by Dr T Fyfield (Agriculture Research Council - Institute of Soil, Climate and Water, Pretoria).

Roots were washed out of the soil cores using ARC-ISCW's root washing facility at Roodeplaat. After collection in a fine mesh sieve, the debris and obvious weed and dead tree roots were removed and the remaining tree roots were air-dried. Root length was then determined using a Geotron WLM1 Root Length Meter. Root length density was calculated per 200 mm depth layer by dividing the total root length by the volume of the soil core.

3.1.7.2 Canopy interception

Seven Delta-T tube solarimeters (Delta-T Devices Ltd, Burwell, Cambridge, England) were installed across the tree row to measure light penetration through the canopy at different

distances from the row. The tube solarimeters were set up parallel to the tree row. This was done at different times during the course of the trial in order to collect data for validation of the two-dimensional canopy radiant interception model. The tube solarimeters were connected to a CR10X data logger and used to record total solar radiation at specified time intervals.

The Delta-T tube solarimeters were regularly serviced during the course of the trial. This involved dismantling some and cleaning glass tubes, repainting checker bar if required, and then re-assembling. Others just required exterior cleaning of glass tubes. Where required, some were re-charged with dry air. This involved connecting the solarimeters to an air-drying column filled with dry silica gel and flushing the solarimeters with dry air for 48 hours. All the solarimeters were regularly re-calibrated against a Precision Eppley thermopile pyranometer.

3.1.7.3 Leaf area index and density

Leaf area index was measured using an LAI-2000 plant canopy analyz er (LI-COR Inc., Lincoln, Nebraska, USA). This measurement was done by activating detector rings 2, 3 and 4 (i.e. switching off rings 1 and 5). Ring 1 was excluded to reduce effects of solid objects immediately above the fish eye, whilst excluding ring 5 reduced the influence of the tree trunk and open spaces under the canopy. While taking measurements, the LAI-2000 optical sensor was fitted with a 45° view cap to restrict the field-of-view along the tree row. The field-of-view was aimed at measuring the leaf area index of only the canopy portion of the tree row and excluding the inter-row region. Measurements were only taken under conditions of diffuse radiation, i.e. before sunrise, after sunset or when uniform cloud cover blocked out direct solar radiation.

Leaf area density (LAD) was determined by converting leaf area index values (I) to leaf area (LAb, m^2 leaves) per canopy base unit area (Acb, m^2 soil) as follows:

$LAb = I * Acb$ (m^2 *leaf* m^{-2} *soil*)

The canopy base unit area is the measured tree row canopy width multiplied by 1 m. Once the leaf area per m of canopy length was known, it was converted to LAD by:

$LAD = LAb / Vc$ (m^2 *leaf* m^{-2} *soil*)

The canopy unit volume (Vc) is the cross-sectional area of the hedgerow canopy multiplied by 1 m. The cross-sectional area of the canopy can either be determined using the formula for the area of an ellipse ($A = \pi\ a\ c$; a = half the width and c = half the height) or by summation of calculated areas of trigonometric sub-units of the cross-section.

3.1.7.4 Canopy size and row orientation

Canopy dimensions (height and breadth) were measured with a calibrated 2 m rod and tape measure, whilst the row orientation was determined with a compass. The reading of the compass was corrected by 15E to account for magnetic declination from true North.

3.1.8. Leucaena trial

An additional field trial was carried out at the Hatfield experimental station on Leucaena (*Leucaena leucocephela*) fodder trees, in order to test the two-dimensional radiant interception model for different environmental conditions (tree size and shape as well as row orientation).

Two single rows of Leucaena were used with spacing between trees ~ 0.5 m. The row orientation was in a N to S axis (10° - 190°) and E to W axis (10° - 280°).

Canopy interception for total solar radiation was measured with tube solarimeters installed at different distances from the row, on both sides of the row. The tube solarimeters were set up parallel to the tree row. This was done for one week for each row.

Leaf area index and density, canopy size as well as row orientation were measured adopting the same method used in the peach trial at Hatfield.

3.2. *Experimental set-up at the University of the North*

3.2.1. Location and environmental characteristics

The field trial at Syferkuil experimental farm (University of the North) was located 30 km East of Pietersburg (23°51' S; 29°40' E; alt. 1250 m), in the summer rainfall region.

The soil in the trial site is a 1 m deep sandy loam Hutton (Soil classification working group, 1991) or Ferralsol (FAO, 1998). Hard plinthic formations are found below 1 m.

3.2.2. Orchard lay-out, irrigation and cultivation practices

Citrus clementine (*Citrus reticulata* cv. Blanco) trees were planted in 1985, in a 7.5 x 3.5 m hedgerow pattern. The tree row orientation is in a SE to NW axis (135° - 315°). Grass in the inter-row spacing was mowed regularly and herbicides applied. Fertilisation and irrigation were applied as required until the beginning of the trial. The irrigation system made use of micro-jets with a wetted diameter of 1.5 m. No insecticide was applied.

3.2.3. Weather monitoring

An automatic weather station was set up, similar to that installed at the Hatfield experimental farm. Air temperature, relative humidity, solar radiation, wind speed and rainfall were monitored and recorded hourly with a CR10X data logger.

3.2.4. Soil measurements

An intensive monitoring site was established, similar to those set up at the Hatfield experimental station. Equipment for measurement of volumetric soil water content and potential was installed on 13-14/10/1999. Twenty-eight heat dissipation sensors (HDS) and time domain reflectometry (TDR) probes were buried in the soil at nodes located on a grid across the row (Figure 3.2). The depths were 0.06, 0.26, 0.56 and 0.86 m. Sensors and probes were installed in the row between two trees, and at distances of 1.25, 2.5 and 3.75 m from the row, on both sides of the row. The TDR probes were pressed into the soil with the rods parallel to the surface.

Soil temperature and matric potential data from heat dissipation sensors were collected and stored with AM416 multiplexers and CR10X loggers. Soil water content data from TDR probes were collected and stored with SDMX50 coax multiplexers, a data logger and a 1502C Tektronix cable tester. HDS sensors and TDR probes were installed at a few centimetres from each other. This enabled us to determine soil water retention functions from measurement of matric potential and water content.

During the installation of HDS and TDR sensors, soil samples were collected at the same node depths and distances from the tree row. The samples were used to determine bulk density, soil texture and hydraulic characteristics, as well as nutritional properties.

3.2.5. Plant measurements

During the installation of the intensive monitoring site, core samples were taken at regular intervals across the tree row / inter-row and at specific depths for root length density determinations. These samples were analysed by Dr T Fyfield (Agriculture Research Council

- Institute of Soil, Climate and Water, Pretoria). The same method was used as for the core samples taken at the Hatfield experimental farm.

Canopy interception of total solar radiation was measured with tube solarimeters installed across the row between two trees, and at distances of 1.25, 2.5 and 3.75 m from the row, on both sides of the row. The tube solarimeters were set up parallel to the tree row. This was done at different times during the course of the trial in order to collect data for validation of the two-dimensional canopy radiant interception model. At the same site and time, line quantum sensors were installed to measure canopy interception of photosynthetically active radiation. The instruments were connected to a CR10X data logger and used to record total solar radiation and photosynthetically active radiation at specified time intervals. The sensors were regularly serviced and calibrated. Leaf area density was measured with an LAI-2000 plant canopy analyzer.

3.3. Field trial at Brits

In order to test the two-dimensional radiant interception model for different environmental conditions (tree size and shape as well as row orientation), field trials were carried out on two commercial farms 15 km North of Brits (25°00'S, 27°46'E, alt. 1107 m).

On the first farm, Empress mandarin (*Citrus reticulata* cv. Blanco) was grown in hedgerows with a planting density of 4 x 4 m and row orientation in a SE to NW axis (145° - 325°). The second farm had Delta Valencia (*Citrus sinensis* [L.] cv. Osbeck) grown in a tramline pattern. The spacing was two rows 4 x 4 m with 8 m gap and row orientation in a SE to NW axis (135° - 315°).

Canopy interception for total solar radiation was measured with tube solarimeters installed at different distances from the row, on both sides of the row. The tube solarimeters were set up parallel to the tree row. This was done for two weeks in each orchard.

Weather data (air temperature, relative humidity, solar radiation, wind speed and rainfall) were monitored and recorded hourly with an automatic weather station.

Leaf area index and density, canopy size as well as row orientation were measured adopting the same method used in the field trial at Hatfield.

CHAPTER 4

MODELLING

4.1. Evaluation of the SWB model

The SWB model was tested according to the guidelines provided by CAMASE (1995). This evaluation included checking internal consistency and units used in the computer program, comparison of model output with independent data sets of real world observations and sensitivity analysis.

Verification of the model comprised the inspection of the internal consistency of the model and its software implementation. In particular, the following actions were taken: analysis of dimensions and units; on-line checks on mass conservation; detection of violation of natural ranges of parameters and variables; inspection of qualitative behaviour of the model and its implementation by checking whether the response of one model output to changing values of one parameter conforms to theoretical insights.

In this Chapter, an example of calibration of the simple quasi-2D FAO-based cascading model is presented for peaches (Section 4.2). This was done by adjusting some FAO crop factors such that the model prediction of soil water deficit was consistent with field measurements. The most important observations gathered in the field trials at Hatfield and Syferkuil, and relevant to the development of the SWB model, are also presented.

Due to the large size of the SWB two-dimensional model, the code for each subroutine was written in separate files or procedures. The model interface was also developed so as to subdivide the model into components. This should improve user-friendliness during the technology transfer phase of the model, and it also facilitated the validation of the various components separately. The two-dimensional energy interception and soil evaporation sub-models were validated separately using independent data sets (Sections 4.3 and 4.4). The two-dimensional soil water balance model integrates the interactions of the various components, as it uses the 2D energy interception and 2D soil evaporation sub-models to split evaporation and transpiration. Comparing the output obtained with the two-dimensional soil water balance model to independent field measurement data then validated the aggregate model (Section 4.5).

Scenario simulations were carried out to perform sensitivity analyses (Section 4.6). Scenarios were simulated by varying one input parameter and retaining the same values for the other inputs. Logical sensitivity analyses were performed to establish by inspection of output results whether the model is sensitive at all to changes in an input (factor screening). This could indicate which input parameters need to be accurately measured or estimated. The sensitivity analyses also provided estimates of scenario effects in order to recommend the most suitable practices for improved water use efficiency under different environmental conditions. One should, however, be aware that the sensitivity to an input may depend on the particular set of values used for other inputs.

The SWB model is written in Delphi v. 5.0 (Inprise Corp.), and is available for use with Windows 95 on an IBM-PC or compatible computer. The minimum requirement is 16 Mb RAM and a CD-ROM drive.

4.2. Calibration of the FAO-type model and field observations

The simple, quasi two-dimensional, cascading soil water balance model was calibrated using data from the peach trial at the Hatfield experimental station. In the process, FAO basal crop coefficients (Kcb) were determined for first and second leaf peach trees.

FAO basal crop coefficients were determined by plotting daily Kc values for the first two growing seasons of peach trees (Figures 4.1 and 4.2). The daily Kc value was calculated using evapotranspiration measurements from the lysimeters and the grass reference evapotranspiration calculated from weather data. The Kcb values for the various growth stages were determined by fitting an appropriate line through the lower values of Kcb, which are taken to reflect the conditions where the soil surface is dry (negligible evaporation) and there is sufficient water not to restrict transpiration. The longer development period during the first season can be expected since it is necessary to develop the tree structure. The drop in actual evapotranspiration measured with lysimeters during the late stage of the first season was caused by water stress (Figure 4.1). The Kcb line during this late stage was estimated.

Simulations of soil water deficit (SWD) with the SWB model were then carried out and compared to measurements obtained with the neutron water meter (Figures 4.3 and 4.4). The Kcb factors in Figures 4.1 and 4.2 were refined by fitting the simulations of soil water deficit to measured data points (Figures 4.3 and 4.4).

The initial period of the first season was not well evaluated, as too few measurements with the NWM were taken (Figure 4.3). Thereafter, more measurements were available, which enabled a better evaluation of model predictions. Generally, there was good agreement between predicted and measured SWD. This should be expected since the calibration data came from the trial. A strip of trees (20 m row length) was stressed in the period from 10 January 1997 to 20 February 1997 in order to check the reliability of SWB under limited water supply. This strip included one neutron water meter (NWM) measurement site. Of interest is that the model adequately predicted soil water deficit for the stressed (Figure 4.3a) and non-stressed treatments (Figure 4.3b).

The accuracy of the predictions of SWD was evaluated by comparison with SWD determined from NWM measurements. When measured SWD for the whole area (tree row and inter-row) is used, the agreement between predicted and measured SWD is acceptable (Figure 4.5). However, if measured SWD is taken only at the centre of the inter-row (2 m from tree), SWB occasionally shows a lower deficit than the measured values since no irrigation water is applied in the inter-row area. When one considers SWD measured at the row centre, SWB frequently shows a greater deficit than measurements since irrigations are concentrated under the trees. It is thus vitally important to realise that in hedgerow plantings the whole area must be borne in mind when assessing soil water content. The practice of using single or restricted locality measurements, as utilised in agronomic crops, can be misleading in orchards.

The reason for this is obviously the effect of the irrigation distribution (Figure 4.6), rain interception by the canopy (Figure 4.7), as well as the variation in radiation interception by the canopy and the irradiance reaching the soil surface as the season progresses (Figures 4.8 and 4.9). Figures 4.8 and 4.9 highlight the variation in canopy radiation interception across the row. It is seen that in winter (4 July; DOY 185), when there is no tree canopy, the irradiance across the tree row is around 10 MJ m^{-2} d^{-1}. Two months later (4 September; DOY 247), with the onset of spring, the daily irradiance has increased to around 17 MJ m^{-2} d^{-1} on the northern side of the hedgerow, whilst on the southern side, due to canopy development, soil irradiance has increased to only about 15 MJ m^{-2} d^{-1}. In mid-summer (28 December, DOY 362), the irradiance in the inter-row region reaches 22.5 MJ m^{-2} d^{-1}, whilst under the canopy the irradiance has decreased to about 2.5 MJ m^{-2} d^{-1}. Figures 4.8 and 4.9 also show how the position of the shadow moves from ~ 1.3 m (Figure 4.8; DOY 185) to virtually under the tree on DOY 362 (Figure 4.9) as the sun elevation increases into summer.

A common assumption with tree crops is that rooting volume is of a similar magnitude to canopy volume. It was therefore interesting to investigate root length densities of peaches at Hatfield and of clementines at Syferkuil. As can be expected, the root length density decreased with depth both in the case of peaches and clementines (Figures 4.10 and 4.11).

It was interesting to note the root length density across the tree row (Figures 4.10 and 4.11). There are at least as many, if not more roots in the inter-row region (i.e. in the 1 to 2 m distance from the tree trunk) than in the canopy drip area (0 to 1 m from tree trunk), in particular for peaches. It is common practice in hedgerow plantings to irrigate only under the tree canopy and not irrigate in the inter-row region at all. It must be noted that there are significant amounts of roots in the inter-row region and thus this portion of the rooting volume must not be disregarded when assessing the contribution of rain to the water balance.

The resultant effect of the root length densities on the profile SWD across the hedgerow into the inter-row is depicted in Figure 4.12 for peaches with grass sod and bare soil in the inter-row area. This Figure depicts the change in SWD through one drying cycle during the development period. On the basis of volumetric soil water content measurements with the neutron water meter at two locations outside the experimental plot, it was assumed that no lateral movement of ground water from or towards the plot occurred. It is apparent that, during the 36 h after irrigation, most water was used from the wetted area. The presence of a grass sod also had an influence on profile SWD. The volumetric soil water content in the inter-row with grass sod decreased more compared to the inter-row with bare soil.

The same effect was observed by analysing data of soil matric potential obtained with heat dissipation sensors. For example, in Figure 4.13, matric potential values decreased (became more negative) at two depths in the soil profile of peaches during a drying cycle after rain. This occurred both for grass sod and bare soil in the inter-row area, but the soil with grass sod dried faster. It is interesting to note that the top soil (6 cm depth) was wetter than the deeper layer (26 cm depth), as the rain was light and the wetting front did not reach 26 cm soil depth.

Figure 4.14. shows the volumetric soil water content across the row for different depths during a drying cycle of clementines at Syferkuil. The drying cycle started after the soil was wetted by heavy rain. It is evident that root water uptake occurred both from the wetted and non-wetted portion of the ground, due to an evenly distributed root system across the row (Figure 4.11).

The effect of the above features on the diurnal variation of soil temperature at a depth of 6 cm during a summer day is depicted in Figure 4.15 for peaches. It is seen that under the tree, soil temperature was around 19 to 20 °C at 06h00 and increased to 22 °C at 14h00. However, in the inter-row region, the 06h00 temperature was 24 °C and increased to 31 °C (short grass inter-row) and 33 °C (clean cultivated inter-row) at 14h00.

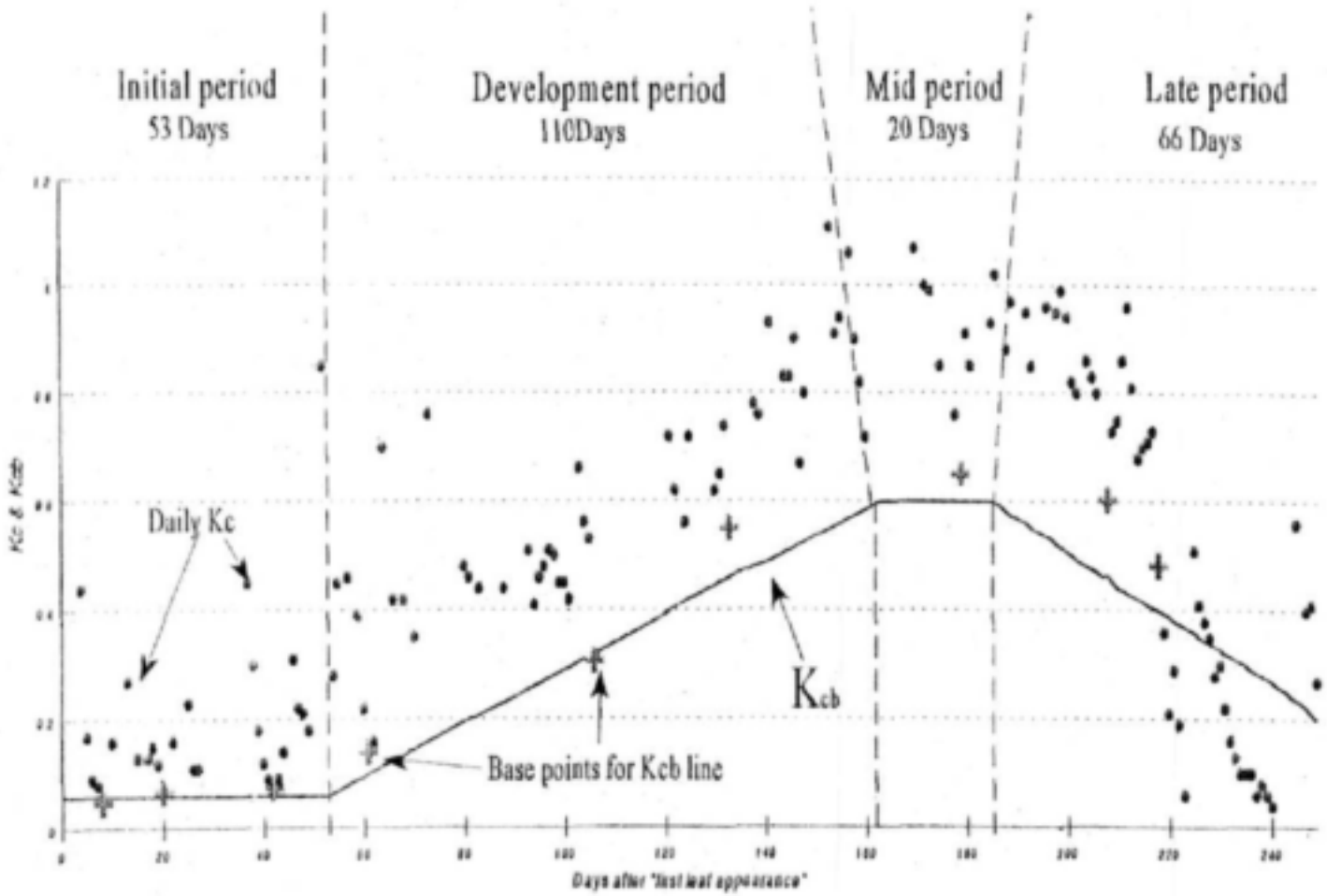

Figure 4.1. Daily Kc and Kcb, as well as growth periods for first leaf season of peaches.

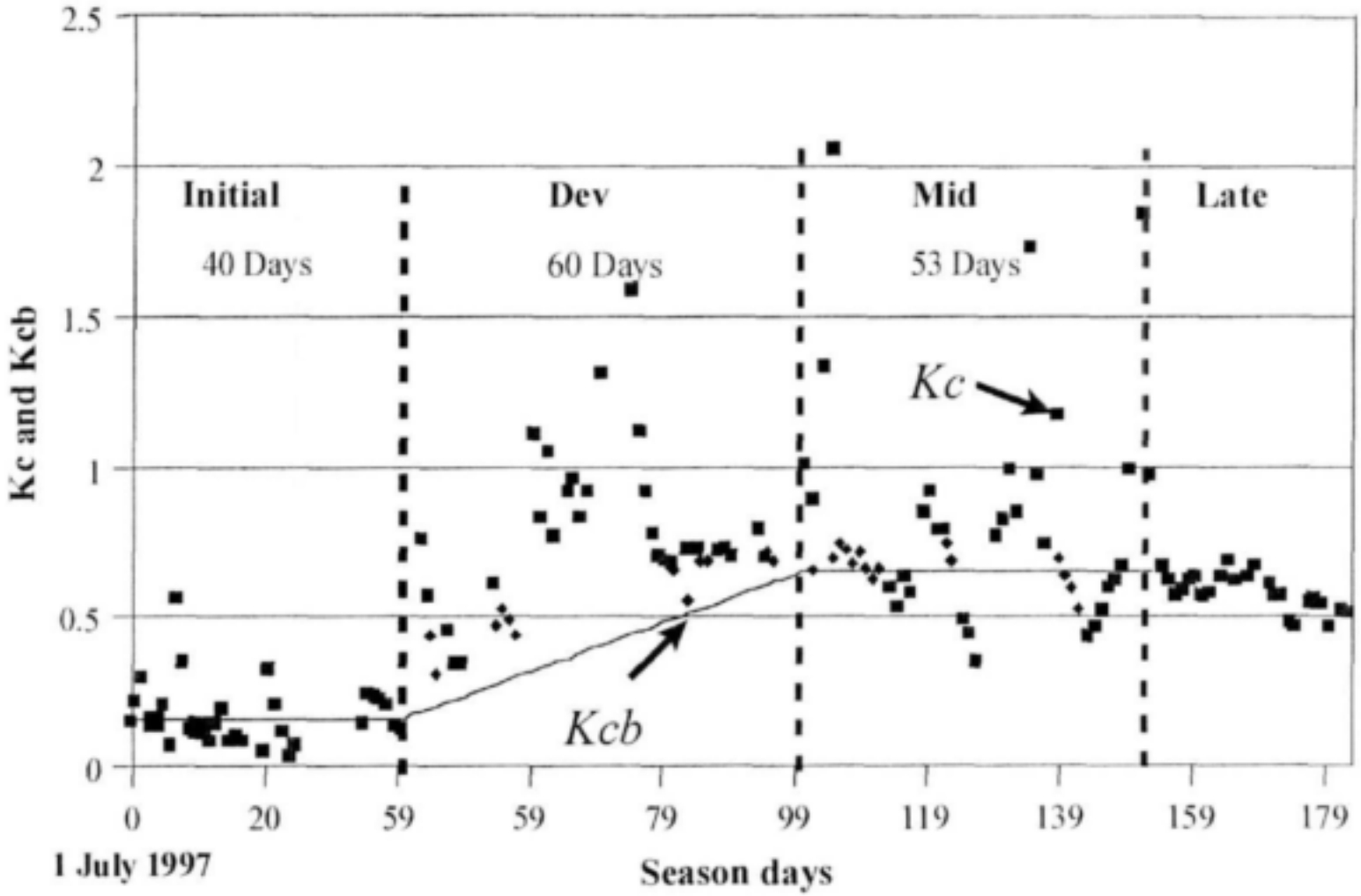

Figure 4.2. Daily Kc and Kcb, as well as growth periods for second leaf season of peaches.

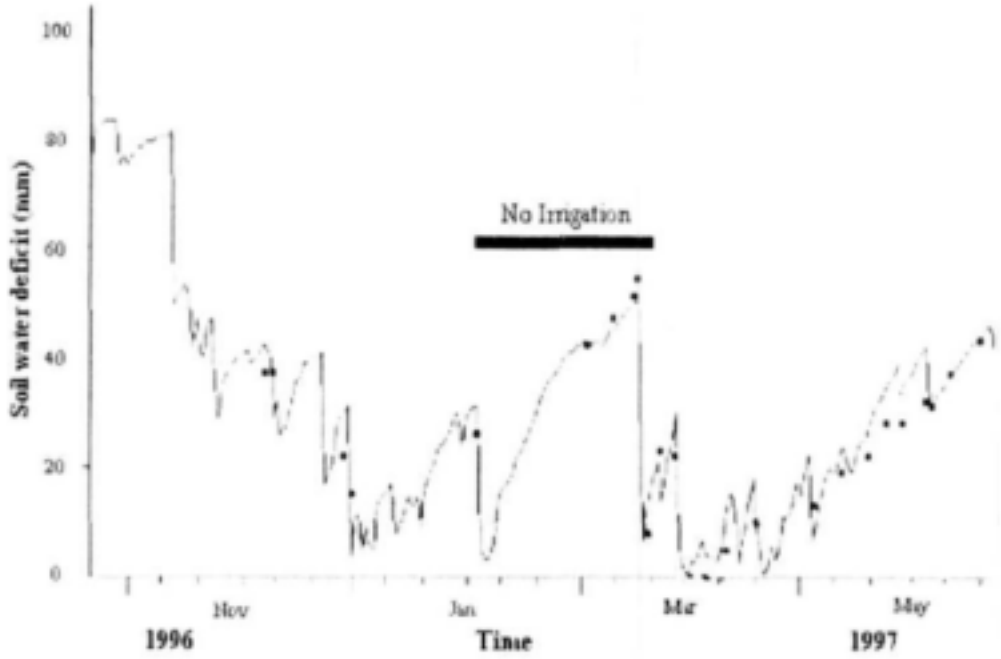

Figure 4.3a. Predicted and measured soil water deficit for first leaf season of peaches (stress treatment).

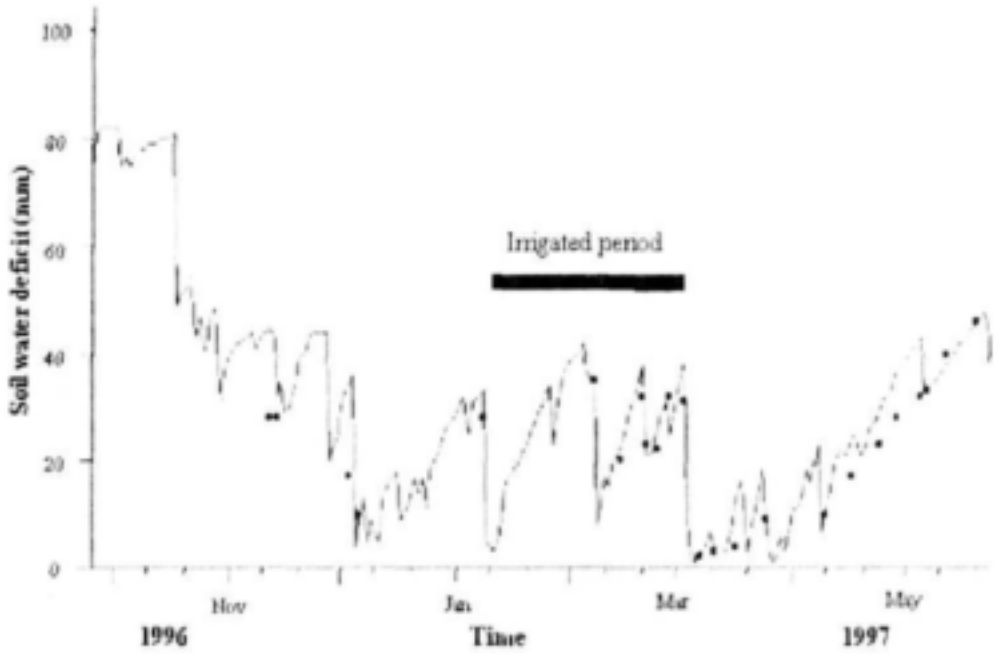

Figure 4.3b. Predicted and measured soil water deficit for first leaf season of peaches (non-stressed treatment).

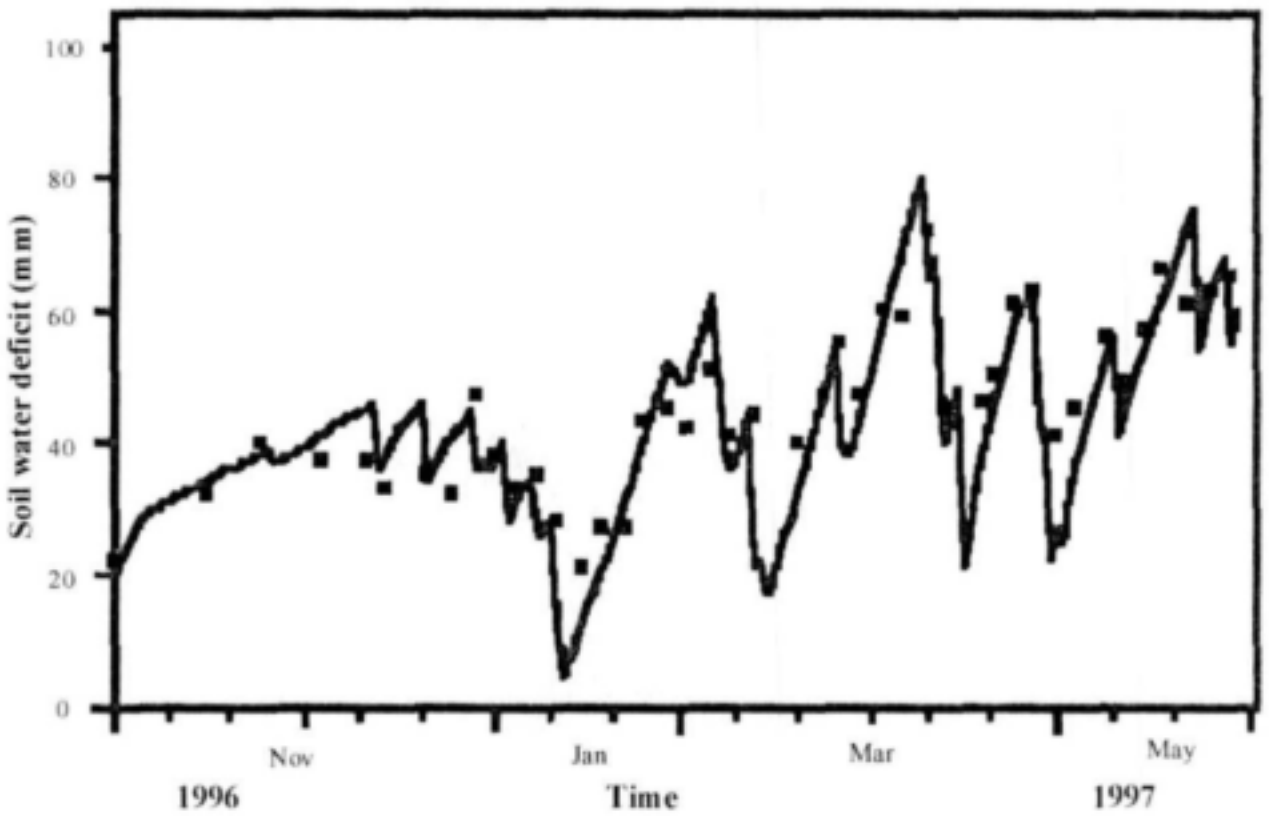

Figure 4.4. Predicted and measured soil water deficit for second leaf season of peaches.

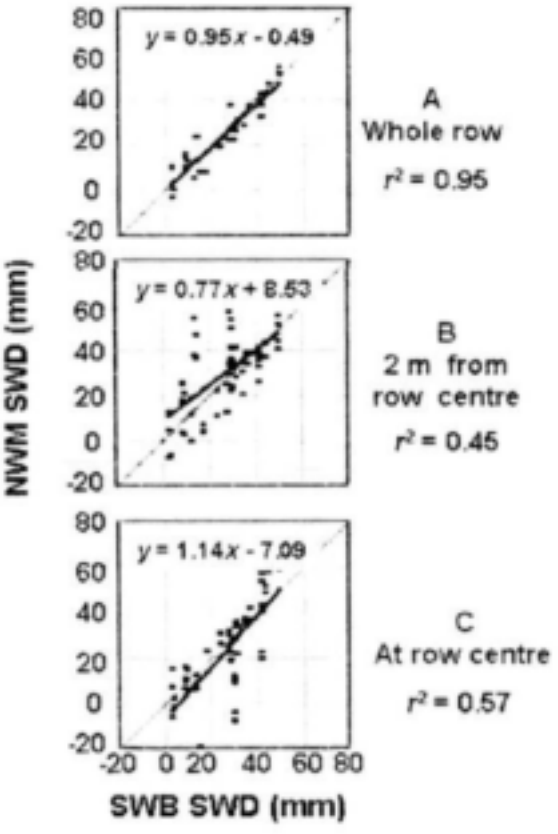

Figure 4.5. Soil water deficit predicted with the SWB model (SWB SWD) vs. measured with the neutron water meter (NWM SWD). The comparison was carried out by using NWM measurements for the whole area, 2 m from tree and at centre of row.

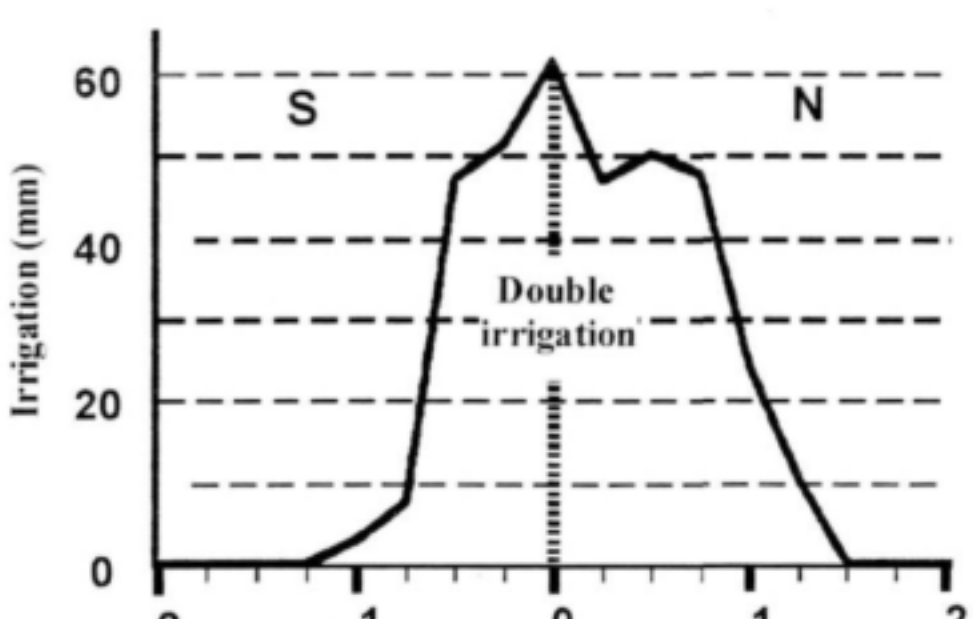

Figure 4.6. Distribution of irrigation application measured with a grid of rain gauges vs. distance from tree row.

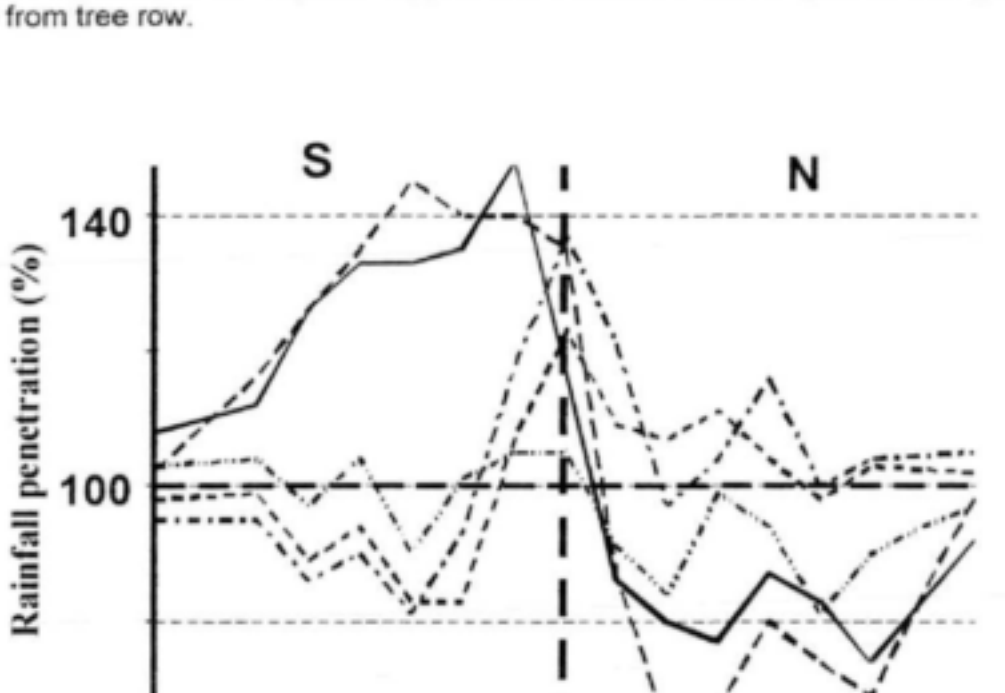

Figure 4.7. Distribution of five rains penetrating the peach canopy, measured with a grid of rain gauges and expressed as % of recorded rainfall vs. distance from tree row.

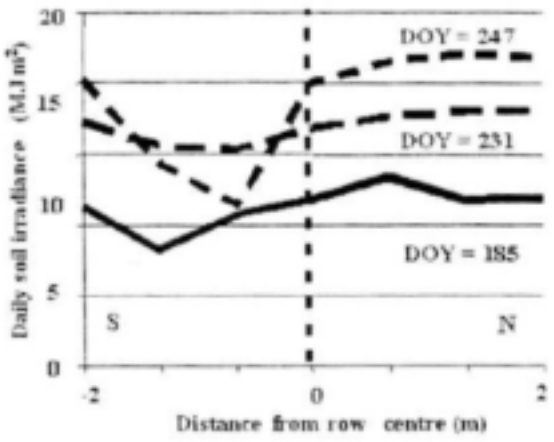

Figure 4.8. Variation of irradiance reaching the soil surface with distance from tree row for three full sunshine days (second leaf peach tree).

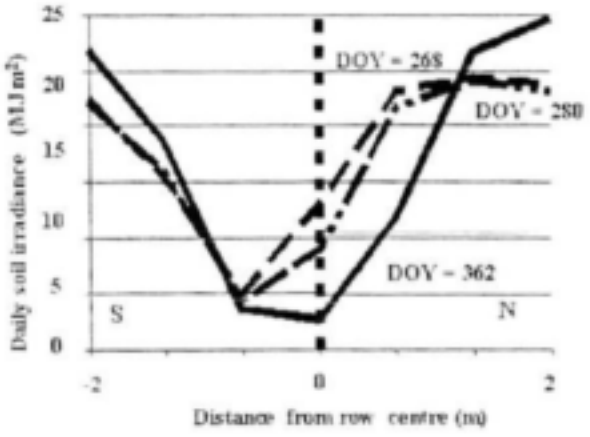

Figure 4.9. Variation of irradiance reaching the soil surface with distance from tree row for three full sunshine days (second leaf peach tree).

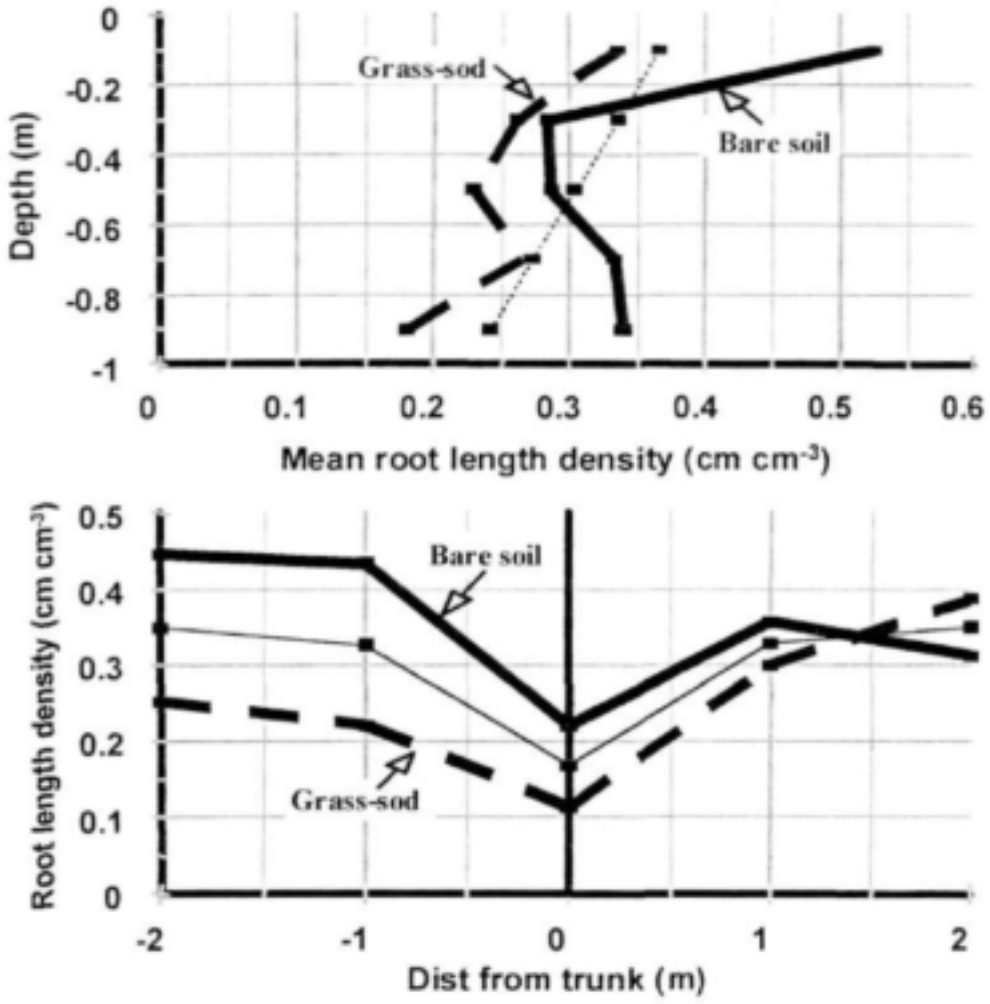

Figure 4.10. Root length density with soil depth and with distance from the trunk for peaches (bare soil or grass sod in the inter-row area).

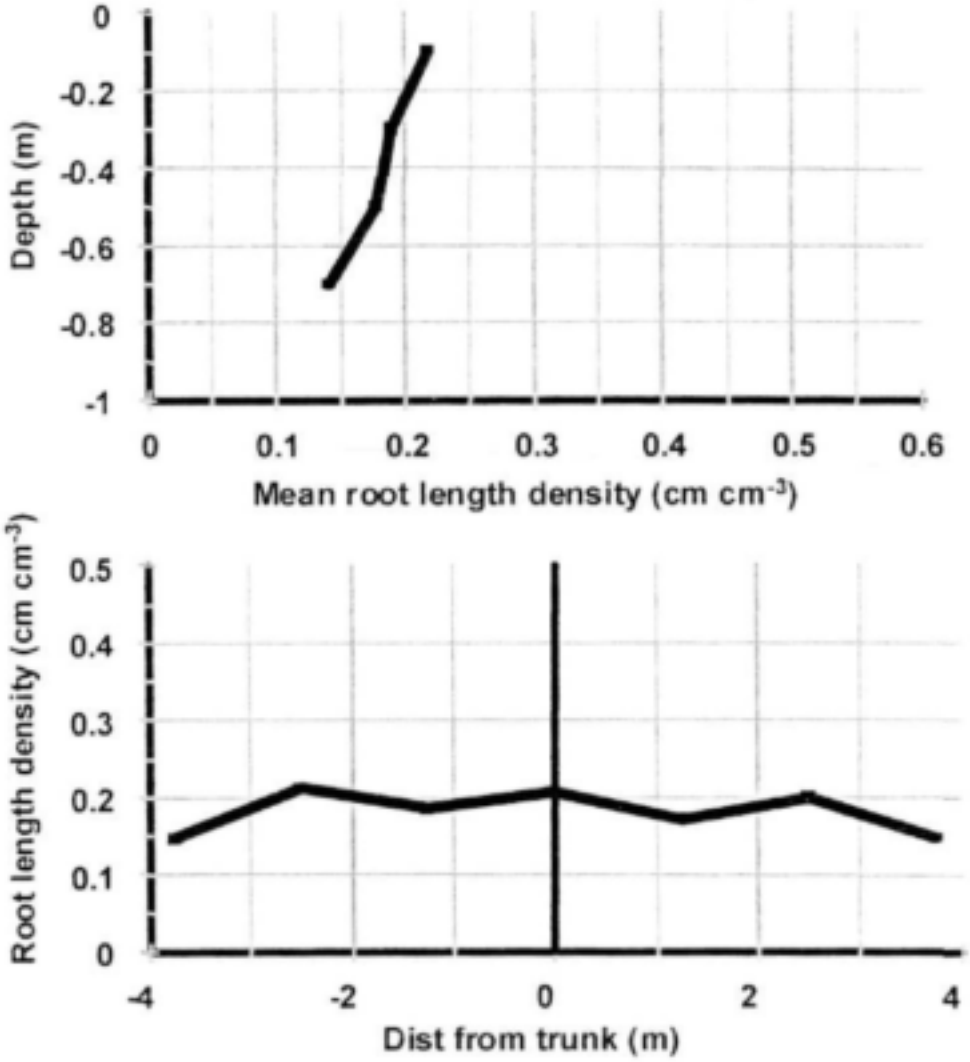

Figure 4.11. Root length density with soil depth and with distance from the trunk for clementines.

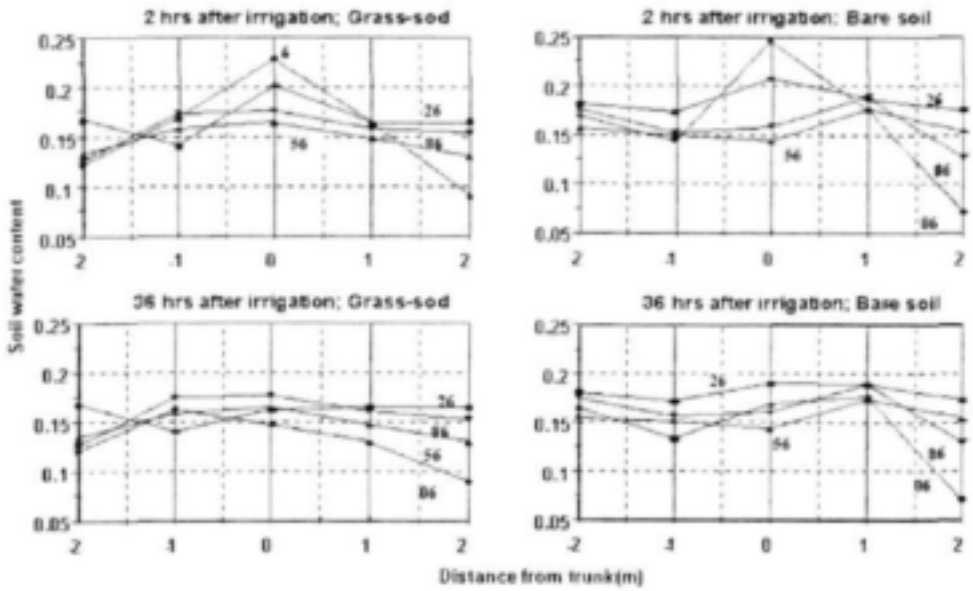

Figure 4.12. Volumetric soil water content across the row at 6, 26, 56 and 86 cm soil depth, and 2 and 36 h after irrigation of peaches (grass sod or bare soil in the inter-row area).

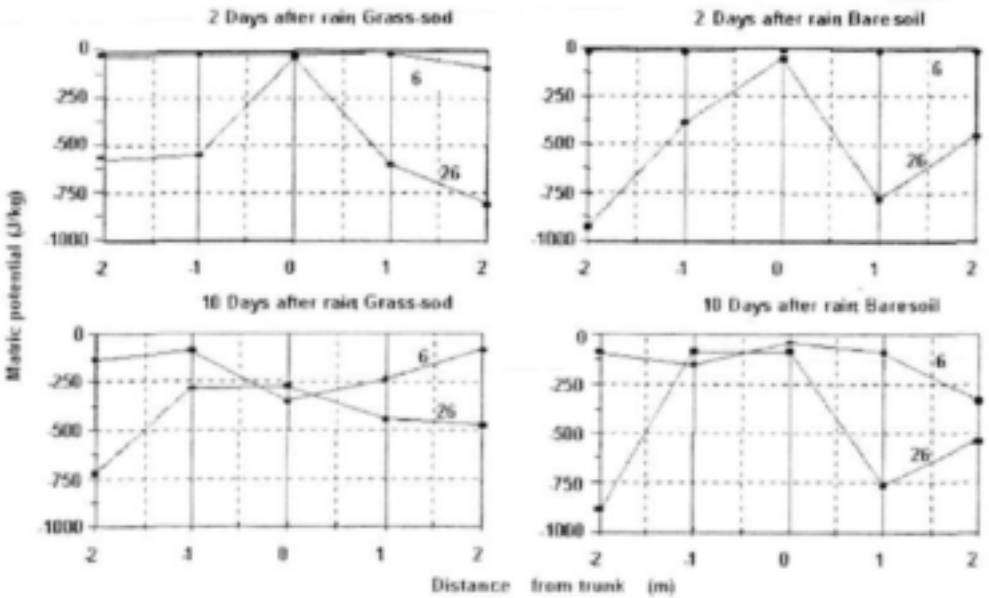

Figure 4.13. Soil matric potential across the row at 6 and 26 cm soil depth, and 2 and 10 days after rainfall for peaches (grass sod or bare soil in the inter-row area).

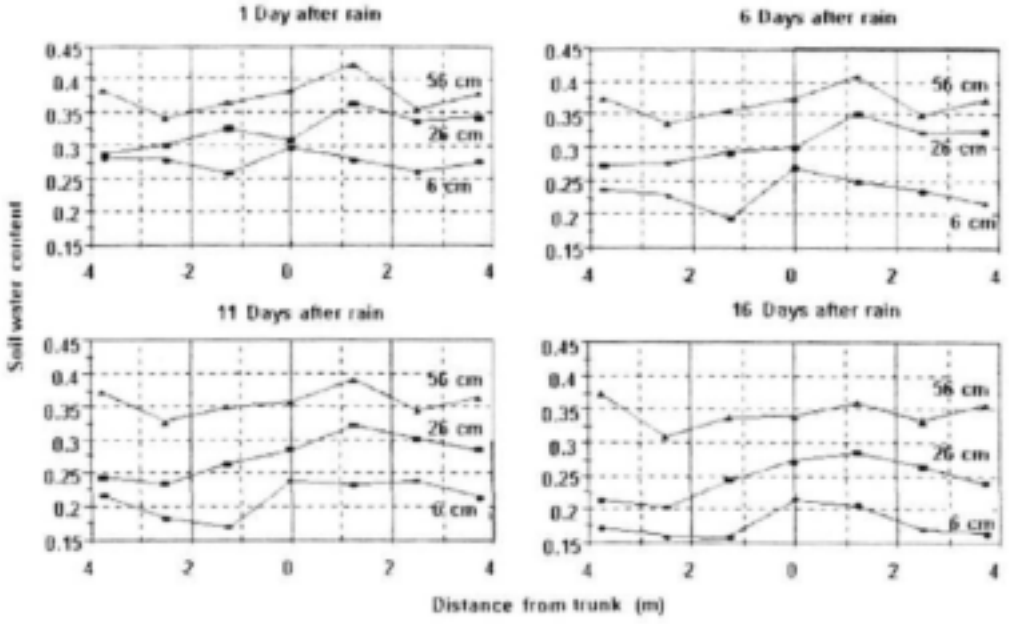

Figure 4.14. Volumetric soil water content across the row at 6, 26 and 56 cm soil depth, and 1, 6, 11 and 16 days after rainfall for clementines.

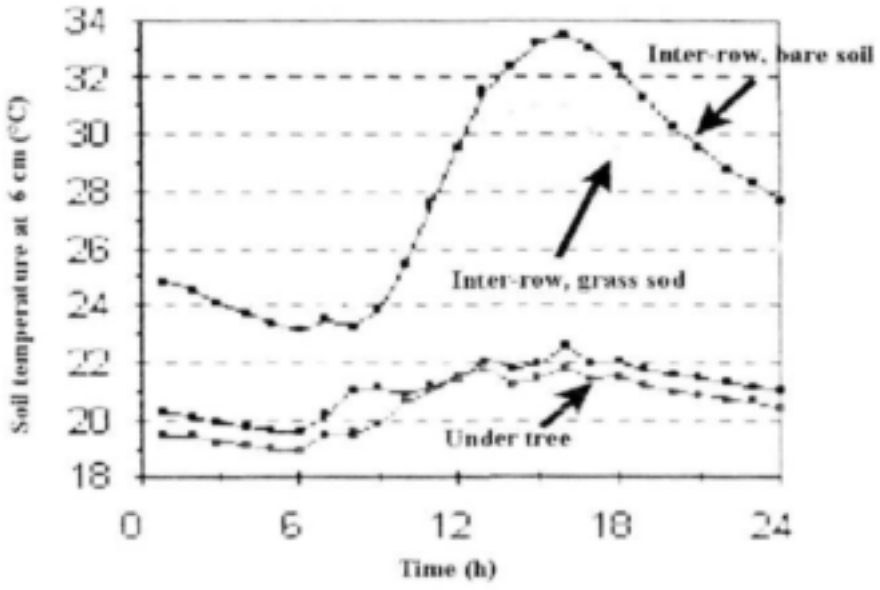

Figure 4.15. Variations in soil temperature measured at 6 cm during a summer day in the peach orchard at Hatfield.

4.3. *Validation of the two-dimensional energy interception model*

4.3.1. Overview of the field trials

The radiant interception model was tested in orchards with differing tree sizes, leaf area densities, shapes and row orientations. Data collected in the peach and Leucaena plantings were used to validate the two-dimensional energy interception model for deciduous tree crops, whilst data obtained from citrus orchards in Syferkuil and Brits were used to validate the model for evergreen tree crops. For the benefit of the reader of this report, locality and orchard planting specifications are summarised in Table 4.1.

There are 11 horizontal surface nodes simulated in the model, but only seven tube solarimeters were available. Solar radiation interception by the canopy was therefore determined with the use of seven tube solarimeters positioned under the canopy and in the inter-row region. Soil irradiance measurements were taken next to the trunk and on each side of the centre of the row. This arrangement created a symmetrical and equidistant pattern of soil surface irradiance. The solarimeter positions for each canopy are presented in Table 4.2. In the case of the tramline Valencia orchard in Brits (Table 4.1), the position mid-way between two adjacent rows was taken as the "tree row" position for the simulation (Table 4.2, tube solarimeter No. 4).

The solarimeters were coupled to a CR10 data-logger through an AM416 multiplexer. Milli-volt readings were taken every 10 s for each solarimeter, converted to solar radiation values (W m^{-2}) with the appropriate calibration value and these values were averaged over one hour intervals. Above canopy radiation was measured at automatic weather stations erected in a nearby open area. The AWS was equipped with a CR10X data logger coupled to a LI 200X pyranometer to measure solar radiation. The data logger was programmed to take readings every 10 s and automatically calculate and record hourly averages. The logged data was regularly downloaded using a laptop computer.

Radiation data were collected from the various sites during the second half of 1999 and collection details are summarised in Table 4.3. In the case of the Leucaena hedgerows, leaves were stripped from the canopy in a uniform manner to give a range of leaf area densities. The peach hedgerow was measured at the beginning of the season when the canopy was in the initial period, approximately a month later during the development period and then when the canopy was fully developed at fruit harvest.

The required parameter values are also presented in Table 4.3. These, as well as the respective values in Tables 4.1 and 4.2, were used as the defining parameters for the hedgerow canopies used in simulating the radiant transmittance. As can be seen in the Tables, a considerable range was covered. Not only were the measurements done from the end of May to early December (i.e. including a good sample of different solar elevations and direct flux densities), the leaf area index ranged from negligible (0.45) to substantial (5.5). These differences contributed to a range in LAD from 0.3 to 2.16 m^2 leaves m^{-3} canopy volume. It must be pointed out that there were also differences in canopy structure; viz. a typical "lollipop" (dense ball stuck on a stem) structure as typified by the clementine orchard to the multiple stem scraggy hedge growth found in the Leucaena. There were also differences in leaf type in that the citrus and peach have simple leaves while the Leucaena has compound leaves. The orchard canopies also varied tremendously in that the Empress mandarin orchard was a relatively dense planting which approximated a one-dimensional system since little direct radiation penetrated to the soil. On the other extreme were the peach trees during the initial stage (i.e. soon after bud-break) when the foliage was sparse. The single row Leucaena site was also very open. The clementine, Valencia and mature peach hedgerows formed distinct two-dimensional systems with a dense high hedgerow canopy and a distinct inter-row region. Leaf absorptivity and the canopy extinction coefficient were assumed to be 0.5 for all simulations of total solar radiation transmission (see Section 2.1).

Table 4.1. List of tree crops monitored and their locality specifications.

Crop	Locality	Latitude	Longitude	Altitude (m)	Planting pattern	Spacing (m)	Row axis
Peach (*Prunus persica* cv. Transvaalia)	Hatfield Experimental Farm, Pretoria	25°45'S	28°16'E	1371	Hedgerow	4.5 x 1.0	E-W (110°-290°)
Leucaena *(Leucaena leucocephela)*	Hatfield Experimental Farm, Pretoria	25°45'S	28°16'E	1372	Single row	0.5	N-S (10°-190°) E-W (100°-280°)
Clementine (*Citrus reticulata* cv. Blanco)	Syferkuil Experimental Farm, Sovenga	23°51'S	29°40'E	1250	Hedgerow	7.5 x 3.5	NW-SE (135°-315°)
Valencia Delta (*Citrus sinesis* [L.] cv. Osbeck)	Commercial orchard, 15 km North of Brits	25°00'S	27°46'E	1107	Tramline	Two rows 4.0 x 4.0 with 8.0 m gap	NW-SE (135°-315°)
Empress mandarin (*Citrus reticulata* cv. Blanco)	Commercial orchard, 15 km North of Brits	25°00'S	27°46'E	1107	Hedgerow	4.0 x 2.0	NW-SE (135°-315°)

Table 4.2. Distances from the trunk (m) of tube solarimeters (No. 1 to 7) installed in different crops.

Crop	No. 4	No. 1 & 7	No. 2 & 6	No. 3 & 5
Peach	At tree trunk	+2 & -2	+1.32 & -1.32	+0.66 & -0.66
Leucaena	At tree trunk	+2.25 & -2.25	+1.5 & -1.5	+0.75 & -0.75
Clementine	At tree trunk	+3.75 & - 3.75	+2.5 & -2.5	+1.25 & 1.25
Valencia Delta	Between two adjacent rows	+6 & -6	+4 & -4	+2 & -2
Empress mandarin	At tree trunk	+2 & -2	+1.32 & -1.32	+0.66 & -0.66

Table 4.3. Radiation data collection programme and canopy parameters for crops monitored.

Crop	Time period (year 1999)		Canopy status	Tree height (m)	Canopy width (m)	Stem height (m)	Leaf area index	Leaf area density ($m^2\ m^{-3}$)
	Date	Day of year						
Peach	9 Sep. to 19 Sep.	252 to 262	Initial canopy	3.0	1.8	0.3	0.45	0.30
	5 Oct. to 31 Oct.	278 to 304	Developing canopy	3.2	2.1	0.3	1.92	0.95
	4 Nov. to 22 Nov.	308 to 326	Full canopy	3.3	2.6	0.4	4.05	1.75
Leucaena	30 May	150	Full canopy (N-S)	2.8	2.8	0	3.39	1.55
	31 May	151	1st Strip (N-S)	2.8	2.8	0	2.67	1.22
	1 June	152	2nd Strip (N-S)	2.8	2.8	0	1.00	0.46
	2 June to 3 June	153 - 154	No leaves (N-S)	2.8	2.8	0	0.51	0.23
	5 June to 9 June	156 -160	Full canopy (E-W)	2.8	3.2	0	3.18	1.40
	10 June	161	1st Strip (E-W)	2.8	3.2	0	2.32	1.00
	11 June	162	No leaves (E-W)	2.8	3.2	0	0.89	0.39
Clementine	3 Dec. to 11 Dec.	337 to 345	Full canopy	3.1	4.0	0.3	5.5	2.16
Valencia Delta	6 July to 20 July	187 to 201	Full canopy	4.3	8.2	0	4.18	1.26
Empress mandarin	20 July to 5 Aug	201 to 217	Full canopy	4.0	2.8	0.4	4.17	1.50

4.3.2. Peach trial (Hatfield)

Figures 4.16 to 4.23 show measured and simulated radiant transmittance at various positions under the canopy of peaches grown in Hatfield. The measured radiant transmittance is represented with symbols, whilst the solid lines are SWB simulations. Next to each graph, the calculated parameters of the statistical analysis between measured and simulated data can be seen. This allows quick, efficient and quantitative evaluation of model performance. The parameters of the statistical analysis are:

i) Number of observations (N);
ii) Coefficient of determination (r^2);
iii) Index of agreement of Willmott (1982) (D);
iv) Root mean square error (RMSE); and
v) Mean absolute error (MAE).

These were recommended by de Jager (1994) to assess model accuracy. He also recommended as model prediction reliability criteria that r^2 and D should be > 0.8, whilst MAE should be < 20%.

The simulations were done for initial, development and mid-stages during the fourth season of growth. The growth stages were associated with different leaf area densities (Table 4.3). This gave the opportunity to test the model under different conditions of canopy size and density.

Data for the initial stage are shown in Figures 4.16 to 4.19. Figure 4.16 represents simulated and measured daily solar radiation in MJ m^{-2} d^{-1}. During the initial stage, i.e. soon after bud-break, the solar radiation reaching the soil surface is well predicted (i.e. little canopy interference). However, it can be noticed that on the southern side at 0.64 and 1.28 m from the tree row, the predicted daily solar radiation is too high. Figure 4.17 shows simulated and measured hourly solar radiation in W m^{-2}. Again, the model appeared to overestimate solar radiation at 0.64 m from the tree row on the southern side. The radiant transmittance across the row for a typical day during the initial stage of the crop, can be seen in Figure 4.18 for 12/09/1999 and in Figure 4.19 for the same day at 13 h. The predicted high soil irradiance in the northern inter-row area, and reducing under the tree as well as on the southern, shaded, inter-row area, was in agreement with the observations. However, the model overestimated irradiance on the southern side, especially at 0.64 m from the tree row. The main reason for the discrepancies between measurements and model predictions was attributed to the presence of trunk and branches shading the tube solarimeters on the southern side of the tree row.

A month later, during the development stage of the crop, the measurements and simulations were repeated. Reasonable agreement was generally observed between measurements and simulations for both daily (Figure 4.20) and hourly solar radiation (Figure 4.21).

Data were also collected during the stage of full canopy development (around harvest, Figures 4.22 and 4.23). During this period, good agreement between measured and simulated values was observed under the tree canopy. The model, however, underestimated daily solar radiation in the inter-row area, in particular at 1.28 m and 1.92 m from the tree row on the northern side. The reason for these discrepancies is primarily due to the shape of the peach hedgerow. Firstly the cross-sectional shape of the canopy was not perfectly elliptical; it would be better approximated by a triangle. Secondly, and most probably more importantly, the long axis of the canopy ellipse was not normal to the soil surface. Instead of this axis being vertical, it was inclined towards the South. In other-words, the hedgerow canopy was not symmetrical but lent to the South. Coupled to this was the fact that there was not a completely uniform distribution of leaves within the canopy.

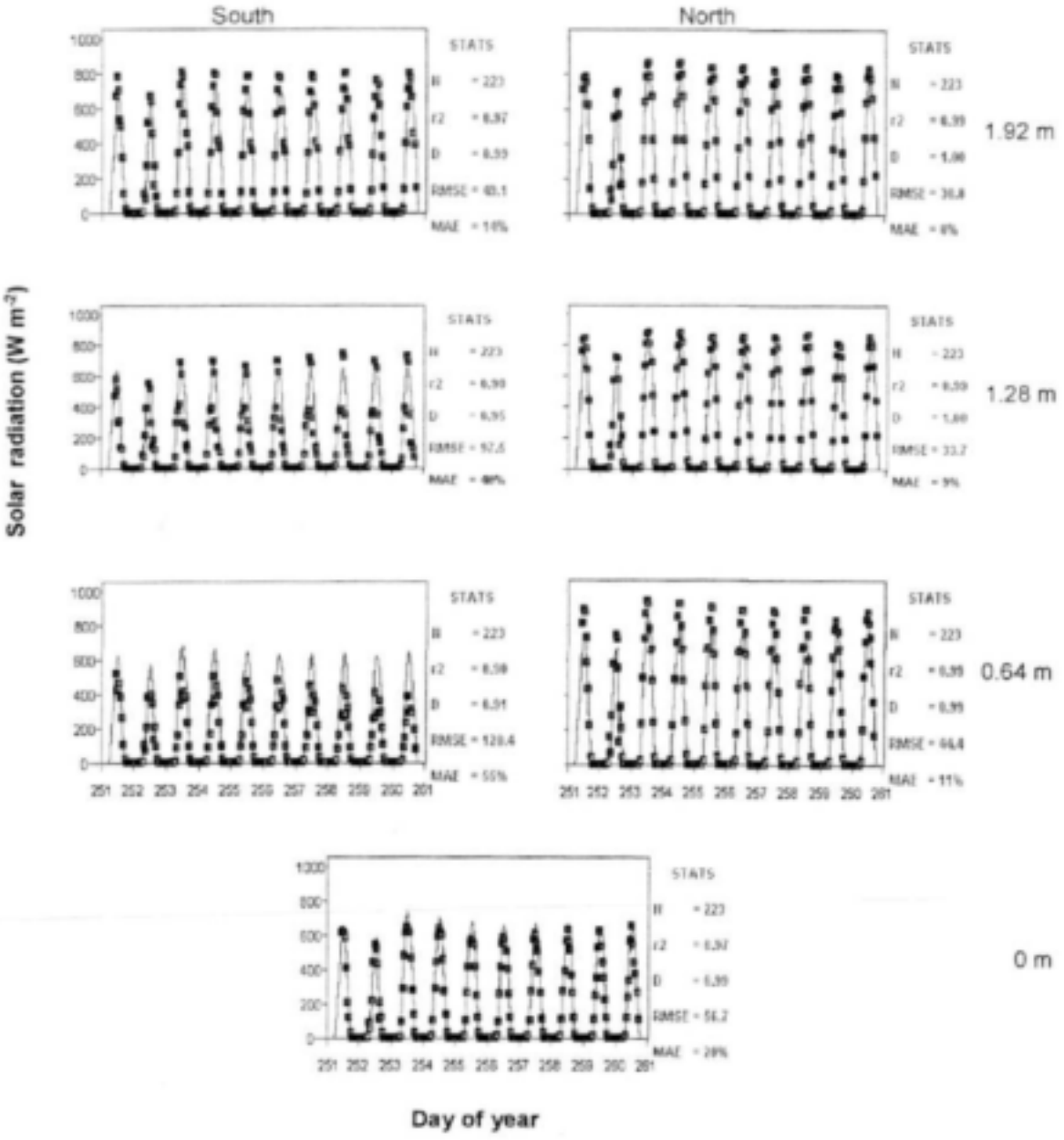

Figure 4.17. Measured (symbols) and simulated (lines) hourly solar radiation at different sides and distances from the tree row in a hedgerow peach orchard (from 09/09/1999 to 19/09/1999, initial stage of the crop).

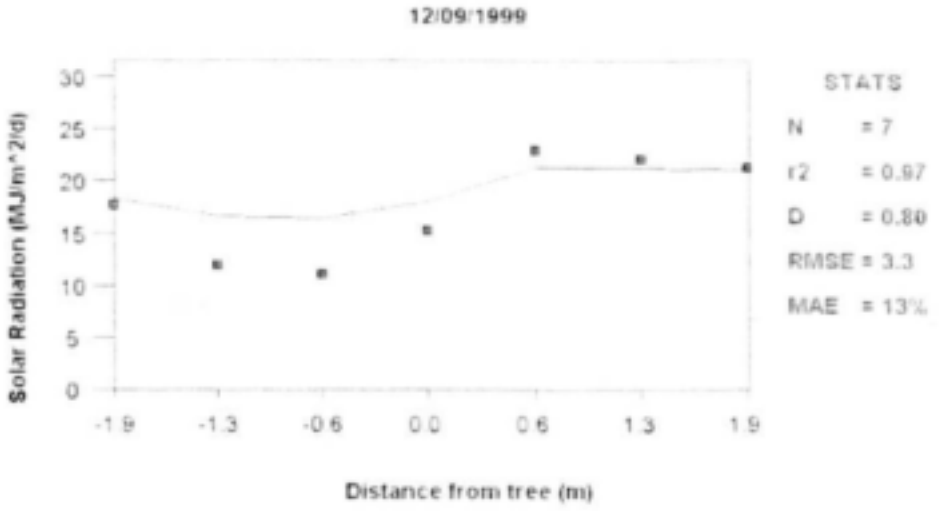

Figure 4.18. Measured (symbols) and simulated (lines) daily solar radiation across the peach hedgerow on 12/09/1999 (initial stage of the crop).

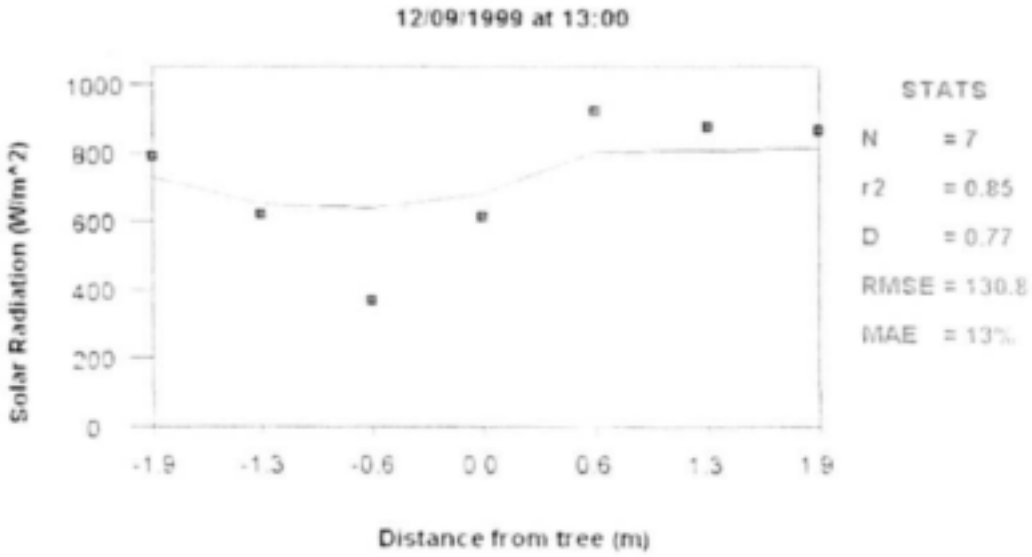

Figure 4.19. Measured (symbols) and simulated (lines) hourly solar radiation across the peach hedgerow on 12/09/1999 at 13 h (initial stage of the crop).

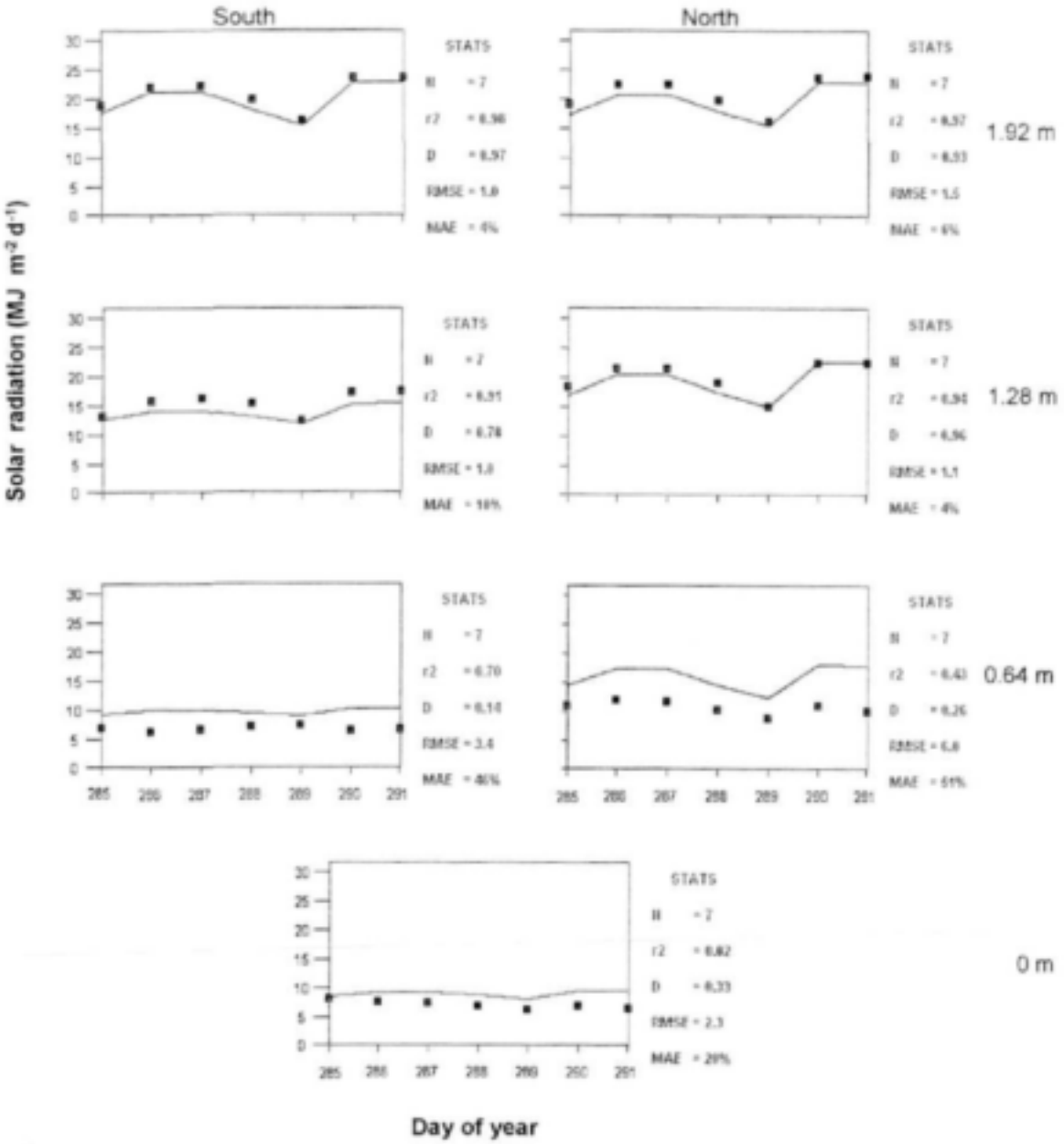

Figure 4.20. Measured (symbols) and simulated (lines) daily solar radiation at different sides and distances from the tree row in a hedgerow peach orchard (from 13/10/1999 to 19/10/1999, development stage of the crop).

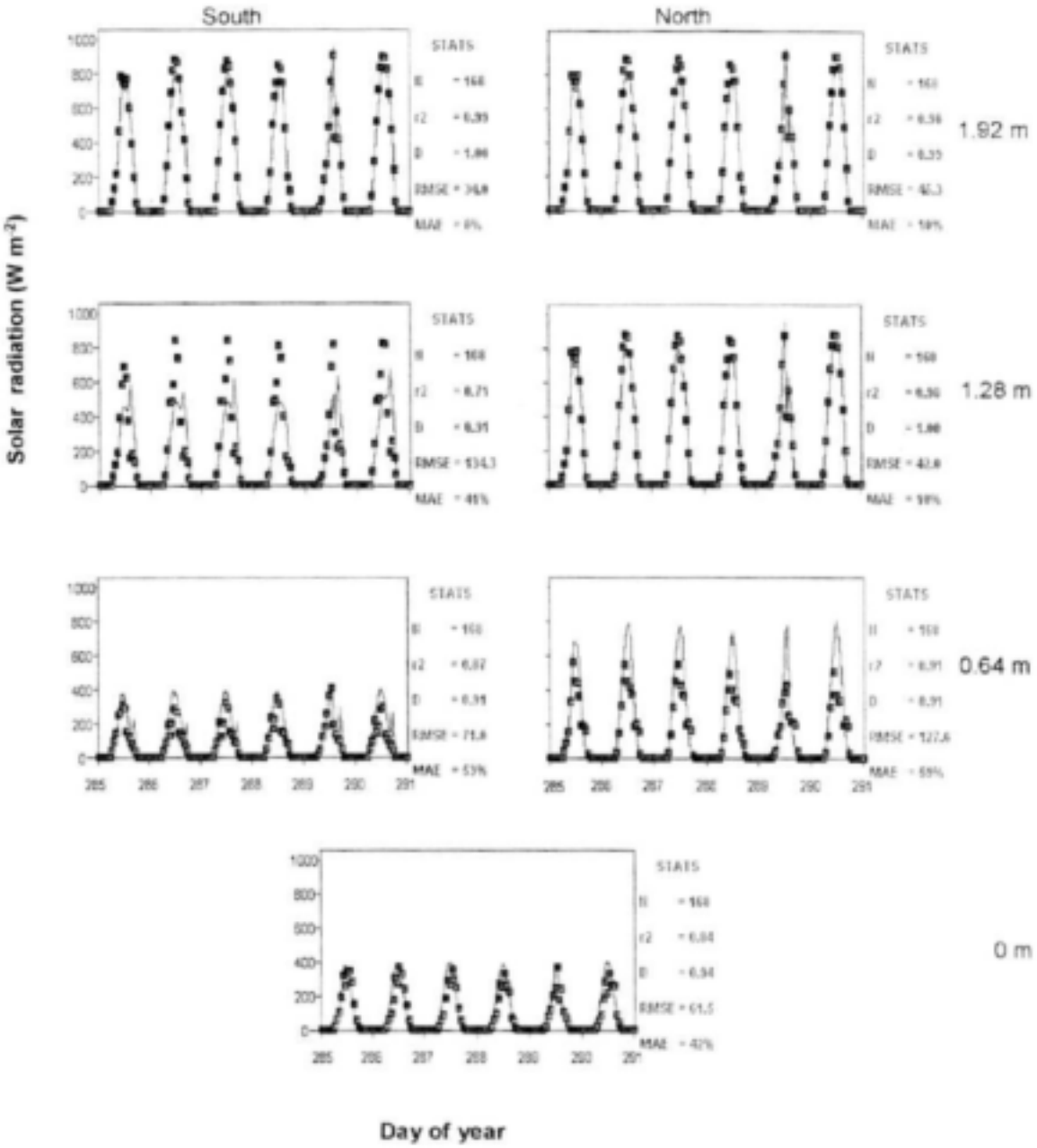

Figure 4.21. Measured (symbols) and simulated (lines) hourly solar radiation at different sides and distances from the tree row in a hedgerow peach orchard (from 13/10/1999 to 19/10/1999, development stage of the crop).

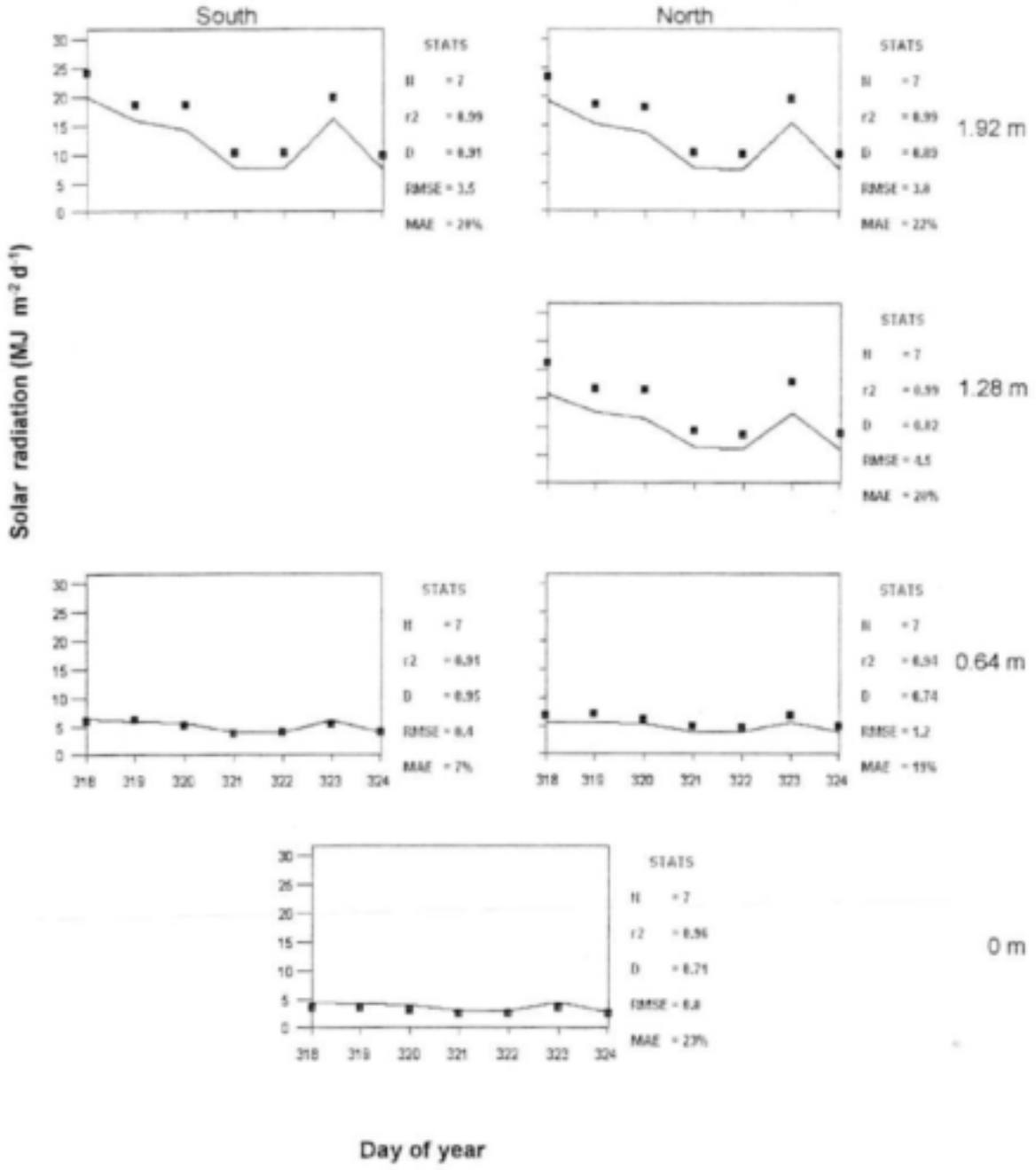

Figure 4.22. Measured (symbols) and simulated (lines) daily solar radiation at different sides and distances from the tree row in a hedgerow peach orchard (from 15/11/1999 to 21/11/1999, at harvest).

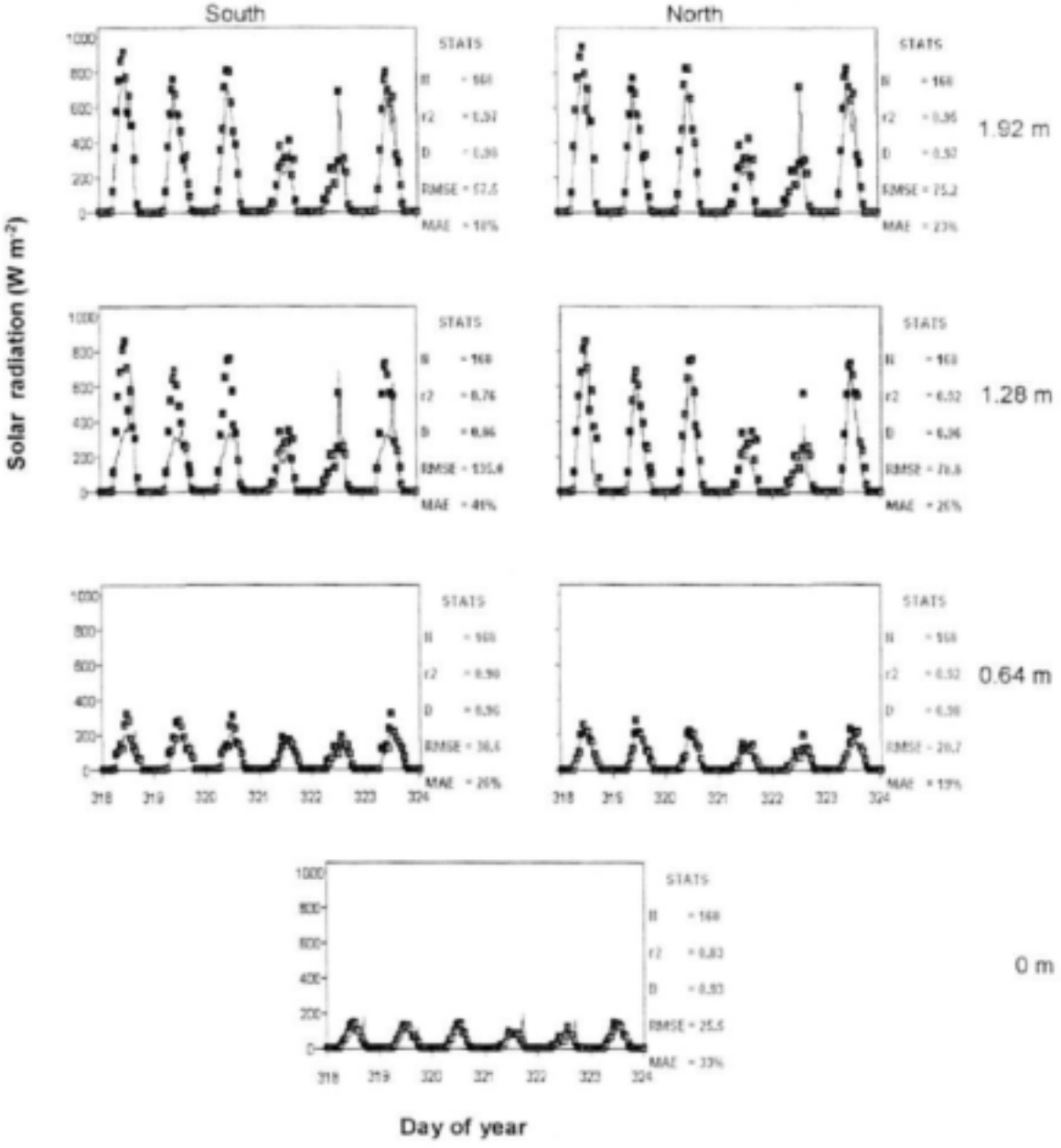

Figure 4.23. Measured (symbols) and simulated (lines) hourly solar radiation at different sides and distances from the tree row in a hedgerow peach orchard (from 15/11/1999 to 21/11/1999, at harvest).

4.3.3. Leucaena trial (Hatfield)

Figures 4.24 to 4.30 show measured and simulated hourly radiant transmittance at various positions under the canopy of Leucaena grown in Hatfield.

The simulations were done for two single tree rows planted in N-S and E-W row axes (Table 4.1) in order to test the model for different row orientations. Also, leaves were uniformly stripped on several occasions during the course of the trial in order to test the model for different leaf area densities (Table 4.3).

The model predicted radiant transmittance through the canopy at different distances from the tree row generally well, as well for different row orientations and canopy densities. However, the model tended to underestimate hourly solar radiation at low values of leaf area density. This is particularly evident in Figures 4.26 and 4.27 (N-S row orientation), as well as in Figures 4.29 and 4.30 (E-W orientation). A possible reason for this discrepancy is the model calculation of diffuse and direct solar radiation. It appeared from the data that the model places too much weight on the diffuse component of solar radiation, which was particularly evident at positions close to the canopy. The presence of the canopy therefore induced a reduction in the calculated radiant transmittance at these nodes. This will have to be investigated further.

The Leucaena hedgerow canopy had similar properties to the peach hedgerow, i.e. non-symmetrical and having a heterogeneous plant material distribution within the canopy (leaves, trunks and branches). This could also be the reason for discrepancies between measurements and simulations.

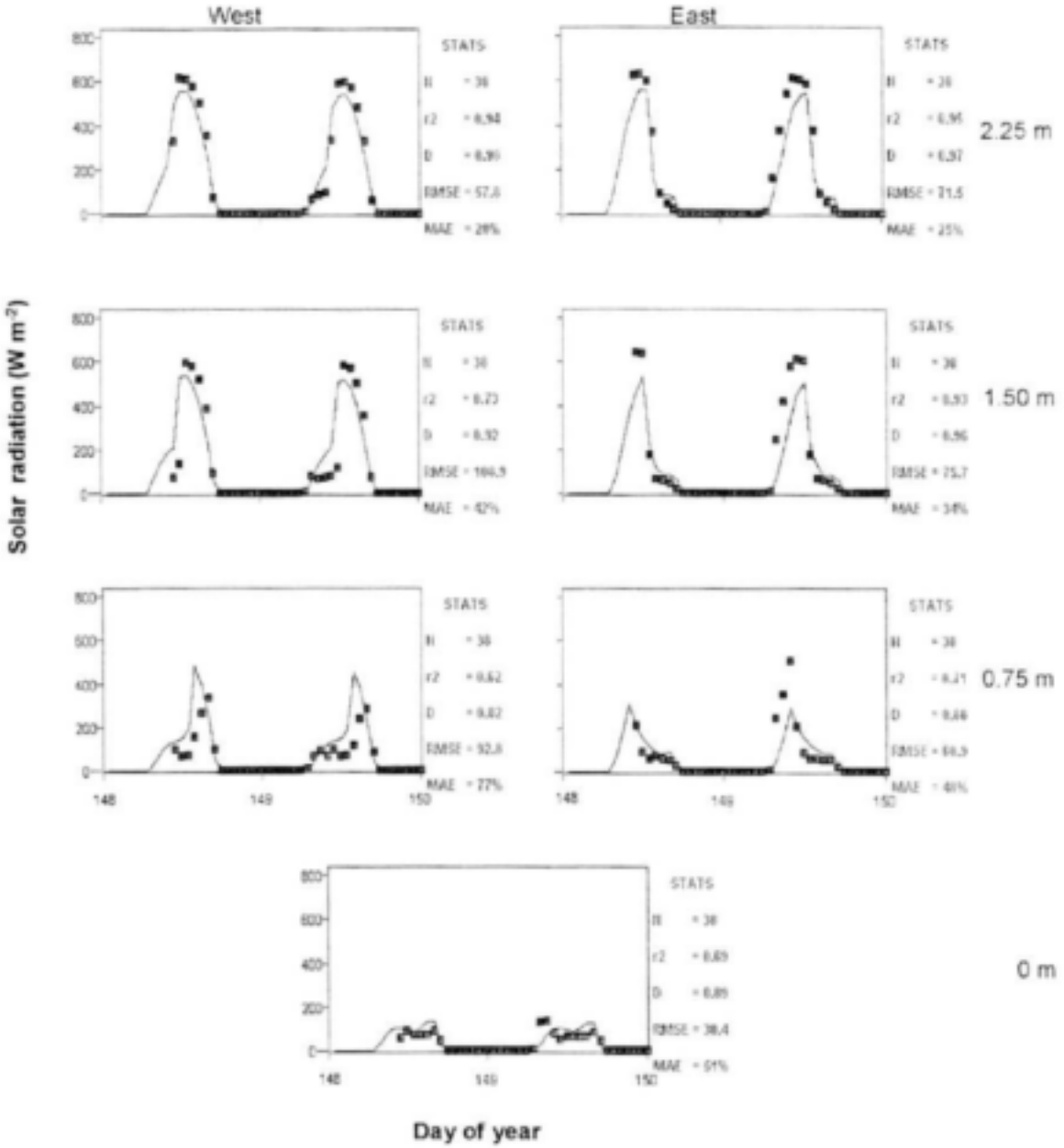

Figure 4.24. Measured (symbols) and simulated (lines) hourly solar radiation at different sides and distances from the tree row in a hedgerow Leucaena planting (from 29/05/1999 to 30/05/1999, row axis N-S; LAD = 1.55 m^2 m^{-3}).

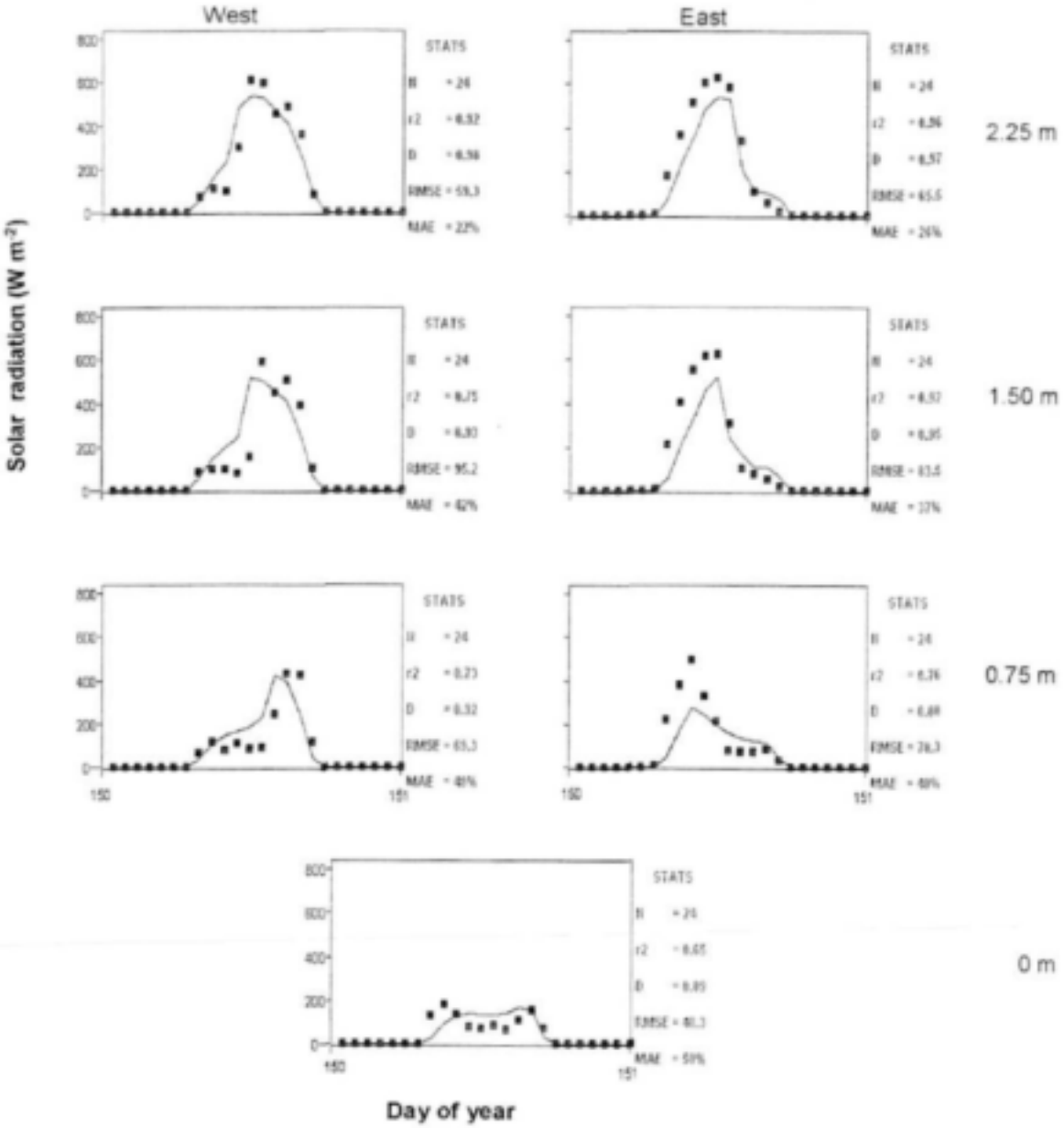

Figure 4.25. Measured (symbols) and simulated (lines) hourly solar radiation at different sides and distances from the tree row in a hedgerow Leucaena planting (on 31/05/1999; row axis N-S; LAD = 1.22 m^2 m^{-3}).

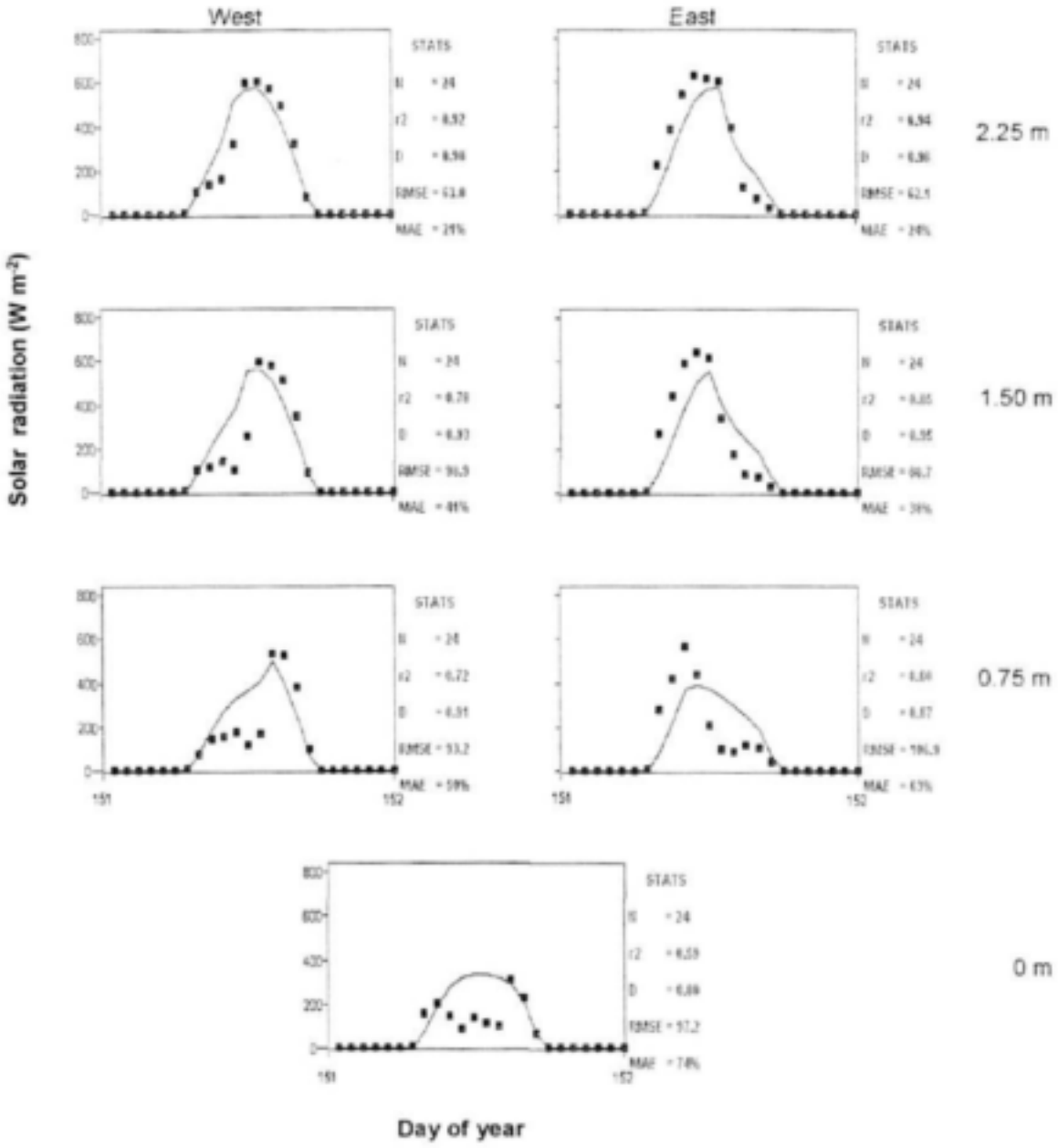

Figure 4.26. Measured (symbols) and simulated (lines) hourly solar radiation at different sides and distances from the tree row in a hedgerow Leucaena planting (on 01/06/1999; row axis N-S; LAD = 0.46 m^2 m^{-3}).

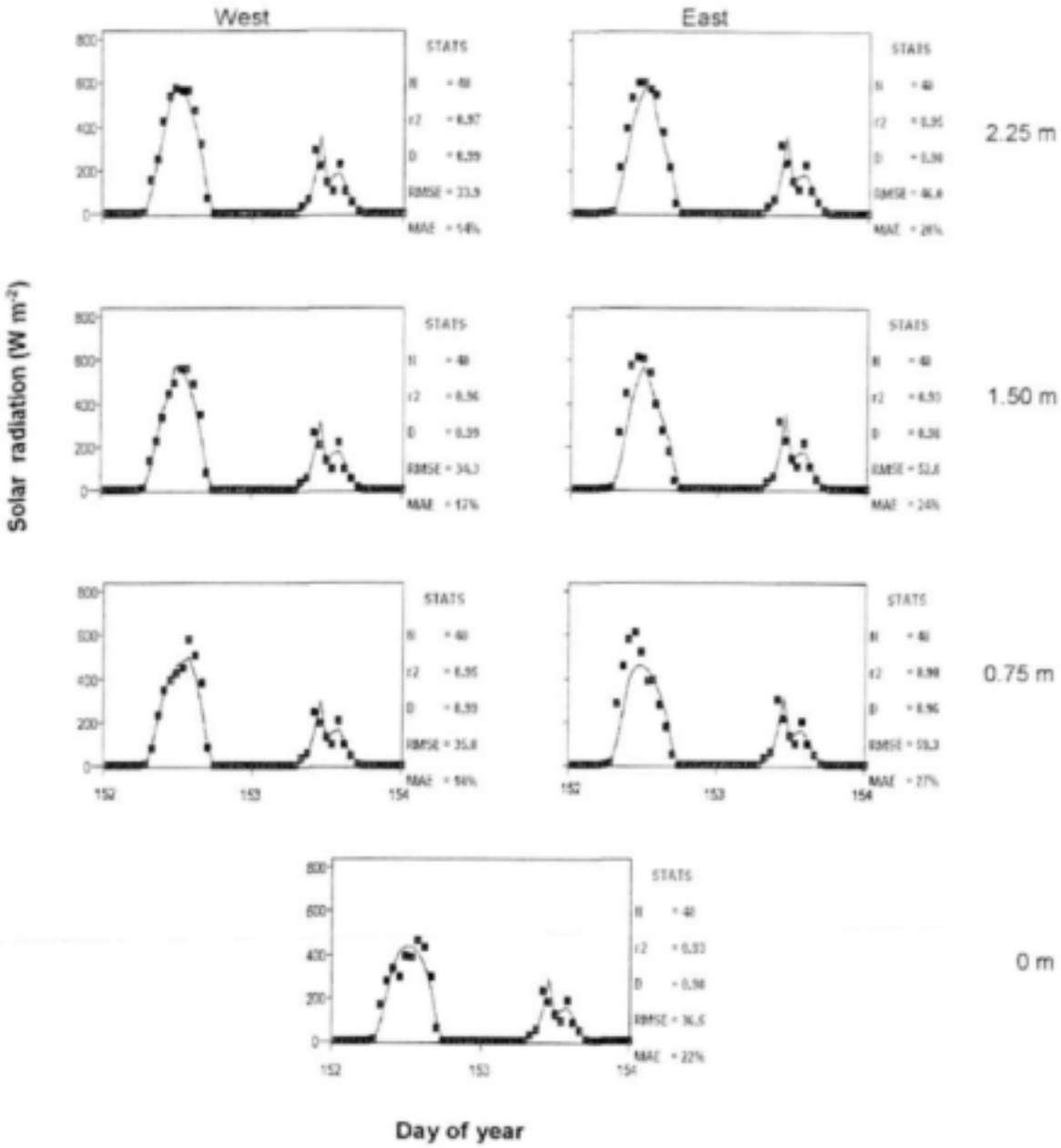

Figure 4.27. Measured (symbols) and simulated (lines) hourly solar radiation at different sides and distances from the tree row in a hedgerow Leucaena planting (from 02/06/1999 to 03/06/1999; row axis N-S; LAD = 0.23 m^2 m^{-3}).

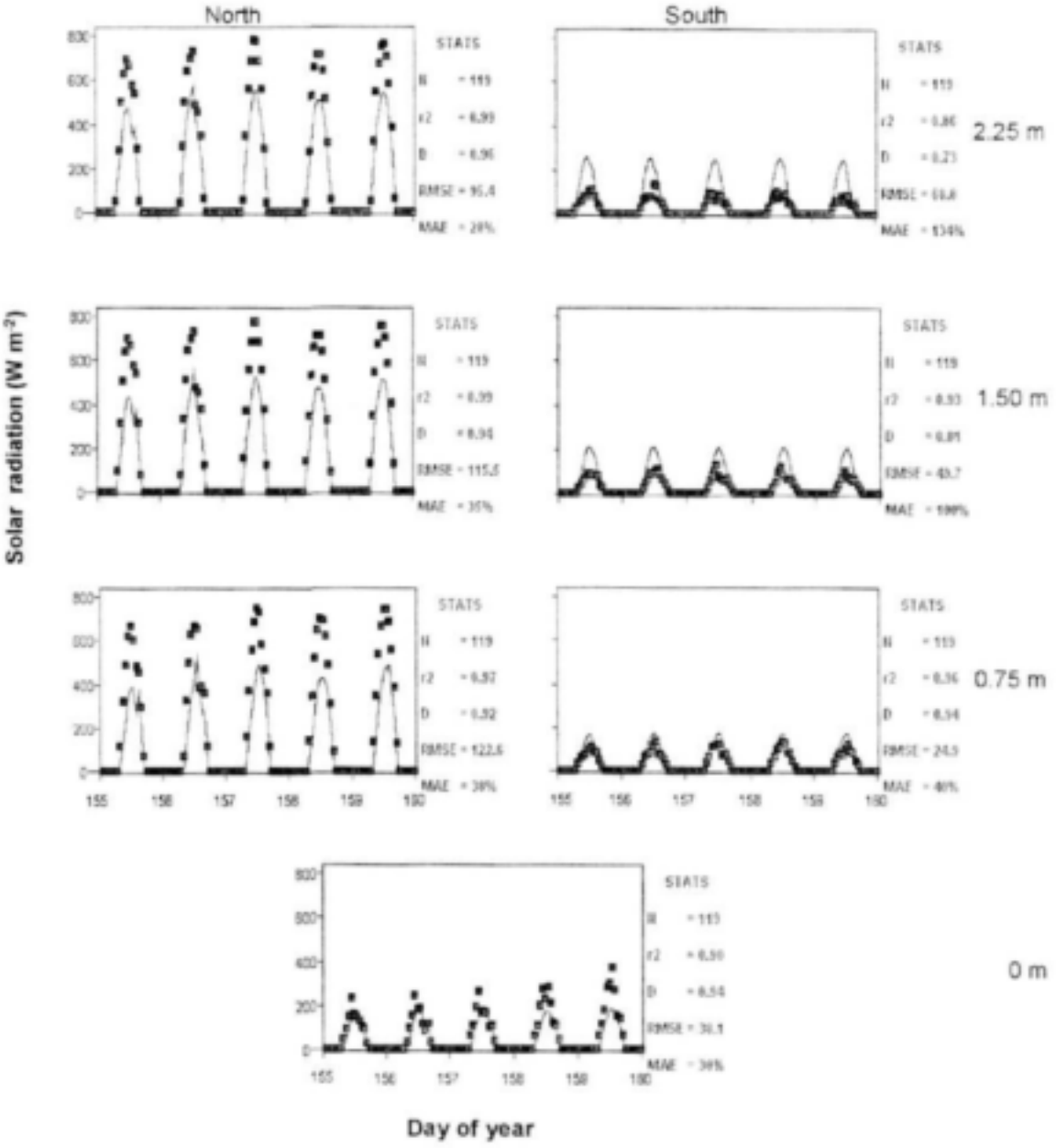

Figure 4.28. Measured (symbols) and simulated (lines) hourly solar radiation at different sides and distances from the tree row in a hedgerow Leucaena planting (from 05/06/1999 to 09/06/1999; row axis E-W; LAD = 1.40 m^2 m^{-3}).

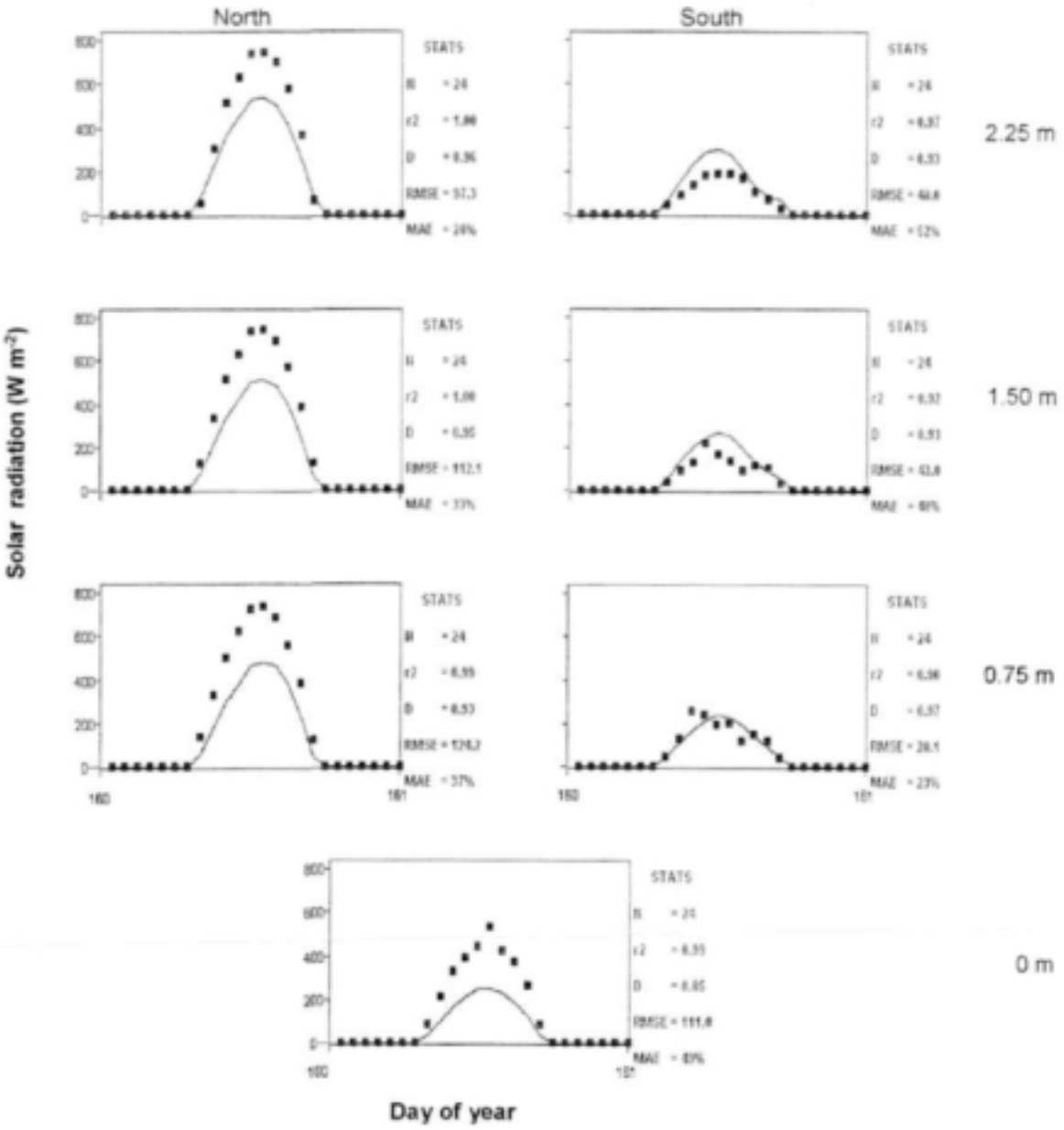

Figure 4.29. Measured (symbols) and simulated (lines) hourly solar radiation at different sides and distances from the tree row in a hedgerow Leucaena planting (on 10/06/1999; row axis E-W; LAD = 1.00 m^2 m^{-3}).

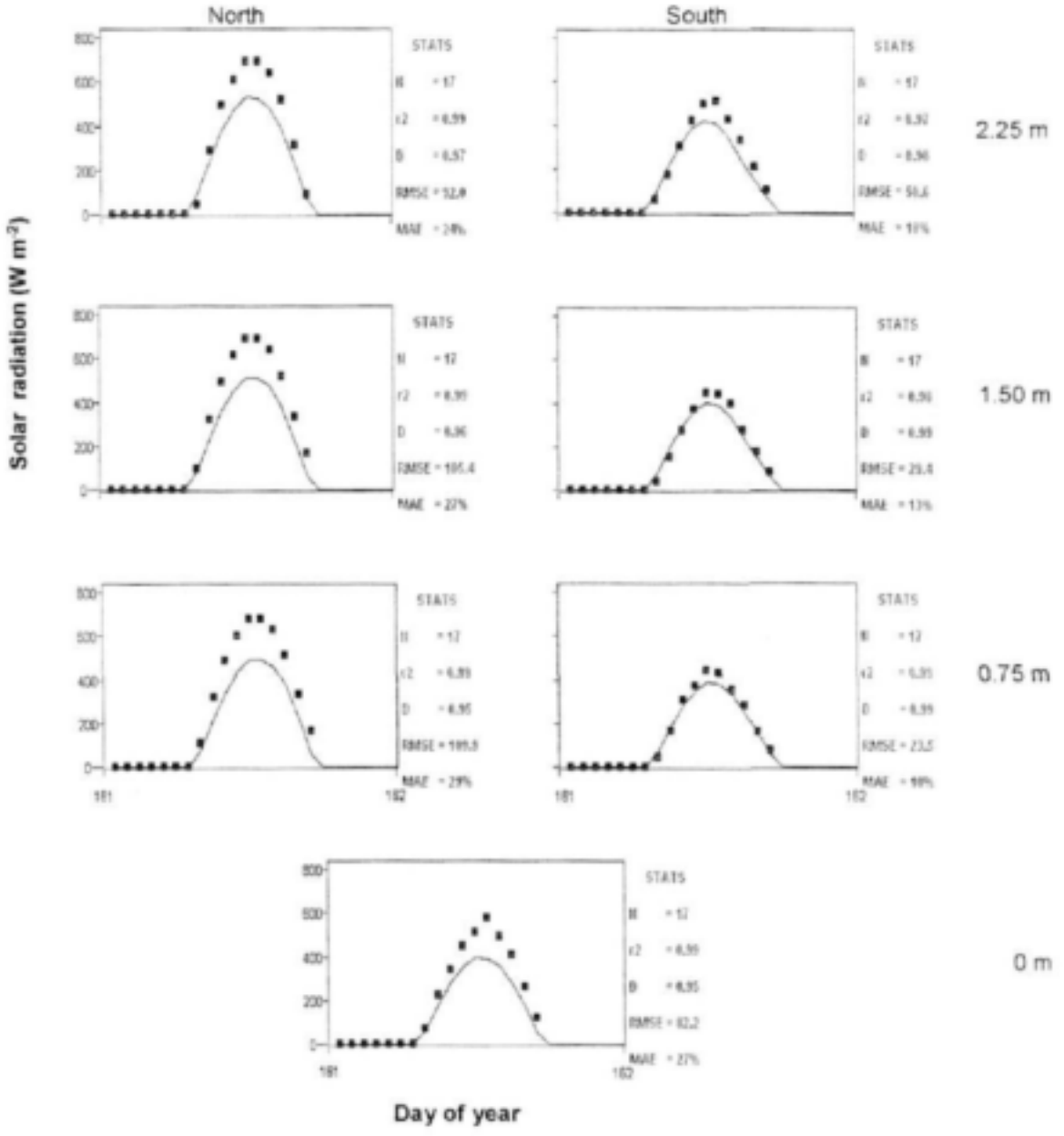

Figure 4.30. Measured (symbols) and simulated (lines) hourly solar radiation at different sides and distances from the tree row in a hedgerow Leucaena planting (on 11/06/1999; row axis E-W; LAD = 0.39 m^2 m^{-3}).

4.3.4. Citrus trial (Syferkuil)

Figures 4.31 and 4.32 depict daily and hourly radiant transmittance in the clementine hedgerow orchard at Syferkuil. Very good agreement between simulated and measured values was observed for all positions under the canopy. The MAE was higher then the reliability criteria of 20% at the tree row and at 1.25 m on either side of the tree row. However, the measured and simulated values at these positions were generally so small that large mean absolute errors were calculated for small discrepancies between measurements and simulations.

An additional simulation was carried out to test the model prediction of transmittance of photosynthetically active radiation (PAR). PAR was measured with line quantum sensors placed adjacent to the tube solarimeters. Leaf absorptivity for PAR was assumed to be 0.8 (Goudriaan, 1977). The canopy extinction coefficient for PAR (K_{PAR}) was calculated to be 0.71 using the procedure described by Jovanovic and Annandale (1998), where:

$$k_{PAR} = k\,(\alpha_p\,\alpha_s)^{0.5}$$

where k is the canopy extinction coefficient for total solar radiation, α_p is leaf absorptivity for PAR and α_s the leaf absorptivity for total solar radiation. k was assumed to be 0.5 (see Section 2.1), α_p is 0.8 (Goudriaan, 1977) and α_s was calculated as the geometric mean of absorptivities in the PAR and near-infrared range (α_n):

$$\alpha_s = (\alpha_p\,\alpha_n)^{0.5}$$

where leaf absorptivity in the near-infrared range (α_n) is equal to 0.2 (Goudriaan, 1977).

Simulated and measured values of PAR (in mol cm^{-2} s^{-1}) are compared in Figure 4.33 for different distances from the tree row. The model predicted PAR generally well.

In the case of the simulations at Syferkuil, the major reason for discrepancies between measured and simulated data for both total solar radiation and PAR, was the presence of irregular branches and a not completely uniform distribution of leaves within the canopy.

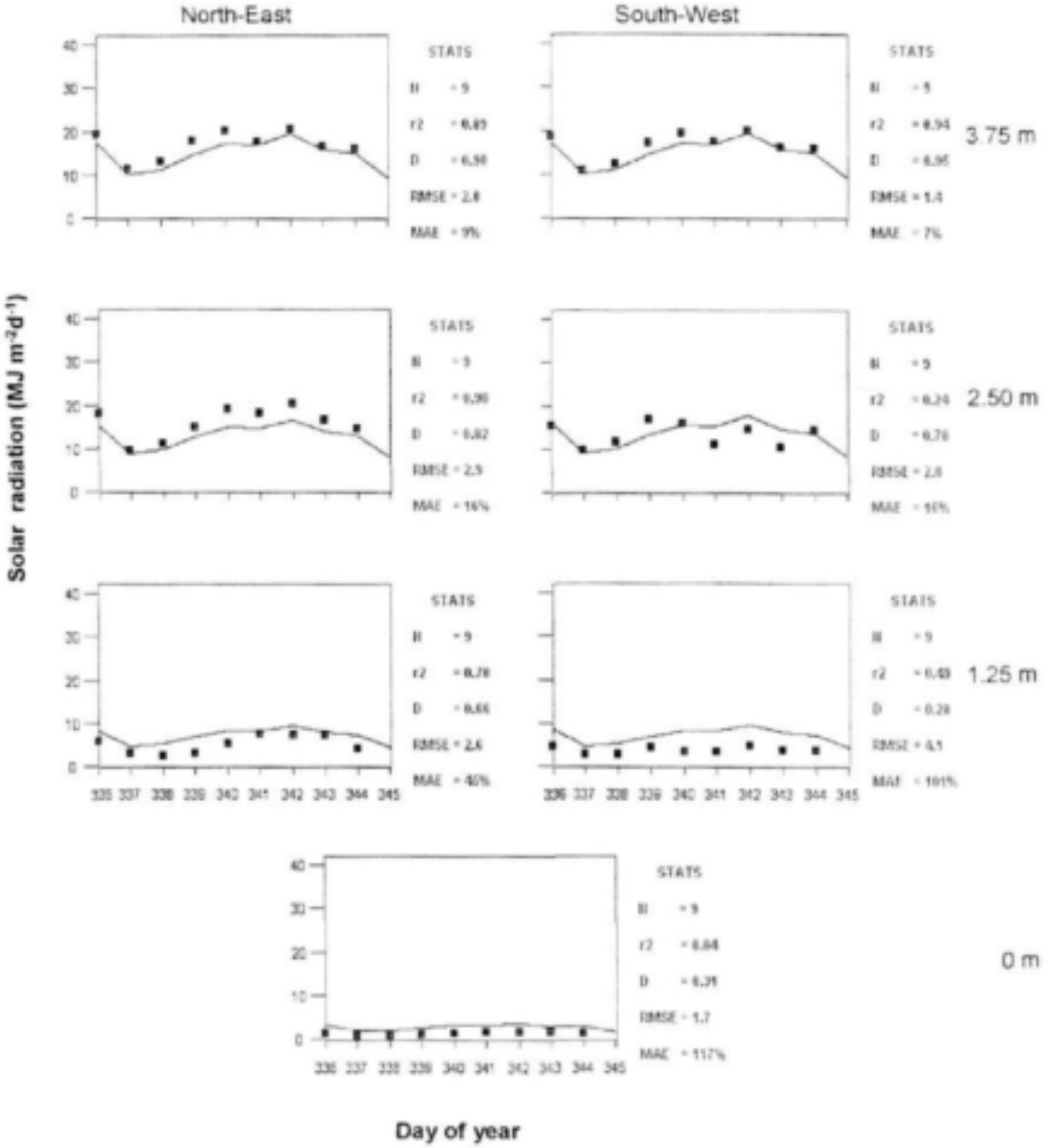

Figure 4.31. Measured (symbols) and simulated (lines) daily solar radiation at different sides and distances from the tree row in a hedgerow clementine orchard (from 03/12/1999 to 11/12/1999).

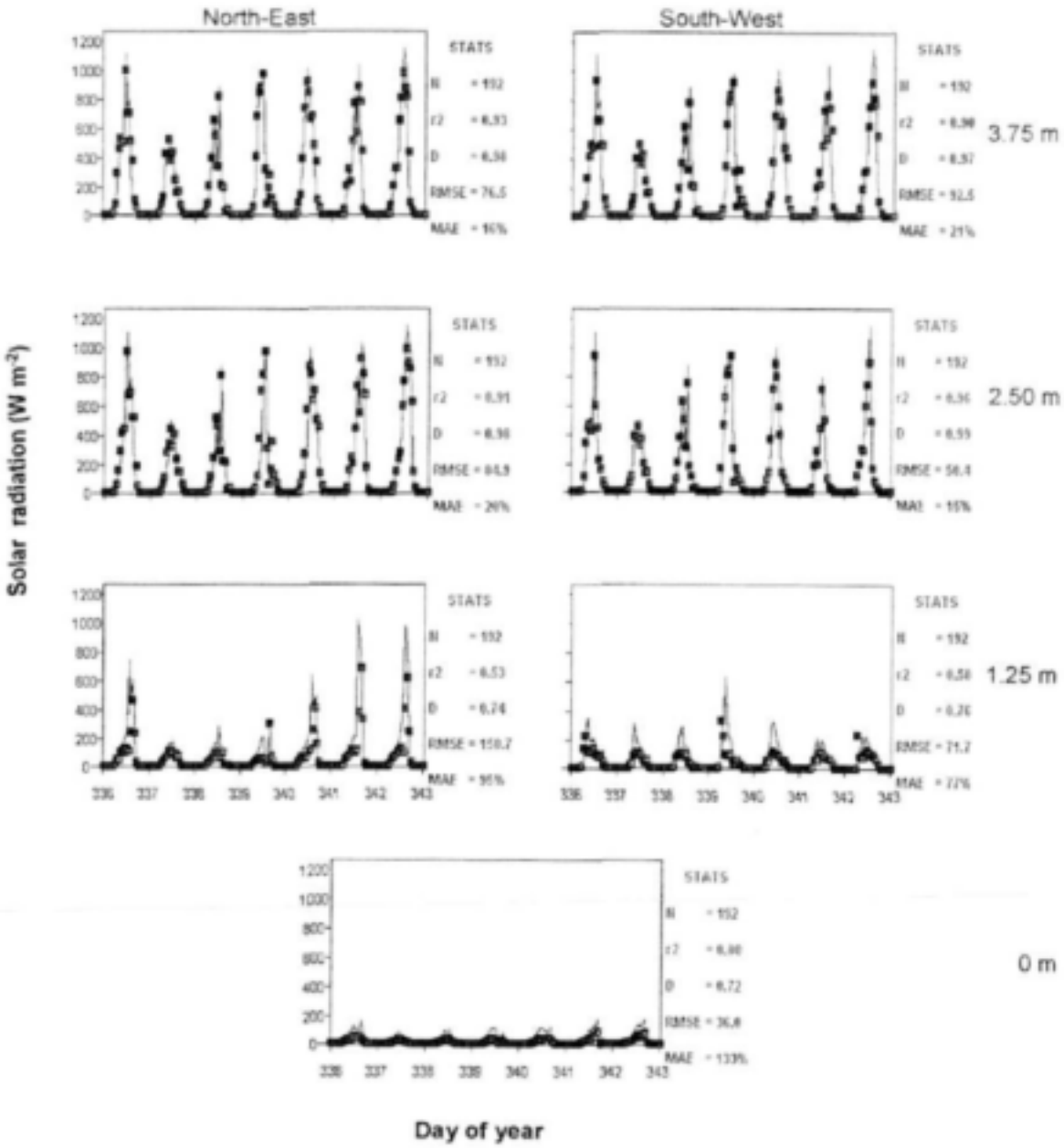

Figure 4.32. Measured (symbols) and simulated (lines) hourly solar radiation at different sides and distances from the tree row in a hedgerow clementine orchard (from 03/12/1999 to 09/12/1999).

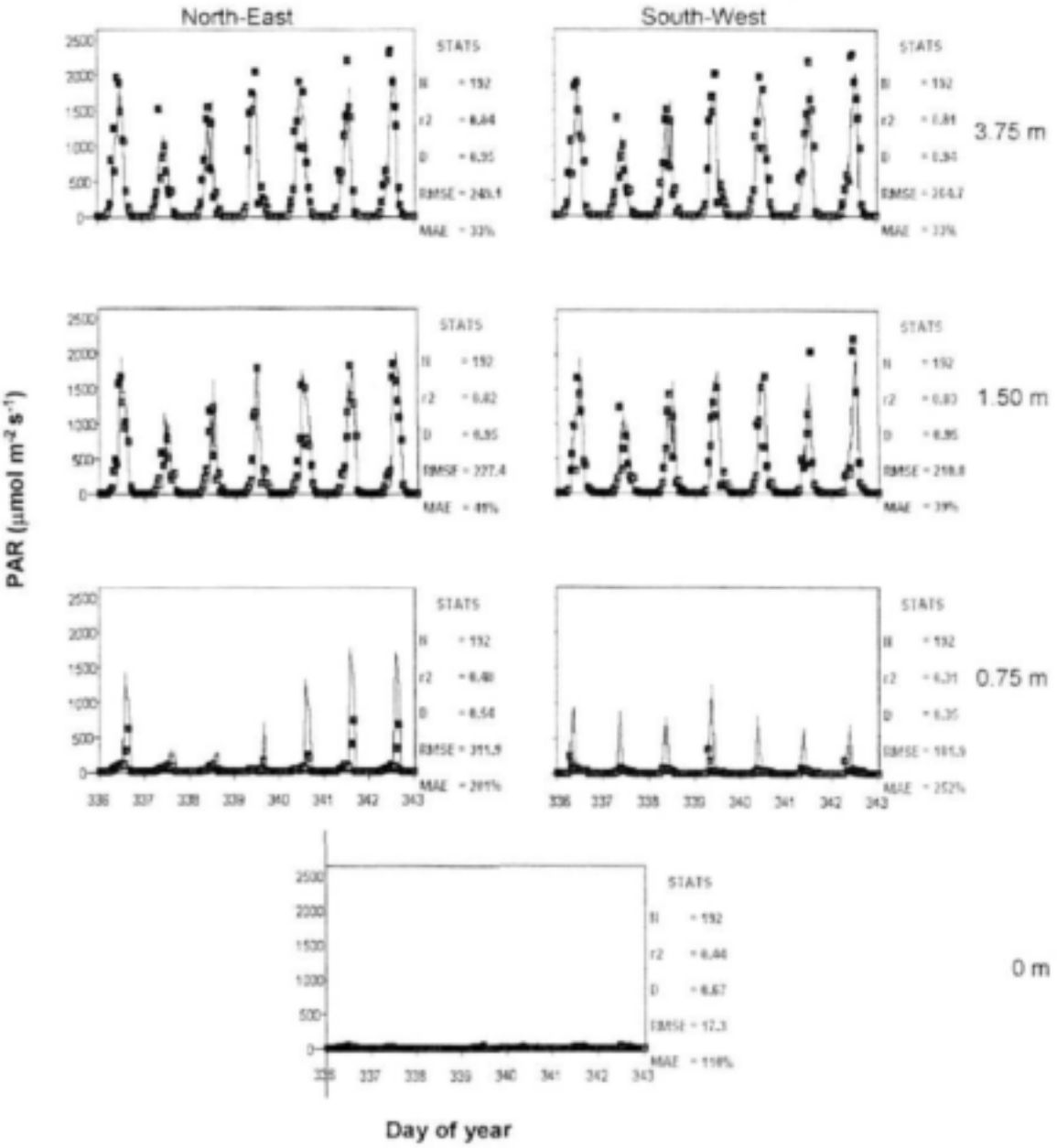

Figure 4.33. Measured (symbols) and simulated (lines) photosynthetically active radiation (PAR) at different sides and distances from the tree row in a hedgerow clementine orchard (from 03/12/1999 to 09/12/1999).

4.3.5. Citrus trial (Brits)

Two radiation trials were carried out in Brits in order to test the two-dimensional radiation interception model for evergreen tree crops under different conditions, in particular for different row orientations (Table 4.1).

The results from the hourly observations and simulations in the tramline Valencia hedgerow orchard are presented in Figure 4.34. Generally, there was reasonable agreement between the predicted and measured values. However, there were some anomalies, in particular at 4 m on the south-western side, and at 2 m on the north-eastern side of the tree row. This was likely due to the placement of the tube solarimeters, as in this tramline orchard the centre between two adjacent rows was assumed to be the "tree row" position (Table 4.2, tube solarimeter No. 4).

The results for the Empress mandarin hedgerow are presented in Figure 4.35 for hourly radiant transmittance. The canopy development of this orchard was extensive. The canopy base was covering 2.8 m of the 4 m row spacing, which gave a canopy cover of 70%. Coupled to this was a canopy height of 4 m. This created a situation where very low soil irradiance values were measured. The model overestimated soil irradiance in the inter-row area (1.32 m and 2 m from the tree row) on both sides of the tree row in the middle hours of the day. It was observed in the field that irregular branches and foliage shaded the tube solarimeters during these periods of the day.

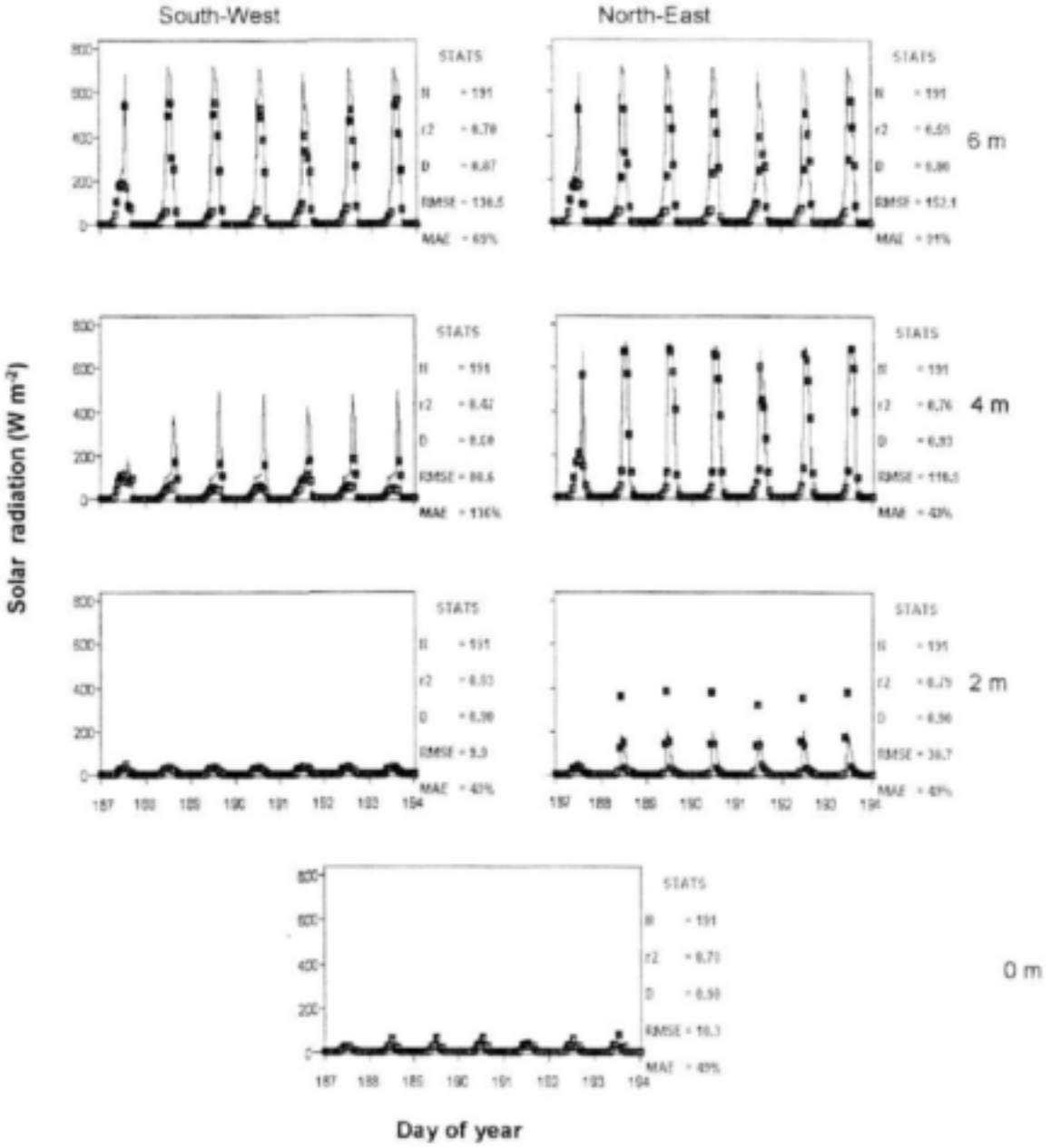

Figure 4.34. Measured (symbols) and simulated (lines) hourly solar radiation at different sides and distances from the tree row in a hedgerow Valencia orchard (from 07/07/1999 to 13/07/1999).

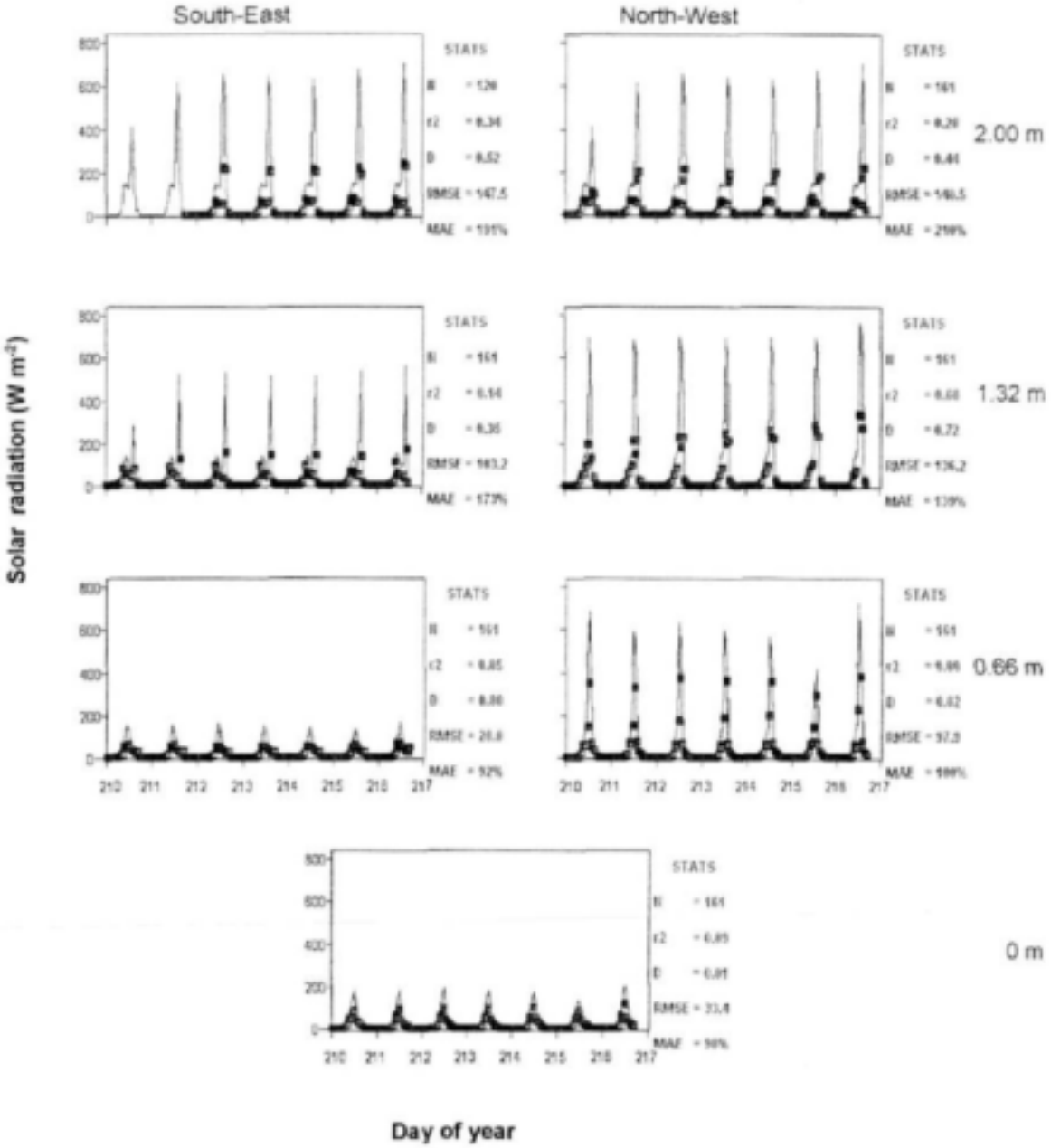

Figure 4.35. Measured (symbols) and simulated (lines) hourly solar radiation at different sides and distances from the tree row in a hedgerow mandarin orchard (from 30/07/1999 to 05/08/1999).

4.4. *Validation of the soil evaporation model*

4.4.1. Theoretical background

The rate of evaporation from a crop is dependent on meteorological conditions such as temperature, wind speed, relative humidity, and solar radiation (Penman, 1948). When crops are grown in widely spaced rows, the crop canopy does not completely cover the soil, and the exposed soil may receive large proportion of the incoming solar radiation, as well as evaporate significant amounts of water. Thus, investigating evaporation in a widely spaced row crop system requires that both the soil and canopy be examined (Tanner and Jury, 1976; Shuttleworth and Wallace, 1985; Lascano et al., 1987). This is particularly true for orchards, in which widely spaced rows bring large diurnal changes in exposure of plants and soil to solar radiation.

One technique available to measure evaporation is micro-lysimetry: it consists of measuring the mass loss by a small volume of wet soil in a container at the soil surface (Shawcroft and Gardner, 1983). The technique has been used extensively for measuring evaporation from bare soil (Caprio et al., 1985, Lascano and Van Bavel, 1986).

However, the practical use of micro-lysimeters is subject to several restrictions. Previous research showed that the rate of evaporation measured with micro-lysimeters and other techniques did often not match. For example, Boast and Robertson (1982), Matthias et al. (1986) and Steiner (1989) found that the measured crop total evapotranspiration exceeded the sum of plant transpiration and soil surface evaporation (measured using micro-lysimeters). On the contrary, soil evaporation values exceeding plant evapotranspiration by almost 125% were reported by Unger and Phillips (1973).

One condition for the micro-lysimeter to give accurate measurement of evaporation is that the soil in the micro-lysimeter be representative of the rest of the orchard. However, installing the lysimeter without disturbing the soil, as Boast and Robertson (1982) proposed, is practically impossible. As a consequence, Shawcroft and Gardner (1983) found that the conditions inside the isolated micro-lysimeters were different from those of the surrounding soil. Also, the interpretation of evaporation measurements made with micro-lysimeters is often difficult. One of the problems is that significant drying of the soil surface usually occurs when the evaporation rate from the surface layer exceeds the rate of water movement toward the surface from the underlying soil layers. Since evaporation depends on the soil surface water content (Black et al., 1970) the rate of evaporation measured with the micro-lysimeter changes over time: after an irrigation event, the soil surface is wet and the evaporation is limited by the net radiation received. Then the supply of water by the soil to the surface becomes limiting and evaporation decreases as the soil becomes drier. Therefore, two stages can be distinguished: the first one is called energy- or demand-limited, whereas the second one is called water- or supply-limited. This behaviour, already reported in previous lysimeter studies (Phillips 1957, Black et al. 1969), was modelled by Ritchie (1972). This model has since then been widely adopted in various lysimeter studies (Villalobos and Fereres 1990, Yanusa et al. 1993).

Theoretical approaches have also been developed to describe and quantify the evaporation process. They are based on the notion of energy fluxes: evaporation being determined by the amount of energy supplied to bring water from the liquid or bound phase to the vapour phase, and can be quantified by estimating radiant and heat fluxes. These studies have provided some clues to explain the discrepancies in experimental measurements. Walker (1984) measured evaporation from a wet soil under a row crop and found that the latent heat flux often exceeded the available radiative energy, suggesting that sensible heat transport from the crop to the soil was influencing evaporation. On the contrary, by examining the within-canopy profiles of heat and water vapour, Begg et al. (1964), as well as Brown and Covey (1966) concluded that there was a sensible heat flux from the soil and lower leaves to

the top of the canopy. Similar observations were reported by Tanner (1960) and Fuchs (1972).

The objectives of this trial were: i) to establish the temporal and spatial patterns of radiative energy interception at the soil surface under the orchard, ii) to measure the spatial and temporal distribution of evaporation in the orchard, iii) to use these data to validate the SWB model for orchards, in particular the procedures concerning radiation interception and evaporation.

4.4.2. Overview of the field trial

A brief overview of the methods used in the soil evaporation trial is given. This study was conducted in the peach trial during the 2000-2001 season at the Hatfield experimental farm. Weather data were collected with an automatic weather station (see Section 3.1.5). Solar radiation interception at the soil surface was determined using seven tube solarimeters (see Section 3.1.7.2). For this particular trial, the tube solarimeters were positioned across one row at distances ranging from -2 m (southern side) to 2 m (northern side) from the row. The data were recorded every 5 minutes with a CR10X data logger.

The main experiment with micro-lysimeters consisted of measurements of evaporation in the orchard. Nineteen micro-lysimeters were installed perpendicular to the rows, at distances ranging from 0 to 2.5 m on either side of the row. Eleven of them had a bare soil surface and were installed in a row where the soil was kept bare, and eight others had a grass-covered surface and were installed in a grass-covered area. After an initial irrigation of 20 mm, applied with sprinklers, soil water evaporation was measured for six days (05-12/03/2001, DOY 64 to 71). Another test experiment was conducted to validate the micro-lysimeter technique. It consisted of measurements of soil water evaporation from eight micro-lysimeters installed in an open field close to the weather station. Four of these micro-lysimeters had a bare soil surface and were located in a bare soil area, and the four others had a grass-covered surface and were located in a grass-covered area. These measurements went on for seven days after an initial irrigation of 20 mm, applied with the same sprinkler system as for the peach orchard.

Evaporation measurements were made by weighing the micro-lysimeters daily. Measurements were taken at 10h00 and 12h00 with an electronic scale, and the average value was retained (in a few cases, discrepancies between these consecutive measurements led to discarding one of them). The evaporation (mm) was calculated as the difference of mass between two consecutive measurements, divided by the product of the density of water and the area of the micro-lysimeter.

4.4.3. Two-dimensional energy interception

The measurements of radiation flux density were used: i) to investigate the daily patterns of radiation interception at the soil surface and ii) to quantify the cumulative solar radiation received daily at different positions in the orchard. These data were used to check the validity of the geometry used to describe tree shape and to predict radiation interception, and to validate the estimations of accumulated energy used for the evaporation part of the model.

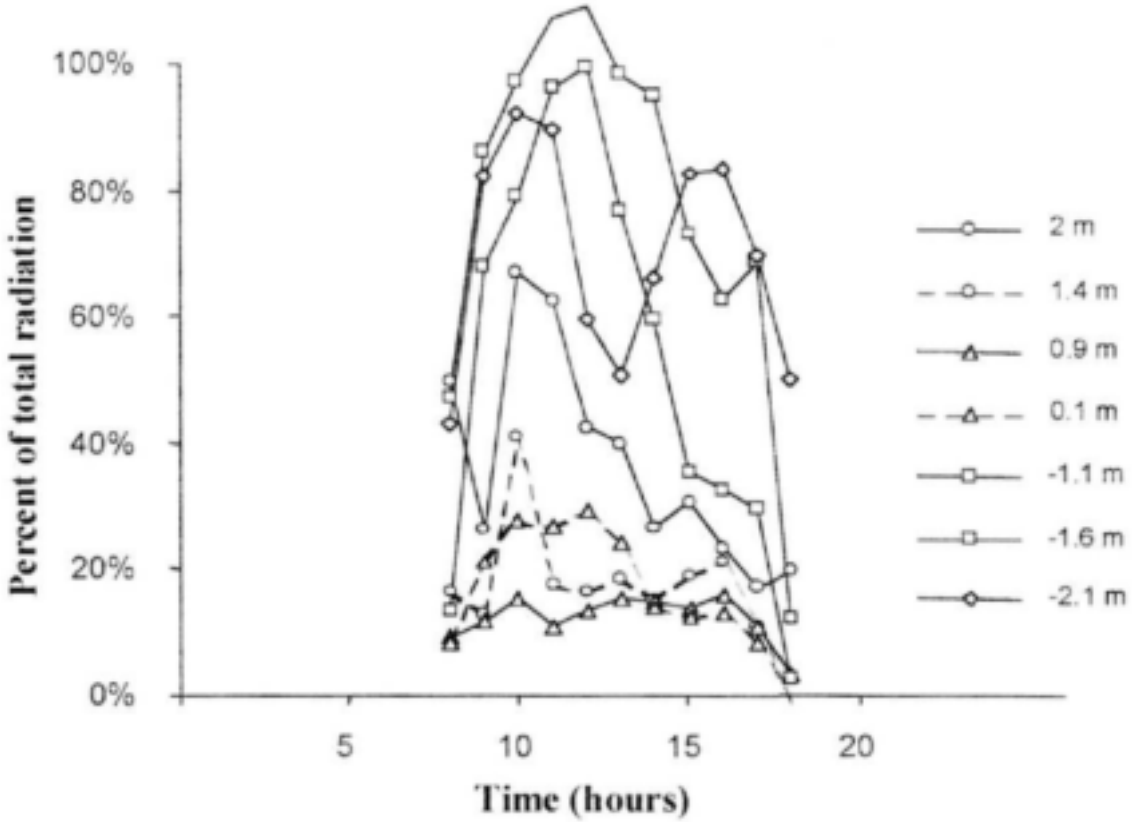

Figure 4.36. Daily patterns of energy interception at different distances from the row, ranging from –2.1 m (northern side) to 2 m (southern side) observed on the first day of the experiment. Radiation received at the soil surface is expressed as the percentage of the total solar radiation (measured by the weather station).

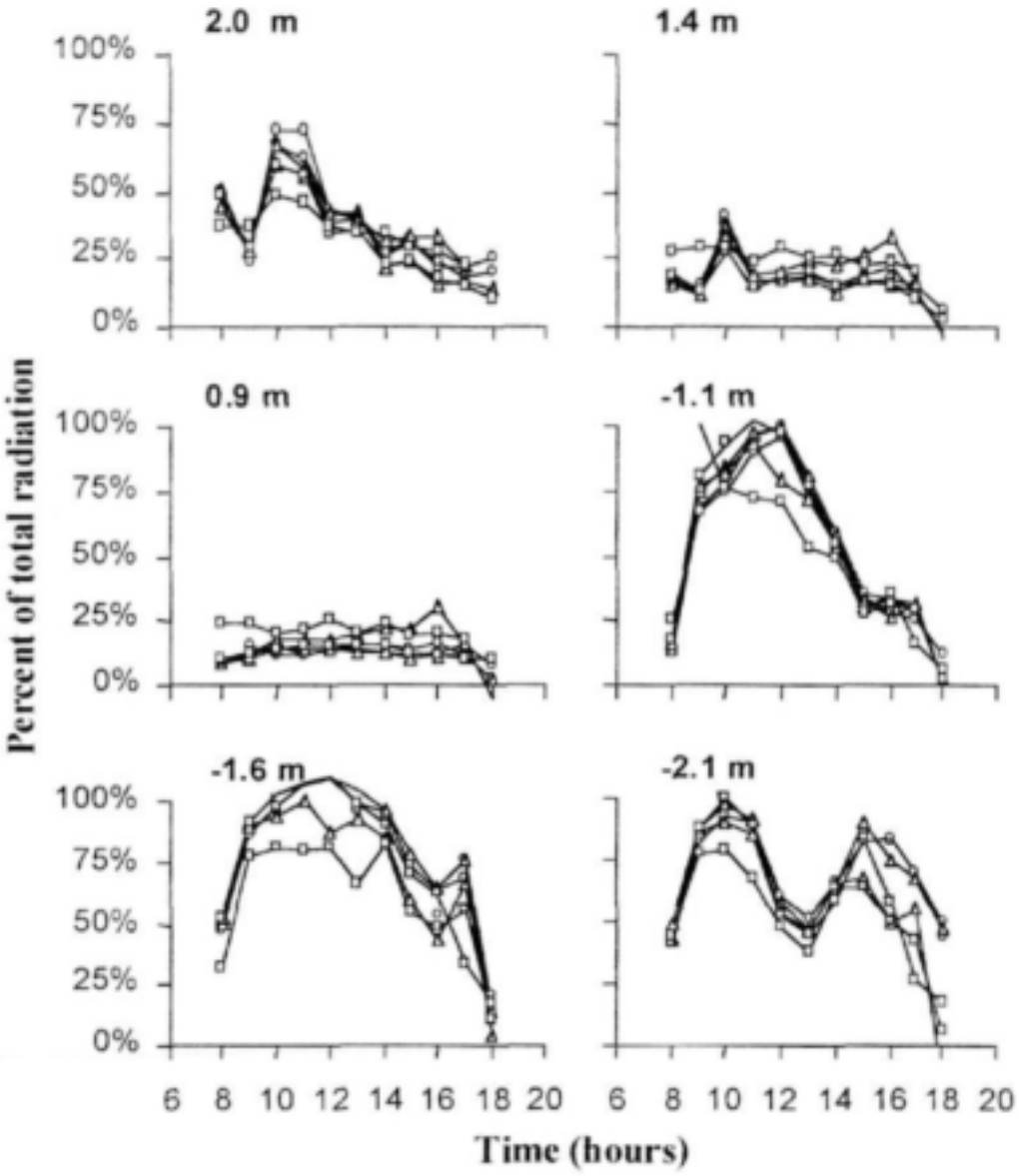

Figure 4.37. Daily patterns of energy interception at different distances from the row, ranging from –2.1 m (northern side) to 2 m (southern side). Each graph represents the percent of the total solar radiation (measured by the weather station) received at the soil surface at a given distance from the row, for the six days of the experiment.

The flux of solar radiation reaching the soil depended on the time of day and on the position in the orchard (Figures 4.36 and 4.37). At 0.9 and 1.4 m on the southern side of the tree, the radiation received at the soil surface was only about 25% of total solar radiation throughout the day. On the contrary, there was full exposure to solar radiation between 10h00 and 12h00 at 1.1 m, and between 9h00 and 13h00 at 1.6 m on the northern side of the tree. Positions half way between the rows exhibited intermediate behaviour, with a peak of about 75% radiation in the morning at -1.90 m and two peaks of about 75% radiation at 2.06 m, one in the morning and one in the afternoon.

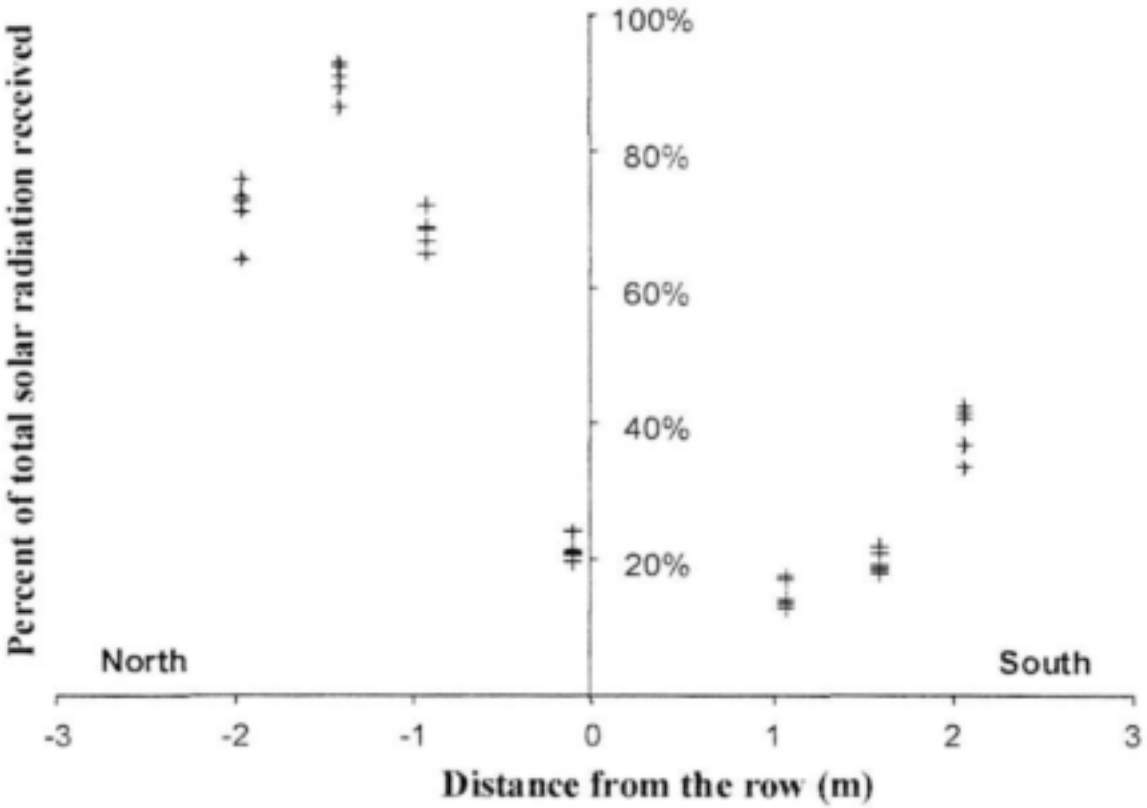

Figure 4.38. Distribution of total amount of energy received daily by solarimeter tubes at different positions under the canopy of the trees (percent of total radiation). The negative values represent the northern side and the positive values are for the southern side of the tree row.

Differences in hourly patterns of energy interception between positions explained the differences in the distribution of daily cumulative energy interception (Figure 4.38). Positions between approximately 0 and -2 m on the southern side of the tree received the lowest level of energy (about 15% of total solar radiation), whereas the highest levels were received between 1 and 2 m on the northern side (with about 90% of solar radiation reaching the soil). This pattern is similar to that described by Pruitt et al. (1984).

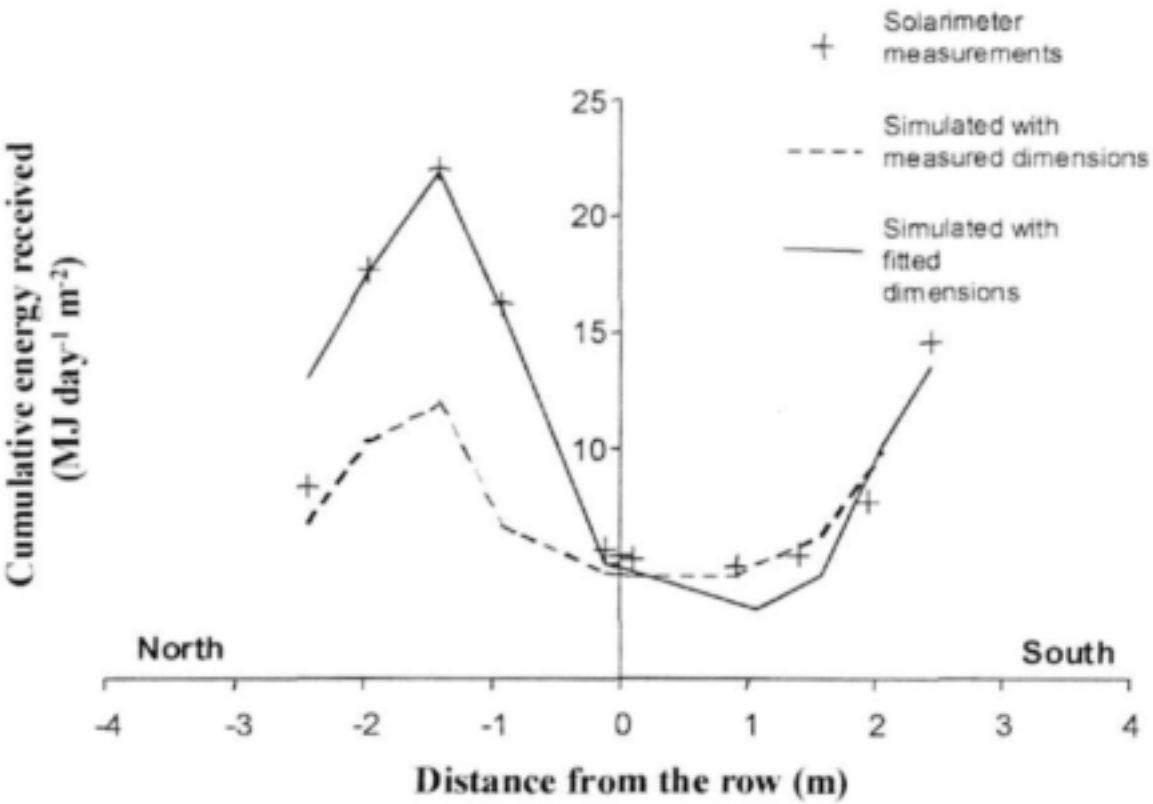

Figure 4.39. Comparison between distribution of energy at the soil surface measured and simulated with the model. The measured dimensions of the tree were: height 3.76 m, width 4.2 m and skirting height 0.45 m. The best fit was obtained for the following tree dimensions: height 3.76 m, width 3.8 m and trunk height 0.9 m.

Simulations were run with the SWB model to validate the predictions of accumulated daily energy interception. The parameters of the model that can be adjusted are the tree dimensions (height, width and skirting height), and the physical values associated with radiation extinction through the canopy (leaf area density, extinction coefficient and absorptivity). Several simulations run with different sets of parameters showed that changing tree dimensions affected the shape of the curve of radiation distribution, whereas changing the parameters associated with radiation extinction led to distributions with similar shapes but different magnitudes.

Using the measured values for tree size (height 3.76 m, width 4.2 m, trunk height 0.45 m), and the following coefficients: leaf area density 1.2 m^2 m^{-3}, extinction coefficient 0.5, and absorptivity 0.5, did not give satisfactory description of energy distribution. Cumulative radiation was underestimated by about half, and the size of the shaded area was over-estimated (Figure 4.39). Adjusting these last three parameters did not help to better predict the shape of the distribution. The best prediction of energy distribution was obtained with the following parameters: height 3.76 m, width 3.8 m, trunk height 0.90 m, leaf area density 1.2, extinction coefficient and absorptivity 0.5 (Figure 4.39). This was the best prediction of radiation interception obtained with trees 40 cm narrower, and with the bottom of the canopy 55 cm higher than measured. Concerning the width of the tree, this is probably due to the fact that the canopy was not exactly ellipsoidal: though the trees had rather few leaves, some scaffold branches at the base extended further than the rest of the canopy. Therefore, the tree width measured in the orchard did not properly reflect the average boundaries of the canopy. Concerning the skirting height, the bias in its estimation was probably related to an irregular distribution of the leaf area density: the branches originating from the base of the

trunk bore fewer shoots and leaves than the rest of the canopy, so that in terms of interception it occurred as if the base of the canopy was higher than measured.

4.4.4. Localised measurement of evaporation

4.4.4.1 Test of the micro-lysimeter technique

In order to test the micro-lysimeters as a tool to measure evaporation, eight of them were placed in open field, and measurements taken for 6 days. Measured evaporation was compared to the ETo calculated using weather station data.

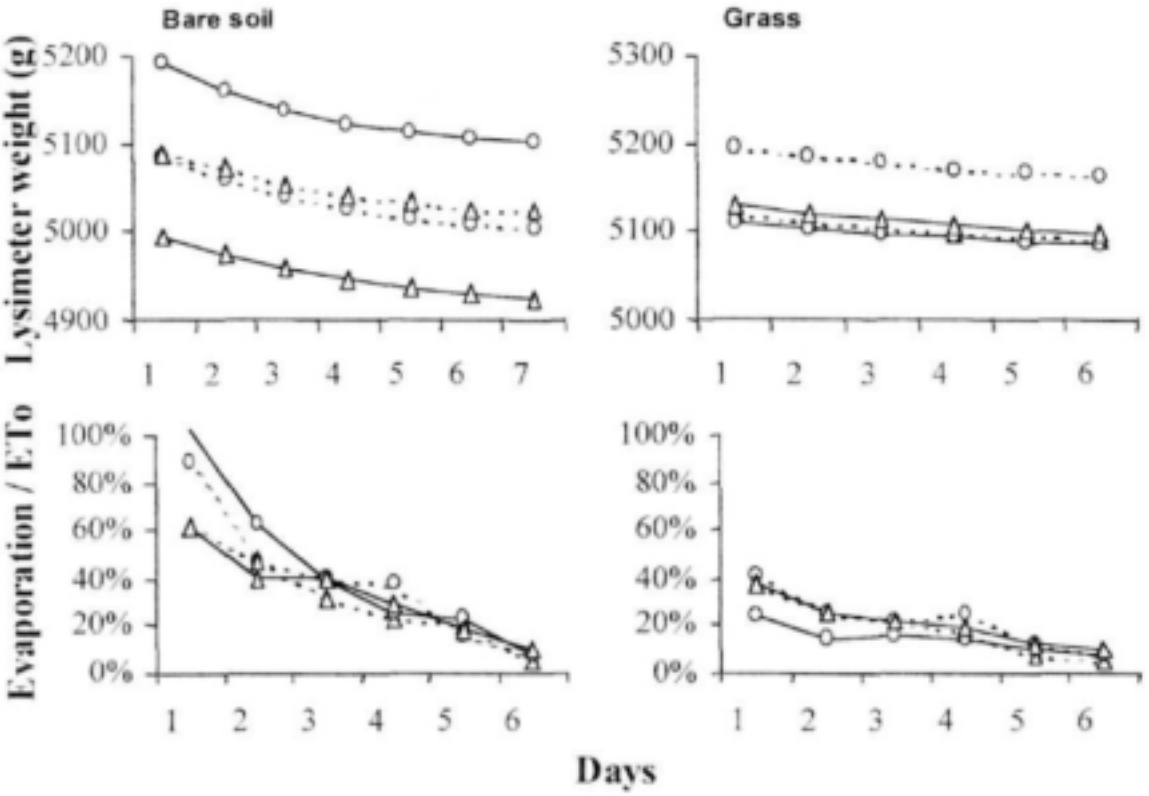

Figure 4.40. Mass loss and evaporation from eight micro-lysimeters installed in open field, four of them in a bare soil area, and four of them in a grass-covered area. The symbols and lines represent replications.

Evaporation appeared to decline from the first day after irrigation. In the bare soil area, the initial values observed during the first day were comparable to ETo (60% to 100% of ETo), but that was not the case for the lysimeters installed in the grass-covered area, with initial evaporations between 20% and 40% of ETo. The fact that evaporation measured by the micro-lysimeters in the bare soil were lower than ETo was probably due to the fact that, while the lysimeter surface was bare soil, ETo is calculated for a grass cover. Also, the fact that the evaporation measured by the lysimeter placed in the grass-covered area was about twice as low as in the bare soil area caused concern. One explanation may be that the grass surrounding the micro-lysimeter created a micro-climate with lower evaporative demand (lower wind and higher humidity); another explanation is that the grass that covered the lysimeter was partially dead, thereby acting as a mulch, preventing radiation from reaching the soil surface and increasing the resistance to vapour transport. The decline in evaporation observed for all micro-lysimeters during the experiment can be described as follows. After irrigation, the soil surface was wet and the evaporation was limited by the net radiation

received (energy-limited stage), then the supply of water by the soil to the surface became limiting and evaporation decreased as the soil became drier (falling rate stage). This behaviour is typical of that reported in previous lysimeter studies (Phillips, 1957). It was modelled as a function of the square root of time by Ritchie (1972) and this model was widely adopted in lysimeter studies (Villalobos and Fereres, 1990; Yanusa et al., 1993).

4.4.4.2 Spatial distribution of evaporation in the orchard

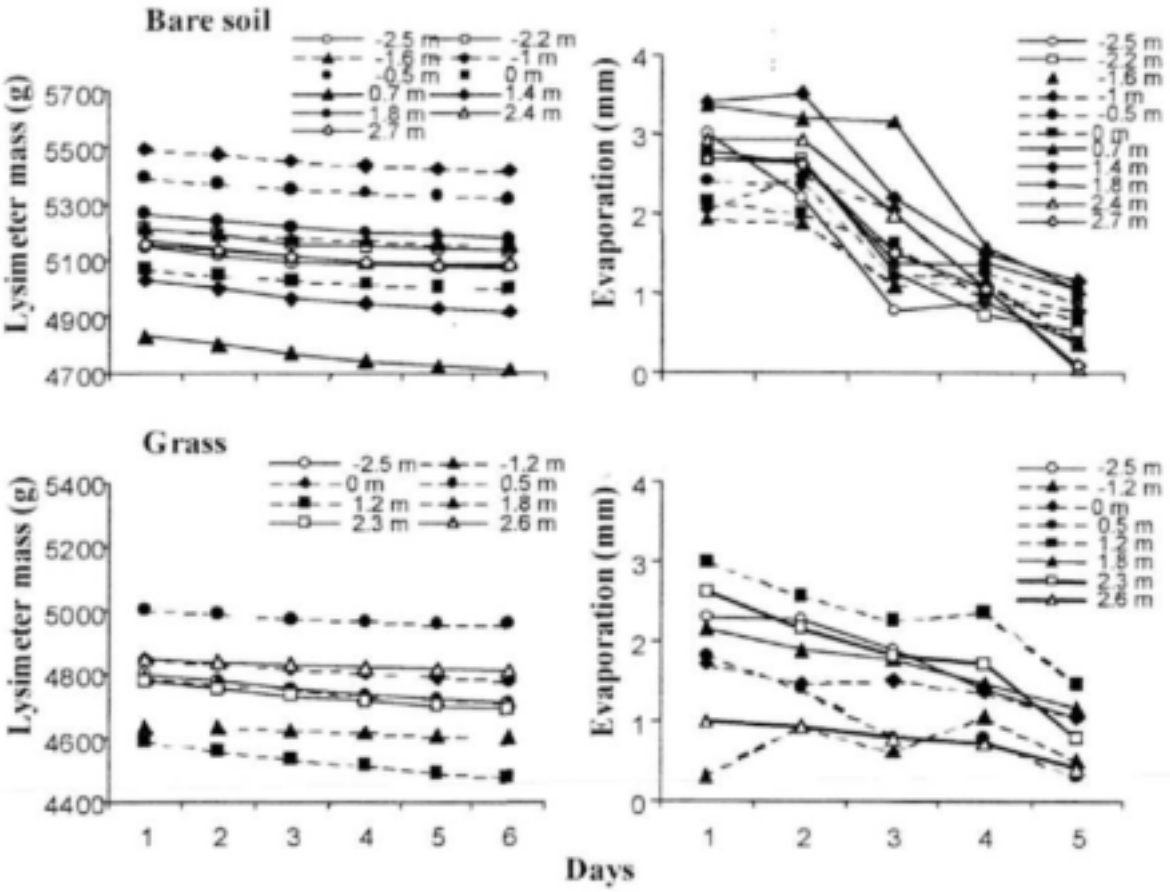

Figure 4.41. Mass loss and corresponding evaporation measured with lysimeters installed at several positions in the orchard. One set of lysimeters was in the bare soil area of the orchard, the other set in the grass-covered area. The positions ranged from distances of -2.5 m from the row (northern side) to 2.7 m (southern side) in the bare soil area, and from -2.5 to 2.6 m in the grass-covered area.

The micro-lysimeter measurements made within the orchard revealed important differences in evaporation (Figure 4.41). The rates of evaporation measured during the first 2 days of the experiment ranged from 1 to 3.5 mm d^{-1}. After the third day, the measured evaporation declined for almost all the lysimeters studied, though the rate of decline differed between lysimeters: in general, it was higher in the bare soil area than in the grass-covered area, and within a given soil cover, higher for the lysimeters that were far from the row.

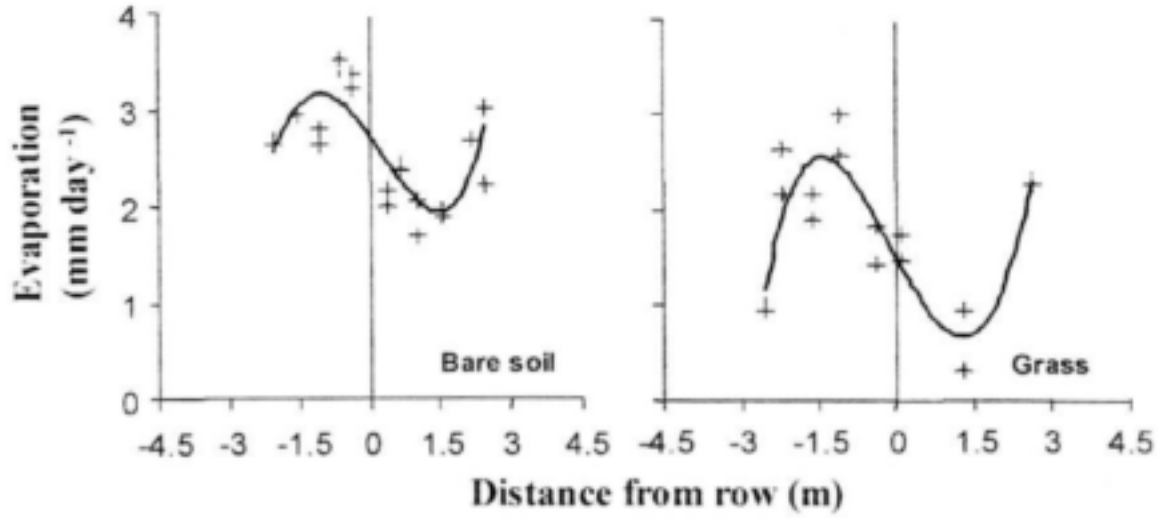

Figure 4.42. Spatial distribution of evaporation across the rows. Measured evaporation is expressed in mm d^{-1} and shown for the bare and grass-covered area of the orchard. The values for the distance of the lysimeter from the row (m) are negative for the northern side and positive for the southern side.

For the first two days of measurements, expected to correspond to the energy-limited stage, a clear distribution of evaporation within the row was observed (Figure 4.42). Evaporation appeared to be a maximum on the northern side of the row (between 1 and 2 m from the row), and a minimum under the trees and on the southern side of the row. This pattern was found both in the bare soil and in the grass-covered areas. However, the evaporation measured in the grass-covered area was lower than that measured at corresponding positions in the bare soil area.

4.4.4.3 Relationships between energy interception and evaporation.

With the patterns of distribution of evaporation (Figure 4.42) and cumulative solar energy received daily (Figure 4.38) being similar, the relations between these two variables were investigated.

A linear correlation between cumulative energy interception and daily evaporation was found for the first 2 days of the experiment (expected to correspond to a situation where evaporation is energy-limited, see below). This correlation was observed for both the bare soil and grass-covered areas (Figure 4.43). Though the slopes of the regression line were similar, the intercepts were not: evaporation was about 1 mm d^{-1} lower in the grass-covered area.

Possible interpretations for the lower rate of evaporation in the grass-covered area are: i) the grass that covered the soil prevented radiation from reaching the soil surface, thus reducing the amount of energy available for water evaporation at the soil surface; ii) grass cover may have created a wetter micro-climate at the soil surface by reducing wind speed and preventing vapour movement by convection.

When measurements for the rest of the experiment (days 3 to 6) were included, the correlation between energy interception and evaporation was lost (data not shown). This suggests that during these days, evaporation was no longer limited by energy interception alone.

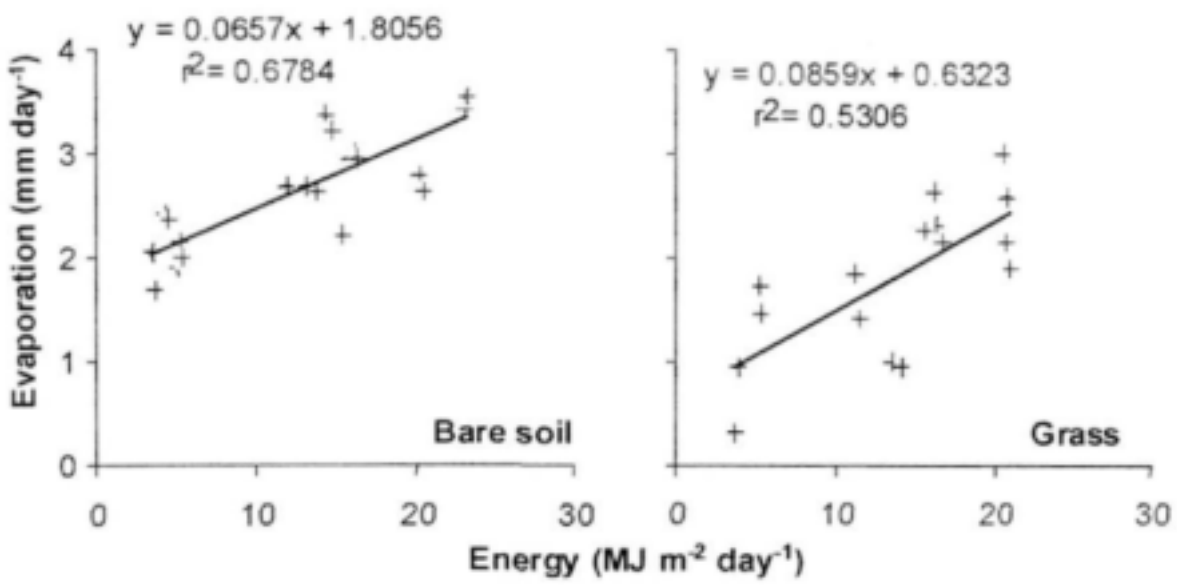

Figure 4.43. Relation between cumulated daily energy interception and evaporation (bare soil and grass-covered area). Only data from the first 2 days of the experiment are shown.

4.4.5. Validation of the evaporation subroutine

The model calculates the spatial distribution of evaporation at the soil surface in two steps:

i) Potential evaporation (PE_j) is estimated at each node by applying the Panman-Monteith equation, using local radiation as input.

ii) Evaporation from the soil surface is then modelled as a function of potential evaporation, air humidity, and humidity of the soil surface (as calculated by the 2D model of water redistribution in the soil).

In the following section evaporation measurements are compared with both modelled potential evaporation and modelled evaporation.

4.4.5.1 Partitioning of potential evapotranspiration

If the assumptions made in the evaporation partitioning subroutine are not violated significantly, the following results are expected:

i) The ratio between measured evaporation and predicted potential evaporation should remain constant at the beginning of the evaporation measurement when evaporation is expected to be energy-limited, then decline with time as evaporation becomes supply-limited.

ii) The initial ratio should be the same and close to unity for all micro-lysimeters.

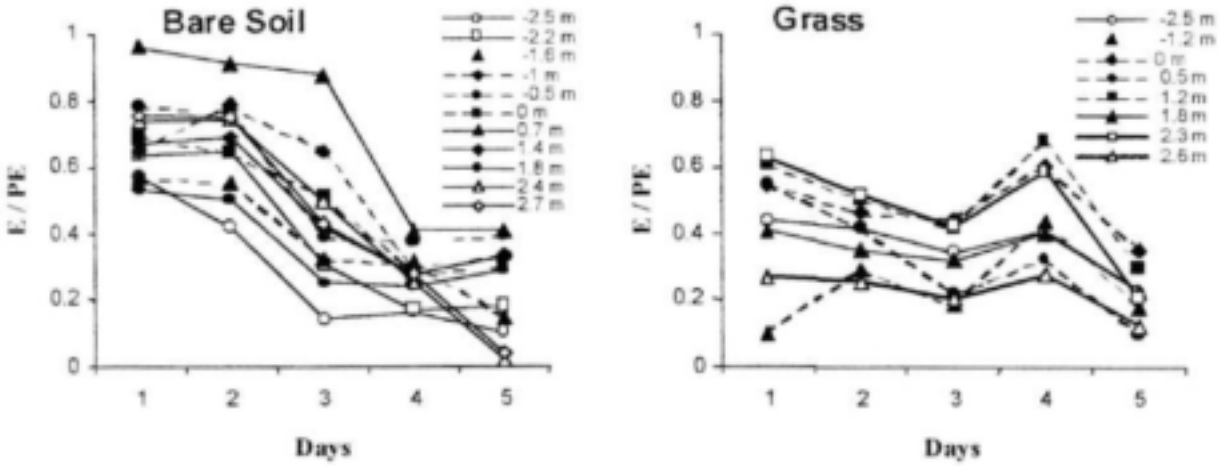

Figure 4.44. Ratio between evaporation measured with micro-lysimeters (E) and potential evaporation (PE) calculated by the model at several positions in the orchard. One set of lysimeters was in the bare soil area of the orchard, the other set in the grass-covered area. The positions ranged from distances of -2.5 m from the row (northern side) to 2.7 m (souhern side) in the bare soil area, and from -2.5 to 2.6 in the grass-covered area.

Most micro-lysimeters installed within the bare soil area gave comparable initial ratios: between 0.6 and 0.8. The ratio between measured evaporation and simulated potential evaporation changed over time as expected (Figure 4.44): it was constant or declined little during the first two days, the decreased during the following days. In the grass area however, the ratio remained between 0.3 and 0.6 during the whole experiment.

These results suggest that in the bare soil area evaporation was energy-limited for the first two days and then became supply-limited for this specific period. The fact that measured evaporation is lower that simulated potential evaporation during the first two day of the experiment is probably due to a bias in the prediction of PE. PE is calculated using the Penman-Monteith equation for ETo, which describes a reference grass cover and not a bare soil. The Penman-Monteith equation is simplified by assuming parameter values for "crop" height, surface resistance and albedo that are applicable to a grass surface, which may lead to an inaccurate estimation of PE for a bare soil surface. Also, within-canopy estimates of wind speed and air humidity would likely improve the accuracy of the simulation. These measurements were, however, not available in the present experiment. Finally, the daily time step at which the potential evaporation is calculated may be too long, as evaporation may become supply-limited during part of a day and could not therefore be expected to match potential evaporation any more.

In the grass-covered part of the orchard, not only the measured initial evaporation is lower than the predicted PE, but there is also no clear shift from an energy-limited to a supply-limited stage, and it seems as if this system is always supply limited. This is quite plausible considering the fact that much of the grass was dead and therefore acted as a mulch.

4.4.5.2 Modelled evaporation

It is necessary to estimate the humidity of the surface layer of the soil to predict evaporation using the Campbell (1985) procedure. The drying of the soil surface has to be simulated using the finite difference SWB model. The simulations were set up as follows: Daily cumulative energy interception was simulated as described earlier, and was in excellent agreement with measured values. Evaporation was modelled using the procedure described in Section 2.1.2. The redistribution of water in the soil was modelled using the two-dimensional finite difference model as described in Section 2.1.3, setting the horizontal nodes (centres of the evaporation areas) at the lysimeter positions, and the vertical nodes at

1, 2, 4, 7, 11 cm depths, and thereafter every 20 cm. The first 5 layers described in this set-up were therefore 1, 1, 2, 3 and 4 cm thick, which made it possible to describe water distribution close to the surface with accuracy. Due to the way the model has been developed, evaporation and redistribution of water in the soil could not be simulated independently (that is, measured evaporation cannot be used as an input to predict soil humidity). One variable used in the model is air humidity (Section 2.1.2). In the current version of the model, air humidity is assumed to be constant and equal to 50 %, which is quite reasonable for a daily time step.

Simulated and measured evaporation were very well correlated in the bare soil area (r^2=0.76), but evaporation was over-estimated by about 30 % (Figure 4.45). In the grass-covered soil area, not only was evaporation grossly over-estimated, but also the correlation between simulated and measured evaporation was low (r^2=0.28). The over-estimation of evaporation is likely to be due to the over-estimation of potential evaporation previously mentioned. The low correlation between simulated and measured evaporation in the grass-covered area is probably due mainly to the dead grass acting as mulch, which is not represented in the model. To a lesser extent, the live grass may also maintain level of transpiration independent of the soil surface humidity. Other possible sources of errors can be in predicting the drying of the soil surface, due to inaccurate estimation of the parameters of soil water redistribution, such as soil hydraulic conductivity (which was not measured but estimated indirectly from the water contents at field capacity and permanent wilting point). However, the fact that the model predicts evaporation very well for the last two days of the experiment, after 3 and 4 days of drying, does not confirm this hypothesis.

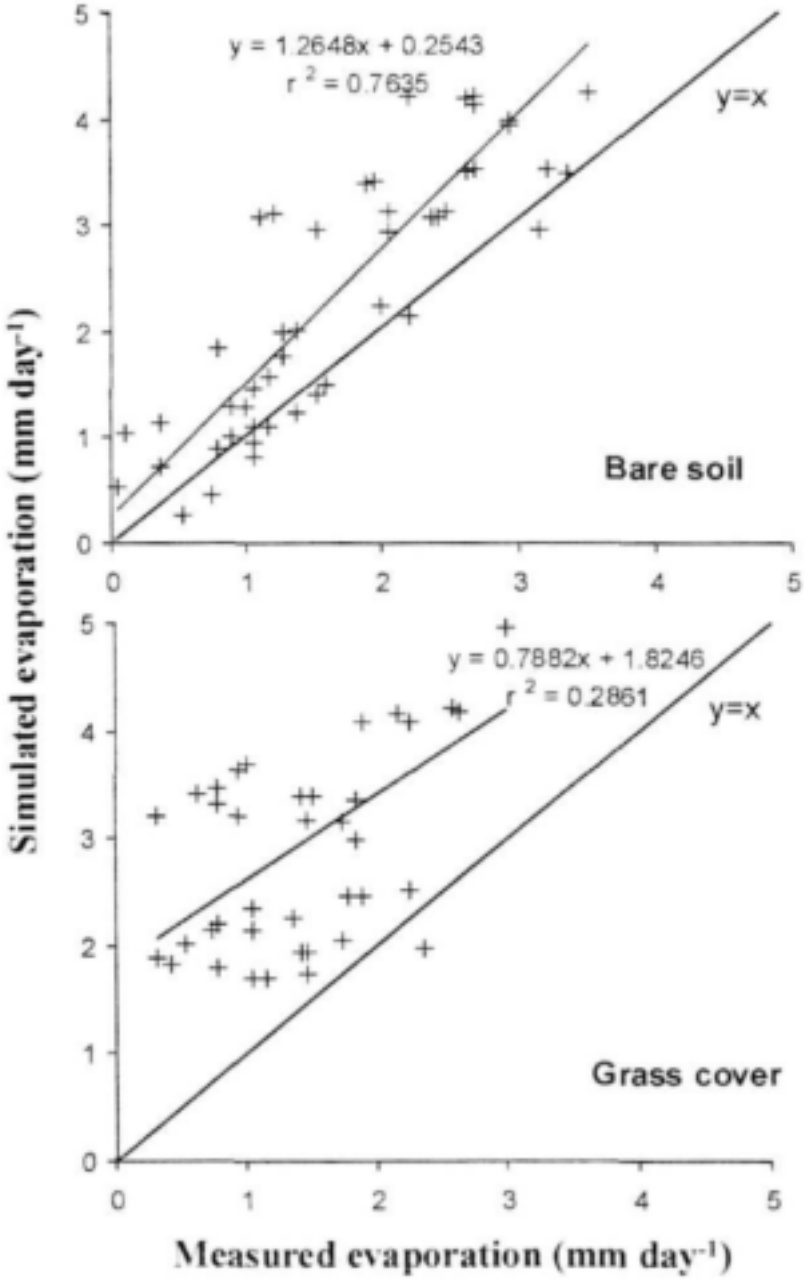

Figure 4.45. Comparison between evaporation measured with the micro-lysimeters and predicted by the model. Air humidity was assumed to be 50 %, which is the default value in the model.

Figure 4.46 shows how the simulations reproduce the transition from a demand-limited to a supply-limited stage in the bare soil area. Simulated PE, simulated E, and measured E are shown for the five days of the experiment. During the first day, the soil surface was wet and simulated evaporation was demand-limited across the whole row. Spatial differences in the surface layer humidity began to appear during days 2 and 3. Whilst simulated evaporation remained equal to potential evaporation under the trees, it decreased in the exposed parts in the middle of the rows. That is, evaporation remained demand-limited under the trees, where the soil surface remained wet, while supply limitations appeared in the middle of the rows where the soil surface dried faster. During days 4 and 5, surface humidity had decreased across the whole row, and evaporation became supply-limited everywhere. In the early

stages when energy limitation is crucial, modelled values overestimated actual evaporation so it is clear that PE needs to be reduced. Once the system, however, became supply limited, simulations matched the evaporation measurements very well, suggesting that the simplified assumptions regarding soil hydraulic conductivity may, indeed, not be serious.

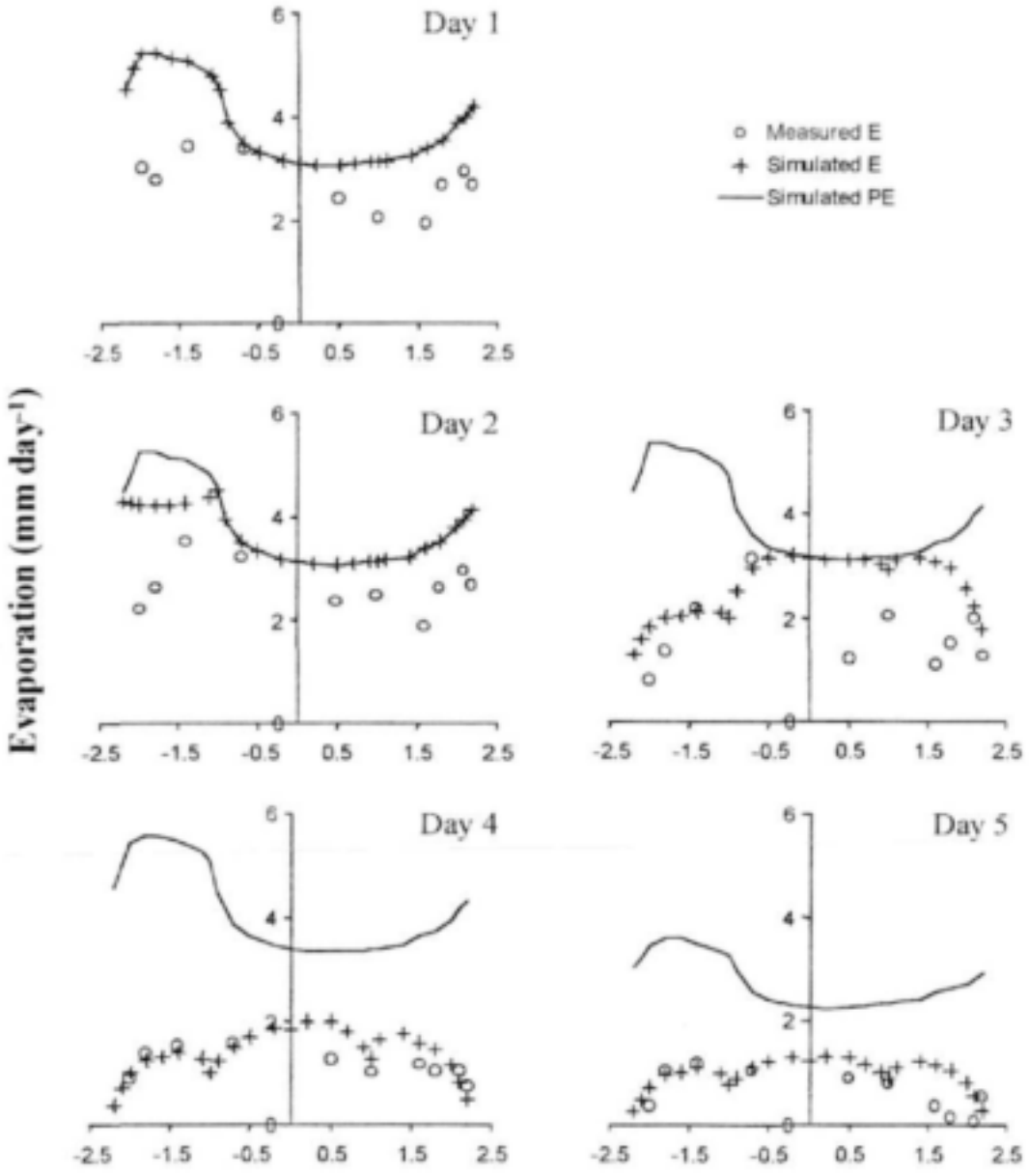

Figure 4.46. Evolutions of evaporation measured with the micro-lysimeters, potential evaporation predicted by the model, and predicted evaporation. Each graph represents evaporation in the bare soil area in one of the 5 days of the experiment.

4.5. Validation of the two-dimensional water balance model

The two-dimensional soil water balance model uses the energy interception and soil evaporation sub-models to split evaporation and transpiration. In this section, the output

obtained with the two-dimensional soil water balance model was compared to independent field measurement data in order to validate the full SWB two-dimensional model.

Volumetric soil water content data collected with the TDR system in the peach and citrus orchards were compared to SWB simulations. In these simulations, it was assumed that the root distribution across the row was uniform, based on the measurements of root density shown in Figures 4.10 and 4.11.

Results of model simulations for drying cycles of the peaches and clementines revealed similar trends, so only results for clementine are presented. It must be noted that the summer 1999/2000 recorded frequent rain and thus the drying cycles for this season were short. The simulations for the 1999/2000 season are presented in Figures 4.47 to 4.49. In Figure 4.47, samples of the model predicted volumetric soil water content compared to measurements are presented for the 6 cm depth. For the most part there was very good agreement with the mean absolute error (MAE) being ~7% for two comparisons and ~17% for the other two. Similar agreement was recorded for the 26 cm depth in Figure 4.48. At the 90 cm depth (Figure 4.49), MAE was greater, ranging from 14 to 22%. Overall results show that the surface layer (6 cm) predictions were generally very accurate which indicates that the procedure used to determine the distribution of solar radiation at the surface used to calculate evaporation works well. However, it was noted that, where differences occurred, the general trend was for the model to predict drier soil than the measurements indicated. This could have been as a result of the very high rainfall causing the surrounding soil to have high water content and there could thus have been an inflow of subsurface water that was not accounted for in the model predictions.

During the 2000/01 summer it was possible to monitor more wetting and drying cycles and the comparisons between measured and simulated volumetric SWC are presented in Figures 4.50 to 4.53 for the clementine hedgerow orchard. In the "a" portion of these figures the comparisons between the measured (blocks) and SWB predicted (line) values for the north-western side of the row are presented. The extreme left column of graphs depicts the comparisons for the nodes at 3.75 m starting at the top with the 6 cm depth, then the 26 cm depth comparison just below, followed by the 56 cm depth and finally at the bottom the values for the 86 cm depth. As one moves to the right, so the 2.5 m, then the 1.25 m and finally the nodes at the row centre are depicted. In the "b" portion of Figures 4.50 to 4.53 the comparisons for the north-eastern side of the row are presented. In these figures the nodes at the row centre are on the left with the 1.25, 2.5 and 3.75 m comparisons presented sequentially as one moves to the right. The comparisons for the upper soil depth, i.e. 6 cm, are presented in the top horizontal row of graphics with the 26, 56 and 86 cm depths being depicted sequentially as one moves down the figures. In this manner, it is possible to graphically present the spatial and daily comparisons of measured and predicted volumetric SWC on each side of the tree row.

Figure 4.50 presents the comparison between measured and predicted daily SWC for a period just before, during and after a heavy under-canopy irrigation. The time period is 9 to 17 February 2001 and the irrigation applied was ~100 mm in a three metre wide band under the tree canopy. If this water had been applied to the whole surface area it would have been equivalent to a 40 mm irrigation. It is seen in Figures 4.50a and b that the nodes at 3.75 and 2.5 m from the row centre show no change in SWC as would be expected since they did not receive any water. The predicted and measured SWC values for these nodes also show close agreement except for the 86 cm deep node at 3.75 m from the row centre in Figure 4.50a. The nodes 1.25 m from the row centre and at the row centre show excellent agreement in absolute value and trends in the values between measured and SWB predicted SWC at the 6 and 26 cm depths. At the 56 cm depth the trends between measured and SWB predicted values are similar but it appears that the SWB predicted SWC increases sooner than the measured values and then it decreases more quickly. At the 86 cm deep nodes the trends in the predicted and measured SWC are similar but the SWB predicted

SWC again tends to increase a bit early. At this depth, the measured SWC is also much higher than the predicted SWC.

Figure 4.51 shows the comparisons for a rainfall event where 22.6 mm of rain were recorded on 19 February 2001. The comparisons presented are from 18 to 26 February 2001. It is seen that at the 6 cm deep nodes there is excellent agreement in the trends and values of SWC for the measured and predicted values. However, at the 26 cm depth an interesting feature is noted: i.e. the measured SWC values do not reflect any increase while the SWB predictions indicate a noticeable increase in SWC between 19 and 20 February. So what is happening in this instance is that, in practice, the wetting front has not penetrated to 26 cm while the model has overestimated the wetting front penetration. At 56 and 86 cm no changes in SWC are measured or predicted. There is good agreement between the measured and predicted SWC values at all the 56 cm deep nodes. In this series the 86 cm nodes show poor agreement between measurements and predictions.

Comparisons of measured and SWB predicted SWC for a good rainfall event, i.e. 34.9 mm on 1 March 2001, are recorded in Figure 4.52. These comparisons run from 26 February to 11 March. Once again there is excellent agreement between the predicted and measured SWC at the 6 cm nodes across the whole row. At the 26 cm deep nodes the model predicted that the wetting front would arrive one day too early (i.e. virtually immediate penetration). At the 56 cm depth the measurements show that there is no change in SWC while the SWB predictions indicate that the wetting front would penetrate to that depth. The 86 cm nodes show negligible change in SWC resulting from the rainfall event with good agreement in trends and values on the S-W side but large differences in SWC values on the N-E side.

The last series of comparisons in Figure 4.53 are for a light rainfall event of 8.3 mm on 19 March 2001. The period considered begins on 18 and ends on 29 March 2001. Looking at the measured values it is noted that only at 2.5 m on the south-western side and at 3.75 m on the north-eastern side is there a slight response in SWC at 6 cm depth. The rest of the nodes show no response in SWC. So this rainfall of 8.3 mm must be regarded as ineffective in altering the SWC. The SWB predictions show no response to this rainfall as well.

A second possible source of discrepancy between measurements and simulations could have been due to spatial variability of soil properties. It is well recognised that spatial variability is a major factor when point measurements of soil water are made with heat dissipation sensors or TDR probes. Due to the high cost of the equipment used, it was not possible to replicate the measurements in order to account for spatial variability.

Another source of error could have been the soil disturbance during the installation of TDR probes. It is clear that, even if soil water sensors are carefully installed according to standard procedures, some disturbance of the soil always occurs. In particular, during the insertion of TDR probes in the soil volume to be measured, some compaction occurs that changes soil bulk density and water retention properties around the rods of the probes. This could cause errors in measurement, especially because the effect of the volume of soil adjacent to the rods has the greatest effect on the measurement (Knight, 1992).

It must be remembered that in the two-dimensional simulations done above there are basically seven profiles that are being evaluated. In the model, it is assumed that the initial water contents are all the same, i.e. only one initial SWC is required per soil depth as an input and this value is then allocated to all the nodes at that specific soil depth. In practice the initial SWC for each node in the 2-D situation is rarely the same and one then uses an average as a beginning point. This is the reason why some measured SWC values begin either above or below the SWB predicted SWC. In some cases, particularly at the 86 cm depth these discrepancies can be rather large as can be seen in Figure 4.52b.

The problems encountered in measuring soil water content, related to spatial variability and point measurements, are highlighted in Figure 4.54. This Figure presents the measured volumetric soil water content (SWC) data (solid circles) at four depths across the clementine

hedgerow, as well as interpolated isolines for two different days. The first day (14 February 2000) was after 48 mm of rain, while 24 February 2000 reflects the water distribution 10 days later. It is important to note the lack of uniformity in the soil water content at the same depth across the hedgerow even after heavy rain. In spite of the fact that most of the profile was very wet (> 34 %), there was a spur of relatively drier soil penetrating to 900 mm. After ten days, the surface layer (6 cm) dried out from around 30 % to ~20%, while the 34% isoline straightened out at a depth of between 400 and 600 mm. This indicates that mainly above this depth the trees were removing water from across the whole inter-row and not from just under the canopy region. It is also important to note that below 600 mm there was a noticeable equilibration of the water content. The water content at 900 mm showed very little change from the original range of 32 to 50 %. This could have been due to the impervious plinthic layer preventing free drainage of the subsoil. The large differences in volumetric soil water content measured across the hedgerow at 900 mm soil depth, however, are mainly attributed to spatial variability in soil properties and sensor placement. It is clear that TDR probes can be used in irrigation scheduling to determine crop water use over certain periods. Caution should, however, be exercised in the interpretation of absolute values of volumetric soil water content obtained from the probes.

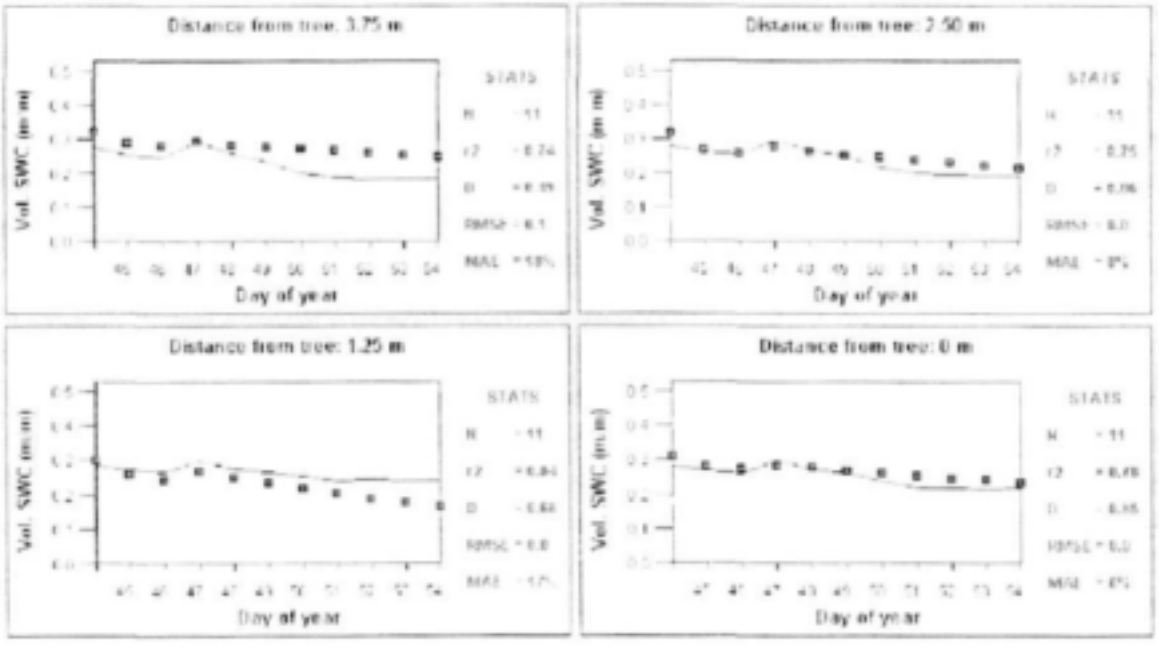

Figure 4.47. Simulated (line) and measured (squares) volumetric soil water content at 6 cm depth, 3.75, 2.5 and 1.25 m on the NE side of the trunk, as well as directly under the tree, for the clementine hedgerow.

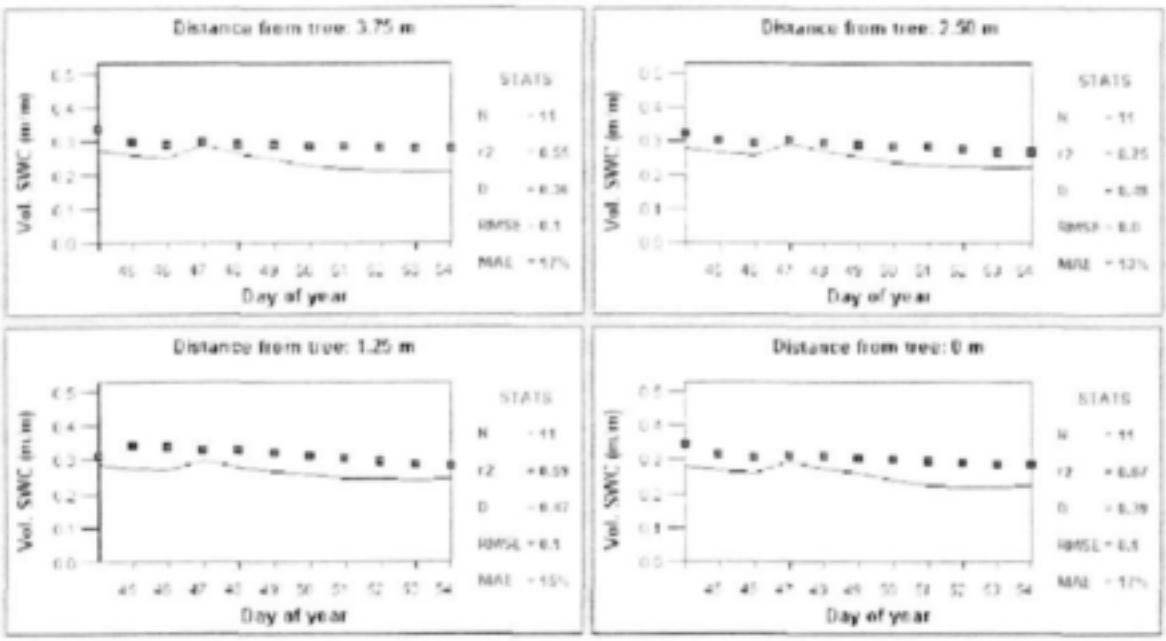

Figure 4.48. Simulated (line) and measured (squares) volumetric soil water content at 26 cm depth, 3.75, 2.5 and 1.25 m on the NE side of the trunk, as well as directly under the tree, for the clementine hedgerow.

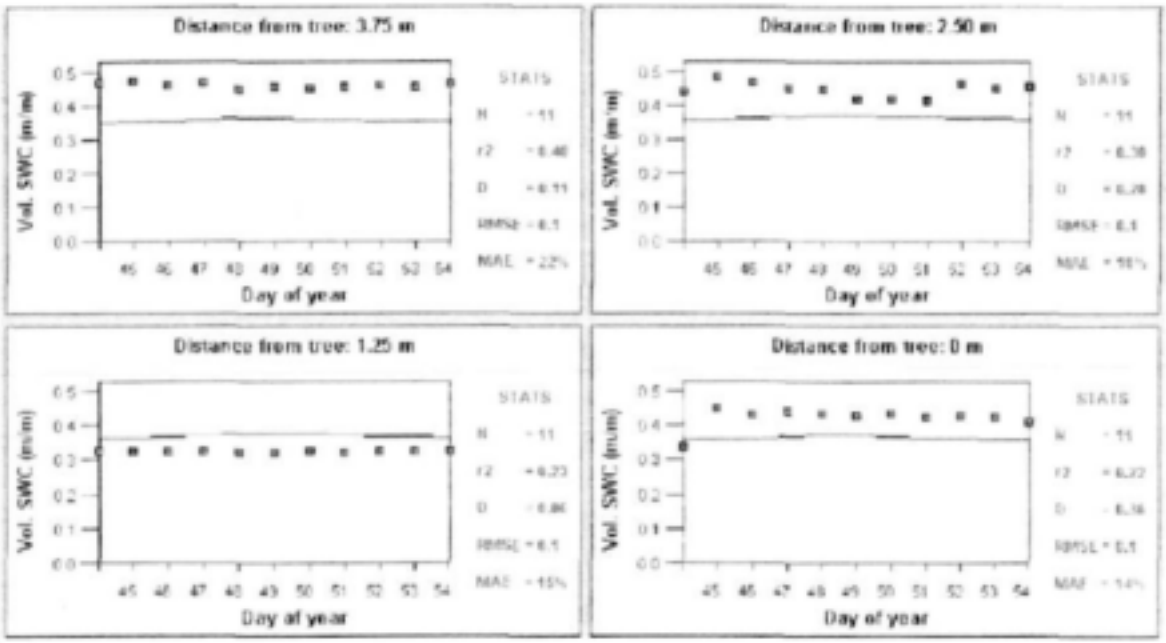

Figure 4.49. Simulated (line) and measured (squares) volumetric soil water content at 90 cm depth, 3.75, 2.5 and 1.25 m on the NE side of the trunk, as well as directly under the tree, for the clementine hedgerow.

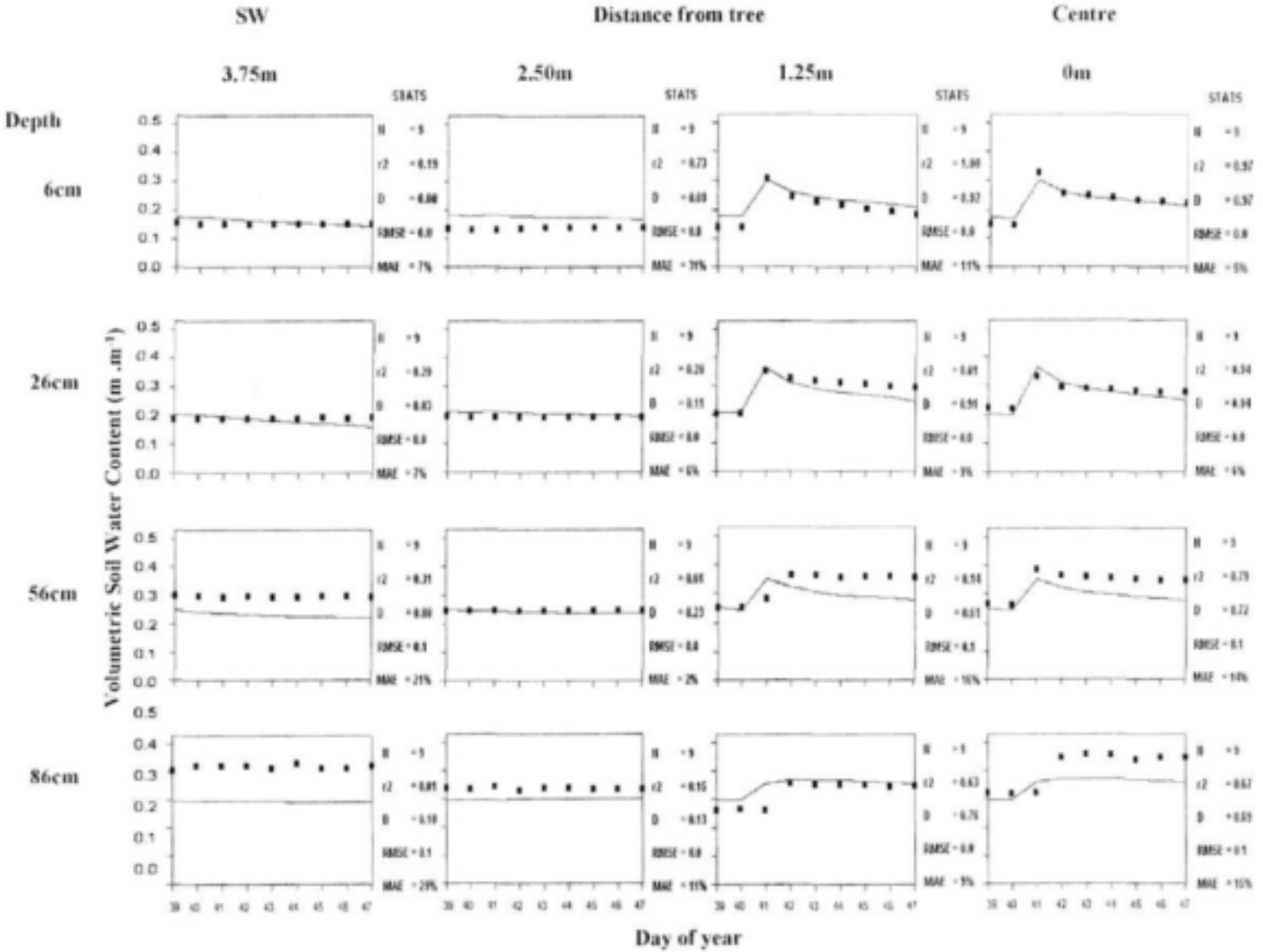

Figure 4.50a. Simulated (line) and measured (squares) volumetric soil water content on the SW side of the clementine hedgerow at 6, 26, 56 and 86 cm depths for the period 9 to 17 February, i.e. during a heavy irrigation event.

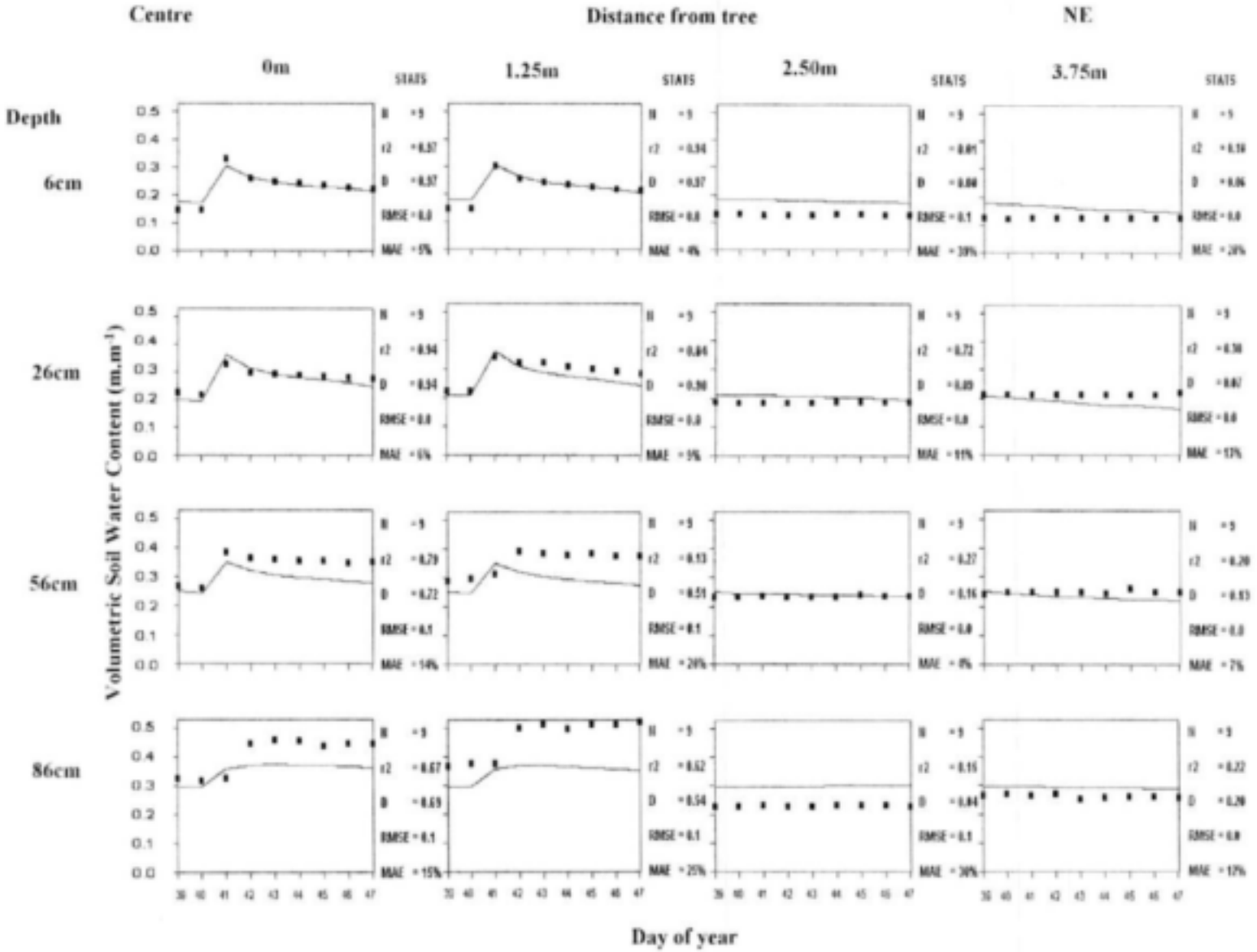

Figure 4.50b. Simulated (line) and measured (squares) volumetric soil water content on the NE side of the clementine hedgerow at 6, 26, 56 and 86 cm depths for the period 9 to 17 February, i.e. during a heavy irrigation event.

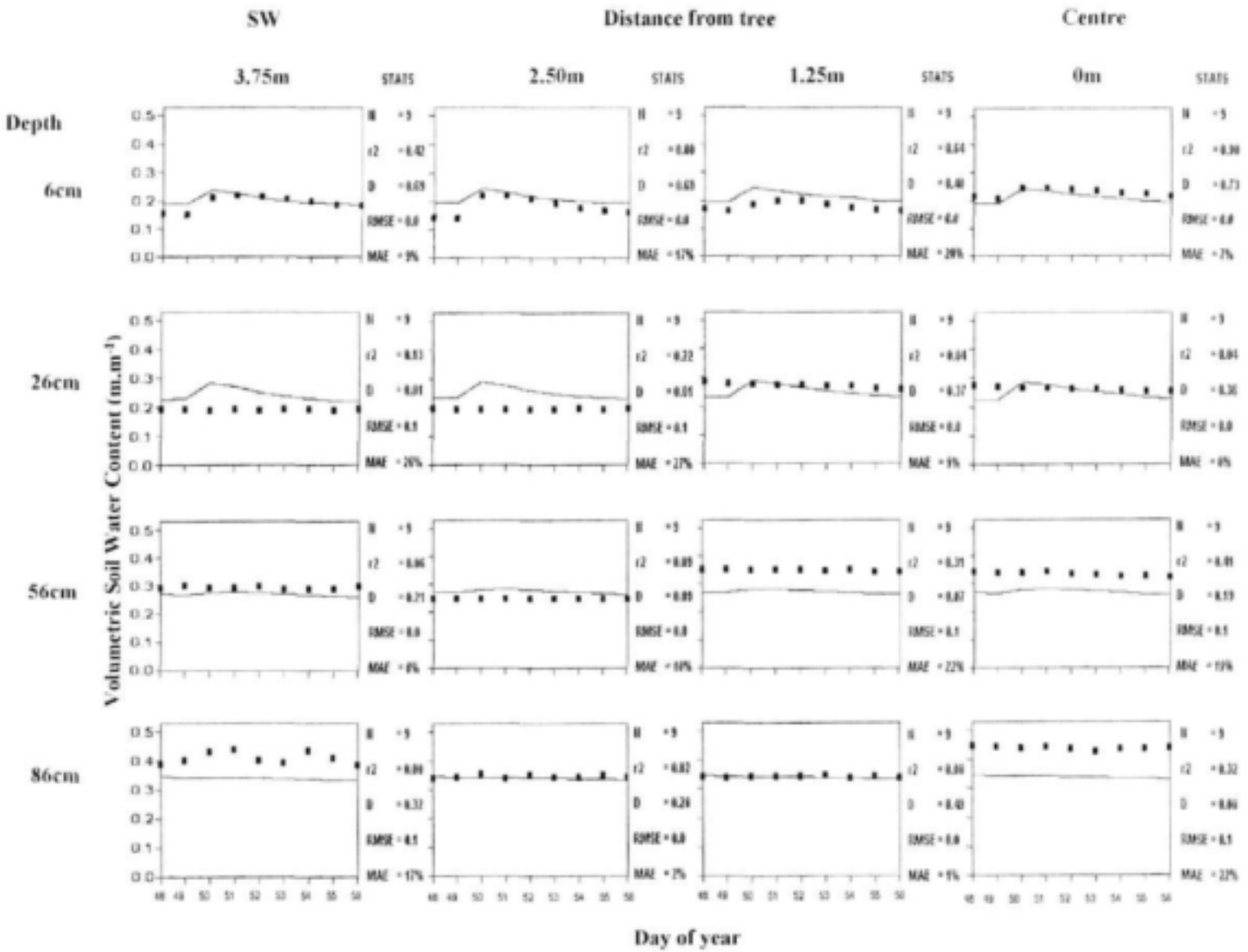

Figure 4.51a. Simulated (line) and measured (squares) volumetric soil water content on the SW side of the clementine hedgerow at 6, 26, 56 and 86 cm depths for the period 18 to 26 February, i.e. during a 22.6 mm rainfall event.

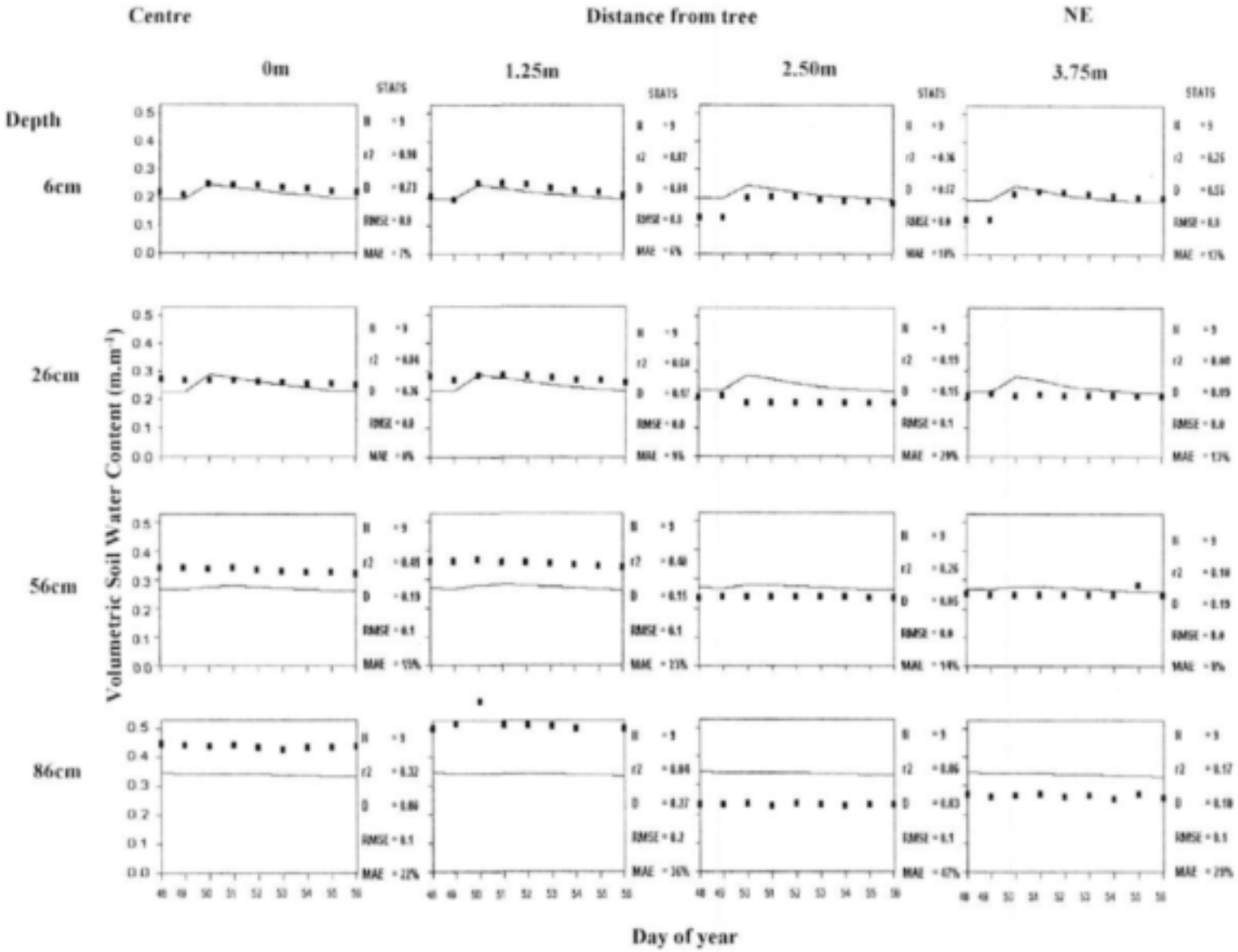

Figure 4.51b. Simulated (line) and measured (squares) volumetric soil water content on the NE side of the clementine hedgerow at 6, 26, 56 and 86 cm depths for the period 18 to 26 February, i.e. during a 22.6 mm rainfall event.

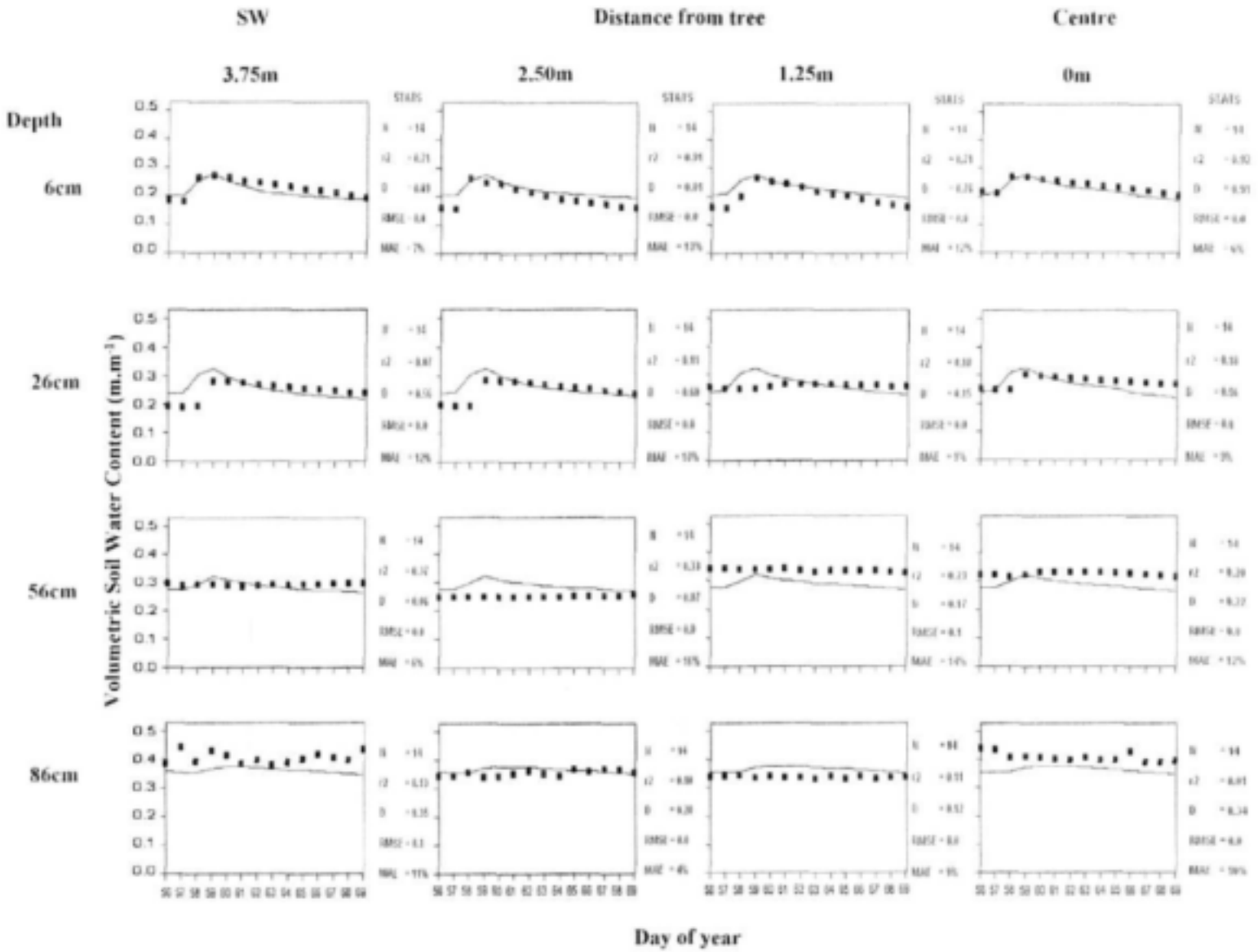

Figure 4.52a. Simulated (line) and measured (squares) volumetric soil water content on the SW side of the clementine hedgerow at 6, 26, 56 and 86 cm depths for the period 26 February to 11 March, i.e. during a heavy rainfall (34.9 mm) event.

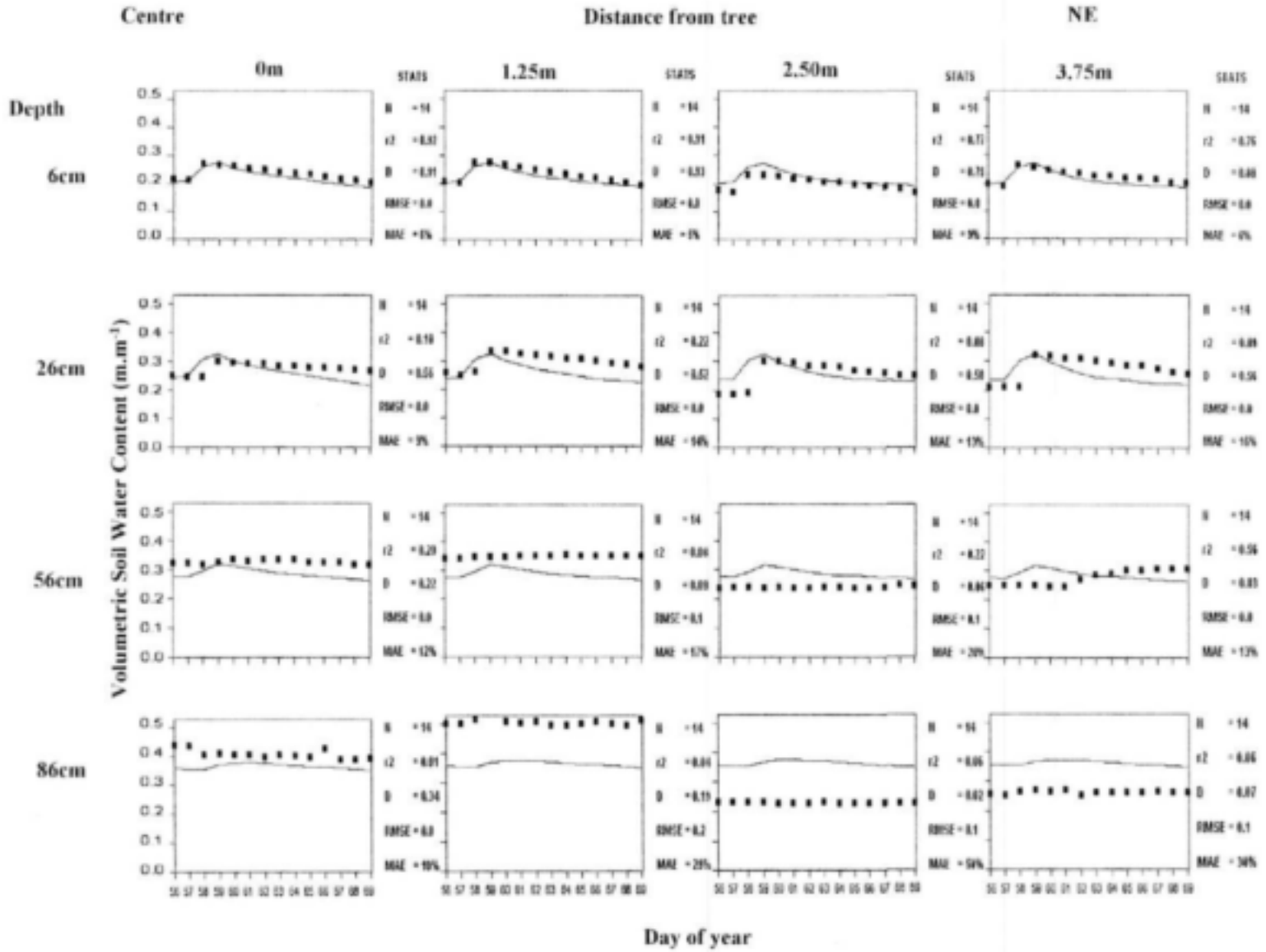

Figure 4.52b. Simulated (line) and measured (squares) volumetric soil water content on the NE side of the clementine hedgerow at 6, 26, 56 and 86 cm depths for the period 26 February to 11 March, i.e. during a heavy rainfall (34.9 mm) event.

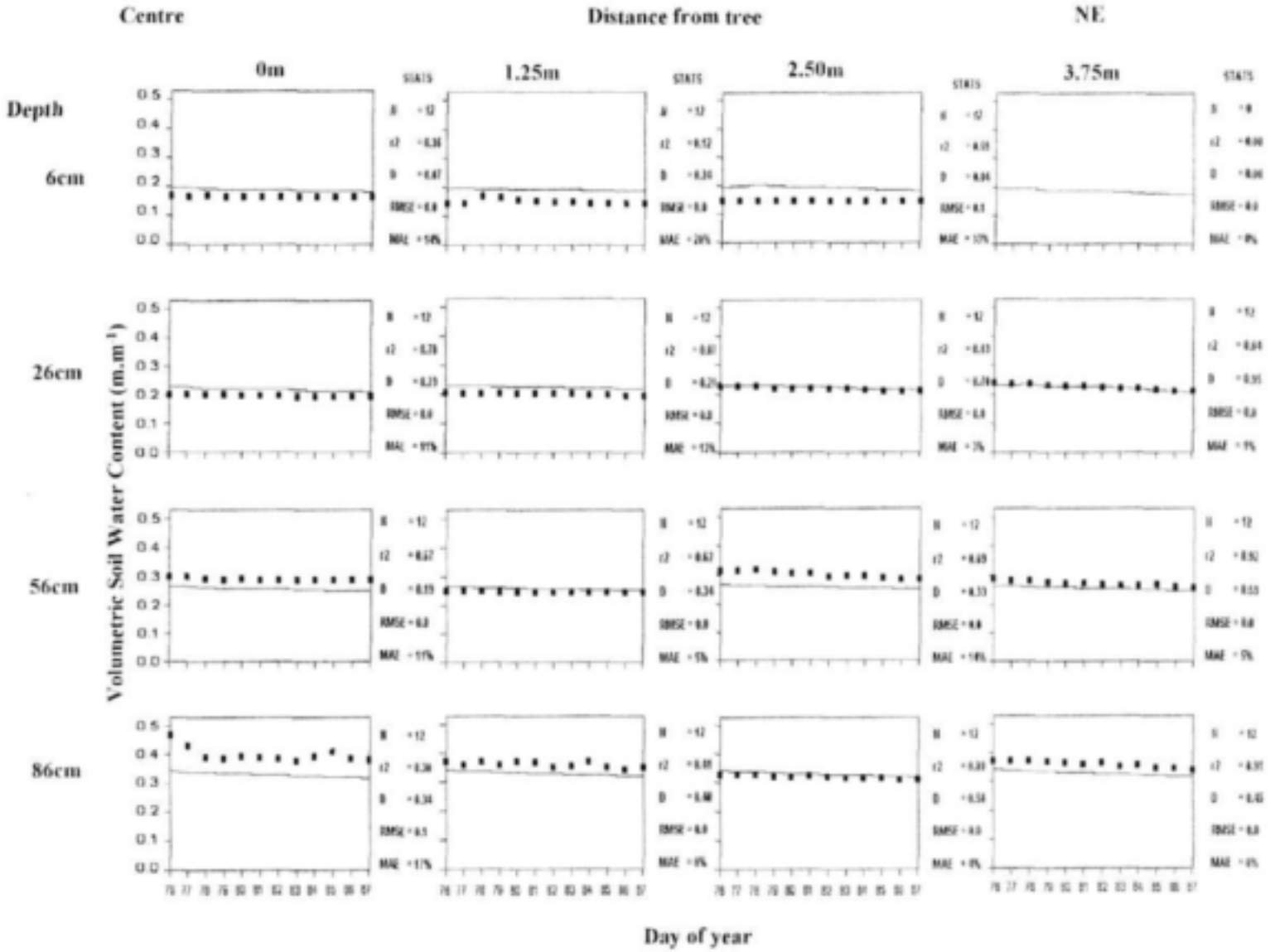

Figure 4.53a. Simulated (line) and measured (squares) volumetric soil water content on the SW side of the clementine hedgerow at 6, 26, 56 and 86 cm depths for the period 18 to 29 March, i.e. during a light rainfall (8.3 mm) event.

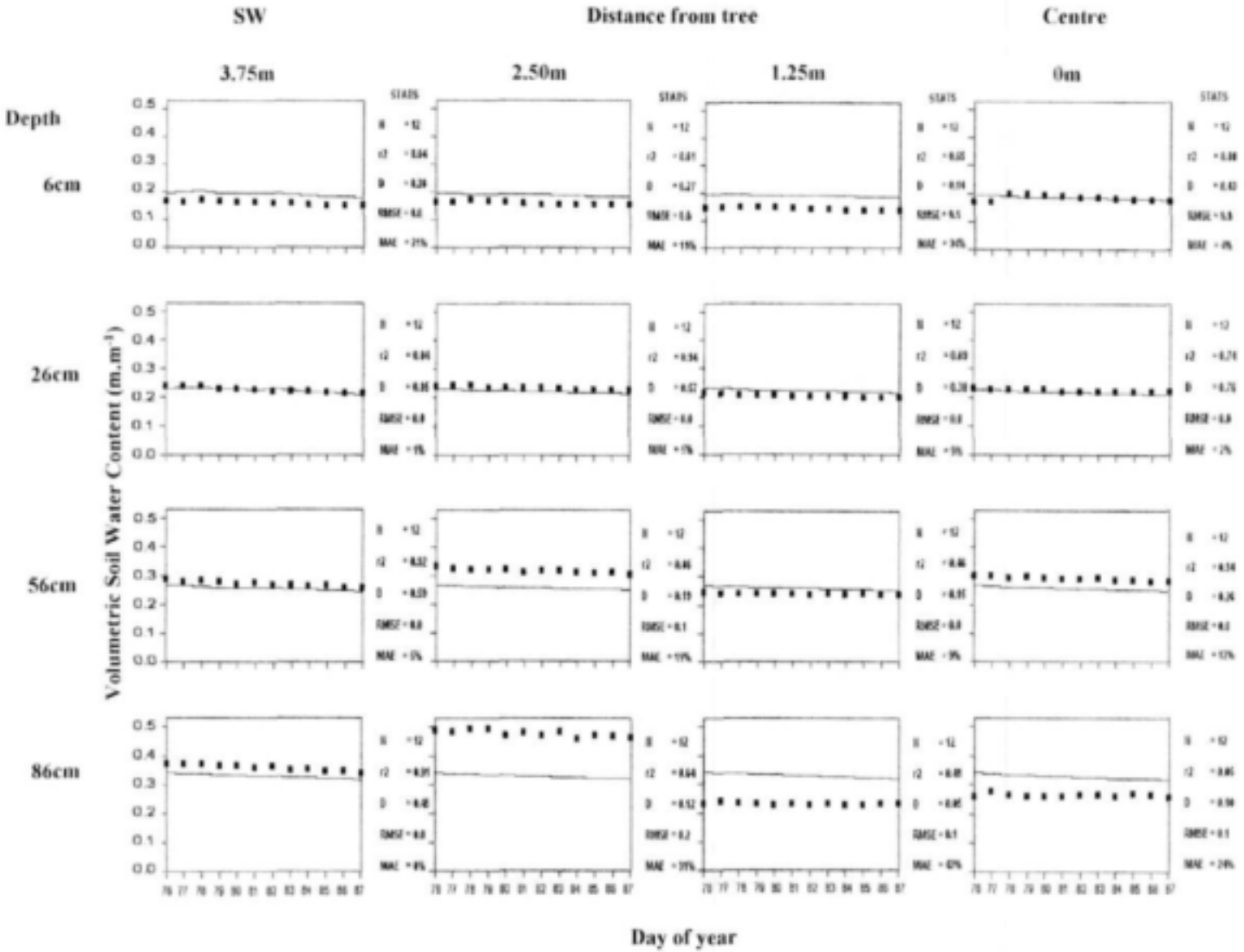

Figure 4.53b. Simulated (line) and measured (squares) volumetric soil water content on the NE side of the clementine hedgerow at 6, 26, 56 and 86 cm depths for the period 18 to 29 March, i.e. during a light rainfall (8.3 mm) event.

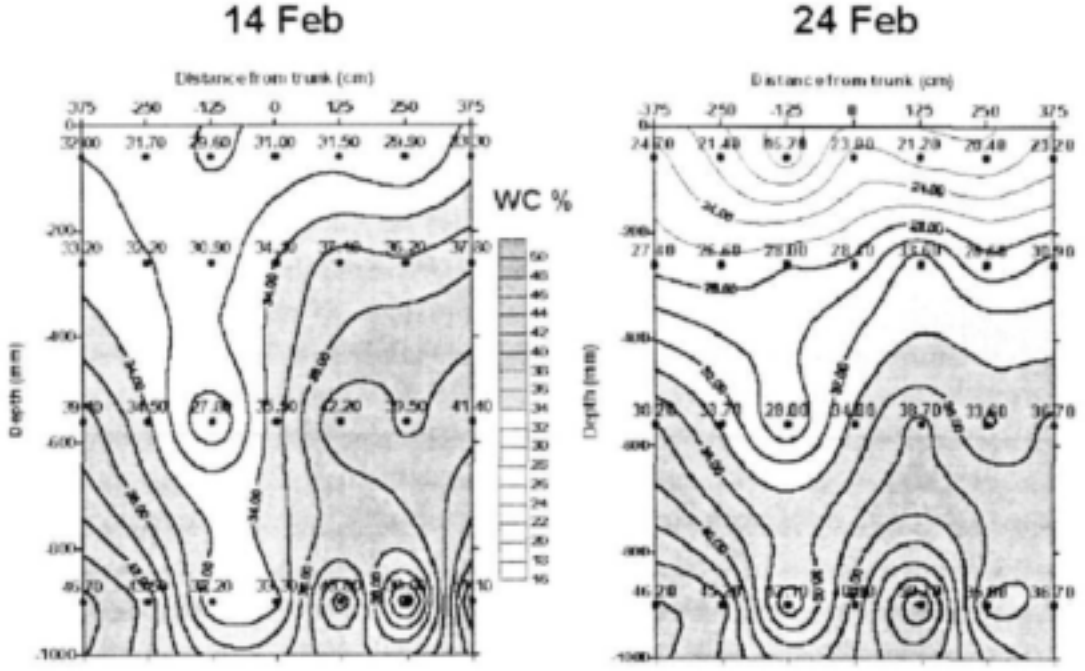

Figure 4.54. Variation in measured volumetric soil water content (WC %) with depth across the clementine hedgerow one day after a 48 mm rainfall (14 February 2000) and 10 days later (24 February 2000). Negative distances on the x-axis are for the SW side of the row, and positive values are for the NE side.

4.6. *Scenario modelling and sensitivity analysis*

Although the two-dimensional SWB was mainly developed as a tool for real-time irrigation scheduling, it can also be used for planning purposes. In this Section, scenario modelling and sensitivity analyses were carried out varying some input parameters and observing variations in certain output variables. The aim of this exercise was to identify the most suitable management practice in order to maximise water use efficiency.

Two case studies were considered for two imaginary orchards, the one in Kakamas (Northern Cape) and the other in Stellenbosch (Western Cape). The two locations were chosen for comparative purposes, as the latitudes and climates differ considerably. The geographic coordinates of Kakamas are 28°46'S and 20°37'E, altitude is 850 m and the climate is dry and hot with an average annual rainfall of ≈ 150 mm, mostly in summer. Stellenbosch (33°54'S; 18°52'E; altitude 146 m) is located in the winter rainfall region (Mediterranean climate) with an average annual rainfall of ≈ 800 mm.

In the imaginary orchard at Kakamas, field capacity was 0.2 m m^{-1} and permanent wilting point was 0.1 m m^{-1}. At Stellenbosch, field capacity was 0.15 m m^{-1} and permanent wilting point was 0.08 m m^{-1}. In both orchards, the depth of the soil profile was 1.1 m, the depth of the root system was 1 m and bulk density was 1.5 Mg m^{-3}. Row width was assumed to be 5 m, which is common practice in orchards in the area.

Weather data sets for the two locations included maximum and minimum temperature, solar radiation, wind speed as well as maximum and minimum relative humidity. The simulations were run from 01/01/1998 until 28/02/1998. This is the period of the year with peak atmospheric evaporative demand at both locations.

The objective of the exercise was to find the row orientation, width of the canopy and width of the irrigated strip that will provide maximum water use efficiency. An additional sensitivity analysis was carried out to investigate the effect of root density in the inter-row area on crop water use. A comparison between the finite difference and cascading model was also carried out using different canopy widths.

Row orientation

Scenario simulations were carried out with optimal conditions of soil water supply. Irrigations were simulated daily on a 1 m wide wetted strip to restore daily water losses through evaporation and transpiration. Canopy width was assumed to be 2 m, which is common practice in the areas considered. Canopy height was 3 m and leaf area density 2 m^2 m^{-3}. Simulations were run varying the row orientation in the two orchards and observing variations in the output results of evaporation and transpiration. The root system was assumed evenly developed in the wetted and non-wetted portions of the profile.

The results are shown in Figure 4.55. Evaporation (E), transpiration (T) and evapotranspiration (ET) were higher in the hot and dry climate of Kakamas compared to Stellenbosch. Transpiration was larger than evaporation at both sites for the specific input data sets used. Expressed as % of ET, E was lowest and T was largest at row orientations close to 0° (N-S row axis). It is therefore recommended that, at both locations, the orchard be planted in a N-S orientation to maximise canopy light interception and minimise water losses through evaporation.

Wetted diameter and canopy width

Scenario simulations were run varying wetted diameter (width of the wetted strip) and canopy width, and observing variations in the output results of evaporation and transpiration. Simulations were run for both case studies with row orientation equal to 0°. Irrigations were simulated daily to restore water losses through evaporation and transpiration. Canopy height

was 3 m and leaf area density 2 m^2 m^{-3}. The root system was assumed to be horizontally evenly developed in the wetted and non-wetted portions of the ground.

Simulated transpiration in mm is shown in Figure 4.56. Transpiration was higher in the hot and dry climate of Kakamas compared to Stellenbosch. It increased by increasing canopy width due to a larger interception of energy by the canopy, and by increasing wetted diameter due to a larger soil water supply. In Figure 4.57, transpiration is expressed as a percent of ET. It is interesting to note that, although T (in % of ET) increased by increasing canopy width, it decreased by increasing wetted diameter as the evaporation losses increased when the wetted area of the soil surface became larger. As a rule of thumb, good water use efficiency can be assumed when more than 70% of the soil water is used for transpiration. A wetted diameter of 0.5 m or less and pruning to reduce the canopy width to 2 m can therefore be recommended for both locations.

Root density

The SWB model allows the user to choose the fraction of roots in the wetted volume of soil. A sensitivity analysis was carried out for both case studies varying the fraction of roots in the wetted volume of soil, and observing variations in the output results of evaporation and transpiration. Simulations were run for both case studies with row orientation equal to 0°, wetted diameter 2 m and canopy width 2 m. Canopy height was 3 m and leaf area density 2 m^2 m^{-3}. As the first two months of 1998 were very dry at Kakamas and Stellenbosch, 50 mm rains were simulated to occur every 10 days. This yielded a total of 300 mm for the two months.

Figure 4.58 shows simulated evaporation and transpiration as a function of the fraction of roots in the wetted volume of soil. A root fraction of 1 indicates that all roots are assumed to be in the wetted volume of soil, a root fraction of 0.9 indicates that 90% of the root are in the wetted volume and 10% in the non-wetted volume, and so on. Maximum transpiration was determined for the particular data sets by simulating daily irrigations to restore water losses through evaporation and transpiration.

It was interesting to note the efficiency of rainfall utilisation by crops having different root densities in the wetted and non-wetted portions of the soil (Figure 4.58). Low T and high E was calculated by assuming all roots are in the wetted volume. By decreasing the root fraction in the wetted volume down to 0.5, T increased and E decreased as the roots in the inter-row volume contributed to crop water uptake. By assuming a root fraction of 0.5 (the same amount of roots in the wetted and non-wetted volume, i.e. root system evenly distributed across the row), T was very close to maximum T and evaporation was the lowest. By further decreasing the root fraction in the wetted volume and assuming there were more roots in the non-wetted volume, T decreased and E increased. This occurred as the major contribution to root water uptake originated from the non-wetted volume of soil, where no shading of the ground generally occurred during the day, evaporation was high and less water was available for transpiration. The effect of root density across the row was more pronounced at Kakamas where the atmospheric evaporative demand is higher compared to Stellenbosch.

Models' comparison

Scenario simulations were run with row orientation 0°, wetted diameter 0.5 m and varying canopy width, using both the finite difference and the cascading soil water balance model of SWB. The aim was to determine if, for these particular case studies, the simpler cascading model yields similar results to the more complex finite difference model. The FAO crop factors (Kcb) for the cascading model were chosen so that the fractional interception of radiation fitted the ratio of canopy width to row width. In this way, fractional interception of radiation was assumed to be equal to canopy cover with no transmittance of radiation through the canopy. The weather data set included very low rainfall for the period simulated

(from 01/01/1998 to 28/02/1998). In order to test the effect of rainfall on soil evaporation from the inter-row area, 30 mm of rain were simulated to occur every 10 days for the period considered. The root system was assumed evenly developed in the wetted and non-wetted portions of the soil for both soil water balance models.

The simulation results are shown in Figure 4.59. It is evident that the cascading model underestimated transpiration at small canopy widths. Transpiration values simulated with the two models were close at large canopy widths. The cascading model underestimated soil evaporation at small canopy widths, but it overestimated it at large widths. The main reason for this disagreement is the different calculation of water redistribution used in the two models. The finite difference model equilibrates water in two dimensions on the basis of matric potential gradients, whilst the cascading model moves water only downwards in the wetted and non-wetted volumes of the soil and simulates evaporation only from the top layer of the soil.

Interpretation of results

According to the scenario simulations, and in order to maximise water use efficiency, the optimal management for the orchards in Kakamas and Stellenbosch imply row orientation 0° (N-S row axis), a wetted diameter of 0.5 m and a canopy width of 2 m. The width of the wetted strip could be increased and similar or higher water use efficiency could be achieved by increasing canopy width. This would, however, reduce the inter-row area and make mechanised management and harvesting more difficult.

It is recommended to take into account possible contributions to crop water uptake from the volume of soil in the inter-row region in order to maximise rainfall use efficiency. As the root fraction in the wetted volume of soil is an input to SWB, information on the development of the rooting system is indispensable for management of irrigations on farm. An accurate estimate of the root fraction in the wetted and non-wetted volume can be obtained by digging a hole across the row, taking soil samples and determining root densities.

The finite difference model, based on sound physical principles, is more reliable than the cascading model, but it also requires more input parameters. In particular, the most difficult parameters to determine will be the leaf area density for the radiation energy part due to the cost of the instrumentation, and the hydraulic conductivity for the soil part due to the specialised knowledge and scientific equipment required. The cascading model also requires calibrated FAO crop factors in order to reasonably partition E and T.

It must be borne in mind that the examples presented in this study are case specific. Different results are to be expected for different conditions and if different input data sets are used. The results of the scenario simulations were obtained assuming the orchard is situated on a level area. It can be expected that under conditions where the orchard surface slopes giving a different aspect, under differing hedgerow orientations as well as at different latitudes, the relative importance of transpiration to evaporation would differ. These variables should be accounted for when planting an orchard. An optimisation program could be built in SWB in order to optimise all input parameters at the same time. This would facilitate the choice of optimal management without having to run simulations by trial and error. Computer software that could be adapted for use with SWB is PEST – ASP (Model-Independent Parameter ESTimation) developed by John Doherty and Watermark Numerical Computing (Australia).

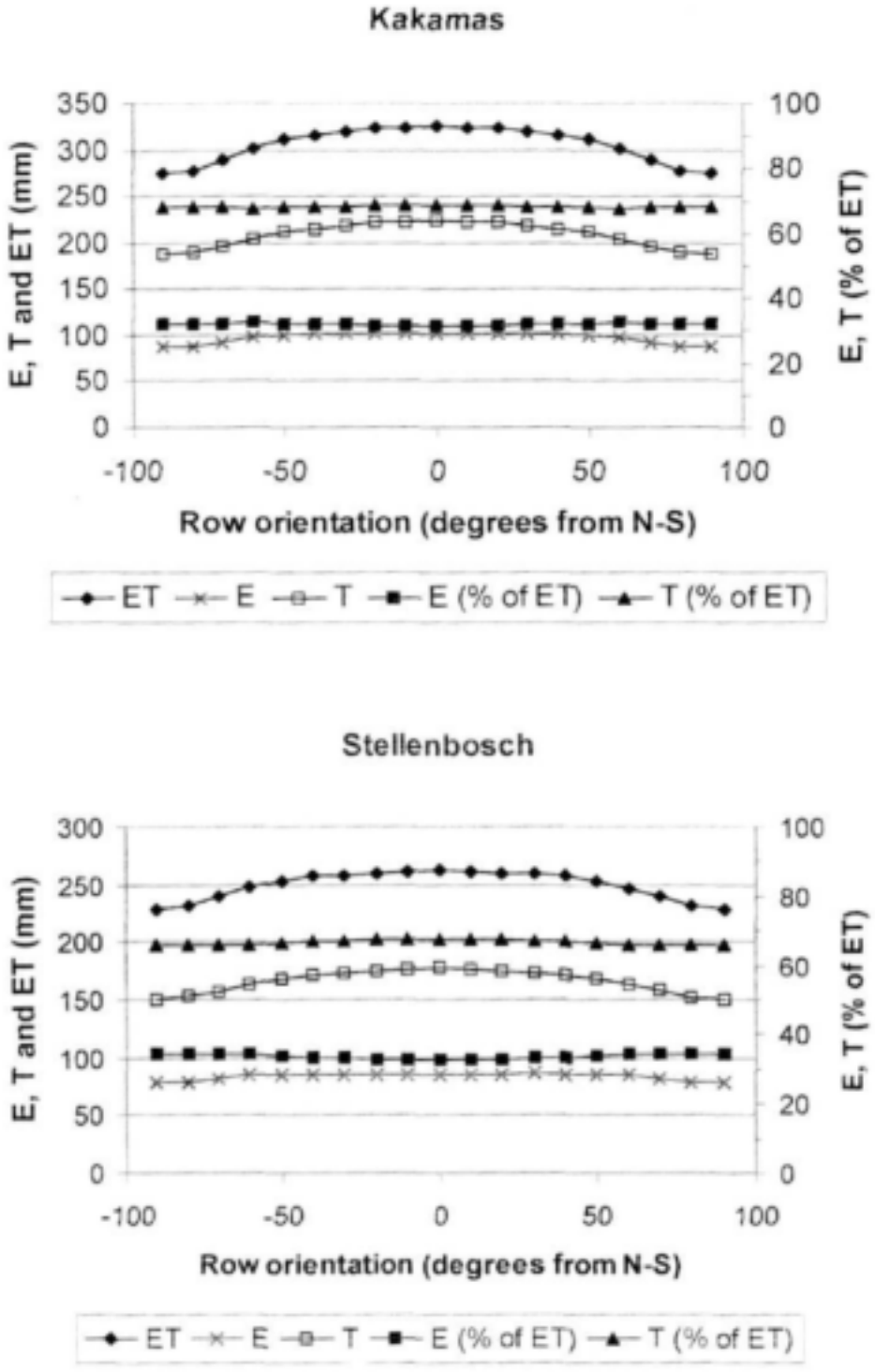

Figure 4.55. Simulated evaporation (E), transpiration (T) and evapotranspiration (ET) as a function of row orientation for two orchards at Kakamas and Stellenbosch (from 01/01/1998 to 28/02/1998).

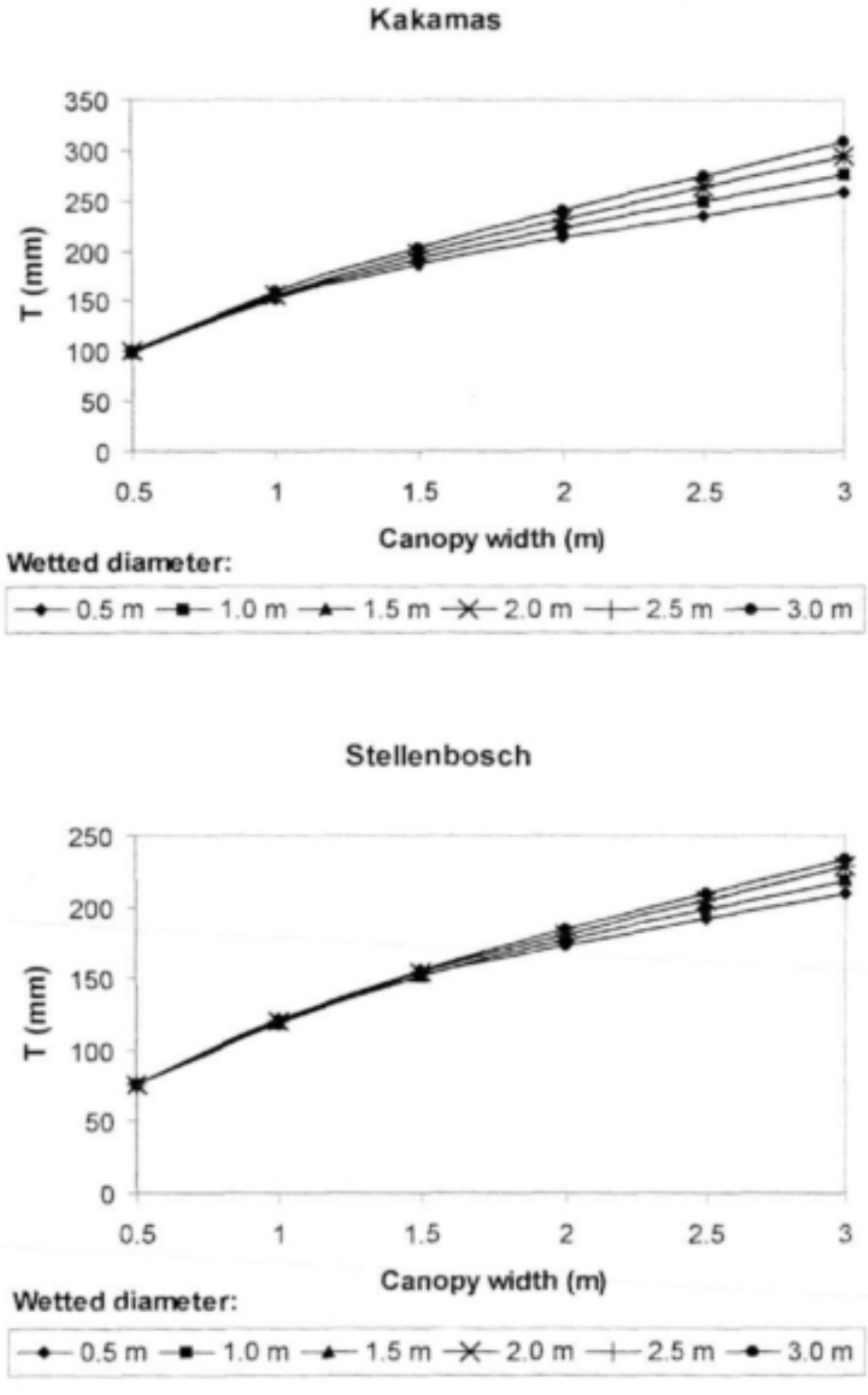

Figure 4.56. Simulated transpiration (T) as a function of canopy width and wetted diameter for two orchards at Kakamas and Stellenbosch (from 01/01/1998 to 28/02/1998).

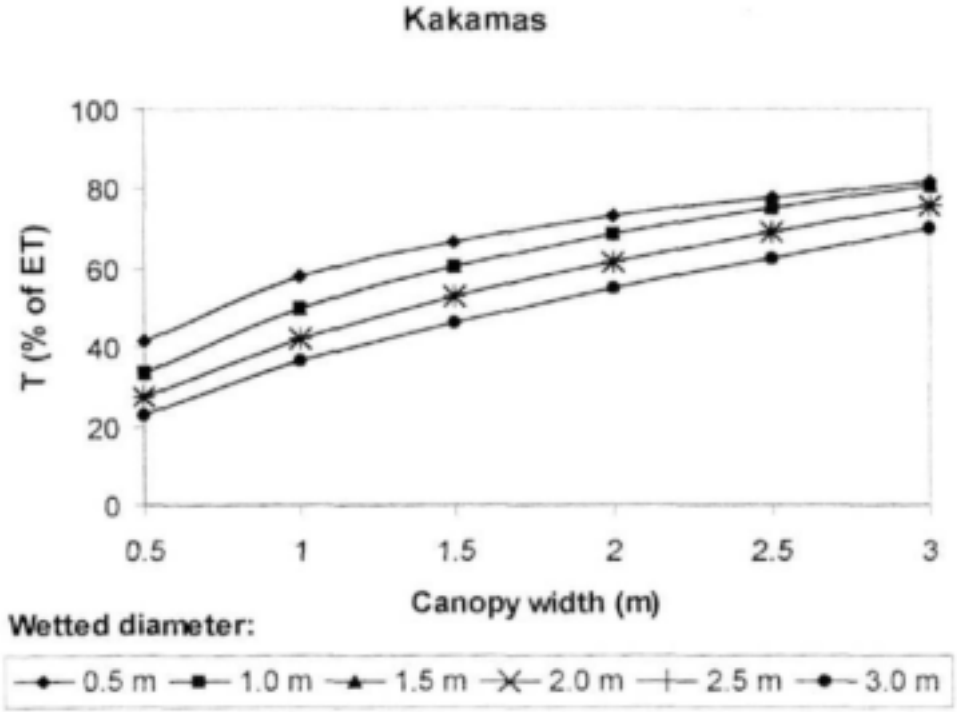

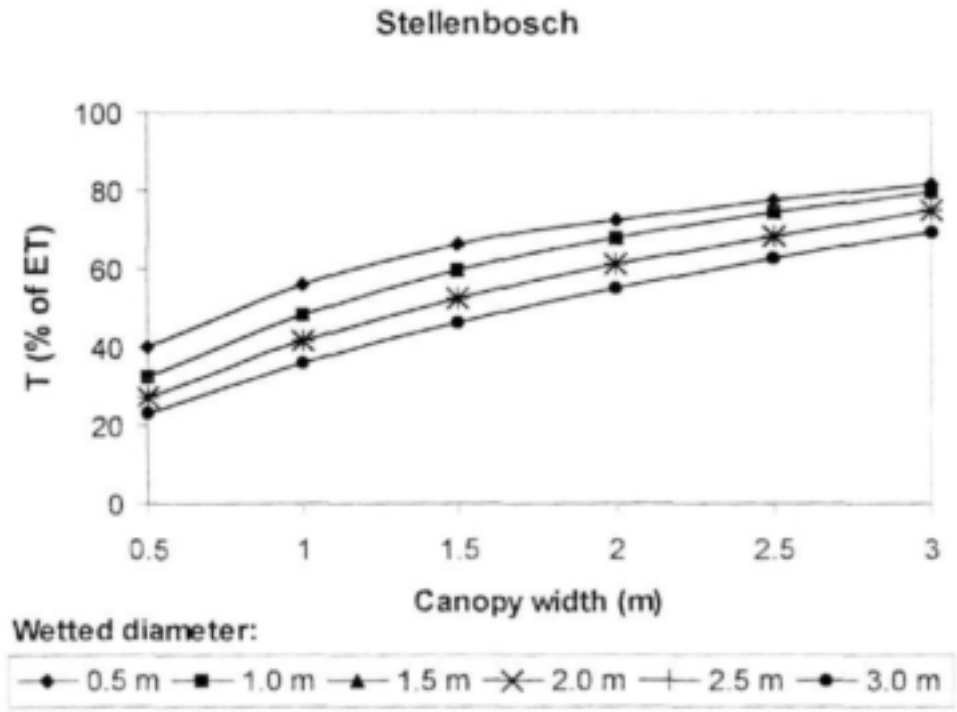

Figure 4.57. Simulated transpiration (T) in % of evapotranspiration (ET) as a function of canopy width and wetted diameter for two orchards at Kakamas and Stellenbosch (from 01/01/1998 to 28/02/1998).

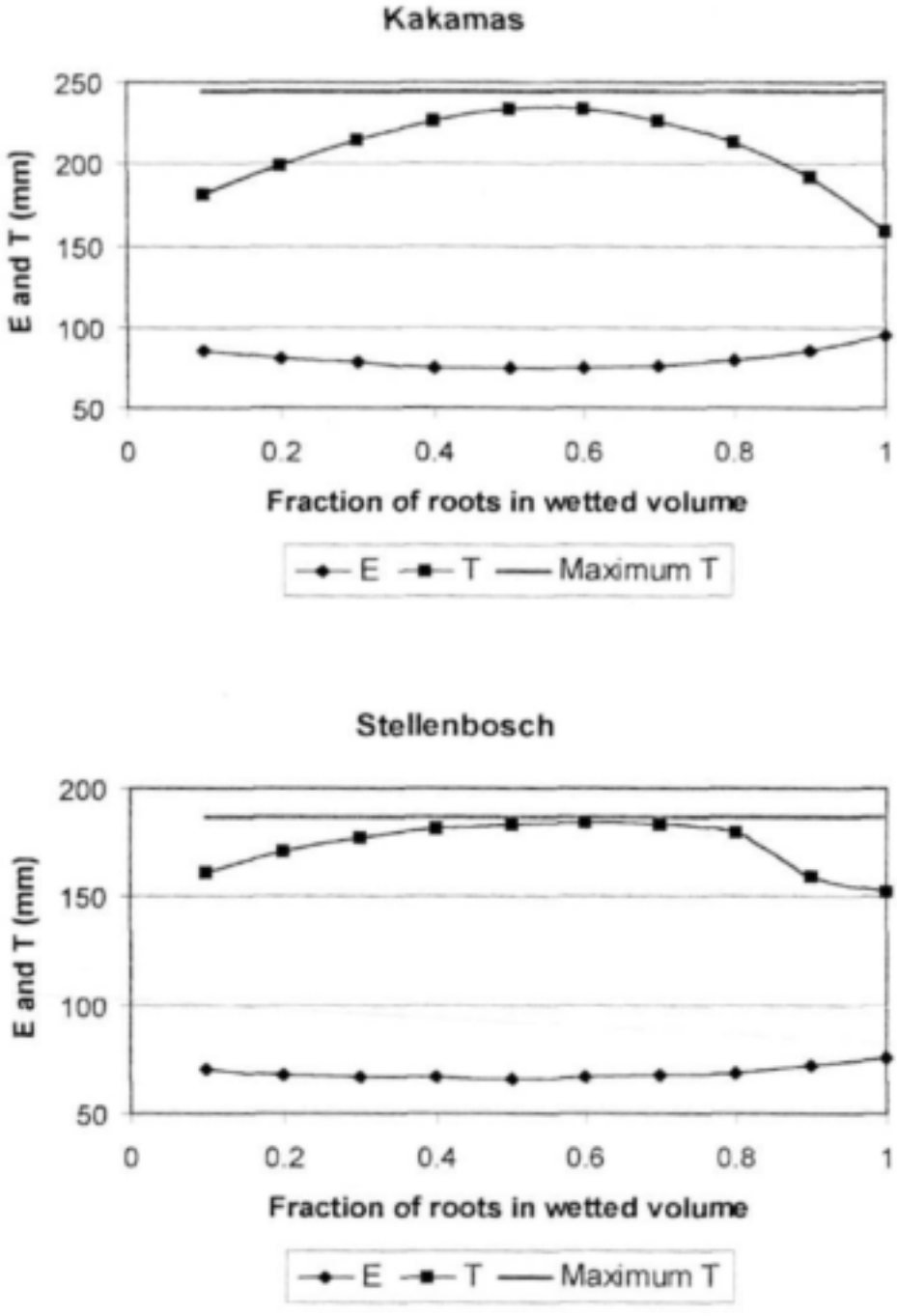

Figure 4.58. Simulated transpiration (T) and evaporation (E) as a function of the fraction of roots in the wetted volume of soil for two orchards at Kakamas and Stellenbosch (from 01/01/1998 to 28/02/1998).

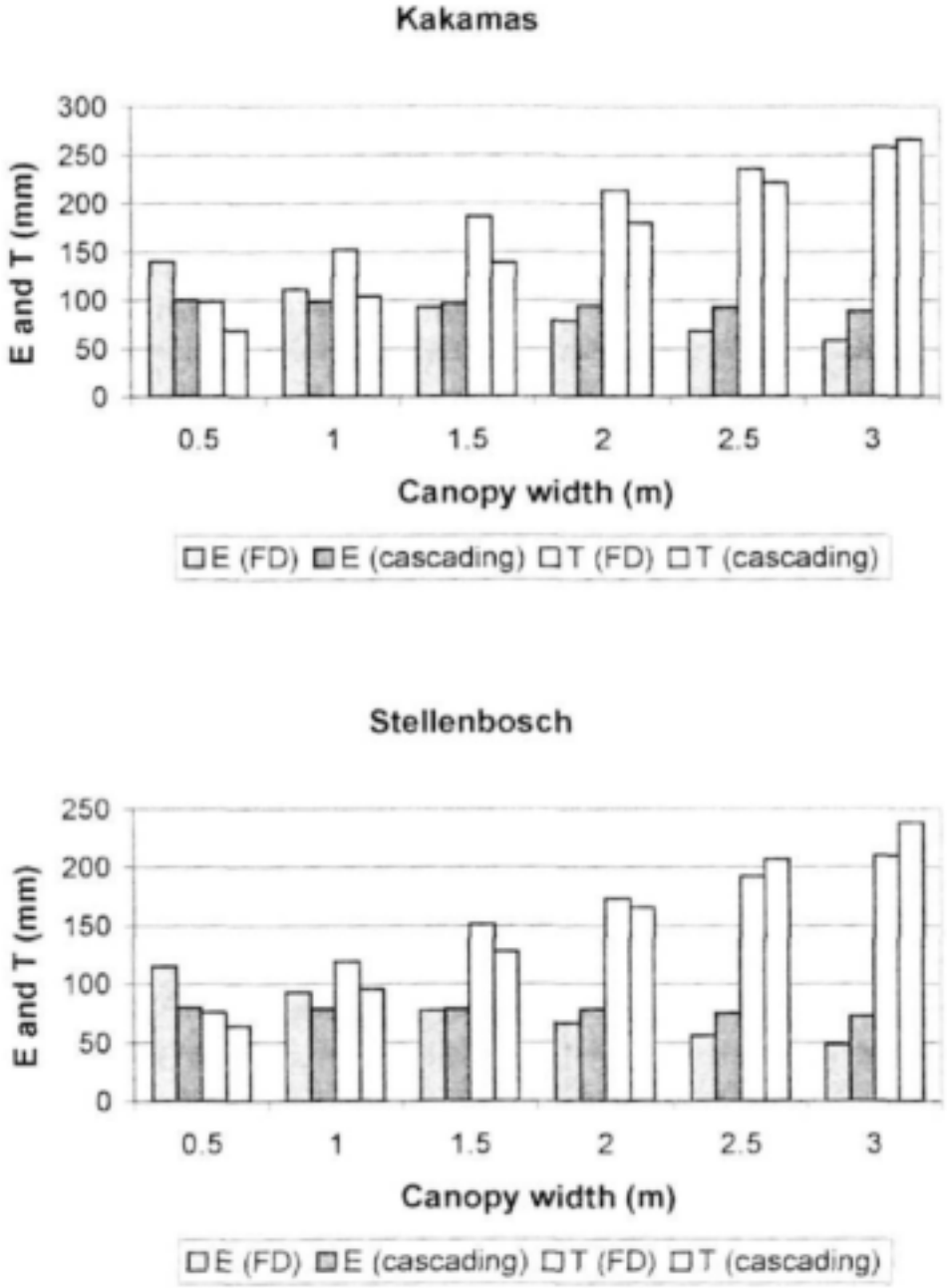

Figure 4.59. Evaporation (E) and transpiration (T) simulated with the cascading and finite difference (FD) model as a function of canopy width for two orchards at Kakamas and Stellenbosch (from 01/01/1998 to 28/02/1998).

CHAPTER 5

CONCLUSIONS AND RECOMMENDATIONS

Conclusions

A two-dimensional energy interception and soil water balance model was developed (objective 1). The model was fully validated for deciduous trees (objective 2) using data obtained in field trials on peaches and Leucaena (Hatfield experimental station, University of Pretoria). For model validation in evergreen citrus orchards (objective 3), data obtained in field trials set up at the Syferkuil experimental station (University of the North) and on two commercial farms in Brits were used. The development of a core of irrigation expertise at the University of the North (objective 4) and the supply of equipment to the University of the North for research and training (objective 5) were also achieved. This is dealt with in detail in the report on capacity building and technology transfer (Chapter 7).

The two-dimensional energy interception and soil water balance model was developed by the research team and included in the Soil Water Balance (SWB) irrigation scheduling model. This should facilitate irrigation water management of micro-irrigated crops. The SWB model is available for use with Windows 95 on an IBM-PC or compatible computer. The minimum requirement is 16 Mb RAM and a CD-ROM drive. The program is supplied in executable code on CD.

Two soil water balance models were included in SWB in order to facilitate irrigation scheduling of hedgerow tree crops. The first model calculates the two-dimensional energy interception for hedgerow tree crops, based on solar and row orientation, tree size and shape, as well as leaf area density. Two-dimensional soil water redistribution is also calculated with a finite difference solution. A simpler model, based on the FAO crop factor approach and a cascading soil water balance, was also developed to enable users to predict crop water requirements with a limited number of input data.

Both the two-dimensional and the cascading soil water balance models account for effects that are typical for localised irrigation in hedgerow orchards, and that have been observed in the field trials. These factors are variability in soil water deficit and irrigation distribution across the row. Root length density is also not always uniform across the row and the SWB model makes provision for this through an input variable, which is defined as the fraction of roots in the wetted volume of soil. In addition, the two-dimensional energy interception model accounts for variations in soil irradiance across the row, and makes provision for shapes of tree canopies that resemble an ellipse with the bottom part cut off (tromboid) to accommodate certain pruning practices.

The FAO-based model and the cascading soil water balance were calibrated for first leaf and second leaf peaches.

The validation of the two-dimensional energy and soil water balance model was done in three steps:

i) Validation of the two-dimensional energy interception sub-model separately using independent data sets collected in all field trials.

ii) Validation of the soil evaporation sub-model separately using independent data sets collected in the peach field trial at Hatfield.

iii) Validation of the aggregate two-dimensional energy and soil water balance model, using independent data sets collected in the field trial at Syferkuil.

The two-dimensional energy interception model was validated for different conditions (latitude, row orientation, size of the canopy and leaf area density). It is fair to say that hourly spatial and temporal variations of radiant transmittance were generally well simulated by the radiant interception model presented in this study. The results obtained show that when one

deals with a symmetrical and elliptical canopy having a uniform leaf distribution, for example the Syferkuil clementine hedgerow, the model follows the diurnal cycle of radiant transmittance exceptionally well. In the case where the canopy is non-symmetric and/or has non-uniform leaf distribution, as can be expected, errors in predictions of solar radiation transmittance will occur.

Irregular trunks and branches could cause inaccuracies in predictions of the energy balance. At low values of leaf area density, the shade from trunks and branches is not accounted for in the SWB model. The subroutine splitting total solar radiation into diffuse and direct radiation should be further tested. The relative importance of the non-symmetric canopy shape as opposed to the non-uniform leaf distribution should be investigated. It would also be interesting to test the model for conditions where the canopy does not have an elliptical shape at all.

The soil evaporation model was tested in a seven days field experiment undertaken to study the distribution of solar radiation and soil water evaporation across a hedgerow peach orchard following irrigation. The variability in irradiance reaching the soil beneath the orchard, due to partial shading by the canopies, was related to that of evaporation: locations which were out of the shade of trees (on the northern side of the row) received almost full solar radiation and had the highest evaporation rates, whereas shaded locations (under the tree and on the southern side of the row) had low evaporation rates.

Simulations of light interception by the two-dimensional SWB model were in good agreement with observations, though the tree dimensions for which the model gave the best predictions were slightly different from those measured in the orchard. Concerning evaporation, model predictions matched the measurements made with the micro-lysimeter with less accuracy. This may be due to errors in both the micro-lysimeter measurements of evaporation, and in the model predictions. The experiment conducted to validate the technique showed that: i) there was a relatively high variability in lysimeter measurements, even for lysimeters placed in similar conditions; ii) evaporation measurements were highly dependent on the local environment (bare soil or grass) in which the micro-lysimeters were installed. The model predictions could have been affected by: i) errors in parameter estimation, iii) cumulative errors in the estimation of water content after a few days, and iii) inaccuracies in describing water transfer in the upper layers of the soil and humidity at the soil surface. It also appeared important to measure air relative humidity in orchards and use it as input in order to predict soil evaporation accurately.

The two-dimensional energy and soil water balance model was validated using data from the citrus trial at Syferkuil. The model predicted the soil water content at different depths in the soil profile and distances from the tree row reasonably well. The major difficulties encountered in the validation of the soil water balance were due to spatial variability of soil properties and disturbance of the soil when the water sensors were installed.

Careful installation is therefore recommended for soil water sensors that give point measurements like those used in this study (heat dissipation sensors and TDR probes). The TDR probes can be used in irrigation scheduling to determine crop water use over certain periods. Caution should, however, be exercised in the interpretation of absolute values of volumetric soil water content obtained as output reading from the probes.

The two-dimensional energy and soil water balance model is primarily meant to be a real-time, irrigation scheduling tool for commercial orchards. Results from this study should guide irrigation scheduling consultants, extension officers and farmers to more efficiently use scarce water resources on high value tree crops. The two-dimensional model, however, can also be used for planning purposes as demonstrated in the scenario simulations. The mechanistic canopy radiation interception routine which has been shown to be very accurate will make it possible to evaluate the effect of row orientation and spacing as well as the effect of wetted diameter and pruning practices on water use.

The biggest contribution of this model is likely to be the quantification of the contribution that rainfall can make to crop water use by taking the non-irrigated inter-row soil reservoir into account. Scenario simulations proved that crop water uptake from the inter-row volume of soil can be high and this needs to be accounted for in irrigation management in order to maximise rainfall use efficiency. It is recommended to accurately estimate the root fraction in the wetted and non-wetted volume of soil by digging a trench across the row, taking soil samples and determining root density.

The two-dimensional energy interception and finite difference soil water balance model is expected to be more accurate than the cascading soil water balance, due to the sound physical principles on which it is based. The mechanistic detailed approach could give guidance with respect to the magnitude of errors made by using simpler, more empirical approaches. However, the two-dimensional model will also require more input parameters compared to the simpler cascading model. In particular, the most difficult parameters to determine will be the leaf area density for the radiation energy part due to the cost of the instrumentation, and the hydraulic conductivity for the soil part due to the specialised knowledge and scientific equipment required. On the other hand, the cascading model requires calibrated FAO crop factors in order to reasonably partition E and T. It would be interesting to compare the cascading and the two-dimensional soil water balance models against field measurements in order to determine the level of accuracy in predictions.

During this project, two user-friendly tools have also been developed, the ETo and HDS calculator. The ETo calculator was developed as a stand-alone tool for the calculation and database storage of the Penman-Monteith reference evapotranspiration (ETo). It can also be used to check what weather measurements can be omitted without experiencing large errors in the estimation of ETo at a particular site. This should facilitate the application of SWB in combination with a weather station, and improve the accuracy of model predictions. The HDS calculator was indispensable for processing data obtained from heat dissipation sensors, which were used to estimate soil matric potential in the field trials. The HDS calculator was used for individual calibration and temperature correction of sensors' readings.

Recommendations for further research

The successful validation of the two-dimensional energy interception and soil water balance model opens the opportunity to develop a useful yield predictor and productivity efficiency measure if one knows the canopy to fruit ratio. This information could also be useful for fruit colour, size and internal quality (sugar content) research, depending on the market requirements for a specific plant species.

As demonstrated with data from the peach trial at Hatfield, soil or cover crops between rows can also have a large effect on the efficient use of rainfall, and this should be further investigated.

Although not common, it is practiced on certain commercial farms to irrigate orchards with drip irrigation systems several times during the day. This implies the need for an hourly time step model in order to accurately predict the soil water balance. The hourly Penman-Monteith reference evapotranspiration procedure has recently been finalised and appears in the Irrigation and Drainage Bulletin No. 56 published by the FAO (Allen et al., 1998). This could also be included in the SWB model for hourly predictions of crop water requirements.

An optimisation program could be built in SWB-2D in order to optimise all input parameters at the same time. This would facilitate the choice of optimal management (row orientation and spacing, wetted diameter and pruning practices) without having to run simulations by trial and error. Computer software that could be adapted for use with SWB is PEST – ASP (Model-Independent Parameter ESTimation) developed by John Doherty and Watermark Numerical Computing (Australia).

REFERENCES

ALLEN RG (1997) Self-calibrating method for estimating solar radiation from air temperature. ASCE J. Hydrol. Eng. 2(2) 56-67.

ALLEN RG, JENSEN ME, WRIGHT JL, BURMAN RD (1989) Operational estimates of evapotranspiration. *Agron. J.* 81 650-662.

ALLEN RG, SMITH M, PRUITT WO and PEREIRA LS (1996) Modifications to the FAO crop coefficient approach. *Proc. of the Int. Conf. on Evapotranspiration and Irrigation Scheduling*. San Antonio, Texas, USA. 124-132.

ALLEN RG, PEREIRA LS, RAES D and SMITH M (1998) *Crop evapotranspiration. Guidelines for computing crop water requirements.* Irrigation and Drainage Paper No. 56. FAO, Rome, Italy.

ANNANDALE JG, BENADÉ N, JOVANOVIC NZ, STEYN JM and DU SAUTOY N (1999) Facilitating Irrigation Scheduling by Means of the Soil Water Balance Model. Water Research Commission Report No. 753/1/99, Pretoria, South Africa.

ANNANDALE JG, CAMPBELL GS, OLIVIER FC and JOVANOVIC NZ (2000) Predicting crop water uptake under full and deficit irrigation: An example using pea (*Pisum sativum* L. cv. Puget). *Irrig. Sci.* 19 65-72.

BEGG JE, BURHUZEN JF, LEMON ER, MISRA DK, SLATYER RO and STERN WR (1964) Diurnal energy and water exchange in bulrush millet in an area of high solar radiation. *Agric. Meteorol.* 1 294-312.

BENNIE ATP, COETZEE MJ, VAN ANTWERPEN R, VAN RENSBURG LD and DU T. BURGER R (1988) 'n Waterbalansmodel vir besproeiing gebaseer op profielwatervoorsieningstempo en gewaswaterbehoeftes. Waternavorsingskommissie Verslag No. 144/1/88, Pretoria, South Africa.

BLACK TC, TANNER CB and GARDNER WR (1970) Evapotranspiration from a snapbean crop. *Agron. J.* 62 66-69.

BOAST CW and ROBERTSON TM (1982) The micro-lysimeter method for determining evaporation from bare soil. Description and laboratory evaluation. *Soil Sci. Soc. Am. J.* 46 689-696.

BOSEN JF (1958) An approximation formula to compute relative humidity from dry bulb and dew point temperatures. *Monthly Weather Rev.* 86(12) 486.

BRISTOW KL, CAMPBELL GS and CALISSENDORFF K (1993) Test of a heat-pulse probe for measuring changes in soil water content. *Soil Sci. Soc. Am. J.* 57 930-934.

BROWN KW and COVEY C (1966) The energy-budget evaluation of the micro meteorological transfer process within a cornfield. *Agric. Meteorol.* 3 73-96.

BURMAN RD, JENSEN ME, ALLEN RG (1987) Thermodynamic factors in evapotranspiration. In: James LG and English MJ (eds.) *Proc. Irrig. and Drain. Spec. Conf., ASCE*, Portland, Oregon, USA. 28-30.

CAMASE (1995) Newsletter of Agro-ecosystems modelling. Extra edition. AB-DLO Publisher, November 1995, Wageningen, The Netherlands, 8 pp.

CAMPBELL GS (1977) *An Introduction to Environmental Biophysics*. Springer, New York.

CAMPBELL GS (1985) *Soil physics with Basic*. Elsevier Science, Amsterdam.

CAMPBELL GS and DIAZ R (1988) Simplified soil-water balance models to predict crop transpiration. In: Bidinger FR and Johansen C (eds.) *Drought research priorities for the dryland tropics*. ICRISAT, India. 15-26.

CAMPBELL GS and GEE GW (1986) Water potential: Miscellaneous methods. In: Klute A (ed.) *Methods of Soil Analysis. Part 1*. Agronomy monograph No. 9. American Society of Agronomy, Soil Science Society of America, Madison, Wisconsin. 619-633.

CAMPBELL GS and NORMAN JM (1998) *An introduction to environmental biophysics*. 2nd ed. Springer, New York.

CAMPBELL GS and STOCKLE CO (1993) Prediction and simulation of water use in agricultural systems. In: *International Crop Science I*. Crop Sci. Soc. of Am., 677 S. Segoe Rd., Madison, WI 53711, USA.

CAMPBELL GS, CALISSENDORFF K and WILLIAMS JH (1991) Probe for measuring soil specific heat using a heat-pulse method. *Soil Sci. Soc. Am. J.* 55 291-293.

CAMPBELL GS, FLINT AL, BILSKIE J and CALISSENDORFF C (2001) Calibration and temperature correction of heat dissipation matric potential sensors. Unpublished.

CAPRIO JM, GRUNWALD GK and SNYDER RD (1985) Effect of standing stubble on soil water by evaporation. *Agric. Forest. Meteorol.* 34 129-144.

CHARLES-EDWARDS DA and THORNLEY HM (1973) Light interception by an isolated plant. A simple model. *Ann. Bot.* 37 919-928

CHARLES -EDWARDS DA and THORPE MR (1976) Interception of diffuse and direct-beam radiation by a hedgerow apple orchard. *Ann. Bot.* 40 603-613.

CROSBY CT (1996) SAPWAT 1.0 - A computer program for estimating irrigation requirements in Southern Africa. Water Research Commission Report No. 379/1/96, Pretoria, South Africa.

DE JAGER JM (1994) Accuracy of vegetation evaporation ratio formulae for estimating final wheat yield. *Water SA* 20(4) 307-315.

DOORENBOS J and PRUITT WO (1977) *Crop water requirements*. FAO Irrigation and Drainage Paper No. 24. FAO, Rome, Italy.

DUFFIE JA, BECKMAN WA (1980) *Solar engineering of thermal processes*. John Wiley and Sons, New York.

FAO (1998) *World Reference Base for Soil Resources*. World Soil Resources Report No. 84. FAO, Rome, Italy.

FUCHS M (1972) The control of the radiation climate of plant communities. In: Hillel D (ed.) Optimizing the Soil Physical Environment toward Greater Crop Yields. *Academic Press, New York*,173-191.

GOUDRIAAN J (1977) *Crop meteorology: a simulation study*. Pudoc, Wageningen.

GREEN GC (1985a) *Estimated irrigation requirements of crops in South Africa. Part 1*. Dept of Agric. and Water Supply, Pretoria, South Africa.

GREEN GC (1985b) *Estimated irrigation requirements of crops in South Africa. Part 2*. Dept of Agric. and Water Supply, Pretoria, South Africa.

HANKS RJ and RITCHIE JT (1991) *Modeling plant and soil systems*. Agronomy Monograph No. 31, ASA-CSSA-SSSA, 677 S. Segoe Rd., Madison, WI 53711. 545 pp.

HARRISON LP (1963) Fundamental concepts and definitions relating to humidity. In: Wexler A (ed.) *Humidity and Moisture, Vol. 3.*, Reinhold Publishing Company, New York.

HILLEL D (1998) *Environmental soil physics*. Academic Press, San Diego, CA, USA.

HODGES T and RITCHIE JT (1991) The CERES-wheat phenology model. In: Hodges T (ed.) *Predicting crop phenology*. CRC Press, Boston.

JACKSON RD and TAYLOR SA (1986) Thermal conductivity and diffusivity. In: Klute A (ed.) *Methods of Soil Analysis. Part 1.* Agronomy monograph No. 9. American Society of Agronomy, Soil Science Society of America, Madison, Wisconsin. 945-956.

JOVANOVIC NZ and ANNANDALE JG (1997) A laboratory evaluation of Watermark electrical resistance and Campbell Scientific 229 heat dissipation matric potential sensors. *Water SA* 23(3) 227-232.

JOVANOVIC NZ and ANNANDALE JG (1998) Measurement of radiant interception of crop canopies with the LAI-2000 plant canopy analyzer. *SA J. Plant and Soil* 15(1) 6-13.

JOVANOVIC NZ and ANNANDALE JG (1999) An FAO type crop factor modification to SWB for inclusion of crops with limited data: Examples for vegetable crops. *Water SA* 25(2) 181-189.

KNIGHT JH (1992) Sensitivity of time domain reflectometry measurements to lateral variations in soil water content. *Water Resour. Res.* 28(9) 2345-2352.

LASCANO RJ and VAN BAVEL CHM (1986) Simulation and measurement of evaporation from a bare soil. *Soil Sci. Soc. Am. J.* 50 1127-1132.

LASCANO RJ, VAN BAVEL CHM, HATFIELD JL and UPCHURCH DR (1987) Energy and water balance of a sparse crop: Simulated and measured soil and crop evaporation. *Soil Sci. Soc. Am. J.* 51 1113-1121.

MATTHIAS AD, SALEHI R and WARRICK AN (1986) Bare soil evaporation near a surface point- source emitter. *Agric. Water Manage.* 11 257-277.

MONTEITH JL (1977) Climate and efficiency of crop production in Britain. *Philos. Trans. R. Soc. London, Ser. B* 281 277-294.

NORMAN JM and WELLES (1983) Radiative transfer in an array of canopies. *Agron. J.* 75 481-488.

OR D, FISHER B, HUBSCHER RA and WRAITH J (1998) WinTDR 98 v. 4.0. Users Guide. Utah State University, Plant, Soils and Biometeorology, Logan, Utah, May 1998.

PENMAN HL (1948) Natural evaporation from open water, bare soil and grass. *Proc R. Soc. Lond (A)* 193 120-145.

PHILLIPS RJ (1957) Evaporation, moisture and heat fields in the soil. *Meteorol. J.* 14 354-366.

PRUITT WD, HENDERSON WD, FERERES E, HAGAN RM, MARTIN PE, TARANTINO E, SINGH H and CHANDIO B (1984) Micro-climate, evapotranspiration, and water use efficiency for drip-irrigation tomatoes. *Transactions of the 12th Congress International Committee on Irrigation and Drainage (A)*, 367-394.

REDINGER GJ, CAMPBELL GS, SAXTON KE and PAPENDICK RI (1984) Infiltration rate of slot mulches: measurement and numerical simulation. *Soil Sci. Soc. Am. J.* 48 982-986.

RITCHIE JT (1972) Model for predicting evaporation from a row crop with incomplete cover. *Water Resour. Res.* 8 1204-1213.

ROSS PJ and BRISTOW KL (1990) Simulating water movement in layered and gradational soils using the Kirchhoff transform. *Soil Sci. Soc. Am. J.* 54 1519-1524.

SHAWCROFT RW and GARDNER HR (1983) Direct evaporation from soil under a row canopy. *Agric. Meteorol.* 28 229-239.

SHUTTLEWORTH JW and WALLACE JS (1985) Evaporation from sparse crops – an energy combination theory. *Q. J. R. Meteorol. Soc.* 111 839-855.

SINCLAIR TR and SELIGMAN NG (1996) Crop modelling: from infancy to maturity. *Agron. J.* 88 698-704.

SINGELS A and DE JAGER JM (1991a) Refinement and validation of PUTU wheat crop growth model. 1. Phenology. *S. A. Plant Soil* 8(2) 59-66.

SINGELS A and DE JAGER JM (1991b) Refinement and validation of PUTU wheat crop growth model. 2. Leaf area expansion. *S. A. Plant Soil* 8(2) 67-72.

SINGELS A and DE JAGER JM (1991c) Refinement and validation of PUTU wheat crop growth model. 3. Grain growth. *S. A. Plant Soil* 8(2) 73-77.

SMITH M (1992a) *CROPWAT - A computer program for irrigation planning and management.* FAO Irrigation and Drainage Paper No. 46. FAO, Rome, Italy.

SMITH M (1992b) Expert consultation on revision of FAO methodologies for crop water requirements. FAO, Rome, Italy, 28-31 May 1990.

SMITH M, ALLEN RG and PEREIRA LS (1996) Revised FAO methodology for crop water requirements. *Proc. of the Int. Conf. on Evapotranspiration and Irrigation Scheduling*, San Antonio, Texas, USA. 133-140.

SOIL CLASSIFICATION WORKING GROUP (1991) *Soil classification. A taxonomic system for South Africa.* Dept of Agricultural Development, Pretoria, South Africa.

STEINER JL (1989) Tillage and surface residue effects on evaporation from soils. *Soil Sci. Soc Am. J.* 53 911-916.

TANNER CB (1960) Energy balance approach to evapotranspiration from crops. *Soil. Sci. Soc. Am. Proc.* 24 1-9.

TANNER CB and JURY WA (1976) Estimating evaporation and transpiration from a row crop during incomplete cover. *Agron. J.* 68 239-243.

TETENS O (1930) Uber einige meteorologische Begriffe. *Z. Geophys.* 6 297-309.

TOPP GC, DAVIS JL and ANNAN AP (1980) Electromagnetic determination of soil water content: measurements in coaxial transmission lines. *Water Resour. Res.* 16(3) 574-582.

UNGER PW and PHILLIPS RE (1973) Soil water evaporation and storage. Proceedings of the national convention, Tillage Conference. *Soil Cons. Soc. Am. J.* 42-54.

VILLALOBOS FJ and FERERES E (1990) Evaporation measurement beneath corn, cotton and sunflower canopies. *Agron. J.* 82 1153-1159.

VAN GENUCHTEN M Th (1980) A closed form equation for predicting the hydraulic conductivity of unsaturated soils. *Soil Sci. Soc. Am. J.* 44 892-898.

WALKER GK (1984) Development and validation of a numerical model simulating evaporation from short cores. *Soil Sci. Soc. Am. J.* 48 960-969.

WHISLER FD, ACOCK B, BAKER DN, FYE RE, HODGES HF, LAMBERT JR, LEMMON HE, MCKINION JM and REDDY VR (1986) Crop simulation models in agronomic systems. *Adv. Agron.* 40 141-208.

WILLMOTT CJ (1982) Some comments on the evaluation of model performance. *Bull. Am. Met. Soc.* 63 1309-1313.

WEISS A and NORMAN JM (1985) Partitioning solar radiation into direct and diffuse, visible and near-infrared components. *Agric. For. Met.* 34 205-213.

YANUSA IAM, SEDGLEY RH, BELFORD RK and TENNANT D (1993) Dynamics of water use in a Mediterranean environment. I. Soil evaporation little affected by presence of plant canopies. *Agric. Water Manage.* 24 205-224.

CAPACITY BUILDING AND TECHNOLOGY TRANSFER

Report to the

Water Research Commission

on the project

"Two-Dimensional Energy Interception and Water Balance Model for Hedgerow Tree Crops"

This report refers to objectives iv) and v) of the research proposal for the project "Two-Dimensional Energy Interception and Water Balance Model for Hedgerow Tree Crops".

Capacity building

Capacity building was a significant aspect of this project.

The Faculty of Agriculture at the University of the North (UNIN) was in dire need of capacity building to enable it to serve the agricultural sector of the Northern Province, particularly with respect to sound irrigation practices.

The importance of capacity building at UNIN was considered. The Northern Province has the highest population density in rural areas of all the Provinces in South Africa. Further, due to the lack of industrial development within the Province, migratory employment in Gauteng is the only real option for domestic income. Thus, for the majority, agriculture (mainly subsistence) is the primary avenue of survival. This situation is compounded by a severe limitation of water resources due to low rainfall and high evaporative demand. These factors make effective water use a vital issue in this Province. One of the aspects of effective water use is effective irrigation. The Faculty of Agriculture at UNIN did not have a recognized irrigation specialist on their staff and thus did not offer satisfactory courses in irrigation. The National Community Water and Sanitation Training Institute (NCWSTI) is addressing, in parallel with other activities, training in aspects of water sanitation, distribution and control in rural areas. Thus, the training of sound irrigation practices was severely neglected within the Province. Coupled to this is the general lack of sound irrigation principles in the region (except in the large commercial undertakings). Short-term training courses for the users of water for irrigation purposes are being contemplated by the authorities in the Province. Commendable as this is, it's only an emergency plan, which does not offer a long-term solution. It was needed to create a core of expertise within the Province, which could then address the long-term issues. It is envisaged that this project is the beginning phase of developing this core of expertise.

The Faculty of Agriculture and the NCWSTI at the University of the North had no qualified irrigation specialist within their ranks. Bearing in mind the arid nature of the Northern Province, and the importance of agriculture in the region, it was imperative that this aspect be rectified. This project addressed this by enabling Mr N Du Sautoy, Senior Lecturer from the UNIN Faculty of Agriculture, to complete the capacity building component initiated in the WRC project "Facilitating Irrigation Scheduling by Means of the SWB Model".

When he joined the SWB modelling group at the University of Pretoria in 1997, Mr N du Sautoy volunteered to change his field of expertise (i.e. citrus production technology and

plant nutrition) to irrigation modelling. This step was taken in recognition of the need for a sound irrigation curriculum at UNIN and has involved concerted input into computer skills, crop physiology and environmental biophysics with respect to principles of water use efficiency. In the process, a unique lysimeter trial site has been established at the Hatfield Experimental Farm (University of Pretoria) for the study of water dynamics in deciduous trees. A sound foundation for very useful fruit tree water balance studies was therefore laid.

A course on irrigation scheduling based on the principles included in the SWB model was organized by the Department of Soil Science (UNIN). This concept was presented at the University of the North Curriculum Development Workshop held on 28/04/1999 at the Ranch Hotel in Pietersburg under the topic "Training in Soil Science". Mr N Du Sautoy organized and presented the course titled "Irrigation and Soil Water Balance" for 3rd and 4th year students at the University of the North. The application of the SWB model forms part of the course practicals.

A workshop on "Crop Modelling and Irrigation Scheduling" was also organized by Mr N Du Sautoy on 24-25/03/1998 in Pietersburg, with the participation of Prof JT Ritchie (Michigan State University, USA). A large number of students, mainly from the University of the North and University of Venda, officials and extensionists (Department of Agriculture) as well as researchers were invited and attended this workshop.

The Faculty of Agriculture (UNIN) has been equipped with the following instrumentation: 28 heat dissipation sensors, 28 time domain reflectometry probes, one 1502C Tektronix cable tester, four data loggers, two AM416 multiplexers, one AM25T multiplexer, one automatic weather station, sap flow meters and tube solarimeters. The total value of the equipment is about R 185,000.

During the installation of the equipment at the Syferkuil experimental farm (UNIN), a large group of students from the University of the North was trained in the theory and application of the techniques used. The students were trained during a two-day session while installing the intensive monitoring site.

Several students of the University of the North have been trained in the application of the following techniques:

i) Heat dissipation sensors for measuring soil matric potential;
ii) Time domain reflectometry for measuring volumetric soil water content;
iii) Soil and root sampling for laboratory analysis;
iv) Tube solarimeters for measuring total solar radiation;
v) Line quantum sensors for measuring photosynthetically active radiation;
vi) Automatic weather station for recording weather data; and
vii) Tension-infiltrometer for measuring soil hydraulic conductivity.

Capacity building was not only directed at UNIN. The Plant Production and Soil Science Department of Pretoria University also benefited.

An M. Inst. Agrar. (Agronomy) student at the University of Pretoria, under the guidance of the project leader, was trained and employed as Research Assistant on this project. Mr NS Mpandeli completed his Bachelor of Agriculture degree majoring in horticulture at the University of Venda in 1997. In 1998, he completed the B. Inst. Agrar. Honours degree at the University of Pretoria. Mr NS Mpandeli was trained in the following fields:

1) Theoretical basis for energy interception and soil water balance modelling.
2) Principles and operation of equipment used to collect field measurements for the validation of the model:

i) Micro-lysimeters for measurement of soil evaporation;
ii) Automatic weather station;
iii) Heat dissipation sensors for measurement of soil water potential;
iv) Time domain reflectometry for measurement of volumetric soil water content;
v) Neutron water meter for measurement of soil water content;

vi) Sunfleck ceptometer for measurement of interception of photosynthetically active radiation;
vii) Tube solarimeters for measurement of total solar radiation; and
viii) Leaf area index and growth analysis.

3) Use of spreadsheets for data processing and analysis.

This was done through course work and participation at workshops and conferences.

The M. Inst. Agrar. work program for Mr Mpandeli was recommended by the project leader and included the following courses:

i) Agronomy 801 and 890
ii) Scientific presentation 783
iii) Microclimatology 312
iv) Irrigation 422
v) Computer information and literacy 171, 172, 173 and 174
vi) Mathematics

Mr NS Mpandeli visited the Oklahoma Climatology Survey Institute (USA) for a training period of 28 days. This trip was invaluable to him in order to get experience in managing and operating meteorological electronic equipment and systems. He also attended the Soil Science Society of South Africa Congress held in Pretoria in June 1999, and participated at the Combined Congress held in Bloemfontein in January 2000 and the Joint Congress held in Pretoria in January 2001.

Based on this training, Mr NS Mpandeli was appointed at the Institute for Soil, Climate and Water (Agricultural Research Council - Pretoria) through the Professional Development Program.

Technology transfer

Results from this project should guide irrigation scheduling consultants, extension officers and farmers in the more efficient use of scarce water resources on high value tree crops. The mechanistic detailed approach will also give guidance with respect to the magnitude of errors made by using simpler more empirical approaches.

Obviously, initially this tool will be beneficial to large commercial concerns, but with the emergence of commercial black farmers (as land redistribution programmes come into effect) their need for technical assistance will be tremendous. This initiative will make a significant contribution to being able to address this need as it arises.

The following papers have been presented at conferences during the course of this project.

ANNANDALE JG, BENADÉ N, JOVANOVIC NZ and DU SAUTOY N (1998) SWB, a user friendly irrigation scheduling model. *Joint Congress, Soils and Crops Towards 2000*. Jan. 1998, Alpine Heath, KwaZulu-Natal, South Africa.

This paper won the Soil Science Society Silver medal for the best paper on implementable technology at the Joint Congress, Soils and Crops Towards 2000, January 1998, Alpine Heath, KwaZulu-Natal, South Africa.

DU SAUTOY N, JOVANOVIC NZ and ANNANDALE JG (1998) Modelling fruit tree water use for irrigation scheduling. *Joint Congress, Soils and Crops Towards 2000*. Jan. 1998, Alpine Heath, KwaZulu-Natal, South Africa.

ANNANDALE JG, CAMPBELL GS, STOCKLE CO, JOVANOVIC NZ and DU SAUTOY N (1999) Two-dimensional water balance modelling of tree crops. *Congress of the SA Society of Crop Production*. Jan. 1999, Stellenbosch, South Africa.

This paper won the Nico Viljoen prize for the best paper at the Congress of the SA Society of Crop Production, January 1999, Stellenbosch, South Africa.

DU SAUTOY N, JOVANOVIC NZ, ANNANDALE JG and NEPFUMBADA MP (1999) Two-dimensional measurement of soil water and energy balance in a hedgerow peach orchard. *Congress of the SA Society of Crop Production*. Jan. 1999, Stellenbosch, South Africa.

PRETORIUS JJB, JOVANOVIC NZ and ANNANDALE JG (1999) Individual calibration of Campbell Scientific 229 heat dissipation sensors. *Congress of the SA Society of Crop Production*. Jan. 1999, Stellenbosch, South Africa.

ANNANDALE JG, CAMPBELL GS, JOVANOVIC NZ and DU SAUTOY N (1999) Modelling hedgerow tree crop water use. *8th Congress of the Southern African Society for Horticultural Sciences*. Jan. 1999, Stellenbosch, South Africa.

DU SAUTOY N, JOVANOVIC NZ and ANNANDALE JG (1999) The use of heat pulse technique to monitor transpiration in peach trees. *8th Congress of the Southern African Society for Horticultural Sciences*. Jan. 1999, Stellenbosch, South Africa.

DU SAUTOY N, JOVANOVIC NZ and ANNANDALE JG (2000) Contribution of inter-row region to the soil water balance in hedge-row plantings. *SASCP, SAWSS, SANCRA Combined Congress*. Jan. 2000, Bloemfontein, South Africa.

ANNANDALE JG, CAMPBELL GS, JOVANOVIC NZ, DU SAUTOY N and BENADE N (2000) Simulating the two-dimensional water and energy balance. *SASCP, SAWSS, SANCRA Combined Congress*. Jan. 2000, Bloemfontein, South Africa.

ANNANDALE JG, JOVANOVIC NZ, CAMPBELL GS, DU SAUTOY N. and BENADÉ N (2000) Improving water use efficiency of widely spaced micro-irrigated crops with a two-dimensional water and energy balance model. *Proc. of the 6th International Micro-Irrigation Congress (Micro 2000)*, 22-27 Oct. 2000, Cape Town, South Africa.

The following papers emanated from previous WRC projects and have been presented at conferences during the course of this project:

JOVANOVIC NZ, ANNANDALE JG and BENNIE ATP (2000) Canopy radiation extinction coefficient accounts for differences in row width. *SASCP, SAWSS, SANCRA Combined Congress*. Jan. 2000, Bloemfontein, South Africa.

JOVANOVIC NZ, ANNANDALE JG and HAMMES PS (2000) Teaching crop physiology with the Soil Water Balance (SWB) model. *SASCP, SAWSS, SANCRA Combined Congress*. Jan. 2000, Bloemfontein, South Africa.

JOVANOVIC NZ, ANNANDALE JG and NEL AA (2000) A mechanistic approach for simulation of deficit irrigation of sunflower (*Helianthus annuus* L.). *SASCP, SAWSS, SANCRA Combined Congress*. Jan.2000, Bloemfontein, South Africa.

The following papers emanated from previous WRC projects and have been published during the course of this project:

JOVANOVIC NZ and ANNANDALE JG (1999) An FAO type crop factor modification to SWB for inclusion of crops with limited data: Examples for vegetable crops. *Water SA* **25**(2) 181-190.

JOVANOVIC NZ, ANNANDALE JG and MHLAULI NC (1999) Field water balance and SWB parameter determination of six winter vegetable species. *Water SA* **25**(2) 191-196.

JOVANOVIC NZ and ANNANDALE JG (2000) Crop growth model parameters of 19 summer vegetable cultivars for use in mechanistic irrigation scheduling models. *Water SA* **26**(1) 67-76.

JOVANOVIC NZ and ANNANDALE JG (2000) SWB (Soil Water Balance): A computer tool for teaching future irrigation water managers. *J. Nat. Resour. Life Sci. Educ.* **29** 15-22.

ANNANDALE JG, CAMPBELL GS, OLIVIER FC and JOVANOVIC NZ (2000) Predicting crop water uptake under full and deficit irrigation: An example using pea (*Pisum sativum* L. cv. Puget). *Irrig. Sci.* **19** 65-72

JOVANOVIC NZ, ANNANDALE JG and HAMMES PS (2000) Teaching crop physiology with the Soil Water Balance (SWB) model. *J. Nat. Resour. Life Sci. Educ.* **29** 23-30.

JOVANOVIC NZ, ANNANDALE JG and NEL A (2000) A mechanistic approach for simulation of deficit irrigation of sunflower (*Helianthus annuus* L.). *S. Afr. J. Plant and Soil* **17**(3) 117-123.

The following papers emanated from this project and have been submitted for publication:

ANNANDALE JG, JOVANOVIC NZ, BENADÉ N and ALLEN RG (2001) User-friendly software for estimation and missing data error analysis of the FAO 56-standardized Penman-Monteith daily reference crop evaporation. *Irrig. Sci.*

ANNANDALE JG, DU SAUTOY N, CAMPBELL GS, JOVANOVIC NZ and LOBIT P (2001) Two-dimensional energy interception model for hedgerow fruit trees. *Agric. For. Meterol.*

ANNANDALE JG, JOVANOVIC NZ, CAMPBELL GS, DU SAUTOY N and BENADE N (2001) A two-dimensional water balance model for hedgerow tree crops. *Irrig. Sci.*

In February 1999, the project leader was invited by OTK to demonstrate the SWB model to their highveld irrigators.

In May 1999, the project leader was invited by the South African Irrigation Institute to present the SWB model to their regional design engineers.

There was cooperation with Ms T Volschenk (Agricultural Research Council - Infruitec, Stellenbosch), and Dr E Hoffman (formerly Agricultural Research Council, Institute for Tropical and Subtropical Crops, Nelspruit).

The SWB model, as well as all data originating in this research project, are available from Neil Du Sautoy (Department of Soil Science, University of the North, P. B. X1106 Sovenga 0727). The reference for the CD is "Tree project WRC K5/945".

Appendix A

2D-Energy partitioning model

```
unit _Tree2D;

interface

uses
  Math,Windows, Messages, SysUtils, Classes, Graphics, Controls,
Forms,
  Dialogs, _IGlob;

type
  TTreeObj = Object
  private
  public
    Test: Integer;
    PE,PT,xp: HNodeType;  {Potential evap, transp and node position}
    PotTransp: Double;
    procedure SetupTree2D;
    procedure CalcDailySTArray;
    procedure InitSite(Hemisphere: Char; Slope,Aspect: Double);
    procedure   InitOrchard(CanopyHeight,CanopyWidth,BareStemHeight:
Double);
    procedure DailyAstroSettings(DOY: integer);
    procedure SetUpRadNodes;
    procedure BeamAndDiffuse(MSolar,cosZA,RelPress: Double);
    function Calc_CD(x_p,a,c,Zo,h,za,phi: Double): Double;
    function Calc_Td(x_p,a,c,Zo,h,Exponent: Double): Double;
    function  DayTreeSolar(MSolar,Td,Exponent,x_p,a,c,Zo,h:  Double):
Double;
    function
HourTreeSolar(hour,MSolar,RelPress,Td,Exponent,x_p,a,c,Zo,h:
Double): Double;
    procedure PartitionPET;
  end;

const
  SolarConst = 1360;      {W/m2 Solar constant}

{*  Latitude = -25.75;      {negative for SH}
  StandardMeridian = 30; {These are at 0, 15, 30 ... 345 degrees.
Generally time
  zones run approximately +7.5 to -7.5 degrees either side of a std
meridian,
  but sometimes this varies depending on political boundaries. Check
an atlas
  for longitude and std meridian}
  Longitude = 28.27;
  Altitude = 1372;        {m}
  Slope = 0;              {degrees from horizontal}
  Aspect = 0;             {degrees from due South in NH?}
```

```
  h = 4.5;                {RowSpacing}
  w = 4.5;                {WettedWidth - dont let canopy width exceed
row spacing}
  bs = 4.5;               {BareSoilWidth}
  RowOrientation = -88;   {negative values are W of N, whilst pos are
E of N -90 to 90}
  CanopyHeight = 3.25;
  CanopyWidth = 2.75;
  BareStemHeight = 0.35; {dont let skirting height exceed height}
  LAD = 1;                {Leaf Area Density}
  k = 0.5;                 {should I rather calc this for za using eq
for Kbe?}
  Absorptivity = 0.5;      {Absorptivity = 0.8 for PAR, 0.2 for NIR
and O>0.5 for solar}
*)
var
  TreeObj: TTreeObj;
  SinLat,
  CosLat,
  LC,                   {longitudinal correction}
  slp,                  {slope}
  asp,                  {aspect}
  SolarNoon,
  SinDec,
  SinLatSinDec,
  CosLatCosDec,
  SinSlope,
  CosSlope,
  Exponent,
  a,
  c,
  Zo,
  x_axis,
  RadFrac,          {Fraction of potential daily radiation}
  PotDailySolar,
  RelPress,
  Sp,Sd:          Double;
  Td:             HNodeType;

implementation

uses
  _Tree2DF, _DM, _IWeathr, _WDayDM, _FieldDM, _SoilFD;

procedure TTreeObj.SetupTree2D;
begin
  if not DM.T2DSetT.FindKey([FieldDM.Field.Value]) then
    Raise           SWBErr.Create('Setup           for           field
'+FieldDM.WeatherID.AsString+ ' does not exist!');
  InitSite('S',DM.T2DSetTSlope.Value,DM.T2DSetTAspect.Value);

InitOrchard(DM.T2DSetTCanopyH.Value,DM.T2DSetTCanopyW.Value,DM.T2DSe
tTStemH.Value);
  SetUpRadNodes;
end;
```

```
procedure TTreeObj.CalcDailySTArray;
var
  j: Integer;
begin
  for j := Lft to Rt do
    DM.DailyST[j]                                                    :=
DayTreeSolar(WDayDM.Solar.Value,Td[j],Exponent,xp[j],a,c,Zo,DM.T2DSe
tTRowWidth.Value);
end;

procedure TTreeObj.InitSite(Hemisphere: Char; Slope,Aspect: Double);
//Convert degrees to radians and calculate longitudinal correction
begin
  if Hemisphere = 'S' then
  begin
    SinLat := Sin(-DM.Lat.Value*Pi/180);
    CosLat := Cos(-DM.Lat.Value*Pi/180);
  end
  else
  begin
    SinLat := Sin(DM.Lat.Value*Pi/180);
    CosLat := Cos(DM.Lat.Value*Pi/180);
  end;
  slp := Slope*pi/180;
  asp := Aspect*pi/180;
  SinSlope := Sin(slp);
  CosSlope := Cos(slp);
  LC  := -1/15*(DM.T2DSetTLong.Value - DM.T2DSetTSTDMer.Value);


   RelPress := exp(-DM.Elev.Value/8200); {Pa/P}
end; {InitSite}

procedure
TTreeObj.InitOrchard(CanopyHeight,CanopyWidth,BareStemHeight:
Double);
begin
  c := (CanopyHeight - BareStemHeight)/2;
  a := CanopyWidth/2;
  Zo := BareStemHeight + c;
  x_axis := (90 + DM.T2DSetTRowOrient.Value)*pi/180;
  Exponent                                    :=                    -
DM.T2DSetTExtCoeff.Value*Sqrt(DM.T2DSetTAbsorb.Value)*DM.T2DSetTLADe
ns.Value; {part of exp term for transmission}
  {Multiply max LAD by Kcb to simulate tree growth}
end;

procedure TTreeObj.DailyAstroSettings(DOY: Integer);
var
  EqOfTime,
  f,
  CosDec,
  Dec,              {in degrees - for error checking}
  HalfDay,
  SinHalfDay,
  CosHalfDay,
```

```
  DayLength:  Double;
  i:          Integer;
begin
  for i := Lft to Rt do
    Td[i]                                                    :=
Calc_Td(xp[i],a,c,Zo,DM.T2DSetTRowWidth.Value,Exponent);
  f := (279.575 + 0.9856*DOY)*Pi/180; {radians}
  EqOfTime       :=       (-104.7*sin(f)+596.2*sin(2*f)+4.3*sin(3*f)-
12.7*sin(4*f)
                -429.3*cos(f)-2*cos(2*f)+19.3*cos(3*f))/3600;
  SolarNoon := 12 - LC - EqOfTime;
  SinDec                                                     :=
0.39785*sin(4.869+0.0172*DOY+0.03345*sin(6.224+0.0172*DOY));
  {if Hemisphere is S then SinDec = -SinDec no! only change lat}

  Dec := arcsin(SinDec);
  CosDec := Cos(Dec);
  SinLatSinDec := SinLat*SinDec;
  CosLatCosDec := CosLat*CosDec;
  CosHalfDay := - SinLatSinDec/CosLatCosDec;
  SinHalfDay := sqrt(1-sqr(CosHalfDay));

  HalfDay := pi/2 - arctan(CosHalfDay/SinHalfDay);{half day length
in radians}

  PotDailySolar                :=              117.5              *
(HalfDay*SinLatSinDec+CosLatCosDec*SinHalfDay)/pi;
  DayLength := 2*HalfDay*12/pi; {day length in hours}

end;

procedure TTreeObj.BeamAndDiffuse(MSolar,cosZA,RelPress: Double);
var
  St,
  m,
  PotPARbeam,
  PotPARdiff,
  PotPAR,
  w,
  PotNIRbeam,
  PotNIRdiff,
  PotNIR,
  PotSolar,
  PAR,
  NIR,
  Ratio,
  FracPARbeam,
  FracNIRbeam,
  Sb:          Double;
begin
  St := MSolar; {measured global radiation}
  if DailySim then
  begin
    St := SolarConst*RadFrac*cosZA;

  end;
```

```
  if St < 0 then St := 0;
  m := 1/cosZA;
  PotPARbeam := 600*exp(-0.185*RelPress*m)*cosZA;
  PotPARdiff := 0.4*(600*cosZA - PotPARbeam);
  PotPAR := PotPARbeam + PotPARdiff;
  w     :=     1320*power(10,(-1.195     +     0.4459*log10(m)     -
0.0345*sqr(log10(m))));
  PotNIRbeam := (720*exp(-0.06*RelPress*m) - w)*cosZA;
  PotNIRdiff := 0.6*((720 - w)*cosZA - PotNIRbeam);
  PotNIR := PotNIRbeam + PotNIRdiff;
  PotSolar := PotPAR + PotNIR;
  PAR := St*(PotPAR/PotSolar);
  NIR := St - PAR;
  Ratio := St/PotSolar;       {with a fraction for an Exponent the
base must > 0}
    if Ratio > 0.9 then FracPARbeam := PotPARbeam/PotPAR else{Ratio
:= 0.9;}
  FracPARbeam     :=     PotPARbeam/PotPAR*(1-     power(((0.9     -
Ratio)/0.7),0.666));
  if FracPARbeam < 0 then FracPARbeam :=0;
    if Ratio > 0.88 then FracNIRbeam := PotNIRbeam/PotNIR else{Ratio
:= 0.88;}
  FracNIRbeam     :=     PotNIRbeam/PotNIR*(1-     power(((0.88     -
Ratio)/0.68),0.666));
  if FracNIRbeam < 0 then FracNIRbeam :=0;
  Sb := FracPARbeam*PAR + FracNIRbeam*NIR; {total beam radiation}
  Sd := St - Sb; {total diffuse radiation}
  Sp := Sb/CosZA;
end; {of procedure BeamAndDiffuse (MSolar,cosZA,RelPress: Double);}

procedure TTreeObj.SetUpRadNodes;  {There are 11 nodes}
var
  Space,
  HalfWet,
  HalfRow: Double;
  i:       Integer;
begin
  HalfRow := DM.T2DSetTRowWidth.Value/2;
  HalfWet := FieldDM.WettedDiam.Value/2;
  xp[1]  := 3*HalfRow;        {symmetry plane}
  xp[6]  := xp[1] + HalfRow; {centre node, in tree row}
  xp[11] := xp[6] + HalfRow; {symmetry plane}

    xp[6]  := 2*DM.T2DSetTRowWidth.Value;
    xp[1]  := xp[6] - DM.RNodeTX1.Value;  //3/2*DM.RowWidth.Value
    xp[2]  := xp[6] - DM.RNodeTX2.Value;  //1.92
    xp[3]  := xp[6] - DM.RNodeTX3.Value;  //1.28
    xp[4]  := xp[6] - DM.RNodeTX4.Value;  //0.64
    xp[5]  := xp[6] - DM.RNodeTX5.Value;  //0.3
    xp[7]  := xp[6] + DM.RNodeTX5.Value;
    xp[8]  := xp[6] + DM.RNodeTX4.Value;
    xp[9]  := xp[6] + DM.RNodeTX3.Value;
    xp[10] := xp[6] + DM.RNodeTX2.Value;
    xp[11] := xp[6] + DM.RNodeTX1.Value;
end;
```

```
function TTreeObj.Calc_CD(x_p,a,c,Zo,h,za,phi: Double): Double;
{CD is Canopy Distance or Intercepted Ray Length - parameter s in CE
& T papers This is based on Charles Edwards and Thorley 1973 and
Charles Edwards and Thorpe 1976. We have been able to simplify the
equations by only solving for path length through the canopy to the
soil surface, i.e. Zp = 0 and by assuming that for row crops the
canopy dimension in the y or row direction (b) will be very large so
that the y2/b2 term falls away. xp position of transect. 3h/2 and
5h/2 are symmetry planes with the tree at 2h and with two rows of
trees on either side of the centre row we are modelling za is zenith
angle az is azimuth angle}
var
  n: integer;
  theta,     {zenith angle}
//  phi,       {azimuth angle}
  st,        {sin theta}
  ct,        {cos theta}
  sp,        {sin phi}
  cp,        {cos phi}
  st2,       {sin theta squared}
  ct2,       {cos theta squared}
  cp2,       { cos phi squared}
  a2,        {a squared}
  c2,
  xp2,
  u,           {coeff of Zq squared term - see Charles Edwards and
Thorley 1973}
  v,           {coeff of Zq}
  w,           {coeff of constant term}
  xdist,       {xp - nh}
  s,           {distance through canopy}
  z: Double;
begin
  theta := za;
  st    := sin(theta);
  ct    := cos(theta);
  st2   := Sqr(st);
  ct2   := Sqr(ct);
  sp    := sin(phi);
  cp    := cos(phi);
  cp2   := Sqr(cp);
  a2    := Sqr(a);
  c2    := Sqr(c);
  xp2   := Sqr(x_p);
  u     := c2*st2*cp2 + a2*ct2;
  s     := 0;
  for n := 0 to 4 do
  begin
    xdist := x_p - n*h; {h is row spacing}
    v     := 2*(c2*st*cp*ct*xdist - a2*ct2*Zo);
    w     := c2*ct2*(Sqr(xdist) + a2*(Sqr(Zo)/c2 - 1));
    z     := Sqr(v) - 4*u*w;
    if z > 0 then
      s := s + sqrt(z)/u/ct;
  end;
```

```
  Result := s;
end;



function TTreeObj.Calc_Td(x_p,a,c,Zo,h,Exponent: Double): Double;
{Td is the diffuse transmission coefficient (Tau d)}
//This does not change over the day and will only need to be updated
if the
//crop grows

var
  sumradd,
  ZAd,
  cosZAd,          {zenith angle diffuse}
  AZd,             {azimuth angle diffuse}
  hradd,
  tdif,
  conv,
  fact: Double;
  iz,              {increment for zenith angle}
  ia: integer;     {increment for azimuth angle}
begin
  sumradd := 0;
  tdif := 0;
  conv := pi/180; {conversion from degrees to radians}
  for iz := 0 to 8 do {account for diffuse radiation at different
zenith angles}
  begin
    ZAd := (5+10*iz)*conv; {zenith angles}
    cosZAd := cos(zad);
    hradd := cosZAd*sin(ZAd); {I moved this up here out of azimuth
loop}
    for ia := 0 to 23 do{account for diffuse radiation at diff
azimuth angles}
    begin
      AZd := (15*ia)*conv; {azimuth angles}
      sumradd := sumradd + hradd; {incremented and accumulated
diffuse
                                   weighting factor?}
      tdif                  :=                  tdif                +
hradd*exp(Exponent*Calc_CD(x_p,a,c,Zo,h,ZAd,AZd));
    end;
  end;
  Result := tdif/sumradd;
end;

function      TTreeObj.DayTreeSolar(MSolar,Td,Exponent,x_p,a,c,Zo,h:
Double): Double;
//This calculates the daily beam transmission coef and uses that and
the diffuse
//transmission coef to calculate daily solar radiation
var
  SinEl,    {sin of elevation angle}
```

```
  CosEl,
  El,
  zab,       {beam zenith angle}
  CosZA,
  AZ,
  CosAZ,
  SinAZ,
  phi,
  Tm,
  ViewFactor,       {view factor for beam radiation eq 11.16}
  Tb,               {beam transmission coef}
  Radiation: Double;  {beam weighting factor}
  hour: Integer;
begin
  RadFrac := MSolar/PotDailySolar;
  Radiation := 0;
  DailySim := True;
  Tb := 0;
  for hour := 1 to 24 do
  begin
    SinEl   :=      SinLatSinDec   +   CosLatCosDec*cos(0.262*(hour-
SolarNoon));
    CosEl := sqrt(1-Sqr(SinEl));
    El := arctan(SinEl/CosEl);
    if El > 0 then  {dont calculate AZ when sun still below horizon}
    begin

      CosAZ := (SinLat*SinEl - SinDec)/(CosLat*CosEl);
      SinAZ := sqrt(1 - Sqr(CosAZ));
      AZ := arctan(SinAZ/CosAZ);
      if hour < 12 then
        AZ := pi - AZ
      else
        AZ := AZ + pi;
      if CosAZ < 0 then
        if AZ > pi then
          AZ := AZ - pi
        else
          AZ := AZ + pi;
      zab := pi/2 - El; {zentih angle for beam is complementary to
elev angle}
      cosZA := cos(zab);
      phi:= AZ - x_axis;
      Tb := exp(Exponent*Calc_CD(x_p,a,c,Zo,h,zab,phi));
      BeamAndDiffuse(MSolar,cosZA,RelPress); {call this and angle
calculations
      - zenith and phi only once hourly - take view factor out as
well}
      ViewFactor :=  CosSlope*cosZA + SinSlope*sin(zab)*cos(AZ-asp);
      Radiation :=  Radiation + Tb*Sp*ViewFactor + Td*Sd;// eq 11.16
page 180
    end;
  end;
  Result := Radiation * 0.0036;  {to convert to MJ/m2/day #}
end;
```

```
function
TTreeObj.HourTreeSolar(hour,MSolar,RelPress,Td,Exponent,x_p,a,c,Zo,h
: Double): Double;
//This calculates the hourly beam transmission coef and uses that
and the
//diffuse transmission coef to calculate hourly solar radiation
var
  SinEl,  {sin of elevation angle}
  CosEl,
  El,
  zab,    {beam zentih angle}
  cosZA,
  AZ,
  CosAZ,
  SinAZ,
  phi,
  ViewFactor,       {view factor for beam radiation eq 11.16}
  Tb,               {beam transmission coef}
  BeamWt: Double;  {beam weighting factor}
begin
  SinEl := SinLatSinDec + CosLatCosDec*cos(0.262*(hour-SolarNoon));
  CosEl := sqrt(1-Sqr(SinEl));
  El := arctan(SinEl/CosEl);
  if El > 0 then  {dont calculate AZ when sun still below horizon}
    begin
      CosAZ := (SinLat*SinEl - SinDec)/(CosLat*CosEl);
      SinAZ := sqrt(1 - Sqr(CosAZ));
      AZ := arctan(SinAZ/CosAZ);
      if hour < 12 then AZ := pi - AZ   {so that AZ = pi when due
south?}
        else AZ := AZ + pi;
      if CosAZ < 0 then
        if AZ > pi then AZ := AZ - pi
          else AZ := AZ + pi;
      zab := pi/2 - El;  {zentih angle for beam is complementary to
elev angle}
      cosZA := cos(zab);
      phi:= AZ - x_axis;
      Tb := exp(Exponent*Calc_CD(x_p,a,c,Zo,h,zab,phi));
      BeamAndDiffuse (MSolar,cosZA,RelPress); {call this and angle
calculations
      - zenith and phi only once hourly - take view factor out as
well}

  {I want Sp so that we can adjust for slope and aspect using eq
11.16}
      ViewFactor :=  CosSlope*cosZA + SinSlope*sin(zab)*cos(AZ-asp);
    // eq 11.16 page 180
//      Result := Tb*Sp*ViewFactor + Td*Sd;
      Result := Tb*Sp*ViewFactor + Td*Sd;  {#}
    end
  else
    Result := 0;
end;

procedure TTreeObj.PartitionPET;
```

```
var
  j:              Integer;
  PEvap,
  PotEvap,
//  PotTransp,
  Transmission,
  TransmittedRad: Double;
begin
  TransmittedRad := 0;
  for j := Lft to Rt do
    TransmittedRad           :=           TransmittedRad           +
DM.DailyST[j]*SoilFD.Surface[j];
  TransmittedRad := TransmittedRad/DM.T2DSetTRowWidth.Value;
  if WDayDM.Solar.Value > 0 then
    Transmission  :=  TransmittedRad/WDayDM.Solar.Value     {fraction
transmitted to surface}
  else
    Raise SWBErr.Create('Division by zero! Daily Solar = 0');
  PotEvap := PET*Transmission;
  PotTransp := PET - PotEvap;
  TTreeObj.CalcDailySTArray;
  for j := Lft to Rt do
  begin

    PE[j] := DM.DailyST[j]/WDayDM.Solar.Value*PET;
    PT[j] := PET-PE[j];
  end;

  {Error checking code}
  PEvap := 0;
  for j := Lft to Rt do
    PEvap                    :=                    PEvap                +
PE[j]*SoilFD.Surface[j]/DM.T2DSetTRowWidth.Value;

  PotTransp := PET - PEvap;
  {Check if PotEvap = PEvap}
end;

end.

procedure TTreeObj.El(hour: Integer): Double;
var
  SinEl,  {sin of elevation angle}
  CosEl,
  El,
  zab: Double;    {beam zentih angle}
begin
  SinEl := SinLatSinDec + CosLatCosDec*cos(0.262*(hour-SolarNoon));
  CosEl := sqrt(1-Sqr(SinEl));
  El := arctan(SinEl/CosEl);
  zab := pi/2 - El;  {zentih angle for beam is complementary to elev
angle}
 // Result := zab;
end;

  if El > 0 then  {dont calculate AZ when sun still below horizon}
```

```
function TTreeObj.AZ(SinEl,hour: Double): Double;
{We are using compass co-ordintes (C&N pg 168)
 N is 0 degrees
 E is 90
 S is 180 and
 W is 270 degrees}
var
  cosZA,
  AZ,
  CosAZ,
  SinAZ: Double;

begin
  CosAZ := (SinLat*SinEl - SinDec)/(CosLat*CosEl);
  SinAZ := sqrt(1 - Sqr(CosAZ));
  AZ    := arctan(SinAZ/CosAZ);
    if hour < 12 then AZ := pi - AZ   {so that AZ = pi when due
south?}
      else AZ := AZ + pi;
    if CosAZ < 0 then
      if AZ > pi then AZ := AZ - pi
        else AZ := AZ + pi;
end;
```

Appendix B

Source code for the 2D-Finite difference water balance model

```
unit _SoilFD;

{The finite difference matric flux potential based water balance
requires that nodes be placed at the interface between layers and
that layers be divided into upper and lower portions. Layers have
uniform properties within themselves but properties can differ
between layers. The layer is referenced to the potential at the top
of the layer. Around each node a control volume is therefore formed
which is made up of the lower half of the layer above it and the
upper half of the layer below it. The mass balance equations for
these control volumes are solved by this model.}

interface

uses SysUtils, Dialogs, Math, _IGlob, _InitSaltDM;

type
  TSoilFD = Object
    procedure FDiffInitSoil;
    procedure FDiffInit2DSoil;
    procedure CalcWaterStatus;
    procedure SurfaceStorage;
    function getStoredWater: Double;
    procedure CalcRootDensityAndConductivity;
    procedure RedistributionAndMassBalance;
    procedure FDiffCalcSoildz;
    procedure FDiffCalcSoildx;
    procedure  CalcCVwaterContent;  {call  during  initialization  and
every day}
    procedure SetUp2Dnodes;
    procedure Infiltration2D;
    procedure Init2DSourceSinkFluxes;
    procedure Zero2DBoundConduct(i,j: Integer);
    procedure SetLowerBoundaryCond2D;
    procedure MassBal2D(i,j:Integer);
    procedure Redist2D;
    procedure WaterFunctions(i,j: Integer);
  private
    MFPu,
    MFPl:         VNodeType;      {soil layers}
    PotentialEvap,
    lim,abv,est,
    dwdp,
    sumf:         Double;
    nlr:          Integer;
    a,ax,b,bx,bl,cx,f,dp,dkdpu,dkdpl,h,jv,kv,wnu,wnl,
    wu,wl,cpu,cpl,ks,ku,kl,ruk,n,nl,fr,Psi,PsiE,PsiI,hc,CVnwc:
VNodeType{SoilVecs};
    si: VNodeType;{USED TO SEE IF PROPERTIES OF ADJACENT LAYERS ARE
THE SAME}
```

```
    SurfStor: Double;
    LWetNode,
    RWetNode: Integer;
    IrrigatedSurf: Double;
    procedure CalcIrrigSurf(WettedWidth: Double);
  public
    jl,CVwc,CVdz,HALFdz:            VNodeType;
    x:                              Distances;
    TwiceWidth,Factor,Surface:      LeachNodes;
    Psi2D,                                        {matric potential}
    hr:                             Nodes;        {humidity}
    ProfileWidth,TwiceProfileWidth: Double;       {row spacing}
    procedure Evap2D(i,j: Integer);
    procedure WaterUptake2D;
    procedure DailyWatBal2D;
    procedure Calc2DRootDensAndConductivity;
  end;

  SoilProps2DType = record
    b,AEP,
    Ks,RhoB,
    WS,n,
    PWP,FC: Array[TopNode..Btm,LftNode..Rt] of Double;
  end; {SoilProps2DType}

  TControlVol = record
    WN1rA,              {New water content * 1/4 area of element}
    WN11A,
    WNurA,
    WNulA,
    URxFlowPath,
    LRxFlowPath,
    ULxFlowPath,
    LLxFlowPath,
    URzFlowPath,
    LRzFlowPath,
    ULzFlowPath,
    LLzFlowPath,
    ACV,                {control volume area}
    W,                  {old volumetric water content, before DT}
    WN,                 {new volumetric water content}
    dWNdPsi,            {differential water capacity}
    Infil,
    Evap,
    dEvap_dPsi,
    froot,              {fraction roots}
    rootuk,             {root uptake conductivity 2D}
    Uptake,
    dUptake_dPsi,

     MassSoil:   Array[Surf..Btm,Lft..Rt] of Double;
  end; {TControlVol}

  TElemVars = record
    Area,                           {area of 1/4 element}
```

```
    WNul,WNur,WNll,WNlr,                {new water content}
    dWNul_dPsi,dWNur_dPsi,              {water capacity}
    dWNll_dPsi,dWNlr_dPsi,              {water capacity}
    Kul,Kur,Kll,Klr,                    {hydraulic conductivities}
    dKul_dPsi,dKll_dPsi,dKur_dPsi,dKlr_dPsi,          {conductivity
derivative }
    MFPlr,MFPll,MFPur,MFPul,            {matric flux potential }
    SoilMass: Array[TopNode..Btm,LftNode..Rt] of Double; {mass of
soil (kg) in 1m row * 1/4 element }
  end; {TElemVars}

var
  SoilFD:  TSoilFD;
  Props2D: SoilProps2DType;
  Elem2D:  TElemVars;
  CV:      TControlVol;
  dX:      Array[LftNode..Rt] of Double;
  Tolerance,                {used in checking mass balance }
  RHcanopy,                 {need to get these from other objects }
  urx,lrx,ulx,llx,urz,lrz,ulz,llz: Double;

implementation

uses _Run, _DM, _CropDM, _SoilDM, _FieldDM, _FCropDM, _ISoil,
_ICrop, _IWeathr,
  _Tree2D;

const
  Mw = 0.018;  {mole mass of H2O, kg/mol }
  R  = 8.31;   {gas constant             }
  Dv = 2.4e-5; {H2O vapor diff. m2/s     }
  Tk = 293;    {soil temperature, kelvins}
  Vd = 0.017;  {vapor density, kg/m3     }
  ha = 0.5;     {humidity of air This we will later make variable
over the day}
  MdivRT = Mw/(R*Tk);
  Cinfil = 0; {concentration of the infiltrating water}
  MBTolerance = 0.0000003; {for soil water flux mass balance
equations}

  im = 1e-10;  {maximum mass balance error (1e-7 kg/m2/s = 0.0086
mm/day)}

procedure TSoilFD.SetUp2Dnodes;
var
  i,j: Integer;
begin
  for i := TopNode to Btm do
    for j := LftNode to Rt do
    with Elem2D do
    begin
      Area[i,j] := (dX[j]*Soil.dZ[i])/4;  {calc area of 1/4 of each
element}
      if (i = TopNode) or (j = LftNode) or (j = Rt) then
        Area[i,j] := 0;
      SoilMass[i,j] := Area[i,j]*1000*Props2D.RhoB[i,j];
```

```
    end;

  for i := Surf to Btm do
    for j := Lft to Rt do
    begin
      CV.URxFlowPath[i,j] := Soil.dz[i-1]/(2*dX[j]);
      CV.LRxFlowPath[i,j] := Soil.dz[i]/(2*dX[j]);
      CV.ULxFlowPath[i,j] := Soil.dz[i-1]/(2*dX[j-1]);
      CV.LLxFlowPath[i,j] := Soil.dz[i]/(2*dX[j-1]);
      CV.LLzFlowPath[i,j] := 1/(4*CV.LLxFlowPath[i,j]);
      CV.ULzFlowPath[i,j] := 1/(4*CV.ULxFlowPath[i,j]);
      CV.LRzFlowPath[i,j] := 1/(4*CV.LRxFlowPath[i,j]);
      CV.URzFlowPath[i,j] := 1/(4*CV.URxFlowPath[i,j]);
      CV.ACV[i,j]              := (Elem2D.Area[i-1,j-1]+Elem2D.Area[i-
1,j]+Elem2D.Area[i,j]+
                                  Elem2D.Area[i,j-1]);
      CV.MassSoil[i,j]                  :=     (Elem2D.SoilMass[i-1,j-
1]+Elem2D.SoilMass[i-1,j]+

Elem2D.SoilMass[i,j]+Elem2D.SoilMass[i,j-1]);
    end;
end; {procedure SetUp2Dnodes}

procedure TSoilFD.Init2DSourceSinkFluxes;
{An infiltration flux is added to each interior node of the grid so
as to generalize the continuity equation. Only surface nodes can
have a non zero value for infiltration so all nodes are set to zero
in this procedure and only surface nodes are recalculated for each
time step. Evaporation  and root water uptake have been added }
begin
  FillChar(CV.Infil,SizeOf(CV.Infil),#0);
  FillChar(CV.Evap,SizeOf(CV.Evap),#0);
  FillChar(CV.dEvap_dPsi,SizeOf(CV.dEvap_dPsi),#0);
  FillChar(CV.Uptake,SizeOf(CV.Uptake),#0);
  FillChar(CV.dUptake_dPsi,SizeOf(CV.dUptake_dPsi),#0);
end; {Init2DSourceSinkFluxes}

procedure TSoilFD.Infiltration2D;
{This PROC must be used to distribute water over the surface It
checks to see if there was irrigation in the previous time step or
in this time step. if not then no change needs to be made to surface
node infiltration. 1mm is 1kg/m2. Divide this by the time step in
seconds to get flux density. For drip or micro if we have a figure
in litres it will be easy to calc a flux by dividing litres by
emitter spacing times row width and then by dt and then multiply by
distance in X axis over which irrigation falls - should set up nodes
so that wetted area falls halfway between two nodes}

var
  i,j:          Integer;
  MassWater,
  WetSurfIrrig,
  SurfaceInf,
  IrrigInf:     Double;
begin
```

```
  Soil.IrrigRed := Soil.IrrigRed - Soil.PrecipRed;

  i := Surf;
  for j := Lft to Rt do
      CV.Infil[i,j] := 0; {reset infiltration to 0 for new day}
  if (Soil.PrecipRed > 0) or (CV.Infil[Surf,6] <> 0) then
  begin


    {Infiltration2D fluxes kg/m(Y)/s }
    i := Surf;


    for j := Lft to Rt do
      CV.Infil[i,j] := CV.Infil[i,j] + Soil.PrecipRed/dt*Surface[j];
  end;

  if (Soil.IrrigRed > 0) or (CV.Infil[Surf,6] <> 0) then
  begin
    MassWater := Soil.IrrigRed*ProfileWidth; {kg water applied to 1m
(Y) row length}
    WetSurfIrrig := MassWater/IrrigatedSurf; {kg/m2 = mm }
    IrrigInf  := WetSurfIrrig/dt;           {flux density at a node
kg/m^2(XY)/s}

    {Infiltration2D fluxes kg/m(Y)/s }
    i := Surf;
    for j := LWetNode to RWetNode do
      CV.Infil[i,j] := CV.Infil[i,j] + IrrigInf*Surface[j];

(*  if (DM.Irrg + DM.Precp > 0) or (CV.Infil[Surf,6] <> 0) then
  begin
    MassWater := DM.Irrg*ProfileWidth; {kg water applied to 1m (Y)
row length}
    WetSurfIrrig := MassWater/IrrigatedSurf; {kg/m2 = mm }
    IrrigInf  := WetSurfIrrig/dt;           {flux density at a node
kg/m^2(XY)/s}

    {Infiltration2D fluxes kg/m(Y)/s }
    i := Surf;
    for j := LWetNode to RWetNode do
      CV.Infil[i,j] := IrrigInf*Surface[j];

    for j := Lft to Rt do
      CV.Infil[i,j] := CV.Infil[i,j] + DM.Precp/dt*Surface[j];*)
  end;
end; {Infiltration2D}

procedure TSoilFD.Zero2DBoundConduct(i,j: Integer);
begin
  with Elem2D do
  begin
    if i = Surf then
    begin
      Klr[i-1,j-1]   := 0;
      MFPlr[i-1,j-1] := 0;
```

```
      Kll[i-1,j]      := 0;
      MFPll[i-1,j]    := 0;
    end;

    if j = Lft then
    begin
      Klr[i-1,j-1]      :=0;
      MFPlr[i-1,j-1]    :=0;
      Kur[i,j-1]        :=0;
      MFPur[i,j-1]      :=0;
      dKur_dPsi[i,j-1] :=0;
    end;

    if j = Rt then
    begin
      Kll[i-1,j]      := 0;
      MFPll[i-1,j]    := 0;
      Kul[i,j]        := 0;
      MFPul[i,j]      := 0;
      dKul_dPsi[i,j] := 0;
    end;


(*    if i = Surf then
    begin
      Klr[i-1,j-1] := 0;
      MFPlr[i-1,j-1] := 0;
      Kll[i-1,j] := 0;
      MFPll[i-1,j] := 0;

      CV.URxFlowPath[i,j] := 0;
      CV.URzFlowPath[i,j] := 0;
      CV.ULxFlowPath[i,j] := 0;
      CV.ULzFlowPath[i,j] := 0;
    end;

    if i = Lft then
    begin
      Klr[i-1,j-1] := 0;
      MFPlr[i-1,j-1] := 0;
      Kur[i,j-1] := 0;
      MFPur[i,j-1] := 0;
      dKur_dPsi[i,j-1] := 0;

      CV.ULxFlowPath[i,j] := 0;
      CV.ULzFlowPath[i,j] := 0;
      CV.LLxFlowPath[i,j] := 0;
      CV.LLzFlowPath[i,j] := 0;
    end;

    if i = Rt then
    begin
      Kll[i-1,j] := 0;
      MFPll[i-1,j] := 0;
      Kul[i,j] := 0;
      MFPul[i,j] := 0;
```

```
      dKl_dPsi[i,j] := 0;

      CV.URxFlowPath[i,j] := 0;
      CV.URzFlowPath[i,j] := 0;
      CV.LRxFlowPath[i,j] := 0;
      CV.LRzFlowPath[i,j] := 0;
    end;

    if i = Surf then
    begin
      Klr[i-1,j-1] := 0;
      MFPlr[i-1,j-1] := 0;
      Kll[i-1,j] := 0;
      MFPll[i-1,j] := 0;

      CV.URxFlowPath[i,j] := 0;
      CV.URzFlowPath[i,j] := 0;
      CV.ULxFlowPath[i,j] := 0;
      CV.ULzFlowPath[i,j] := 0;
    end;*)


  end; {with}
end; {Zero2DBoundConduct;}

procedure TSoilFD.MassBal2D(i,j:Integer);
var
  MBE2D,           {Mass balance error }
  dMBEdPsi,        {derivative of MBE wrt water potential}
  dPsi,
  dHflux,dVflux,S,RR,E,
  stor,
  MaxDP:      Double;
begin
  { Fluxes towards node [i,j] are positive }
  with CV,Elem2D do
  begin
    urx := (MFPlr[i-1,j]-MFPll[i-1,j])*URxFlowPath[i,j];
    urz  :=  (MFPul[i-1,j]-MFPll[i-1,j])*URzFlowPath[i,j]+g/2*Kul[i-
1,j]*dX[j];

    lrx := (MFPur[i,j]-MFPul[i,j])*LRxFlowPath[i,j];
    lrz          :=          (MFPll[i,j]-MFPul[i,j])*LRzFlowPath[i,j]-
g/2*Kul[i,j]*dX[j];

    ulx := (MFPll[i-1,j-1]-MFPlr[i-1,j-1])*ULxFlowPath[i,j];
    ulz                  :=                  (MFPur[i-1,j-1]-MFPlr[i-1,j-
1])*ULzFlowPath[i,j]+g/2*Kur[i-1,j-1]*dX[j-1];

    llx := (MFPul[i,j-1]-MFPur[i,j-1])*LLxFlowPath[i,j];
    llz := (MFPlr[i,j-1]-MFPur[i,j-1])*LLzFlowPath[i,j]-g/2*Kur[i,j-
1]*dX[j-1];

    stor        :=    -Rho_w*(WN[i,j]-W[i,j])*ACV[i,j]/dt+Infil[i,j]-
Evap[i,j]-Uptake[i,j];
    MBE2D :=  urx+lrx+ulx+llx+lrz+llz+urz+ulz+stor;
```

```
  {dMBEdPsi}
    dHflux          :=          -Elem2D.Kll[i-1,j]*URxFlowPath[i,j]-
Elem2D.Kul[i,j]*LRxFlowPath[i,j]
                -Elem2D.Klr[i-1,j-1]*ULxFlowPath[i,j]-Elem2D.Kur[i,j-
1]*LLxFlowPath[i,j];
    dVflux          :=          -Elem2D.Kll[i-1,j]*URzFlowPath[i,j]-
Elem2D.Kul[i,j]*LRzFlowPath[i,j]
                -Elem2D.Klr[i-1,j-1]*ULzFlowPath[i,j]-Elem2D.Kur[i,j-
1]*LLzFlowPath[i,j];

    S    :=    -g/2*(Elem2D.dKul_dPsi[i,j]*dX[j]+Elem2D.dKur_dPsi[i,j-
1]*dX[j-1]);


    RR := -Rho_w*dWNdPsi[i,j]/dt; {This term does not show the ACV
which cancels out
                                  with the ACV term which is contained
in the
                                  dWNdPsi equation  }
    E := -dEvap_dPsi[i,j];
    dMBEdPSI  := dHflux + dVflux + S + RR + E - dUptake_dPsi[i,j];
    Tolerance := Tolerance + ABS(MBE2D);
    dPsi      := MBE2D/dMBEdPsi;

    if SoilFD.Psi2D[i,j] < -0.01 then
    begin
      MaxDP := -0.8*SoilFD.Psi2D[i,j];
      if abs(dPsi) > MaxDP then
        if dPsi > 0 then
          dPsi := MaxDP
        else
          dPsi := -MaxDP;
    end;
    SoilFD.Psi2D[i,j]  :=  SoilFD.Psi2D[i,j]-dPsi;     {update  water
potential }
  end; {with}
end; {MassBal2D}

(*
procedure TSoilFD.Evaporate(i,j: Integer);
var
  HumSoil: Double;
begin
  if i = Surf then
  begin
    HumSoil := exp(MdivRT*SoilFD.Psi2D[i,j]);
    CV^[i,j].Evap     :=     TreeObj.PE[j]/dt*(HumSoil-RHcanopy)/(1-
RHcanopy)*SoilFD.Surface[j];
    CV^[i,j].dEvap_dPsi    :=    TreeObj.PE[j]/dt*HumSoil*MdivRT/(1-
RHcanopy)*SoilFD.Surface[j];
  end;
end; {procedure Evaporate}
*)

procedure TSoilFD.Redist2D;
```

```
var
  iteration,
  i,j,hour: Integer;
begin

  RHcanopy := 0.5;
  Iteration := 0;
  SoilFD.Infiltration2D;
  Calc2DRootDensAndConductivity;
  WaterUptake2D;
  repeat
    Tolerance := 0;
    for i := Surf to Btm do
      for j := Lft to Rt do
      begin
        MassBal2D(i,j);
        if i = Surf then
          Evap2D(i,j);
        WaterFunctions(i,j);
        SoilFD.Zero2DBoundConduct(i,j);

      end;
    SoilFD.SetLowerBoundaryCond2D;
    Inc(Iteration);
  until (Tolerance <= MBTolerance) or (Iteration = 20000);
  if Iteration = 20000 then
    ShowMessage('20000 Iterations DOY = '+IntToStr(DOY));


  Write(Psi2DFVar,DateToStr(RunDate));
  for i := 1 to nl do
    for j := 1 to nl do
      Write(Psi2DFVar,' ',Format('%12.2f',[CV.WN[i,j]]));
  WriteLn(Psi2DFVar);

  for i := 1 to nl do
    for j := 1 to nl do
    begin
      if
DM.WBal2DT.Locate('FIELD;DATE;I;J',VarArrayOf([FieldDM.Field.Value,R
unDate,i,j]),[]) then
        DM.WBal2DT.Edit
      else
      begin
        DM.WBal2DT.Insert;
        DM.WBal2DTField.Value := FieldDM.Field.Value;
        DM.WBal2DTDate.Value  := RunDate;
        DM.WBal2DTI.Value     := i;
        DM.WBal2DTJ.Value     := j;
      end;
      DM.WBal2DTPsi.Value := SoilFD.Psi2D[i,j];
      DM.WBal2DTWC.Value  := CV.WN[i,j];
      DM.WBal2DT.Post;
    end;
end; {procedure Redist2D;}
```

```
procedure TSoilFD.SetLowerBoundaryCond2D;
var
  j: Integer;
begin
  for j := Lft to Rt do
  begin
    case FieldDM.FieldTblBoundCond.Value of
      0: begin
           Elem2D.MFPll[Btm,j]   := Elem2D.MFPul[Btm,j];
           Elem2D.MFPlr[Btm,j-1] := Elem2D.MFPur[Btm,j-1];
         end;
         {Gravity will drain the profile as there is no matric flux
potential gradient}
      1: begin
           Elem2D.MFPll[Btm,j]   := Elem2D.MFPul[Btm,j];
           Elem2D.MFPlr[Btm,j-1] := Elem2D.MFPur[Btm,j-1];

           Elem2D.Kul[Btm,j]   :=0;
           Elem2D.Kur[Btm,j-1] :=0;
         end;
         {set zero-flux lower boundary, set drainage = 0}
    end;
  end;
end; {SetLowerBoundaryCond2D}

procedure TSoilFD.CalcIrrigSurf(WettedWidth: Double);
var
  i: Integer;
begin
  for i := 1 to 11 do
    if x[i] >= (x[6] - WettedWidth/2) then
    begin
      LWetNode := i;
      Break;
    end;
  for i := 11 downto 1 do
    if x[i] <= (x[6] + WettedWidth/2) then
    begin
      RWetNode := i;
      Break;
    end;
  IrrigatedSurf := 0;
  for i := LWetNode to RWetNode do
    IrrigatedSurf := IrrigatedSurf + SoilFD.Surface[i];
end;

procedure TSoilFD.FDiffCalcSoildx;
{This procedure sets the horizontal node spacing in metres}
var
  i,j: Integer;
begin
  {Set up horizontal node spacing}
  x[0] := -1;
  x[1] := 0;     { Left symmetry plane}
  for j := 2 to Rt do
    x[j] := TreeObj.xp[j]-TreeObj.xp[1];
```

```
  x[RtNode] := x[Rt]+1;  { Right symmetry plane }

  for j := LftNode to Rt do
    dX[j] := x[j+1]-x[j];

        { Calculate surface area covered by each surface node }
        { This is needed to calculate infiltration and evaporation }


  for j := Lft+1 to Rt-1 do
    Surface[j] := (dX[j-1] + dX[j])/2;

  Surface[Rt]  := dX[Rt-1]/2;
  Surface[Lft] := dX[1]/2;
  CalcIrrigSurf(FieldDM.WettedDiam.Value);

 { TwiceWidth and Factor are needed to calculate percolation and
leaching.
   They are calculated here to prevent them being recalculated with
each
   time step. }

   for j := Lft to Rt do
     TwiceWidth[j] := 2*Surface[j];

   ProfileWidth := X[Rt]-X[Lft]; //should be same as row width
   TwiceProfileWidth := ProfileWidth*2;

   for j := Lft to Rt do
     if TwiceWidth[j] <> 0 then
       Factor[j] := -2*dt/TwiceWidth[j]
     else
       Factor[j] := 0;
    // LeachFactor[j]:=-20000/TwiceWidth[j];
end; {FDiffCalcSoildx}

procedure TSoilFD.FDiffCalcSoildz;
 {I am adding a thin layer 1 cm thick to the standard 11 layer
model. We may have to add a warning if someone tries to enter the
thickness of layer 1 at less than 1 cm}
var
  i: Integer;
begin       {GAYLON dz[0]:=1e6; dz[1]:=0.01; Surf layer is always 1
cm}
  Soil.dz[0] := 1e6;  {not sure why Gaylon wants this air space so
big as we specify
                  the surface liquid flux and evap doesn't use a
resistance term
                  explicitly}
 {don't allow user to input layer 1 < 1 cm}
  Soil.dz[1] := 0.01;
  Soil.dz[2] := SoilData.z[1]-Soil.dz[1];
  for i := 2 to nl do
    Soil.dz[i+1] := SoilData.z[i] - SoilData.z[i-1];
  for i := 0 to nl+1 do
    HALFdz[i] := Soil.dz[i]/2;
```

```
  CVdz[0] := HALFdz[0];
  CVdz[1] := HALFdz[1];
  CVdz[nl+2] := HALFdz[nl+1];
  for i := 2 to nl+1 do
    CVdz[i] := HALFdz[i] + HALFdz[i-1];
end; {procedure FDiffCalcSoildz}

procedure Hydraulics(Psi,PsiE,PsiI,bl,SatWC,n,nl,hc,ks: Double; var
wc,k,MFP,
  dwdp: Double);
begin
  if Psi < PsiI  then
  begin
    wc   := SatWC*Power(PsiE/Psi,bl);
    dwdp := -wc*bl/Psi ;
  end
  else if Psi < 0 then
  begin
    wc := SatWC*(1-hc*Sqr(Psi));
    dwdp := -2*hc*SatWC*Psi;
  end
  else {if p >= 0 then}
  begin
    wc   := SatWC;
    dwdp := 0;  {Gaylon made this 1e-5, concerned about div by 0?}
  end;


  if Psi < PsiE  then
  begin
    k   := Ks*Power(PsiE/Psi,n);
    MFP := k*Psi/nl;
  end
  else
  begin
    k   := Ks;
    MFP := Ks*(PsiE*n/nl+Psi);
  end;
end; {procedure Hydraulics}

procedure TSoilFD.CalcCVwaterContent;
var
  i: Integer;
begin
  i := 1;
  CVwc[i] := CVnwc[i];
  CVnwc[i] := wnu[i];
  for i := 2 to nl+1 do
  begin
    CVwc[i] := CVnwc[i];
    CVnwc[i] := (HALFdz[i-1]*wnl[i-1]+HALFdz[i]*wnu[i])/CVdz[i];
  end;
end;

function Humidity(Psi,PsiE: Double): Double;
begin
```

```
  if Psi < PsiE then {Humidity := Exp(Mw*p/(R*Tk))}
    Result := Exp(MdivRT*Psi)  {to save calculating MwR/T each time}
  else
    Result := 1;
end;

procedure TSoilFD.FDiffInitSoil;
var
  i,LayerNr: Integer;
  ac:        Double;
begin

  SoilData.fcwc[0]  := SoilData.fcwc[1];
  SoilData.pwpwc[0] := SoilData.pwpwc[1];
  SoilData.SatWC[0] := SoilData.SatWC[1];
  SoilData.WC[0]    := SoilData.WC[1];
  SoilData.bd[0]    := SoilData.bd[1];
  for i := Btm downto Surf+1 do
  begin
    SoilData.fcwc[i]  := SoilData.fcwc[i-1];
    SoilData.pwpwc[i] := SoilData.pwpwc[i-1];
    SoilData.SatWC[i] := SoilData.SatWC[i-1];
    SoilData.WC[i]    := SoilData.WC[i-1];
    SoilData.bd[i]    := SoilData.bd[i-1];
  end;

  FDiffCalcSoildz;

     wnu[1]:= SoilData.WC[2];
     wnl[1]:= SoilData.WC[2];

  for i := Btm downto Surf+1 do
    begin
       wnu[i]:= SoilData.WC[i-1];
       wnl[i]:= SoilData.WC[i-1];
    end;

  CalcCVwaterContent;
  if RunF.SimSalts.Checked then
    InitSaltDM.GetFDInitSalts(FieldDM.Field.Value);

  for i := 1 to nl+1 do
  begin
    SoilData.WCDry[i] := SoilData.WC[i];
    SoilData.SatWC[i] := 1 - SoilData.BD[i]/2.65;
    Soil.b[i]                                                    :=
ln(SoilData.PsiPWP/SoilData.PsiFC)/ln(SoilData.fcwc[i]/SoilData.pwpw
c[i]);
    Soil.a[i]          :=          Exp(ln(-SoilData.PsiPWP)          +
Soil.b[i]*ln(SoilData.pwpwc[i]));
    if FieldDM.Model.Value = 0 then {Growth}
      SoilData.pwpwc[i]                  :=                Exp(-ln(-
3*CropDM.Psilm.Value/(2*Soil.a[i]))/Soil.b[i])         {plant  lower
limit}
    else
```

```
      SoilData.pwpwc[i]                    :=                    Exp(-ln(-
3*FCropDM.FPot.Value/(2*Soil.a[i]))/Soil.b[i]);          {plant  lower
limit}
    if SoilData.wc[i] > SoilData.SatWC[i] then
    begin
      SoilData.wc[i] := SoilData.SatWC[i];
      ShowMessage(FieldDM.Field.Value+': Initial WC['+IntToStr(i)+']
exceeds saturation');
    end; {if}

    if RunF.SimSalts.Checked then
    begin
      FillChar(Soil.ElCond,SizeOf(Soil.ElCond),#0);
      FillChar(Soil.ElCondDry,SizeOf(Soil.ElCondDry),#0);

      Soil.MassCa[i]                                                    :=
InitSaltDM.InitCa[i]*SoilData.bd[i]*SoilFD.CVdz[i];
      Soil.MolCa[i]  := Soil.MassCa[i]/AtomicMassCa;
      Soil.CaConc[i]                                                    :=
Soil.MolCa[i]/(SoilFD.CVnwc[i]*Rho_w*SoilFD.CVdz[i]);

      Soil.MassMg[i]                                                    :=
InitSaltDM.InitMg[i]*SoilData.bd[i]*SoilFD.CVdz[i];
      Soil.MolMg[i]  := Soil.MassMg[i]/AtomicMassMg;
      Soil.MgConc[i]                                                    :=
Soil.MolMg[i]/(SoilFD.CVnwc[i]*Rho_w*SoilFD.CVdz[i]);

      Soil.MassNa[i]                                                    :=
InitSaltDM.InitNa[i]*SoilData.bd[i]*SoilFD.CVdz[i];
      Soil.MolNa[i]  := Soil.MassNa[i]/AtomicMassNa;
      Soil.NaConc[i]                                                    :=
Soil.MolNa[i]/(SoilFD.CVnwc[i]*Rho_w*SoilFD.CVdz[i]);

      Soil.MassK[i]                                                     :=
InitSaltDM.InitK[i]*SoilData.bd[i]*SoilFD.CVdz[i];
      Soil.MolK[i]  := Soil.MassK[i]/AtomicMassK;
      Soil.KConc[i]                                                     :=
Soil.MolK[i]/(SoilFD.CVnwc[i]*Rho_w*SoilFD.CVdz[i]);

      Soil.MassCl[i]                                                    :=
InitSaltDM.InitCl[i]*SoilData.bd[i]*SoilFD.CVdz[i];
      Soil.MolCl[i]  := Soil.MassCl[i]/AtomicMassCl;
      Soil.ClConc[i]                                                    :=
Soil.MolCl[i]/(SoilFD.CVnwc[i]*Rho_w*SoilFD.CVdz[i]);

      Soil.MassSO4[i]                                                   :=
InitSaltDM.InitSO4[i]*SoilData.bd[i]*SoilFD.CVdz[i];
      Soil.MolSO4[i]  := Soil.MassSO4[i]/AtomicMassSO4;
      Soil.SO4Conc[i]                                                   :=
Soil.MolSO4[i]/(SoilFD.CVnwc[i]*Rho_w*SoilFD.CVdz[i]);

      Soil.Gypsum[i] := InitSaltDM.InitGyp[i];
      Soil.Lime[i]   := InitSaltDM.InitLime[i];

      Soil.InitProfileGypsum     :=     Soil.InitProfileGypsum     +
Soil.Gypsum[i];
```

```
      Soil.InitProfileLime   := Soil.InitProfileLime + Soil.Lime[i];
      Soil.InitMassSoilSolution    :=    Soil.InitMassSoilSolution    +
Soil.MassCa[i]
                                   + Soil.MassSO4[i] + Soil.MassMg[i]
                                   + Soil.MassNa[i]  + Soil.MassK[i]
                                   + Soil.MassCl[i];
    end;
  end; {for}

  Soil.CaConc[13] := Soil.CaConc[12];
  Soil.MassCa[13] := Soil.MassCa[12];
  Soil.MolCa[13]  := Soil.MolCa[12];

  Soil.MgConc[13] := Soil.MgConc[12];
  Soil.MassMg[13] := Soil.MassMg[12];
  Soil.MolMg[13]  := Soil.MolMg[12];

  Soil.NaConc[13] := Soil.NaConc[12];
  Soil.MassNa[13] := Soil.MassNa[12];
  Soil.MolNa[13]  := Soil.MolNa[12];

  Soil.KConc[13]  := Soil.KConc[12];
  Soil.MassK[13]  := Soil.MassK[12];
  Soil.MolK[13]   := Soil.MolK[12];

  Soil.ClConc[13] := Soil.ClConc[12];
  Soil.MassCl[13] := Soil.MassCl[12];
  Soil.MolCl[13]  := Soil.MolCl[12];

  Soil.SO4Conc[13] := Soil.SO4Conc[12];
  Soil.MassSO4[13] := Soil.MassSO4[12];
  Soil.MolSO4[13]  := Soil.MolSO4[12];

  Soil.ActualTrsp := 0;
  FillChar(a,SizeOf(a),#0);
  FillChar(si,SizeOf(si),#0);



  b     := a;
  bx    := a;
  bl    := a;
  cx    := a;
  f     := a;
  jl    := a;
  dp    := a;
  PsiE  := a;
  MFPl  := a;
  MFPu  := a;
  dkdpu := a;
  wnu   := a;
  wnl   := a;
  wu    := a;
  wl    := a;
  cpu   := a;
  cpl   := a;
```

```
  ks     := a;
  dkdpl  := a;
  ku     := a;
  kl     := a;
  n      := a;
  n1     := a;
  h      := a;
  jv     := a;
  kv     := a;
  fr     := a;
  ruk    := a;

 {assign properties from cascading layers to FD layers}

  SoilData.ProfFC                                                    :=
Round(FD_SoilStoredWater(SoilData.FCWC,Soil.dz));
  SoilData.ProfSAT                                                   :=
Round(FD_SoilStoredWater(SoilData.SATWC,Soil.dz));
  SoilData.ProfPWP                                                   :=
Round(FD_SoilStoredWater(SoilData.PWPWC,Soil.dz));

  SurfStor := 0;
  LayerNr := 0;
  si[0] := -1;       {needed to force recalculation of upper half of
layer 1}
  si[1] := LayerNr;
  si[2] := LayerNr; {Layer 1 and 2 will have same props - layer 1 is
just a
                     small bit of layer 2}
  for i := 3 to Btm do
  begin
    if      (SoilData.fcwc[i-1]      <>      SoilData.fcwc[i])      or
(SoilData.pwpwc[i-1]<>
       SoilData.pwpwc[i]) or (SoilData.bd[i-1] <> SoilData.bd[i])
then
      Inc(LayerNr);
   {This looks to see if layers have different props, we will have
to
    change this to look at b, PsiE, Ks once we have them as varying
input}
    si[i] := LayerNr;
  end;
  for i := TopNode{Surf} to Btm do
  begin
    SoilData.SatWC[i] := 1 - SoilData.bd[i]/2.65;{Nico hierdie word
dalk
                                                  elders gedoen
    soos  waar  gronde  initialize  word?  THIS  IS  SOIL.SATwc  -  WE
ALREADY KNOW IT?
    if not read from input then calc b, PsiE and Ks}
    b[i]                                                             :=
ln(SoilData.PsiPWP/SoilData.PsiFC)/ln(SoilData.fcwc[i]/SoilData.pwpw
c[i]);
    a[i] := Exp(ln(-SoilData.PsiPWP) + b[i]*ln(SoilData.pwpwc[i]));
    PsiE[i]                                                          :=
SoilData.PsiFC*Power(SoilData.fcwc[i]/SoilData.SatWC[i],b[i]);
```

```
    ks[i] := 0.2*1e-3/Sqr(PsiE[i]); {Change here saturated hydraulic
conductivity}
    n[i]  := 2+3/b[i];
    n1[i] := 1-n[i];
    b1[i] := 1/b[i];
    ac    := 2*b[i]/(1 + 2*b[i]);          {Hutson & Cass a     value}
    PsiI[i] := PsiE[i]*Power(ac,-b[i]);  {Hutson & Cass Psi i value}
    hc[i]   := (1-ac)/Sqr(PsiI[i]);      {Hutson & Cass c     value}
    Psi[i]      :=   PsiE[i]*Power(SoilData.WC[i]/SoilData.SatWC[i],-
b[i]);
    {set initial Psi from water content of layer below it, not quite
right but
    OK for this one off}
    if FieldDM.Model.Value = 0 then {Growth}
      SoilData.pwpwc[i]                    :=                  Exp(-ln(-
3*CropDM.Psilm.Value/(2*a[i]))/b[i]){plant lower limit}
    else
      SoilData.pwpwc[i]                    :=                  Exp(-ln(-
3*FCropDM.FPot.Value/(2*a[i]))/b[i]);{plant lower limit}
  end;

  Psi[n1+2] := Psi[n1+1]; {set lower boundary potential}
  dkdpu[0] := 0;
  dkdpl[0] := 0; {upper conductivities 0 - no liquid
                  flux into air, evaporation does, however, occur}
  for i := Surf to Btm do
  begin
    {First give the potential at bottom of a layer to determine the
     lower new water content wn1, the lower conductivity k1, the
lower matric
     flux potential MFP1 and d theta d psi (dwdp) or the slope
     of the water retention function (differential water capacity).
Note that
     dwdp is not an array, we use the number straight away (not here
though)
     and therefore dont need to remember it.}

Hydraulics(Psi[i+1],PsiE[i],PsiI[i],b1[i],SoilData.SatWC[i],n[i],n1[
i],hc[i],ks[i],
               wn1[i],k1[i],MFP1[i],dwdp);

Hydraulics(Psi[i],PsiE[i],PsiI[i],b1[i],SoilData.SatWC[i],n[i],n1[i]
,hc[i],ks[i],
               wnu[i],ku[i],MFPu[i],dwdp);
    h[i] := Humidity(Psi[i],PsiE[i]);



    wu[i] := wnu[i];
    wl[i] := wn1[i];
  end;
  FD_CalcLayerWC(wnu,wn1);
  Soil.InitialWC := FD_SoilStoredWater(SoilData.WC,Soil.dz);
  CalcCVwaterContent;
  h[n1+2] := h[n1+1]; {lower boundary}
  h[0]    := 0.5;
```

```
  Psi[0]   := -1e5; {upper boundary  -will change this to have h[0]
the
                    atmospheric Humidity vary over the day and from
that
                    Psi[0] can be calculated}
end;

procedure TSoilFD.FDiffInit2DSoil;
var
  i,j: Integer;
begin
  for i := TopNode to BtmNode do
    for j := LftNode to RtNode do
    begin
      Psi2D[i,j] := Psi[i];
      hr[i,j]    := h[i];
    end;

  for i := TopNode to Btm do
    for j := LftNode to Rt do
    begin
      Props2D.b[i,j]    := b[i];

      Props2D.AEP[i,j]  := PsiE[i];
      Props2D.Ks[i,j]   := Ks[i];
      Props2D.RhoB[i,j] := SoilData.bd[i];
      Props2D.WS[i,j]   := SoilData.SatWC[i];
      Props2D.n[i,j]    := n[i];

      Props2D.PWP[i,j]  := SoilData.pwpwc[i];
      Props2D.FC[i,j]   := SoilData.fcwc[i];

      Elem2D.WNul[i,j]  := wnu[i];
      Elem2D.WNur[i,j]  := wnu[i];

      Elem2D.WNll[i,j]  := wnl[i];
      Elem2D.WNlr[i,j]  := wnl[i];

      Elem2D.Kul[i,j]   := ku[i];
      Elem2D.Kur[i,j]   := ku[i];
      Elem2D.Kll[i,j]   := kl[i];
      Elem2D.Klr[i,j]   := kl[i];
      Elem2D.MFPul[i,j] := MFPu[i];
      Elem2D.MFPur[i,j] := MFPu[i];
      Elem2D.MFPll[i,j] := MFPl[i];
      Elem2D.MFPlr[i,j] := MFPl[i];
    end;
  for i := Surf to Btm do
    for j := Lft to Rt do
    begin
      CV.W[i,j]  := CVwc[i];
      CV.WN[i,j] := CVnwc[i];
    end;

  j := LftNode;
  for i := TopNode to Btm do
```

```
    begin
      Elem2D.Kll[i,j]      := 0;
      Elem2D.MFPll[i,j]    := 0;
      Elem2D.Kul[i,j]        := 0;
      Elem2D.MFPul[i,j]      := 0;
      Elem2D.dKul_dPsi[i,j] := 0;
      Elem2D.dKll_dPsi[i,j] := 0;
    end;

  j := RtNode;
  for i := TopNode to Btm do
    begin
      Elem2D.Klr[i,j-1]      := 0;
      Elem2D.MFPlr[i,j-1]    := 0;
      Elem2D.Kur[i,j-1]        := 0;
      Elem2D.MFPur[i,j-1]      := 0;
      Elem2D.dKur_dPsi[i,j-1] := 0;
      Elem2D.dKlr_dPsi[i,j-1] := 0;
    end;

  i := Btm;
  for j := LftNode to Rt do
    begin
      Elem2D.Kll[i,j]      := 0;
      Elem2D.MFPll[i,j]    := 0;
      Elem2D.Klr[i,j]        := 0;
      Elem2D.MFPlr[i,j]      := 0;
      Elem2D.dKlr_dPsi[i,j] := 0;
      Elem2D.dKll_dPsi[i,j] := 0;
    end;

  {set all boundary conductancies to zero here}

end; {FDiffInit2DSoil}

procedure TSoilFD.SurfaceStorage;
var
  MaxPrecip: Double;
begin
  {SumPrecip := SumPrecip + Precip.Precip; }
  SurfStor  := SurfStor + Soil.PrecipRed;//DM.Precp;
  MaxPrecip := g*ks[1]*dt;  {max infil in a time step? Is this a way
of
                              preventing it from crashing?}
  if SurfStor > MaxPrecip then
  begin
    SurfStor := SurfStor-MaxPrecip;{stores excess water on surface -
perhaps
    we need to add a max storage parameter and let the rest runoff?
Perhaps
    the  surface  storage  should  be  allowed  to  vary  over  time
(rainfall energy
    dependent - see SWIM). It can be restored by cultivation}
    DM.Precp := MaxPrecip;

  end
```

```
  else
  begin
    DM.Precp := SurfStor;
//    Soil.PrecipRed := SurfStor;
    SurfStor := 0;
  end;
    {Ons sal 'n nuwe afloop routine moet skryf - soos dit nou is sal
niks
     afloop nie - this would be true if we did not call runoff
already}
end; {procedure TSoilFD.SurfaceStorage}

procedure TSoilFD.CalcRootDensityAndConductivity;
var
  i:          Integer;
  Emax,
  z_rd,Oldz: Double; {yes z_rd is local}
begin
  Soil.ActualTrsp := 0;
  Soil.ECRoot := 0;
  Soil.ECRootSat := 0;
  if (Crop.RD > 0) and (Crop.FItransp > 0) then
  begin
    sumf := 0;
    z_rd := Soil.dz[1] + HALFdz[2];
    i := 2;
    repeat    {transpiration if crop}

      if Psi[i] < 2*CropDM.Psilm.Value then
        f[i] := 0 {no roots in dry layers-does cascading have this?}
      else
      begin
        if z_rd <= Crop.Rd then
          fr[i]                :=              Soil.dz[i]*(2*(Crop.Rd-
z_rd)+Soil.dz[i])/Sqr(Crop.Rd)
        else
          fr[i] := Sqr((Crop.Rd-z_rd+Soil.dz[i])/Crop.Rd);
      end;
      sumf := sumf + fr[i];
      Oldz := z_rd;
      Inc(i);
      if i <= nl+1 then
        z_rd := z_rd + CVdz[i];
    until (i > nl+1) or (Oldz > Crop.Rd);
    nlr := i-1;
    case FieldDM.Model.Value of
      0: Emax := CropDM.MaxTrans.Value;    {Growth}
      1: Emax := FCropDM.FMaxTrans.Value; {FAO}
    end;
    est := PET/Emax;
    if sumf > 0 then
      for i := 1 to nl+1 do
      begin
        fr[i]  := fr[i]/sumf; {normalize f}
        ruk[i]              :=            Crop.FItransp*Emax*fr[i]/(-
0.67*CropDM.Psilm.Value*dt);
```

```
      end;
  end {if (Crop.RD > 0) and (Crop.FItransp > 0)}
  else
    for i := 1 to n1+1 do
    begin
      fr[i]  := 0;
      ruk[i] := 0;
    end;
end;  {CalcRootDensityAndConductivity;}

procedure TSoilFD.CalcWaterStatus;
var
  i: Integer;
begin
  for i := Surf to Btm do
  begin

Hydraulics(Psi[i+1],PsiE[i],PsiI[i],b1[i],SoilData.SatWC[i],n[i],n1[
i],hc[i],ks[i],
                wn1[i],k1[i],MFP1[i],dwdp);
    h[i] := Humidity(Psi[i],PsiE[i]);
    cp1[i] := Rho_W*dwdp/dt;
    if si[i] = si[i-1] then {if layer below has same props as one
above}
    begin
      ku[i]   := k1[i-1];
      MFPu[i] := MFP1[i-1];
      cpu[i]  := cp1[i-1];
      wnu[i]  := wn1[i-1];
    end
    else
    begin

Hydraulics(Psi[i],PsiE[i],PsiI[i],b1[i],SoilData.SatWC[i],n[i],
                 n1[i],hc[i],ks[i],wnu[i],ku[i],MFPu[i],dwdp);
      cpu[i] := Rho_W*dwdp/dt;
    end;
  end;
end; {CalcWaterStatus}

procedure TSoilFD.RedistributionAndMassBalance;
var
  TmpI,
  i:        Integer;
  MBE,
  swt,{space weighting factor for gravity flux - 0.5 is central
space weighting
       and 1 full upstream weighting - this may become variable when
       oscillations occur- see SWIM pg 11,44,45}
  swt1,{1-swt}  {CLAIRE - LOOK AT THIS FOR US PLEASE}
  ust,
  Psix,
  estar,
  AvePsi,
  AvePstar: Double;
begin
```

```
  TmpI := 0;
  PotentialEvap := (1-Crop.Flevap)*PET/dt;   {a flux kg/m2/s}
  kv[0] := PotentialEvap/(1-h[0]);              {transfer coef for
evap}
 {Main daily iteration loop begins to find potentials that will
satisfy balance}
  repeat
    if sumf > 0 then
    begin
      AvePsi := 0;
      for i := 2 to nlr do
        AvePsi := AvePsi + fr[i]*Psi[i];
      AvePstar := AvePsi/CropDM.Psilm.Value;
      if AvePstar < 1.5 then
        ust := 1-0.67*AvePstar
      else
        ust := 0;
      if est < ust then
        estar := est
      else
        estar := ust;
      if estar < 0 then
        estar := 0;
      psix := CropDM.Psilm.Value*(AvePstar+0.67*estar);
    end
    else
      psix := 0;

    MBE  := 0; {accumulates mass balance error of each control
volume}
    swt := 0.5;
    swt1 := 1-swt;
    jl[0] := DM.Precp/dt; {constant flux upper boudary-take out of
loop
                                unless we introduce variable time
step?}
    jv[0]  :=  -kv[0]*(h[1]-h[0]); {upper boundary vapour flux -
evaporation}

    Psi[nl+2] := Psi[nl+1];
    CalcWaterStatus;

    if FieldDM.FieldTblBoundCond.Value = 1 then
    begin
      ku[nl+1] := 0;    {enable these to set drainage to zero}
      kl[nl+1] := 0;    {CHECK}
    end;

    for i := 1 to nl+1 do {calculate fluxes and derivatives}
    begin
      if Psi[i] = Psi[i+1] then
      begin  {save some calculations for lower bound?}
        jl[i] := g*ku[i];  {upper and lower k will be the same, no
space weighting needed}
        jv[i] := 0;        {no matric potential induced vapour flux}
```

```
        if Psi[i] >= PsiE[i] then
        begin
          dkdpu[i] := 0;
          dkdpl[i] := 0;
        end
        else
        begin
          dkdpu[i] := -n[i]*ku[i]/Psi[i];
          dkdpl[i] := dkdpu[i];
        end;
      end
      else {adjacent potentials not equal}
      begin
        {jl[i] := (phil[i]-phiu[i])*(1/dz[i]+Gr/(Psi[i]-Psi[i+1]));}
        {Gaylon has a different term and sign for the gravity
component}
        jl[i]                          :=                          (MFPu[i]-
MFPl[i])/Soil.dz[i]+g*(swt*ku[i]+swt1*kl[i]);
            {kv[i]:=0.66*Dv*Vd*(ws[i]-
(wu[i]+wnu[i]+wl[i]+wnl[i])/4)*
            (h[i+1]-h[i])/((Psi[i+1]-Psi[i])*dz[i]);}
        {kv[i]            :=          2.6928e-7*(SoilData.SatWC[i]-
(wu[i]+wnu[i]+wl[i]+wnl[i])/4)*
              (h[i+1]-h[i])/((Psi[i+1]-Psi[i])*dz[i]); }
            {uses avg wc of Surf and bottom of layer at both old
and new time step}
        kv[i]             :=          2.6928e-7*(SoilData.SatWC[i]-
(wu[i]+wnu[i]+wl[i]+wnl[i])/4)/Soil.dz[i];
        jv[i] := -kv[i]*(h[i+1]-h[i]);

        if Psi[i] < PsiE[i] then
          {dkdpu[i] := (kbar[i]-ku[i])/(Psi[i+1]-Psi[i])}
          dkdpu[i] := -n[i]*ku[i]/Psi[i]
        else
          dkdpu[i] := 0;
        if Psi[i+1] < PsiE[i] then
          {dkdpl[i] := (kl[i]-kbar[i])/(Psi[i+1]-Psi[i])}
          dkdpl[i] := -n[i]*kl[i]/Psi[i+1]
        else
          dkdpl[i] := 0
      end; {else}

      {Derivatives of mass balance equation needed for Newton
Raphson}

      bx[i]                    :=                    kl[i-1]/Soil.dz[i-
1]+ku[i]/Soil.dz[i]+MdivRT*h[i]*kv[i-1]+MdivRT*h[i]*kv[i]+
            cpu[i]*HALFdz[i]+cpl[i-1]*HALFdz[i-1]-g*swt1*dkdpl[i-
1]
            +g*swt*dkdpu[i]+ruk[i]; {Gaylon has + lower g term}
      {Mass balance of control volume i}
      {Derivative wrt psi[i-1]}
      ax[i]   :=   -ku[i-1]/Soil.dz[i-1]-g*swt*dkdpu[i-1]-MdivRT*h[i-
1]*kv[i-1];
      {Derivative wrt psi[i+1]}
```

```
      cx[i]          :=          -kl[i]/Soil.dz[i]+g*swtl*dkdpl[i]-
MdivRT*h[i+1]*kv[i];  {Gaylon has - g term}
      {Derivative wrt psi[i]}
      f[i]     :=     Rho_W*((wnu[i]-wu[i])*HALFdz[i]+(wnl[i-1]-wl[i-
1])*HALFdz[i-1])/dt
                -jl[i-1]+jl[i]-jv[i-1]+jv[i]-ruk[i]*(psix-Psi[i]);
      MBE := MBE + abs(f[i]);
    end; {for}

   {Thomas algorithm (pg 19,SPWB)to solve matrix of simultaneous
equations
   -we are looking for the potentials that will minimize mass
balance error}

    for i := 1 to nl  do
    begin
      cx[i]   := cx[i]/bx[i];
      f[i]    := f[i]/bx[i];
      bx[i+1] := bx[i+1]-ax[i+1]*cx[i];
      f[i+1]  := f[i+1]-ax[i+1]*f[i];
    end;
    dp[nl+1]  := f[nl+1]/bx[nl+1];
    Psi[nl+1] := Psi[nl+1]-dp[nl+1];
    for i := nl downto 1 do          {was for i := nl-1 downto 1 do}
    begin
      dp[i] := f[i]-cx[i]*dp[i+1]; {change in potentials}
      if Abs(Psi[i]) > 0.01 then
        lim:= 0.8*Abs(Psi[i]);       {restrict change in pot}
      abv:= Abs(dp[i]);
      if abv>lim then
        dp[i] := lim*dp[i]/abv;
      Psi[i] := Psi[i]-dp[i];        {next guess at potential}
    end;
    Psi[nl+2] := Psi[nl+1];
    Inc(TmpI);
  until (MBE < im) or (TmpI > 100000);
  if TmpI > 100000 then
    Raise SWBErr.Create('FD: Did not converge!');
  {end of main daily iteration loop to find potentials that will
satisfy mass balance}

  CalcWaterStatus;
  FD_CalcLayerWC(wnu,wnl);

  CalcCVwaterContent;

  {Calculate transpiration from each layer for new potentials}
  Soil.ActualTrsp := 0;
  for i := 1 to nl+1 do {could do this for nlr surely - layers with
roots}
  begin
    Soil.ActualTrsp      :=      Soil.ActualTrsp-ruk[i]*(psix-Psi[i]);
{kg/m2/s}
    wl[i] := wnl[i]; {reset old wc to new wc}
    wu[i] := wnu[i];
  end;
```

```
  Soil.ActualTrsp := Soil.ActualTrsp*dt; {mm}


  if Soil.ActualTrsp < 0 then
    Soil.ActualTrsp := 0;
  Soil.TransDOY  :=  Soil.ActualTrsp;    {NB  remember  to  accumulate
during the day for timesteps < 1 day}

  if Crop.FItransp > 0 then
  begin
    Soil.SI := Soil.ActualTrsp/(Crop.FItransp*PET);
{      if Soil.SI > 1 then
      begin
        ShowMessage('Soil.SI > 1!!');
        Soil.SI := 1;
      end;}
  end
  else
    Soil.SI := 0;
  {SumDrain := SumDrain + jl[nl]*dt; mm}
  Soil.DrainDOY  :=  jl[nl+1]*dt;  {mm}  {NB  remember  to  accumulate
during the day for timesteps < 1 day}
  {SumEvap := SumEvap - jv[0]*dt;}
  Soil.EvapDoy  :=  -jv[0]*dt;  {mm}      {NB  remember  to  accumulate
during the day for timesteps < 1 day}

  Write(PsiFVar,DateToStr(RunDate));
  for i := 1 to nl+1 do
    Write(PsiFVar,' ',Format('%12.2f',[Psi[i]]));
  WriteLn(PsiFVar);
end;  {procedure RedistributionAndMassBalance}

function TSoilFD.getStoredWater: Double;
var
  sw,wc: Double;
  i:     integer;
begin
  sw := 0;
  for i := 1 to nl+1 do
  begin
    wc := 0.5*(wnu[i] + wnl[i]); {vol wc}
    {!!  Nico hierdie kan nou teruggestuur word na res van die model
waar jy toets
     vir   massa   balans   en   bereken   deficits   ens   -   na
ProcInsertResutls?}

    sw := sw + wc*Soil.dz[i]*Rho_W;   {mm}

  end;
  Result := sw;
end;

procedure TSoilFD.WaterFunctions(i,j: Integer);
begin
  with Props2D,Elem2D do
```

```
  if SoilFD.Psi2D[i,j] < AEP[i,j-1] then
  begin
    Kur[i,j-1]                          :=   Ks[i,j-1]*Power((AEP[i,j-
1]/SoilFD.Psi2D[i,j]),n[i,j-1]);
    MFPur[i,j-1]       := Kur[i,j-1]*SoilFD.Psi2D[i,j]/(1-n[i,j-1]);
    dKur_dPsi[i,j-1]   := -n[i,j-1]*Kur[i,j-1]/SoilFD.Psi2D[i,j];
    WNur[i,j-1]        := WS[i,j-1]*Power((SoilFD.Psi2D[i,j]/AEP[i,j-
1]),-1/b[i,j-1]);
    dWNur_dPsi[i,j-1] := -WNur[i,j-1]/(b[i,j-1]*SoilFD.Psi2D[i,j]);
  end
  else
  begin
    Kur[i,j-1]         := Ks[i,j-1];
    MFPur[i,j-1]                        :=Ks[i,j-1]*(AEP[i,j-1]/(1-n[i,j-
1])+SoilFD.Psi2D[i,j]-AEP[i,j-1]);
    dKur_dPsi[i,j-1]   := 0;
    WNur[i,j-1]        := WS[i,j-1];
    dWNur_dPsi[i,j-1] := 0;
  end;


{First calculate the upper right conductance and then compare soil
properties
in adjacent elements to reduce number of calculations using
transcendental
functions.}

  with Props2D, Elem2D do
  begin
    if (n[i,j] = n[i,j-1]) and (Ks[i,j] = Ks[i,j-1]) and (AEP[i,j] =
AEP[i,j-1]) and
       (WS[i,j] = WS[i,j-1]) then
    begin
      Kul[i,j]         := Elem2D.Kur[i,j-1];
      MFPul[i,j]       := Elem2D.MFPur[i,j-1];
      dKul_dPsi[i,j]   := Elem2D.dKur_dPsi[i,j-1];
      WNul[i,j]        := Elem2D.WNur[i,j-1];
      dWNul_dPsi[i,j] := Elem2D.dWNur_dPsi[i,j-1];
    end
    else
    begin
      if SoilFD.Psi2D[i,j] < AEP[i,j] then
      begin
        Kul[i,j]                                                    :=
Ks[i,j]*Power((AEP[i,j]/SoilFD.Psi2D[i,j]),n[i,j]);
        MFPul[i,j]       := Kul[i,j]*SoilFD.Psi2D[i,j]/(1-n[i,j]);
        dKul_dPsi[i,j]   := -n[i,j]*Kul[i,j]/SoilFD.Psi2D[i,j];
        WNul[i,j]                                                   :=
WS[i,j]*Power((SoilFD.Psi2D[i,j]/AEP[i,j]),-1/b[i,j]);
        dWNul_dPsi[i,j] := -WNul[i,j]/(b[i,j]*SoilFD.Psi2D[i,j]);
      end
      else
      begin
        Kul[i,j]         := Ks[i,j];
        MFPul[i,j]                          :=    Ks[i,j]*(AEP[i,j]/(1-
n[i,j])+SoilFD.Psi2D[i,j]-AEP[i,j]);
```

```
        dKul_dPsi[i,j]  := 0;
        WNul[i,j]       := WS[i,j];
        dWNul_dPsi[i,j] := 0;
      end;
    end;    { of if properties are not identical }
  end;   {of with Props[i,j] and with Elem2D^[i,j] }

  with Props2D, Elem2D do
  begin
    if (n[i-1,j-1]   = n[i,j-1])   and (Ks[i-1,j-1] = Ks[i,j-1]) and
       (AEP[i-1,j-1]  =  AEP[i,j-1])  and  (WS[i-1,j-1]  =  WS[i,j-1])
then
    begin
      Klr[i-1,j-1]         := Elem2D.Kur[i,j-1];
      MFPlr[i-1,j-1]       := Elem2D.MFPur[i,j-1];
      WNlr[i-1,j-1]        := Elem2D.WNur[i,j-1];
      dWNlr_dPsi[i-1,j-1] := Elem2D.dWNur_dPsi[i,j-1];
    end
    else
    begin
      if SoilFD.Psi2D[i,j] < AEP[i-1,j-1] then
      begin
        Klr[i-1,j-1]                  :=  Ks[i-1,j-1]*Power((AEP[i-1,j-
1]/SoilFD.Psi2D[i,j]),n[i-1,j-1]);
        MFPlr[i-1,j-1]          := Klr[i-1,j-1]*SoilFD.Psi2D[i,j]/(1-
n[i-1,j-1]);
        WNlr[i-1,j-1]                                    :=    WS[i-1,j-
1]*Power((SoilFD.Psi2D[i,j]/AEP[i-1,j-1]),-1/b[i-1,j-1]);
        dWNlr_dPsi[i-1,j-1]        :=        -WNlr[i-1,j-1]/(b[i-1,j-
1]*SoilFD.Psi2D[i,j]);
      end       { of if then }
      else
      begin
        Klr[i-1,j-1]         := Ks[i-1,j-1];
        MFPlr[i-1,j-1]       := Ks[i-1,j-1]*(AEP[i-1,j-1]/(1-n[i-1,j-
1])+SoilFD.Psi2D[i,j]-AEP[i-1,j-1]);
        WNlr[i-1,j-1]        := WS[i-1,j-1];
        dWNlr_dPsi[i-1,j-1] := 0;
      end;  { of else }
    end;   { of if properties not identical }
  end;   {of with Props[i-1,j-1] and with Elem2D^[i-1,j-1] }

  with Props2D,Elem2D do
  begin
    if (n[i-1,j]  = n[i-1,j-1])   and (Ks[i-1,j] = Ks[i-1,j-1]) and
       (AEP[i-1,j]= AEP[i-1,j-1]) and (WS[i-1,j] = WS[i-1,j-1]) then
    begin
      Kll[i-1,j]         := Elem2D.Klr[i-1,j-1];
      MFPll[i-1,j]       := Elem2D.MFPlr[i-1,j-1];
      WNll[i-1,j]        := Elem2D.WNlr[i-1,j-1];
      dWNll_dPsi[i-1,j] := Elem2D.dWNlr_dPsi[i-1,j-1];
    end
    else
    begin
      if SoilFD.Psi2D[i,j]<AEP[i-1,j] then
      begin
```

```
        Kl1[i-1,j]                          :=   Ks[i-1,j]*Power((AEP[i-
1,j]/SoilFD.Psi2D[i,j]),n[i-1,j]);
        MFPl1[i-1,j]          := Kl1[i-1,j]*SoilFD.Psi2D[i,j]/(1-n[i-
1,j]);
        WNl1[i-1,j]                                              :=     WS[i-
1,j]*Power((SoilFD.Psi2D[i,j]/AEP[i-1,j]),-1/b[i-1,j]);
        dWNl1_dPsi[i-1,j]             :=            -WNl1[i-1,j]/(b[i-
1,j]*SoilFD.Psi2D[i,j]);
      end
      else
      begin
        Kl1[i-1,j]         := Ks[i-1,j];
        MFPl1[i-1,j]                :=  Ks[i-1,j]*(AEP[i-1,j]/(1-n[i-
1,j])+SoilFD.Psi2D[i,j]-AEP[i-1,j]);
        WNl1[i-1,j]        := WS[i-1,j];
        dWNl1_dPsi[i-1,j] := 0;
      end;
    end;  { of if properties not identical }
  end;   {of with Props[i-1,j] and Elem2D^[i-1,j] }

  with CV do
  begin
    WNlrA[i,j] := Elem2D.WNlr[i-1,j-1]*Elem2D.Area[i-1,j-1];
    WNlA[i,j] := Elem2D.WNl1[i-1,j]*Elem2D.Area[i-1,j];
    WNurA[i,j] := Elem2D.WNur[i,j-1]*Elem2D.Area[i,j-1];
    WNulA[i,j] := Elem2D.WNul[i,j]*Elem2D.Area[i,j];
    WN[i,j]                                                          :=
(WNlrA[i,j]+WNlA[i,j]+WNurA[i,j]+WNulA[i,j])/ACV[i,j];


    dWNdPsi[i,j] := (Elem2D.dWNlr_dPsi[i-1,j-1]*Elem2D.Area[i-1,j-1]
                    +Elem2D.dWNl1_dPsi[i-1,j]*Elem2D.Area[i-1,j]
                    +Elem2D.dWNur_dPsi[i,j-1]*Elem2D.Area[i,j-1]
                    +Elem2D.dWNul_dPsi[i,j]*Elem2D.Area[i,j]);
    {dWNdPsi term is actually divided by ACV but is omitted here
     as the only place dWNdPsi is used is in the derivative of the
     storage term and a multiplication by ACV occurs in this term
     so it saves computation time to omit it here }
  end;
end; {WaterFunctions }


procedure TSoilFD.Evap2D(i,j: Integer);
var
  HumSoil: Double;
begin
  {PE[j] kg/m2/s from partition PET in Tree2D}
  {i is top otherwise won't enter this procedure}
  {replace RHCanopy with RH Air?}
  HumSoil := Humidity(Psi2D[i,j],Props2D.AEP[i,j]);
  CV.Evap[i,j]       :=       TreeObj.PE[j]/dt*(HumSoil-RHCanopy)/(1-
RHCanopy)*Surface[j];
  CV.dEvap_dPsi[i,j]      :=      TreeObj.PE[j]/dt*HumSoil*MdivRT/(1-
RHCanopy)*Surface[j];
```

```
end;

procedure TSoilFD.Calc2DRootDensAndConductivity;
var
  i,j:       Integer;
  Emax,
  z_rd,Oldz: Double; {yes z_rd is local}
begin
  if (Crop.RD > 0) and (Crop.FItransp > 0) then
  begin
    sumf := 0;
    z_rd := Soil.dz[1] + HALFdz[2];
    i := 2;
    repeat    {transpiration if crop}

      for j := Lft to Rt do
      begin
        if Psi2D[i,j] < 2*CropDM.Psilm.Value then
          CV.froot[i,j] := 0
        else
        begin


          if z_rd <= Crop.Rd then begin
            CV.froot[i,j]          :=          Soil.dz[i]*(2*(Crop.Rd-
z_rd)+Soil.dz[i])/Sqr(Crop.Rd)/Rt*(1-FieldDM.FRootWetZone.Value);
              if (j >= LWetNode) and (j <= RWetNode) then
                CV.froot[i,j]        :=        Soil.dz[i]*(2*(Crop.Rd-
z_rd)+Soil.dz[i])/Sqr(Crop.Rd)/Rt*FieldDM.FRootWetZone.Value;
            end
            else
              if z_rd > Crop.Rd then begin
                CV.froot[i,j]              :=              Sqr((Crop.Rd-
z_rd+Soil.dz[i])/Crop.Rd)/Rt*(1-FieldDM.FRootWetZone.Value);
              if (j >= LWetNode) and (j <= RWetNode) then
                CV.froot[i,j]              :=              Sqr((Crop.Rd-
z_rd+Soil.dz[i])/Crop.Rd)/Rt*(FieldDM.FRootWetZone.Value);
            end;
        end;
        sumf := sumf + CV.froot[i,j];
      end;
      Oldz := z_rd;
      Inc(i);
      if i <= Btm then
        z_rd := z_rd + CVdz[i];
    until (i > Btm) or (Oldz > Crop.Rd);
    nlr := i-1;
    case FieldDM.Model.Value of
      0: Emax := CropDM.MaxTrans.Value;    {Growth}
      1: Emax := FCropDM.FMaxTrans.Value; {FAO}
    end;
    est := PET/Emax;
    if sumf > 0 then
      for i := Surf to Btm do
        for j := Lft to Rt do
        begin
```

```
          CV.froot[i,j]  := CV.froot[i,j]/sumf; {normalize f}
          CV.rootuk[i,j]                                          :=
TreeObj.PotTransp(Crop.FItransp*Emax}*CV.froot[i,j]/(-
0.67*CropDM.Psilm.Value*dt);
        end;
  end {if (Crop.RD > 0) and (Crop.FItransp > 0)}
  else
  for i := Surf to Btm do
    for j := Lft to Rt do
    begin
      CV.froot[i,j]  := 0;
      CV.rootuk[i,j] := 0;
    end;
end;

procedure TSoilFD.WaterUptake2D;
var
  ust2D,
  Psix2D,
  estar2D,
  AvePsi2D,
  AvePstar2D: Double;
  i,j:        Integer;
begin
  if sumf > 0 then    {there are roots}
  begin
    AvePsi2D := 0;
    for i := 2 to nlr do
      for j := Lft to Rt do
        AvePsi2D := AvePsi2D + CV.froot[i,j]*Psi2D[i,j];
    AvePstar2D := AvePsi2D/CropDM.Psilm.Value;
    if AvePstar2D < 1.5 then
      ust2D := 1-0.67*AvePstar2D
    else
      ust2D := 0;
    if est < ust2D then
      estar2D := est
    else
      estar2D := ust2D;
    if estar2D < 0 then
      estar2D := 0;
    Psix2D := CropDM.Psilm.Value*(AvePstar2D+0.67*estar2D);
  end
  else
    Psix2D := 0;

  Soil.ActualTrsp := 0;
  for i := Surf to Btm do {could do this for nlr surely - layers
with roots}
    for j := Lft to Rt do
    begin
      CV.Uptake[i,j]                    :=   -CV.rootuk[i,j]*(Psix2D-
Psi2D[i,j])*ProfileWidth;      {kg/m/s}
      CV.dUptake_dPsi[i,j]                                    :=
CV.rootuk[i,j]*ProfileWidth;//*Surface[j];  {or  Profile  width?  page
116 thesis}
```

```
      Soil.ActualTrsp                                                    :=
Soil.ActualTrsp+CV.Uptake[i,j]/ProfileWidth;///Surface[j]; {kg/m2/s}
    end;
  Soil.ActualTrsp := Soil.ActualTrsp*dt; {mm}
  if Soil.ActualTrsp < 0 then
    Soil.ActualTrsp := 0;
  Soil.TransDOY  :=  Soil.ActualTrsp;    {NB  remember  to  accumulate
during the day for timesteps < 1 day}
end;

procedure TSoilFD.DailyWatBal2D;
var
  i,j:  Integer;
begin
  Soil.EvapDOY := 0;
  for j := Lft to Rt do
    Soil.EvapDOY   :=   Soil.EvapDOY+CV.Evap[Surf,j]/ProfileWidth*dt;
{kg/m2 or mm}
  Soil.DrainDOY := 0;

  for j := Lft to Rt do
  begin
    MassBal2D(Btm,j);
    Soil.DrainDOY := Soil.DrainDOY-(llz + lrz);
  end;
  Soil.DrainDOY := Soil.DrainDOY*dt/ProfileWidth;  {kg/m2 or mm}
end;

end.
```

Appendix C

User-friendly software for calculation and missing data error analysis of FAO 56-standardized Penman-Monteith daily reference crop evaporation

Introduction

Atmospheric evaporative demand driven estimates of crop water requirements are being increasingly used to complement soil water and plant measurements. Many of these methods were reviewed in FAO (Food and Agriculture Organization of the United Nations, Rome, Italy) No. 24, Irrigation and Drainage Bulletin (Doorenbos and Pruitt 1977). During a consultation of experts and researchers held in Rome (Italy) in 1990, the FAO methodologies for crop water requirements were reviewed, and the conceptual framework for their revision and standardization were established (Smith 1992b). In the following years, much work was done worldwide to standardize the procedures (Smith et al. 1996). Different methodologies were tested with data obtained from many locations in the world, and this resulted in the recently published FAO No. 56, Irrigation and Drainage Bulletin (Allen et al. 1998). In this publication, the FAO recommends using the Penman-Monteith equation as reference (*ETo*).

The FAO approach for the calculation of daily *ETo* requires solar radiation (R_s), minimum (T_{min}) and maximum temperature (T_{max}), vapour pressure (*VP*) and wind speed (*U*) data. In the absence of a complete data set, the FAO still advises using the Penman-Monteith equation, but with recommended procedures for estimating missing values (Smith 1992b; Smith et al. 1996; Allen et al. 1998). The objective of this study was to develop user-friendly software for the calculation of daily FAO-56 *ETo*, and for the estimation of errors that can arise if solar radiation, wind and vapour pressure data are not available and have to be estimated.

ETo calculator

A user-friendly computer tool was developed to facilitate the estimation of daily *ETo*, according to the FAO recommendations (Smith 1992b; Smith et al. 1996; Allen et al. 1998). The equations and procedures used in the calculation of *ETo* are given in detail in the Addendum at the end of this Appendix. Context sensitive help files can be accessed from any menu by pressing F1 on the keyboard. The help files include user guidelines and theoretical background. Related topics can be accessed using links and bitmaps with hotspots, in order to facilitate the operational and technical understanding of the software.

A screen printout of the *ETo* calculator is shown in Figure C.1. Essential input data are: date, daily maximum and minimum temperatures, latitude, hemisphere and elevation. In the absence of measured data, solar radiation is calculated with Eq. C.6 (Addendum) as a function of sunshine hours, or estimated with Eq. C.12. The transmissivity coefficients (a_s and b_s) used to calculate R_s from sunshine hours [Eq. C.6] are often locally calibrated. These can be entered in the appropriate blocks. The user can also enter an adjustment coefficient for interior or coastal locations (k_{Rs}) when using Eq. C.12 to estimate R_s. Wind speed can be estimated using the guidelines given in the Addendum (Allen et al. 1998). Vapour pressure can be calculated with Eqs. C.22, C.23 or C.24, or by assuming that the daily minimum temperature is equal to dew point temperature and using Eq. C.22. Allen et al. (1998) recommend using a dew point temperature of T_{min} - 2 for arid and semi-arid climates. A dew

point offset to T_{min} in °C can be entered in the appropriate block for the estimation of vapour pressure from daily T_{min}. Daily *ETo* is calculated by clicking on the "Calc" button (Figure C.1).

The *ETo* calculator makes use of a Paradox database and is written in Delphi 5 (Inprise Corp.). Weather input data can be seen in grid format in Figure C.2. The top window includes information on the weather station, whilst the bottom grid contains the daily weather data. Daily weather data can be imported from comma, tab or space delimited files by clicking an icon in the menu bar. The column order of the data in the import file and the units can be specified by the user, as can realistic ranges for these data for error checking purposes.

Daily *ETo* values calculated using full data sets and *ETo* with estimated R_s, *U* and *VP* can be seen in grid format (Figure C.3). A default value for wind speed can be entered in the bottom part of the screen. The *ETo* calculator uses this value when it calculates *ETo* with estimated *U*. The default values for dew point offset to T_{min} in °C, as well as for the coefficients a_s, b_s and k_{Rs} can also be entered in the bottom part of the screen. Averages of daily *ETo* can also be calculated for a time interval specified by the user in order to estimate errors over a typical irrigation cycle. These are stored and displayed in a separate grid. Daily weather data, daily *ETo* and averages of daily *ETo* can be written to comma delimited files by clicking an icon in the menu bar.

The correctness of this *ETo* calculator was tested against the REF-ET program developed at the University of Idaho and available on the web (http://www.kimberly.uidaho.edu/ref-et/). The REF-ET software contains more than 15 reference evaporation methods and is intended to perform standardized calculations of *ETo*. The main purpose of the *ETo* calculator developed in this study is to calculate FAO-56 Penman-Monteith *ETo* under various levels of data availability. The two software packages, therefore, complement each other.

The *ETo* calculator is a Windows based program with a user-friendly interface. The Figures presented in the next section of this study are examples of printable output graphs. The *ETo* calculator is available for use with Windows 95 on an IBM-PC or compatible computer. The program is supplied in executable code on CD. Copies of the program are available through John G. Annandale, Dept. Plant Production and Soil Science, Univ. of Pretoria, 0001 Pretoria, South Africa (e-mail address: jannanda@postino.up.ac.za).

Error estimation if weather parameters are not available

The *ETo* calculator displays graphically and processes statistically daily *ETo* values calculated from full and incomplete data sets. This should facilitate the estimation of the error made when some weather input parameters are not available. This will indicate how important it is to measure all the parameters affecting evaporation, and under which conditions the FAO procedures for estimating missing data give acceptable accuracy. For this study, full weather data sets were collected from three weather stations, representing very different climatic regions in South Africa:

Nietvoorbij (District: Stellenbosch, South Africa; Latitude 33°54'S; Longitude 18°52'E; Altitude 146 m) from August 1995 to May 1999;

Ukulinga Research Station (District: Pietermaritzburg, South Africa; Latitude 29°40'S; Longitude 30°24'E; Altitude 775 m) from August 1995 to November 1998; and

Kromhout Boerdery (District: Kakamas, South Africa; Latitude 28°46'S; Longitude 20°37'E; Altitude 850 m) from June 1996 to July 1999.

Stellenbosch is located in the winter rainfall region (Mediterranean climate) with an average annual rainfall of ~ 800 mm. The climate of Pietermaritzburg is subtropical (hot, humid, summer rainfall region) with an average annual rainfall of ~ 850 mm. Kakamas is in a dry, hot, summer rainfall climate region (average annual rainfall is ~ 150 mm). Daily *ETo* values were calculated for these locations from full weather data sets, and from the same sets but with estimated R_s, *U* and *VP*. All weather data sets included daily maximum (RH_{max}) and

minimum relative humidity (RH_{min}). The default values of U were calculated as the average daily wind speed for the periods considered. These were 2.72 m s^{-1} for Stellenbosch, 2.04 m s^{-1} for Pietermaritzburg and 1.68 m s^{-1} for Kakamas (areas of light to moderate wind) (Allen et al. 1998). The adjustment coefficients k_{Rs} were 0.16, which is the value recommended for interior locations (Addendum). Typical seasonal trends of *ETo* calculated with full weather data sets are shown in Figure C.4 for the three locations. Missing *ETo* values on the graphs in Figure C.4 indicate that no weather data were available for some days. The average ratios between the radiation term, including net radiation (Rn), and the aerodynamic term, including vapour pressure deficit (VPD) [Eq. (1)], were calculated in order to generalize the climatic conditions for the three sites. For the periods considered, these ratios were 54/46 for Stellenbosch, 68/32 for Pietermaritzburg and 64/36 for Kakamas.

Figure C.5 presents the correlation between daily *ETo* calculated using a full data set and *ETo* with estimated R_s [Eq. C.12] for Stellenbosch. In the top right corner of the graph, the parameters of the statistical analysis are shown. These are number of observations (N), coefficient of determination (r^2), as well as the slope and the constant of the linear regression between daily *ETo* calculated with a full data set and *ETo* with estimated R_s. Table C.1 summarizes the statistical analysis between daily *ETo* calculated using full data sets and *ETo* obtained with estimated R_s [Eq. C.12], U (2.72, 2.04 or 1.68 m s^{-1}) and *VP* (assuming T_{min} reaches dew point) for the three locations. It is evident that the scatter of data points increases (lower r^2) by increasing the number of estimated weather parameters in the calculation of *ETo*. This underlines the importance of measuring all factors involved in the prediction of crop water use. The inconsistencies in the data where *VP* is estimated is not to be entirely attributed to the assumption that T_{min} reaches dew point, as *ETo* calculated with full data sets includes errors in the measurement of relative humidity as well as errors in the prediction of *VP* from RH_{max} and RH_{min}. The slope and constant of such linear regressions could be used to correct the *ETo* predictions when some weather data are not available in a particular climatic region.

Figure C.6 presents the difference between daily *ETo* calculated with estimated R_s and *ETo* calculated with a full data set for Stellenbosch. In the top right corner, the root mean square error (RMSE) and the mean absolute error (MAE) are shown. The errors are summarized in Table C.1 for all cases of estimated weather parameters and locations. The error generally increased by increasing the number of estimated weather parameters. It is interesting to note that the error arising from estimating *U* and *VP* at Pietermaritzburg, was smaller than the error caused by estimating only R_s. The error analysis could be helpful in determining which measurements are indispensable, and those that can be omitted in a particular climatic region and still get a reasonable estimate of *ETo*. The criteria for maximum permissible RMSE and MAE are subjective and depend on the particular application.

The error analysis indicated that, at Stellenbosch, the error from estimating R_s with Eq. C.12 is relatively low especially in winter, but could increase considerably during the dry summer months due to occasional cloudiness. This coincides with the period when high radiation levels occur (Figure C.7). The measurements of *U* and *VP* at this location appear to be quite important and should not be omitted if one is to obtain accurate predictions of *ETo*. At Pietermaritzburg, a very small error in the prediction of *ETo* arises by assuming an average wind speed of 2.04 m s^{-1}. The comparison between measured and estimated *U* is shown in Figure C.8. The measurement of wind speed could be omitted at this location, but R_s and *VP* should definitely be measured. At Kakamas, large errors may arise when estimating any of the weather parameters. It is therefore recommended to record the full set of measurements in order to accurately predict *ETo* at this location. It was interesting to note that *ETo* obtained with estimated *VP* tended to be lower than *ETo* obtained from a full set of weather data. This occurred because estimated *VP* was generally higher than measured *VP* (Figure C.9). As a result, the vapour pressure deficit calculated with Eq. C.21 was smaller causing lower predicted *ETo* [Eq. C.1]. It is therefore clear that minimum air temperature rarely drops to dew point in the dry and arid region of Kakamas, and this assumption for the estimation of

VP does not hold. The dew point temperature can be reduced below minimum air temperature by using the dew point offset option of the *ETo* calculator.

A sensitivity analysis was carried out using averages of daily *ETo* to determine if errors from estimating R_s, *U* and *VP* are reduced when the time period considered is extended. The statistical analyses between average daily *ETo* calculated using a full data set and average daily *ETo* with estimated R_s, *U* and *VP* are presented in Table C.1 for a typical irrigation interval of 5 days. A reduction in scatter of data points and higher r^2 values were generally observed when using 5-day averages of *ETo* compared to daily *ETo*. The calculated RMSE and MAE were smaller using 5-day averages of *ETo* compared to daily *ETo*. This indicates that over- and under-estimates of daily *ETo* compensate each other somewhat over longer time periods. The practical implication is an improved accuracy in the prediction of crop water requirements based on the estimation of some weather parameters required to calculate *ETo*.

Another sensitivity analysis was carried out to compare errors implicit in weather measurements to errors induced by predicting these weather parameters. For this purpose, *ETo* values were calculated by assuming the following errors (± 2 standard deviation at 95% confidence interval): ± 1.5 °C for T_{max} and T_{min}, ± 8% of measured RH_{max} and RH_{min}, ± 5% for R_s and ± 10% for *U*. These values represent typical error bands due to biases internal to electronic sensors, as well as impacts of the environment, shield and data logger. The worst case RMSE and MAE encountered in the estimate of *ETo* due to measurement errors are presented in Table C.2. The error in calculated *ETo* due to estimation of missing data (Table C.1) was generally in the range of possible errors that could be resident in the weather measurements (Table C.2).

Conclusions and recommendations

User-friendly software, the *ETo* calculator, has been developed for the calculation of daily *ETo*, and for the estimation of errors that can arise if solar radiation, wind and vapour pressure data are not available. The theoretical background of the *ETo* calculator is based on the recommendations of the FAO (Allen et al. 1998). Several applications of the software are possible, with the user-friendly interface facilitating the handling of weather databases. The *ETo* calculator can be used to determine correction factors for particular climatic regions when weather data are not available. It can be used, for example, to determine the long-term average value of wind speed that minimises errors in the estimation of evaporation. It can also be used to check what weather measurements can be omitted without experiencing large errors in the estimation of *ETo* at a particular site. As more weather stations are installed in a region as part of a station densification effort, the procedure demonstrated in this work can indicate whether these new stations can contain a reduced set of sensors. This would reduce costs for the new stations and may allow the installation of even more stations. The omitted measurements could be estimated as they have been in this paper, or they could be borrowed from a nearby or regional, fully instrumented station, after testing, to remove any biases due to the transfer in space. In addition, for stations having a full set of sensors, the error analyses point out those measurements that are critical for accurate *ETo* estimates. Therefore, in future measurements, if a particular sensor is shown to be, or is suspected to be faulty, the user will know whether the measurements from this sensor can be dropped from the *ETo* computation process and estimated instead. If the measurements have been shown to be critical to the accuracy of the *ETo* estimate, some means should be applied to retain and correct the faulty data.

In the examples shown in this study, the error analyses carried out with the *ETo* calculator indicated that the measurement of R_s could be omitted at Stellenbosch (Mediterranean climate) during winter without large errors arising in the prediction of *ETo*. In the humid climate of Pietermaritzburg, the measurement of *U* can be omitted and an average of 2.04 m s^{-1} can be assumed. In the arid climate of Kakamas, all weather parameters should be

measured in order to determine *ETo* accurately. The error in predicting *ETo* using estimated R_s, *U* and *VP* is reduced by using 5-day averages of *ETo* rather than daily values. This is advantageous for practical applications in irrigation scheduling. The error in the calculated *ETo* due to prediction of missing weather data was generally in the range of the error induced by assuming a 95% confidence interval in the measurements of T_{max} and T_{min}, RH_{max} and RH_{min}, as well as R_s and *U*. Therefore, although an error is encountered by estimating weather parameters, this is somewhat compensated for by the absence of error that would have been resident in the measurements.

Acknowledgements

The authors thank Karl Monnik and Gert de Nysschen (Agricultural Research Council - Institute of Soil, Climate and Water, Pretoria, South Africa) for making weather data available.

Addendum

Procedure for the calculation of FAO Penman-Monteith grass reference evaporation

The *ETo* calculator computes daily *ETo* in mm d^{-1} according to the following equation (Allen et al. 1998):

$$ETo = [0.408\Delta (R_n - G) + \gamma 900 / (T_{avg} + 273) U_2 VPD] / [\Delta + \gamma (1 + 0.34 U_2)] \quad (C.1)$$

where Δ = slope of the saturation vapour pressure curve (kPa $°C^{-1}$), R_n = net radiation (MJ m^{-2} d^{-1}), G = soil heat flux (MJ m^{-2} d^{-1}), γ = psychrometer constant (kPa $°C^{-1}$), T_{avg} = daily average air temperature (°C), U_2 = daily average wind speed measured at 2 m height (m s^{-1}), VPD = vapour pressure deficit (kPa). The slope of the saturation vapour pressure curve is calculated as follows:

$$\Delta = 4098 \times 0.6108 \exp[17.27 T_{avg} / (T_{avg} + 237.3)] / (T_{avg} + 237.3)^2 \quad (C.2)$$

Daily average air temperature is assumed to be:

$$T_{avg} = (T_{max} + T_{min}) / 2 \quad (C.3)$$

where daily maximum (T_{max}) and minimum temperature (T_{min}) in °C are essential input values.

Net radiation is calculated as follows:

$$R_n = R_{ns} - R_{nl} \quad (C.4)$$

where R_{ns} = net incoming solar short-wave radiation (MJ m^{-2} d^{-1}), R_{nl} = net outgoing terrestrial long-wave radiation (MJ m^{-2} d^{-1}). Assuming the albedo of the reference crop (grass) is 0.23, R_{ns} is:

$$R_{ns} = (1-0.23) R_s \quad (C.5)$$

where R_s = solar radiation (MJ m^{-2} d^{-1}). Solar radiation is an input value. In the absence of measured data, the *ETo* calculator computes R_s as a function of relative sunshine duration (n/N), and if that is not available, from T_{max} and T_{min}. Solar radiation can be calculated with the Ångstrom formula, which relates R_s to extraterrestrial radiation and relative sunshine duration:

$$R_s = (a_s + b_s n / N) R_a \quad (C.6)$$

where a_s = regression constant, expressing the fraction of extraterrestrial radiation reaching the earth on overcast days (n = 0), $a_s + b_s$ = fraction of extraterrestrial radiation reaching the earth on clear days (n = N), n = actual duration of sunshine (h), N = maximum possible duration of sunshine or daylight hours (h), R_a = potential (extraterrestrial) solar radiation (MJ m^{-2} d^{-1}). In the absence of locally calibrated values, the *ETo* calculator assumes a_s = 0.25 and b_s = 0.50. The actual duration of sunshine is an input. The daylight hours are calculated as follows:

$$N = \omega_s \, 24 / \pi \qquad (C.7)$$

where ω_s = sunset hour angle (rad). Sunset hour angle is calculated as follows:

$$\omega_s = arccos[-tan(Lat) \, tan(Dec)] \qquad (C.8)$$

where *Lat* = latitude (rad), *Dec* = solar declination (rad). Latitude is an input value in degrees. The *ETo* calculator converts *Lat* from degrees into radians. The sign of *Lat* in Eq. (8) is positive for the northern and negative for the southern hemisphere. The value entered in the *ETo* calculator is, however, always positive and the user needs to specify the hemisphere. The sign of *Lat* is converted by the program into negative if southern hemisphere is specified. Solar declination is calculated as follows (Duffie and Beckman 1980):

$$Dec = 0.409 \, sin(2 \, B / 365 \, DOY - 1.39) \qquad (C.9)$$

Day of year (*DOY*) is calculated from date which is an input parameter. Potential (extraterrestrial) solar radiation is calculated as follows:

$$R_a = 118.08 \, D_{rel} / \pi \, [\omega_s \, sin(Lat) \, sin(Dec) + sin(\omega_s) \, cos(Lat) \, cos(Dec)] \qquad (C.10)$$

where D_{rel} = inverse relative distance between earth and sun. The factor "118.08" represents the solar constant in MJ m^{-2} d^{-1}. The inverse relative distance of the earth from the sun is calculated as follows:

$$D_{rel} = 1 + 0.033 \, cos(2 \, \pi \, DOY / 365) \qquad (C.11)$$

If the actual duration of sunshine is not available, the *ETo* calculator estimates R_s as follows:

$$R_s = k_{Rs} \, (1 + 2.7x10^{-5} \, Alt) \, (T_{max} - T_{min})^{0.5} \, R_a \qquad (C.12)$$

where k_{Rs} = adjustment coefficient for interior or coastal regions, *Alt* = Altitude (m). The adjustment coefficient k_{Rs} is 0.16 for interior locations, where land mass dominates and air masses are not strongly influenced by a large water body. It is 0.19 for coastal locations, situated on or adjacent to the coast of a large land mass and where air masses are influenced by a nearby water body. Altitude is an input parameter linked to a particular weather station. The "$2.7x10^{-5}$" coefficient is equal to "$2x10^{-5}$" taken from Eq. (15) divided by 0.75. The coefficient is a modification to the recommendation in FAO-56 (Allen et al. 1998) for predicting R_s and is added to account for effects of reduced atmospheric thickness on R_s. A need for an elevation correction was indicated by Allen (1997) for nine U.S. locations. The minimum required input data to calculate R_s are therefore T_{max}, T_{min}, *Alt*, *DOY(date)* and *Lat*.

Kelvin air temperatures are used to calculate net outgoing terrestrial radiation:

$$R_{nl} = f_c \, \prod \Phi \, (T_{max}^4 + T_{min}^4) / 2 \qquad (C.13)$$

where f_c = cloudiness factor, $\prod$ = clear sky net emissivity of the earth's atmosphere, Φ = Stefan-Boltzmann constant ($4.9x10^{-9}$ MJ m^{-2} K^{-4}). The cloudiness factor is calculated as follows:

$$f_c = 1.35 \, R_s / R_{so} - 0.35 \qquad (C.14)$$

with R_{so} = short-wave radiation during bright sunshine (MJ m^{-2} d^{-1}).

$$R_{so} = (0.75 + 2x10^{-5} Alt)\ R_a \qquad (C.15)$$

The constant "0.75" represents the maximum clear sky transmissivity of the atmosphere. Clear sky net emissivity of the earth's atmosphere is calculated as follows:

$$[] = 0.34 - 0.14\ VP^{0.5} \qquad (C.16)$$

where VP = actual vapour pressure (kPa). Actual vapour pressure is an input parameter, or it can be calculated as a function of dew point temperature [Eq. C.22], minimum and maximum relative humidity [Eq. C.23], or dry and wet bulb temperature [Eq. C.24].

As the magnitude of daily soil heat flux beneath the grass reference surface is relatively small, G is assumed to be 0.

The psychrometric constant is calculated as follows:

$$\gamma = 0.00163\ P_a / \lambda \qquad (C.17)$$

where P_a = atmospheric pressure (kPa), λ = latent heat of vaporization (MJ kg^{-1}). Atmospheric pressure is calculated from altitude (Burman et al. 1987), as follows:

$$P_a = P_0\ [(T_0 - \alpha\ Alt) / T_0]^{g / (\alpha\ Rg)} \qquad (C.18)$$

where P_0 = standard atmospheric pressure at sea level (101.3 kPa), T_0 = standard temperature at sea level (293 K), α = adiabatic lapse rate (K m^{-1}), g = gravitational acceleration (9.8 m s^{-2}), Rg = specific gas constant for dry air (286.9 J kg^{-1} K^{-1}). The adiabatic lapse rate is assumed to be 0.0065 K m^{-1} for saturated air. The latent heat of vaporization can be calculated as follows (Harrison 1963):

$$\lambda = 2.501 - 2.361x10^{-3}\ T_{avg} \qquad (C.19)$$

Wind speed (normally daily average over 24 h) measured at 2 m is an input value. If U_2 is not measured, this can be assumed to be $\leq$ 1 m s^{-1} (light wind), 1-3 m s^{-1} (light to moderate), 3-5 m s^{-1} (moderate to strong) or $\geq$ 5 m s^{-1} (strong) according to the guidelines given by Allen et al. (1998). If wind speed (U) is not measured at 2 m height, the logarithmic wind speed profile function is applied to calculate U_2 (Allen et al. 1989), as follows:

$$U_2 = U\ 4.87 / ln(67.8\ H_U - 5.42) \qquad (C.20)$$

where H_U = height at which wind speed is measured (m). The height at which wind speed is measured, is an input value. If this value is not entered in the *ETo* calculator, a default height of 2 m is assumed.

Vapour pressure deficit is calculated adopting the following equation:

$$VPD = [e_s(T_{max}) + e_s(T_{min})] / 2 - VP \qquad (C.21)$$

where e_s = saturated vapour pressure (kPa). Saturated vapour pressure is estimated from air temperature (T), as follows (Tetens 1930):

$$e_s = 0.6108\ exp[17.27\ T / (T + 237.3)] \qquad (C.22)$$

Saturated vapour pressure at T_{max} and T_{min} in Eq. (21) is calculated using T_{max} and T_{min} in Eq. C.22. The actual vapour pressure (VP) is preferably an input variable. If VP is not measured directly, e_s is calculated using dew point temperature in Eq. C.22 and this is then taken as VP in Eq. C.21. If dew point temperature is not available, VP is calculated from measured minimum (RH_{min}) and maximum relative humidity (RH_{max}), and if that is not available, from

measured wet bulb (T_{wet}) and dry bulb temperature (T_{dry}) in °C. Actual vapour pressure can be calculated as a function of percent relative humidity as follows:

$$VP = [e_s(T_{min}) RH_{max} / 100 + e_s(T_{max}) RH_{min} / 100] / 2 \quad (C.23)$$

or from psychrometer readings (Bosen 1958) with

$$VP = e_s(T_{wet}) - 0.0008 (T_{dry} - T_{wet}) P_a \quad (C.24)$$

Saturated vapour pressure at T_{wet} is calculated using T_{wet} in Eq. C.22. If no atmospheric vapour measurements are available, the *ETo* calculator assumes T_{min} reaches dew point, and VP is equal to e_s at T_{min} [Eq. C.22]. Allen et al. (1998) recommended correction procedures for cases when T_{min} is not equal to dew point temperature. The *ETo* calculator includes an option where T_{min} can be reduced in Eq. C.22 by a user-specified value in °C.

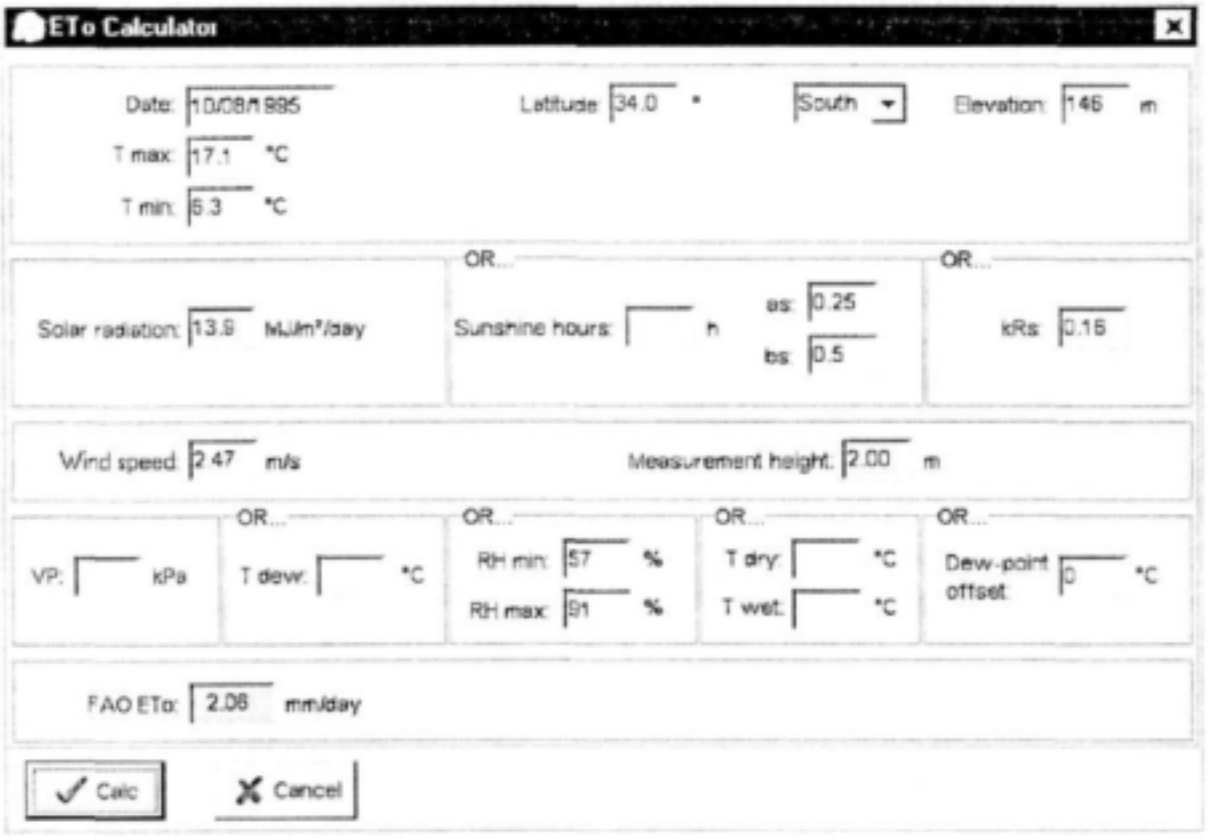

Figure C.1. Screen printout of the FAO Penman-Monteith grass reference evapotranspiration (ETo) calculator. T_{max} and T_{min} are daily maximum and minimum temperatures, a_s and b_s are transmissivity coefficients used to calculate solar radiation (R_s) from sunshine hours [Eq. C.6, Addendum], k_{Rs} is the adjustment coefficient for the calculation of R_s with Eq. (12), VP is actual vapour pressure, T_{dew} is dew point temperature, RH_{min} and RH_{max} are minimum and maximum relative humidities, T_{dry} and T_{wet} are dry and wet bulb temperatures, and dew point offset is used to estimate vapour pressure from T_{min}.

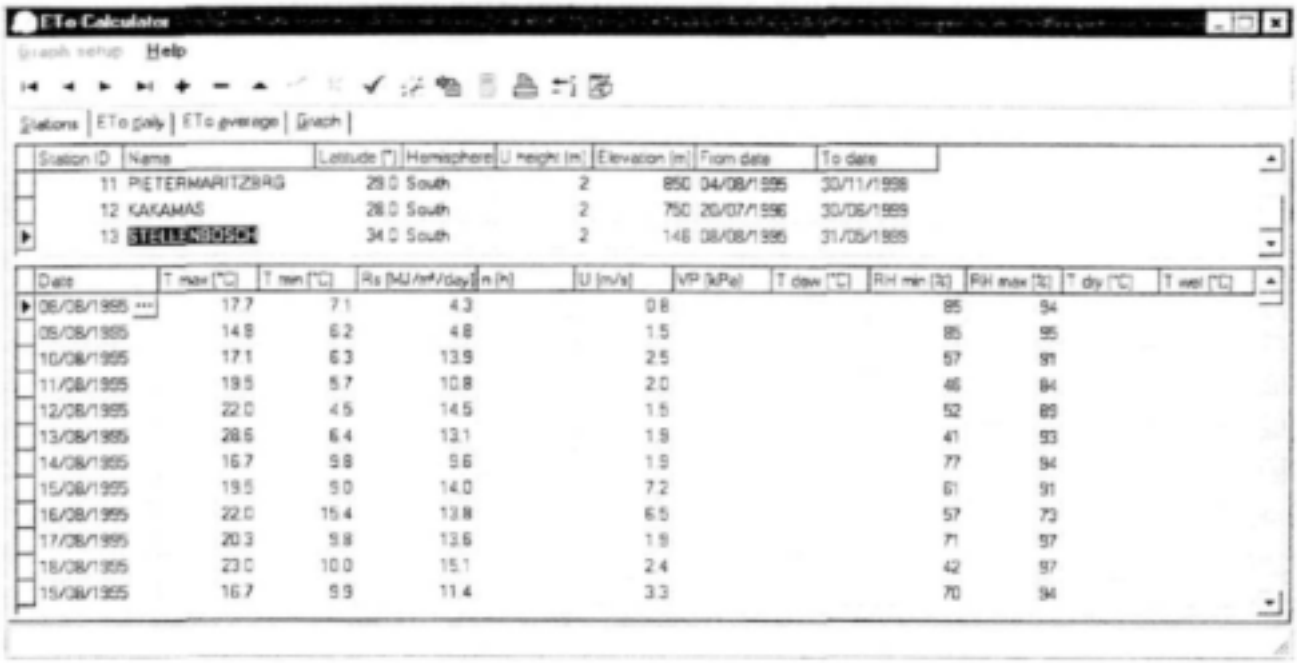

Figure C.2. Screen printout of the weather database. The columns in the top grid are (from left to right): station identification number, name of weather station, latitude, hemisphere, height of measurement of wind speed (m), elevation (m) and range of dates. The columns in the bottom grid are (from left to right): date, maximum and minimum temperature (°C), solar radiation (MJ m^{-2} d^{-1}), sunshine hours (h), wind speed (m s^{-1}), vapour pressure (kPa), dew point temperature (°C), minimum and maximum relative humidity (%), and dry and wet bulb temperature (°C).

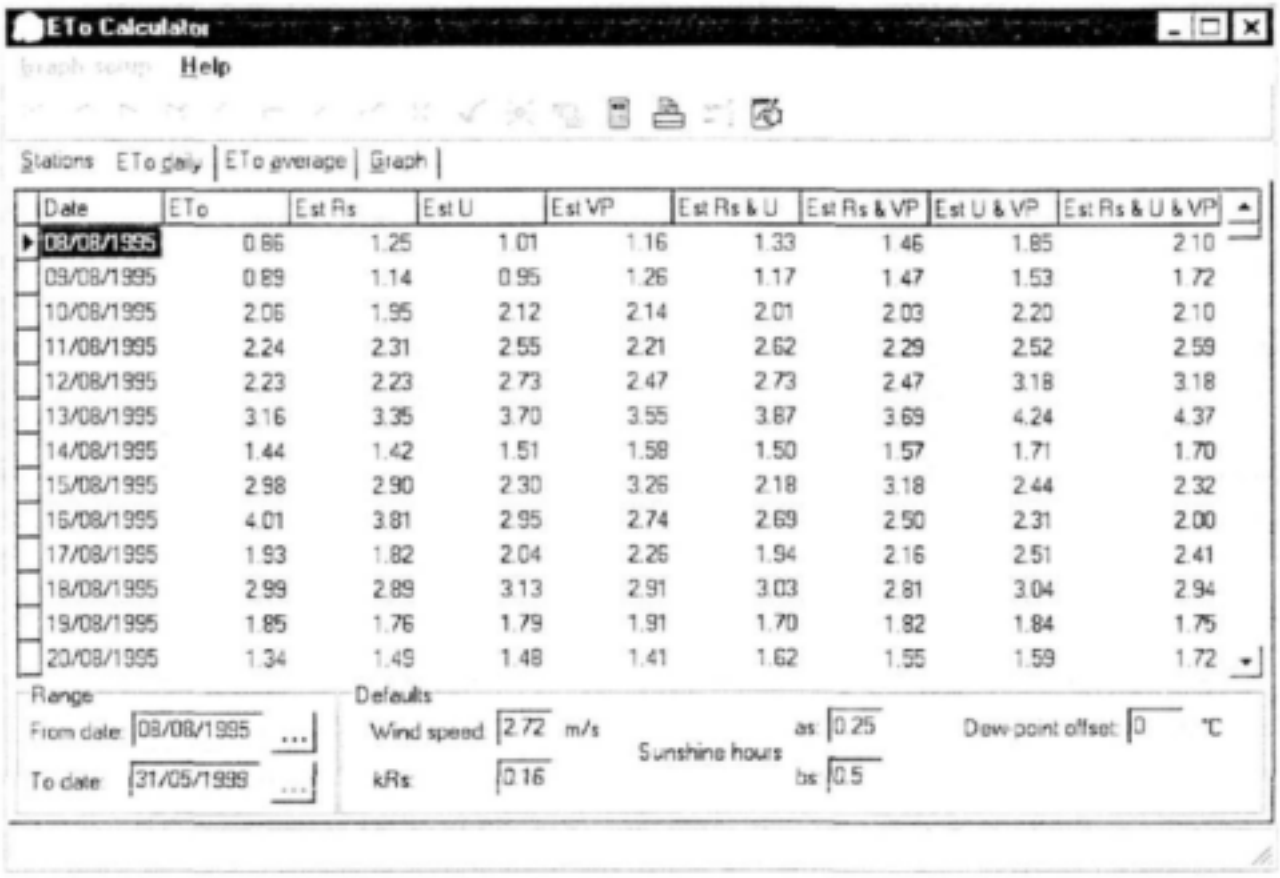

Date	ETo	Est Rs	Est U	Est VP	Est Rs & U	Est Rs & VP	Est U & VP	Est Rs & U & VP
08/08/1995	0.86	1.25	1.01	1.16	1.33	1.46	1.85	2.10
09/08/1995	0.89	1.14	0.95	1.26	1.17	1.47	1.53	1.72
10/08/1995	2.06	1.95	2.12	2.14	2.01	2.03	2.20	2.10
11/08/1995	2.24	2.31	2.55	2.21	2.62	2.29	2.52	2.59
12/08/1995	2.23	2.23	2.73	2.47	2.73	2.47	3.18	3.18
13/08/1995	3.16	3.35	3.70	3.55	3.87	3.69	4.24	4.37
14/08/1995	1.44	1.42	1.51	1.58	1.50	1.57	1.71	1.70
15/08/1995	2.98	2.90	2.30	3.26	2.18	3.18	2.44	2.32
16/08/1995	4.01	3.81	2.95	2.74	2.69	2.50	2.31	2.00
17/08/1995	1.93	1.82	2.04	2.26	1.94	2.16	2.51	2.41
18/08/1995	2.99	2.89	3.13	2.91	3.03	2.81	3.04	2.94
19/08/1995	1.85	1.76	1.79	1.91	1.70	1.82	1.84	1.75
20/08/1995	1.34	1.49	1.48	1.41	1.62	1.55	1.59	1.72

Figure C.3. Screen printout of the reference evapotranspiration (ETo) database. The columns represent (from left to right) daily ETo in mm calculated from a full weather data set, and from the same set with estimated solar radiation (R_s), wind speed (U) and vapour pressure (VP). Range of dates, as well as default values for wind speed, dew point offset used to estimate vapour pressure from minimum temperature, transmissivity coefficients (a_s and b_s) for the calculation of R_s from sunshine hours [Eq. C.6, Addendum] and the adjustment coefficient (k_{Rs}) for the calculation of R_s with Eq. C.12 are entered in the bottom part of the screen.

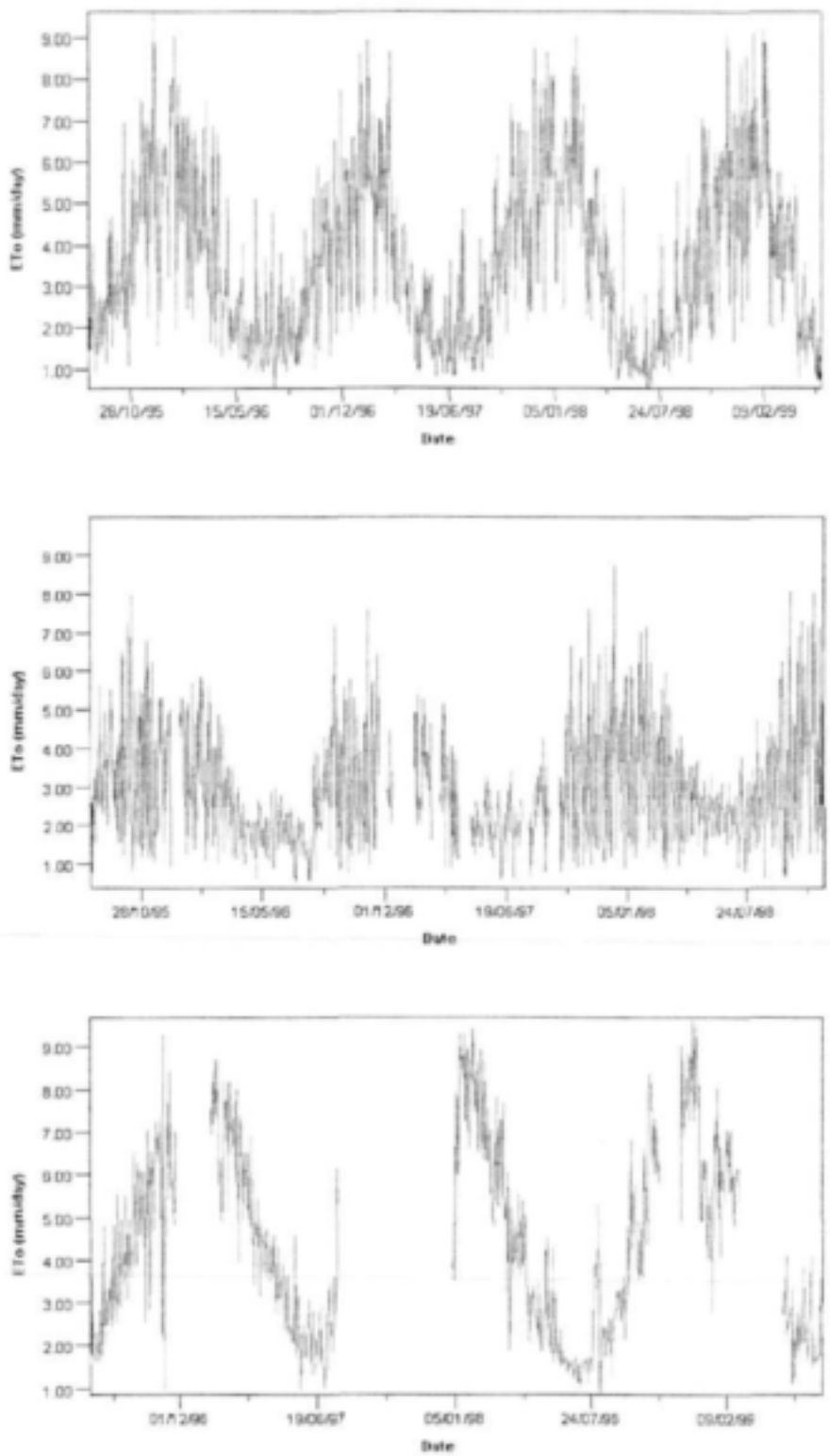

Figure C.4. Seasonal trends of daily ETo calculated with full weather data sets for Stellenbosch (top), Pietermaritzburg (middle) and Kakamas (bottom).

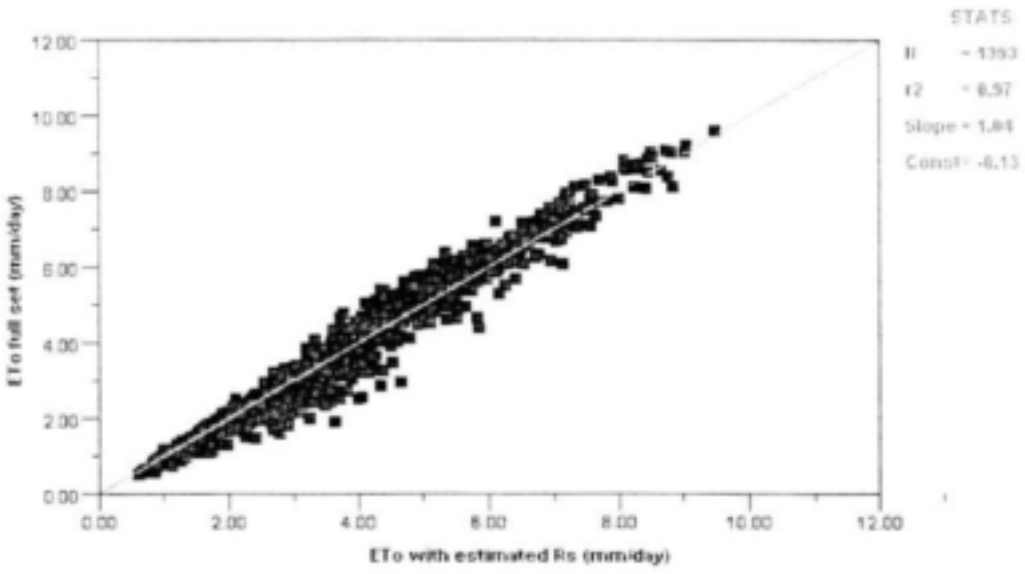

Figure C.5. Correlation between daily ETo calculated from a full weather data set and ETo with estimated solar radiation (R_s) for Stellenbosch (South Africa). The parameters of the statistical analysis are number of observations (N), coefficient of determination (r^2), as well as the slope and the constant of the linear regression.

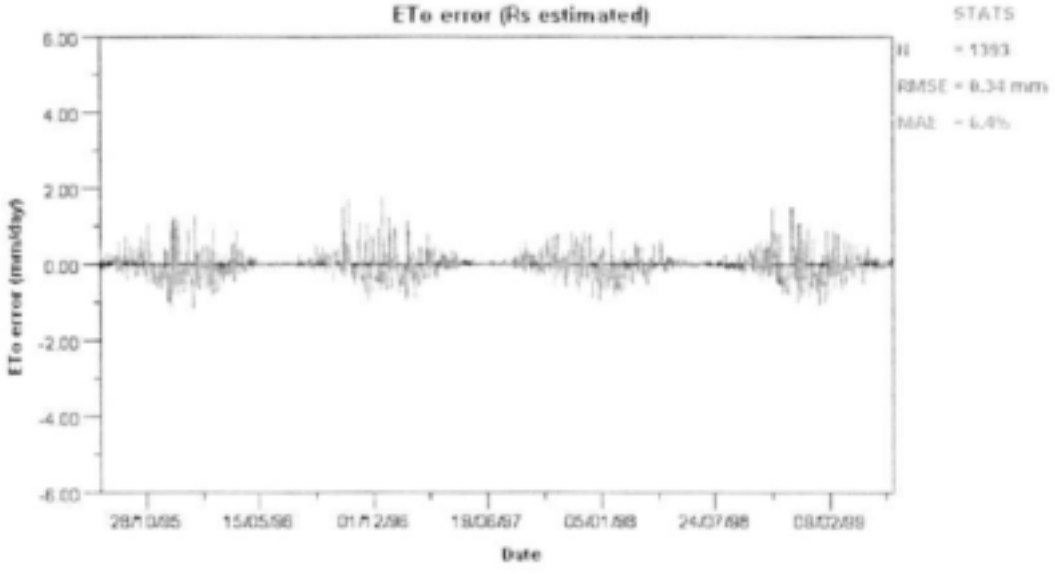

Figure C.6. Difference between daily ETo calculated with estimated solar radiation (R_s) and ETo calculated from a full weather data set for Stellenbosch (South Africa). The parameters of the statistical analysis are root mean square error (RMSE) and mean absolute error (MAE).

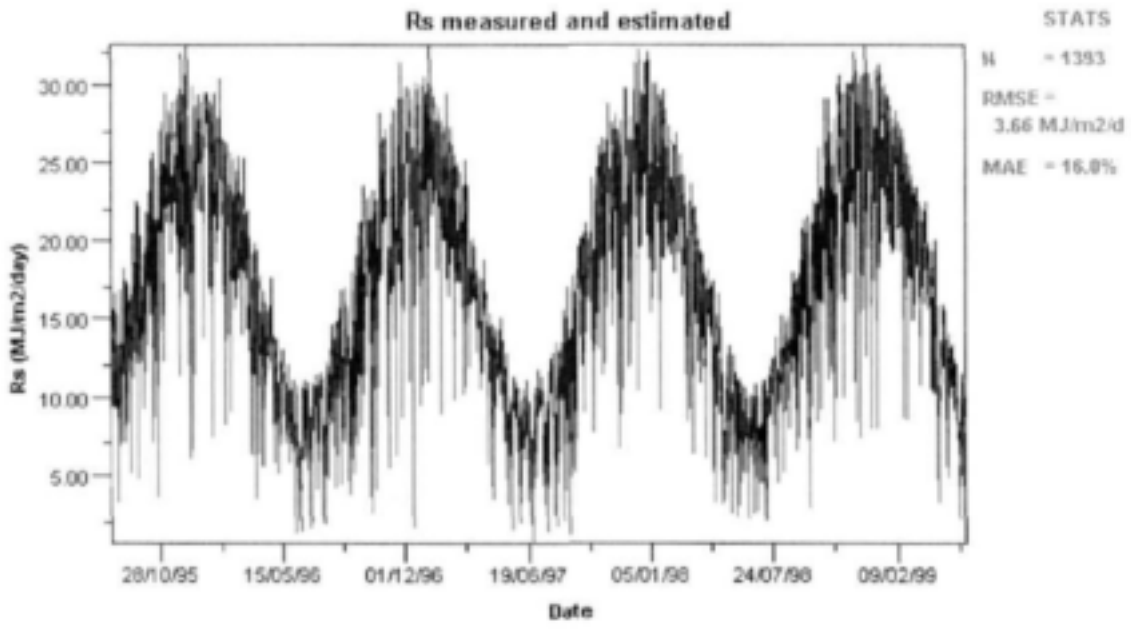

Figure C.7. Measured (bold line) and estimated (thin line) solar radiation (R_s) at Stellenbosch (South Africa).

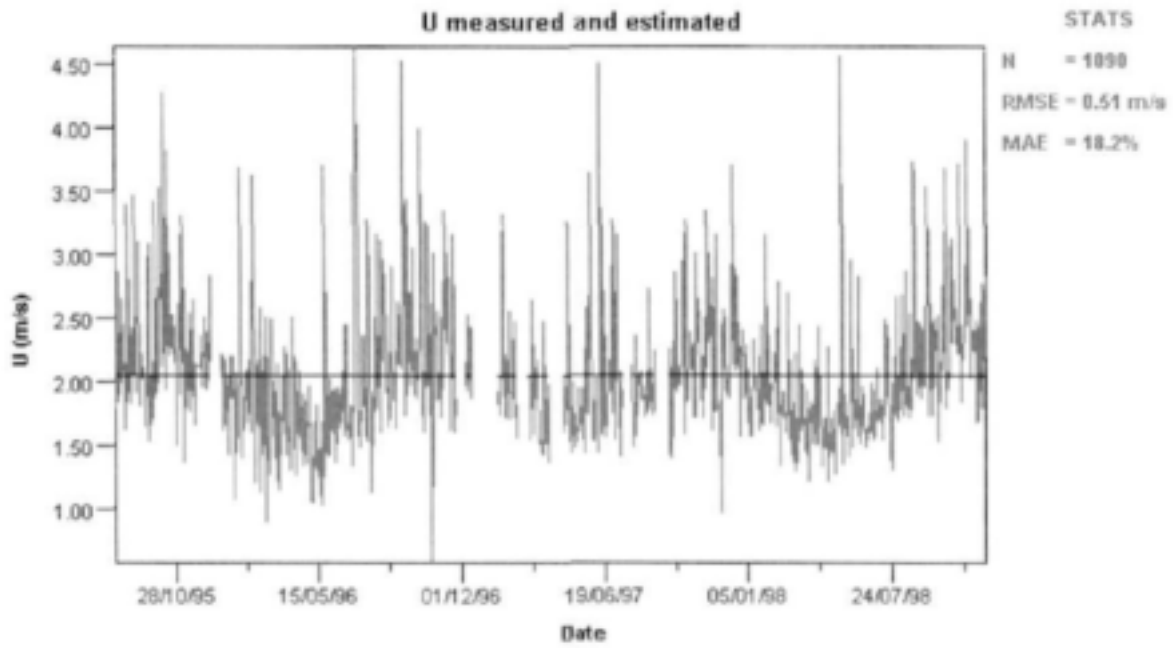

Figure C8. Measured (bold line) and estimated (thin line) wind speed (U) at Pietermaritzburg (South Africa).

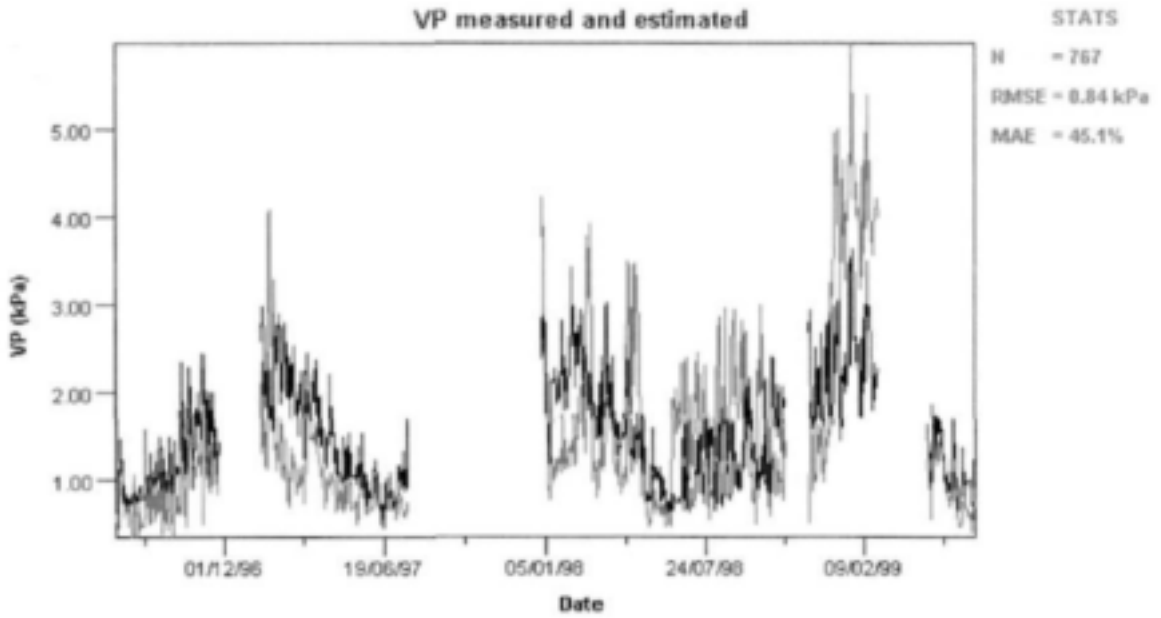

Figure C.9. Measured (bold line) and estimated (thin line) vapour pressure (VP) at Kakamas (South Africa).

Table C.1. Coefficient of determination (r^2), slope and constant of the linear regression, root mean square error (RMSE) and mean absolute error (MAE) of the correlation between daily and 5-days average ETo calculated with estimated solar radiation (R_s), wind speed (U) and vapour pressure (VP), and ETo calculated from a full weather data set for three locations in South Africa.

Location	Statistical parameter	Estimated														Number of observations
		R_s		U		VP		R_s and U		R_s and VP		U and VP		R_s, U and VP		
		Daily	5-days average	Daily	5-days average	Daily	5-days average	Daily	5-days average	Daily	5-days average	Daily	5-days average	Daily	5-days average	
Stellenbosch	r^2	0.97	0.99	0.95	0.98	0.93	0.96	0.89	0.96	0.88	0.94	0.86	0.93	0.78	0.89	1393
	Slope	1.04	1.05	1.06	1.08	1.05	1.06	1.08	1.13	1.08	1.11	1.07	1.13	1.07	1.18	
	Constant	-0.13	-0.14	-0.24	-0.33	-0.09	-0.13	-0.29	-0.48	-0.16	-0.26	-0.26	-0.47	-0.23	-0.61	
	RMSE (mm)	0.34	0.19	0.46	0.30	0.54	0.38	0.67	0.42	0.71	0.48	0.74	0.51	0.93	0.62	
	MAE (%)	6.4	3.5	8.0	5.7	9.1	7.2	13.0	8.5	12.6	8.9	14.3	10.4	18.2	12.5	
Pietermaritzburg	r^2	0.87	0.90	0.98	0.99	0.96	0.94	0.86	0.90	0.81	0.82	0.93	0.92	0.80	0.82	1090
	Slope	0.93	0.82	1.04	1.04	0.96	0.96	0.99	0.86	0.87	0.76	1.00	1.00	0.93	0.80	
	Constant	-0.03	0.32	-0.11	-0.09	-0.08	-0.06	-0.18	0.22	-0.01	0.36	-0.20	-0.18	-0.18	0.23	
	RMSE (mm)	0.59	0.43	0.20	0.12	0.36	0.30	0.58	0.40	0.79	0.64	0.42	0.32	0.78	0.62	
	MAE (%)	13.6	10.2	3.2	2.6	9.2	7.9	13.9	9.8	19.1	16.5	10.8	8.7	19.6	16.5	
Kakamas	r^2	0.96	0.98	0.91	0.97	0.88	0.91	0.86	0.95	0.83	0.88	0.82	0.89	0.76	0.86	767
	Slope	1.01	1.02	1.09	1.10	0.98	0.98	1.09	1.13	0.98	1.00	1.07	1.10	1.06	1.12	
	Constant	0.02	-0.02	-0.45	-0.50	0.11	0.09	-0.42	-0.55	0.19	0.09	-0.36	-0.49	-0.24	-0.51	
	RMSE (mm)	0.46	0.29	0.67	0.43	0.75	0.63	0.83	0.53	0.91	0.71	0.92	0.71	1.08	0.79	
	MAE (%)	6.5	4.2	11.3	7.2	11.9	10.9	14.2	9.2	14.7	12.1	17.3	13.1	19.1	14.1	

Table C.2. Root mean square error (RMSE) and mean absolute error (MAE) of the estimate of ETo calculated including uncertainty in measured weather parameters for three locations in South Africa.

Location	Measurement error	RMSE (mm)	MAE (%)
Stellenbosch	ETo overestimated[a]	0.60	15.39
	ETo underestimated[b]	0.54	13.62
Pietermaritzburg	ETo overestimated	0.48	15.48
	ETo underestimated	0.42	13.60
Kakamas	ETo overestimated	0.54	11.23
	ETo underestimated	0.50	10.38

[a] T_{max} and T_{min} + 1.5°C; RH_{max} and RH_{min} - 8%; R_s + 5%; U + 10%
[b] T_{max} and T_{min} - 1.5°C; RH_{max} and RH_{min} + 8%; R_s - 5%; U - 10%

Appendix D

HDS calculator

Campbell Scientific 229 heat dissipation sensors infer the matric potential (P_m) of soil by equilibrating a porous ceramic with the soil matric potential and then measuring the thermal diffusivity of the matrix. In practice, heat dissipation is determined by applying a heat pulse to a heater within the sensor and monitoring the temperature at the centre of the block before and after heating. The temperature rise (ΔT) is a function of thermal diffusivity, and therefore of the matric potential of the block (Jovanovic and Annandale, 1997).

Two problems were identified with the use of heat dissipation sensors:

i) Calibration varies from sensor to sensor; and
ii) Calibration varies depending on ambient temperature.

Campbell et al. (2001) developed a normalization procedure, which simplifies calibration of individual sensors using the dimensionless temperature rise (T^*):

$$T^* = (\Delta T_d - \Delta T) / (\Delta T_d - \Delta T_w) \qquad (D.1)$$

where

ΔT_d - Temperature rise for oven dry sensor matrix (°C)
ΔT_w - Temperature rise for fully saturated matrix (°C)

An iterative procedure then corrects T^* and P_m for temperature to the value it would have at 20 °C.

The steps involved are:

1) The temperature rise (ΔT) in °C is used to make an initial estimate (T_o^*) of the normalized, dimensionless temperature rise using Eq. D.1:

$$T_o^* = (\Delta T_d - \Delta T) / (\Delta T_d - \Delta T_w)$$

2) T_o^* from step (1) is used in the following empirical equation:

$$s^* = -0.0133\, T_o^{*5} + 0.0559\, T_o^{*4} - 0.0747\, T_o^{*3} + 0.0203\, T_o^{*2} + 0.011\, T_o^* + 0.0013 \qquad (D.2)$$

where s^* is the thermal conductivity response of the sensor.

3) A new estimate of T^* is computed from:

$$T^* = T_o^* - s^* (T - 20) \qquad (D.3)$$

where T is the actual temperature of the medium (°C).

4) A new estimate of s^* is obtained using the new T^* and Eq. D.2:

$$s^* = -0.0133\, T^{*5} + 0.0559\, T^{*4} - 0.0747\, T^{*3} + 0.0203\, T^{*2} + 0.011\, T^* + 0.0013$$

Steps 3 and 4 are repeated until T^* changes less than 10^{-3}.

T^* is converted to soil matric potential using the following calibration equation:

$$P_m = P_o (T^{*n} - 1)^m \qquad (D.4)$$

where P_o = - 56.2 J kg^{-1}, n = 2.22 and m = 1.0. The shape of this calibration equation is similar to the Van Genuchten (1980) water retention function for soil. The mean absolute

deviation of measurements from predictions with Eq. D.4, was found to be 22.8% for data between -10 and -35000 J kg^{-1} (Campbell et al., 2001).

The input data required to determine soil water potential from a particular sensor therefore are:

1) Oven dry (ΔT_d) and vacuum saturated (ΔT_w) readings;
2) Actual temperature of the medium (T); and
3) Temperature rise (ΔT).

The procedure for calibration and temperature correction of heat dissipation sensors was written in a user-friendly programme in Delphi v. 5.0. The programme, called HDS calculator, facilitates the processing of long data series collected in the field. The input screen of the HDS calculator is shown in Figure D.1.

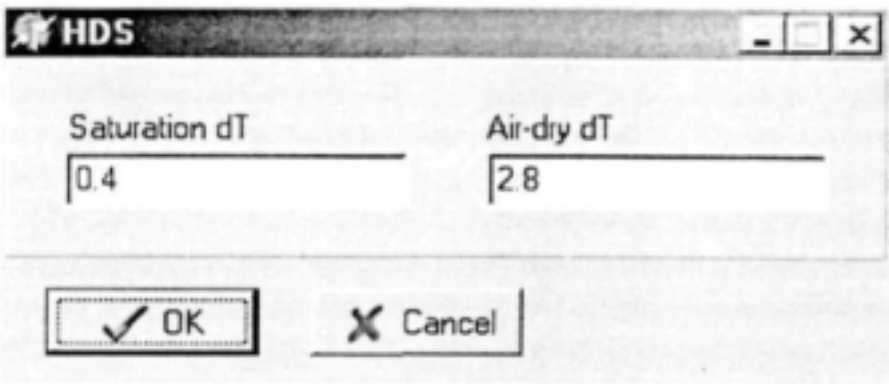

Figure D.1. Input screen of the HDS calculator.

The values of ΔT_w and ΔT_d for the individual sensor are typed in the "Saturation dT" and "Air-dry dT" cells. By clicking on the "OK" button, the HDS calculator prompts the user to select an input ASCII file consisting of two columns, the first with ambient temperatures (T) and the second for matching sensor readings of temperature rise (ΔT). The input ASCII file can be generated in a spreadsheet as a *.txt file. After the user has selected the input file, the program runs the calibration and temperature correction procedure for each pair of T and ΔT values, and generates an output ASCII file in the same folder. The output file includes one column with calculated P_m. It has the same name as the input file, but with the extension *.out.

The HDS calculator is available for use with Windows 95 on an IBM-PC or compatible computer. The program is supplied in executable code on 3.5-inch disks. Copies of the program are available through John G. Annandale, Dept. Plant Production and Soil Science, Univ. of Pretoria, 0001 Pretoria, South Africa (e-mail address: annan@scientia.up.ac.za).

Appendix E

Program for use of heat dissipation sensors with Campbell Scientific CR10 and CR10X data loggers

Program Title: HDS28SE.CSI

This program was drafted to read 28 Heat Dissipation Sensors (HDS) using the single ended (SE) thermocouple (T/c) measurement instruction (Instruction 13). The preference of the SE measurement instruction above the use of the differential (DIFF) approach was because the execution time to complete a cycle of measurements when using the AM416 multiplexer and the Temp DIF command (Instruction 14) was too long. This resulted in inaccuracies in results recorded. It was thus necessary to only excite eight HDS at a time through one CE8 channel and complete the required measurement cycle before proceeding to measure the following group of eight HDS. Coupled to this, it was necessary to include instructions so that the AM416 would skip to the correct channels to record the appropriate thermocouples of the group of 8 HDS that had been activated.

The thermocouple wires for the first group of 8 HDSs were connected directly to the CR10X with the "High line" being connected to the SE 1 to 8 analog input on the CR10X wiring panel while the "low line" was connected to an AG port. The balance of the HDS thermocouples was connected to the AM416 as follows: the "High line" being connected on Set 1 H1 through to Set 10 H2 with the corresponding "Low line" being connected to Set 1 L1 through to Set10 L2. The AM416 was linked to CR10X through the SE analog input 9 and 10. The AM416 was "clocked/pulsed" through port C5 and reset with port C6. The red lead of a thermocouple reference temperature unit (10TCRT) was connected to the analog input SE 12 of the CR10 while the black lead was connected to the data logger excitation channel E3 and the clear lead was connected to an AG terminal.

The four CE8s were separately activated through the control ports C1 to C4.

The output for the program was the reference temperature (RefT) when each series of measurements was taken, the temperature of the soil (SoilT) at the beginning of each series of measurements and the difference in temperature recorded after heating for 1 s and a further 20 s heating period (dT). In the program presented below, the measurements were done every 2 hours.

This specific program was drafted and tested during the period 9/12/99 to 14/12/99. Explanatory text is in italics and follows a semi colon, e.g. ;*This instruction is to set the time interval*

```
*Table 1 Program
  01: 1          Execution Interval (seconds)

1:  If time is (P92)
 1: 0          Minutes (Seconds --) into a
 2: 120        Interval (same units as above)
 3: 11         Set Flag 1 High
;This instruction is to set the time interval to carry out the
measurements ;at 120 minutes as well as giving the option to
manually set flag 1 high to ;initiate the program when required.

2:  If Flag/Port (P91)
 1: 21         Do if Flag 1 is Low
```

```
 2: 0         Go to end of Program Table

3:  AC Half Bridge (P5)
 1: 1         Reps
 2: 22        7.5 mV 60 Hz Rejection Range
 3: 12        SE Channel
 4: 3         Excite all reps w/Exchan 3
 5: 2000      mV Excitation
 6: 3         Loc [ TCRT       ]
 7: 800       Mult
 8: 0         Offset

4:  Polynomial (P55)
 1: 1         Reps
 2: 3         X Loc [ TCRT       ]
 3: 1         F(X) Loc [ RefTemp    ]
 4: -53.46    C0
 5: 90.807    C1
 6: -83.257   C2
 7: 52.283    C3
 8: -16.723   C4
 9: 2.211     C5
; Determine reference Temp & recorded in Loc 1
NOTE: The 10TCRT is designed to be connected to SE1 and using
Instruction 11. If it is connected to any other input channel
Instruction 5 and 55 must be used.

5:  Batt Voltage (P10)
 1: 2         Loc [ Battery    ]
;To record the battery level

;                MEASUREMENTS FOR 1st 8 T/c's
6:  Thermocouple Temp (SE) (P13)
 1: 8         Reps
 2: 22        7.5 mV 60 Hz Rejection Range
 3: 1         SE Channel
 4: 1         Type T (Copper-Constantan)
 5: 1         Ref Temp (Deg. C) Loc [ RefTemp    ]
 6: 5         Loc [ SoilT_1    ]
 7: 1.0       Mult
 8: 0.0       Offset
;Determine Soil Temp of 1st 8 T/c's linked to CR10X; Recorded in
Locs 5 to 12 inclusive

7:  Do (P86)
 1: 41        Set Port 1 High
;Activates 1st CE8 thru' C1

8:  Beginning of Loop (P87)
 1: 0         Delay
 2: 2         Loop Count

9:  Excitation with Delay (P22)
 1: 1         Ex Channel
 2: 0         Delay W/Ex (units = 0.01 sec)
 3: 50        Delay After Ex (units = 0.01 sec)
```

```
 4: 0         mV Excitation

10:  End (P95)
;Create 1 sec period (2 X 50 X 0.01 = 1 sec)
;   i.e. activates CE8 for 1 sec

11:  Thermocouple Temp (SE) (P13)
 1: 8         Reps
 2: 22        7.5 mV 60 Hz Rejection Range
 3: 1         SE Channel
 4: 1         Type T (Copper-Constantan)
 5: 1         Ref Temp (Deg. C) Loc [ RefTemp    ]
 6: 33        Loc [ Sec1_1     ]
 7: 1.0       Mult
 8: 0.0       Offset
;Records Temp of 1st 8 T/c's after 1 sec heating in Locs 33 to 40
inclusive

12:  Beginning of Loop (P87)
 1: 0         Delay
 2: 40        Loop Count

13:  Excitation with Delay (P22)
 1: 1         Ex Channel
 2: 0         Delay W/Ex (units = 0.01 sec)
 3: 50        Delay After Ex (units = 0.01 sec)
 4: 0         mV Excitation

14:  End (P95)
;Creates 20 sec delay; i.e. continue heating for 20 sec

15:  Thermocouple Temp (SE) (P13)
 1: 8         Reps
 2: 22        7.5 mV 60 Hz Rejection Range
 3: 1         SE Channel
 4: 1         Type T (Copper-Constantan)
 5: 1         Ref Temp (Deg. C) Loc [ RefTemp    ]
 6: 61        Loc [ T20s_1     ]
 7: 1.0       Mult
 8: 0.0       Offset
;Determines Temp of 1st T/c's after a total of 21 sec heating;
recorded in Locs 61 to 68 inclusive

16:  Do (P86)
 1: 51        Set Port 1 Low
;Deactivate CE8 No 1
;                COMPLETED MEASUREMENTS FOR 1st 8 T/c's

;                MEASURE SOIL TEMP FOR BALANCE OF T/c's

17:  Do (P86)
 1: 46        Set Port 6 High
;Activate AM416 thru' Control Port 6 (Res - C6)

18:  Beginning of Loop (P87)
 1: 0         Delay
```

```
 2: 10        Loop Count
;10 loops with 2 SE sensors per set: 10 X 2 = 20 (i.e. balance of
T/c's)

19:  Do (P86)
 1: 75        Pulse Port 5
;Pulses AM416 thru" C5 (CLK = C5)

20:  Step Loop Index (P90)
 1: 2         Step
;Necessary not to over-write readings

21:  Thermocouple Temp (SE) (P13)
 1: 2         Reps
 2: 22        7.5 mV 60 Hz Rejection Range
 3: 9         SE Channel
 4: 1         Type T (Copper-Constantan)
 5: 1         Ref Temp (Deg. C) Loc [ RefTemp    ]
 6: 13     -- Loc [ SoilT_9    ]
 7: 1.0       Mult
 8: 0.0       Offset

22:  End (P95)
;Ends measurements of 20 soil Temp measurements (i.e. balance of 28
T/c's)
;Temps recorded in Loc 13 to 32 inclusive.

23:  Do (P86)
 1: 56        Set Port 6 Low
;Resets AM416 to beginning

;                MEASUREMENTS FOR 2nd GROUP OF 8 T/c's

24:  Do (P86)
 1: 42        Set Port 2 High
;Activates 2nd CE8 thru' C2

25:  Beginning of Loop (P87)
 1: 0         Delay
 2: 2         Loop Count

26:  Excitation with Delay (P22)
 1: 1         Ex Channel
 2: 0         Delay W/Ex (units = 0.01 sec)
 3: 50        Delay After Ex (units = 0.01 sec)
 4: 0         mV Excitation

27:  End (P95)
;Create 1 sec period for second set of 8 T/c's linked to CE8 No 2

28:  Do (P86)
 1: 46        Set Port 6 High
;Activates AM416

29:  Beginning of Loop (P87)
 1: 0         Delay
```

```
 2: 4         Loop Count

30:  Do (P86)
 1: 75        Pulse Port 5

31:  Step Loop Index (P90)
 1: 2         Step

32:  Thermocouple Temp (SE) (P13)
 1: 2         Reps
 2: 22        7.5 mV 60 Hz Rejection Range
 3: 9         SE Channel
 4: 1         Type T (Copper-Constantan)
 5: 1         Ref Temp (Deg. C) Loc [ RefTemp    ]
 6: 41     -- Loc [ Sec1_9     ]
 7: 1.0       Mult
 8: 0.0       Offset

33:  End (P95)
;Completes 8 measurements (4 loops X 2 Reps = 8 sensors) of Temp
after 1 sec heating
;Measurements in Locs 41 to 48 inclusive

34:  Do (P86)
 1: 56        Set Port 6 Low
;Resets AM416 back to channel 1

35:  Beginning of Loop (P87)
 1: 0         Delay
 2: 40        Loop Count

36:  Excitation with Delay (P22)
 1: 1         Ex Channel
 2: 0         Delay W/Ex (units = 0.01 sec)
 3: 50        Delay After Ex (units = 0.01 sec)
 4: 0         mV Excitation

37:  End (P95)
;Creates 20s heating period for 2nd CE8; i.e. continue heating for
20 sec

38:  Do (P86)
 1: 46        Set Port 6 High
;Activates AM416

39:  Beginning of Loop (P87)
 1: 0         Delay
 2: 4         Loop Count

40:  Do (P86)
 1: 75        Pulse Port 5

41:  Step Loop Index (P90)
 1: 2         Step

42:  Thermocouple Temp (SE) (P13)
```

```
 1: 2         Reps
 2: 21        2.5 mV 60 Hz Rejection Range
 3: 9         SE Channel
 4: 1         Type T (Copper-Constantan)
 5: 1         Ref Temp (Deg. C) Loc [ RefTemp    ]
 6: 69     -- Loc [ T20s_9     ]
 7: 1.0       Mult
 8: 0.0       Offset

43:  End (P95)
;Measures Temp after 21 sec heating & recorded in Locs 69 to 76
inclusive

44:  Do (P86)
 1: 52        Set Port 2 Low
;Deactivates CE8 No 2
;END OF 2nd GROUP OF 8 T/c's ASSOCIATED WITH 2nd SE8

;                MEASUREMENTS FOR 3rd GROUP OF 8 T/c's

; NNB The AM416 has NOT been reset back to Channel 1 but left to
begin
;         reading at SET 5 where T/c not 17 is connected!

45:  Do (P86)
 1: 43        Set Port 3 High
;Activates 3rd CE8 thru' C3

46:  Beginning of Loop (P87)
 1: 0         Delay
 2: 2         Loop Count

47:  Excitation with Delay (P22)
 1: 1         Ex Channel
 2: 0         Delay W/Ex (units = 0.01 sec)
 3: 50        Delay After Ex (units = 0.01 sec)
 4: 0         mV Excitation

48:  End (P95)
;Create 1 sec period for 3rd CE8

49:  Beginning of Loop (P87)
 1: 0         Delay
 2: 4         Loop Count

50:  Do (P86)
 1: 75        Pulse Port 5

51:  Step Loop Index (P90)
 1: 2         Step

52:  Thermocouple Temp (SE) (P13)
 1: 2         Reps
 2: 22        7.5 mV 60 Hz Rejection Range
 3: 9         SE Channel
 4: 1         Type T (Copper-Constantan)
```

```
 5: 1        Ref Temp (Deg. C) Loc [ RefTemp    ]
 6: 49    -- Loc [ Sec1_17    ]
 7: 1.0      Mult
 8: 0.0      Offset

53:  End (P95)

54:  Do (P86)
 1: 56       Set Port 6 Low
;Resets AM416 to channel 1

55:  Do (P86)
 1: 46       Set Port 6 High
;Activates AM416

56:  Beginning of Loop (P87)
 1: 0        Delay
 2: 4        Loop Count

57:  Do (P86)
 1: 75       Pulse Port 5

58:  Do (P86)
 1: 75       Pulse Port 5

59:  End (P95)
;Steps AM416 thru 8 channels; i.e. to SET 5

60:  Beginning of Loop (P87)
 1: 0        Delay
 2: 40       Loop Count

61:  Excitation with Delay (P22)
 1: 1        Ex Channel
 2: 0        Delay W/Ex (units = 0.01 sec)
 3: 50       Delay After Ex (units = 0.01 sec)
 4: 0        mV Excitation

62:  End (P95)
;Creates 20 sec delay; i.e. continue heating 3rd CE8 for 20 sec

63:  Beginning of Loop (P87)
 1: 0        Delay
 2: 4        Loop Count

64:  Do (P86)
 1: 75       Pulse Port 5

65:  Step Loop Index (P90)
 1: 2        Step

66:  Thermocouple Temp (SE) (P13)
 1: 2        Reps
 2: 22       7.5 mV 60 Hz Rejection Range
 3: 9        SE Channel
 4: 1        Type T (Copper-Constantan)
```

```
 5: 1        Ref Temp (Deg. C) Loc [ RefTemp   ]
 6: 77    -- Loc [ T20s_17   ]
 7: 1.0      Mult
 8: 0.0      Offset

67:  End (P95)
;Ends Temp 21 sec measurements for 3rd SE8
;Temp 21 sec for T/c's 17 to 24 recorded in LOcs 77 to 84 inclusive.

68:  Do (P86)
 1: 56       Set Port 6 Low
;Resets AM416 to channel 1

69:  Do (P86)
 1: 53       Set Port 3 Low
;Deactivates CE8 N0 3
;ENDS MEASUREMENTS FOR 3rd GROUP OF 8 T/c's ASSOCIATED WITH 3rd CE8

;                BEGIN MEASUREMENTS OF LAST 4 T/c's

70:  Do (P86)
 1: 46       Set Port 6 High
;Activates AM416

71:  Beginning of Loop (P87)
 1: 0        Delay
 2: 8        Loop Count

72:  Do (P86)
 1: 75       Pulse Port 5

73:  Do (P86)
 1: 75       Pulse Port 5

74:  End (P95)
;Advances AM416 to SET 9, i.e. where T/c 25 is connected

75:  Do (P86)
 1: 44       Set Port 4 High
;Activates 4th CE8 thru' C4

76:  Beginning of Loop (P87)
 1: 0        Delay
 2: 2        Loop Count

77:  Excitation with Delay (P22)
 1: 1        Ex Channel
 2: 0        Delay W/Ex (units = 0.01 sec)
 3: 50       Delay After Ex (units = 0.01 sec)
 4: 0        mV Excitation

78:  End (P95)
;Create 1 sec period (2 X 50 X 0.01 = 1 sec);
;       i.e. activate 4th CE8 for 1 sec

79:  Do (P86)
```

```
 1: 46       Set Port 6 High
;Activates AM416

80:  Beginning of Loop (P87)
 1: 0        Delay
 2: 2        Loop Count

81:  Do (P86)
 1: 75       Pulse Port 5

82:  Step Loop Index (P90)
 1: 2        Step

83:  Thermocouple Temp (SE) (P13)
 1: 2        Reps
 2: 22       7.5 mV 60 Hz Rejection Range
 3: 9        SE Channel
 4: 1        Type T (Copper-Constantan)
 5: 1        Ref Temp (Deg. C) Loc [ RefTemp    ]
 6: 57    -- Loc [ Sec1_25    ]
 7: 1.0      Mult
 8: 0.0      Offset

84:  End (P95)
;Complete 4 T/c's Temp after 1 sec heating for CE8 No 4 (i.e. T/c No
25 to 28)
;Measurements recorded in Locs 57 to 60 inclusive.

85:  Do (P86)
 1: 56       Set Port 6 Low
;Resets AM416 to channel 1

86:  Do (P86)
 1: 46       Set Port 6 High
;Activates AM416
87:  Beginning of Loop (P87)
 1: 0        Delay
 2: 8        Loop Count

88:  Do (P86)
 1: 75       Pulse Port 5

89:  Do (P86)
 1: 75       Pulse Port 5

90:  End (P95)

91:  Beginning of Loop (P87)
 1: 0        Delay
 2: 40       Loop Count

92:  Excitation with Delay (P22)
 1: 1        Ex Channel
 2: 0        Delay W/Ex (units = 0.01 sec)
 3: 50       Delay After Ex (units = 0.01 sec)
 4: 0        mV Excitation
```

```
93:  End (P95)
;Creates 20 sec delay; i.e. continue heating for 20 sec

94:  Beginning of Loop (P87)
 1: 0         Delay
 2: 4         Loop Count

95:  Do (P86)
 1: 75        Pulse Port 5

96:  Step Loop Index (P90)
 1: 2         Step

97:  Thermocouple Temp (SE) (P13)
 1: 2         Reps
 2: 22        7.5 mV 60 Hz Rejection Range
 3: 9         SE Channel
 4: 1         Type T (Copper-Constantan)
 5: 1         Ref Temp (Deg. C) Loc [ RefTemp    ]
 6: 85     -- Loc [ T20s_25    ]
 7: 1.0       Mult
 8: 0.0       Offset

98:  End (P95)

99:  Do (P86)
 1: 56        Set Port 6 Low
;Ends Temp measurements after 21 sec heating & resets AM416
;Temp 21 sec (T20s_X) for T/c's 25 to 28 recorded in Locs 85 to 88
inclusive.

100:  Do (P86)
 1: 54        Set Port 4 Low
;Deactivates CE8 No 4
;ENDS MEASUREMENTS FOR LAST 4 T/c's CONNECTED TO 4th CE8

;                BEGIN CALCULATIONS TO DETERMINE dT FOR EACH T/c

101:  Beginning of Loop (P87)
 1: 0         Delay
 2: 28        Loop Count

102:  Z=X-Y (P35)
 1: 61     -- X Loc [ T20s_1     ]
 2: 33     -- Y Loc [ Sec1_1     ]
 3: 89     -- Z Loc [ dT_1       ]
;Calculates dT for 28 sensors and places result in
;   Locs 89 to 116 inclusive

103:  End (P95)
;Ends dT calc loop

104:  Do (P86)
 1: 10        Set Output Flag High (Flag 0)
```

```
105:  Set Active Storage Area (P80)
 1: 1         Final Storage Area 1
 2: 111       Array ID

106:  Real Time (P77)
 1: 1220      Year,Day,Hour/Minute (midnight = 2400)

107:  Minimize (P74)
 1: 1         Reps
 2: 0         Value Only
 3: 2         Loc [ Battery    ]

108:  Average (P71)
 1: 1         Reps
 2: 1         Loc [ RefTemp    ]

109:  Sample (P70)
 1: 28        Reps
 2: 5         Loc [ SoilT_1    ]

110:  Do (P86)
 1: 10        Set Output Flag High (Flag 0)

111:  Set Active Storage Area (P80)
 1: 1         Final Storage Area 1
 2: 222       Array ID

112:  Real Time (P77)
 1: 1220      Year,Day,Hour/Minute (midnight = 2400)

113:  Sample (P70)
 1: 28        Reps
 2: 89        Loc [ dT_1       ]

114:  Do (P86)
 1: 21        Set Flag 1 Low

*Table 2 Program
  02: 0.0000    Execution Interval (seconds)

*Table 3 Subroutines

End Program
-Input Locations-
1     RefTemp          41    Sec1_9           81    T20s_21
2     Battery          42    Sec1_10          82    T20s_22
3     TCRT             43    Sec1_11          83    T20s_23
4     _________        44    Sec1_12          84    T20s_24
5     SoilT_1          45    Sec1_13          85    T20s_25
6     SoilT_2          46    Sec1_14          86    T20s_26
7     SoilT_3          47    Sec1_15          87    T20s_27
8     SoilT_4          48    Sec1_16          88    T20s_28
9     SoilT_5          49    Sec1_17          89    dT_1
10    SoilT_6          50    Sec1_18          90    dT_2
11    SoilT_7          51    Sec1_19          91    dT_3
12    SoilT_8          52    Sec1_20          92    dT_4
```

```
13    SoilT_9          53    Sec1_21          93    dT_5
14    SoilT_10         54    Sec1_22          94    dT_6
15    SoilT_11         55    Sec1_23          95    dT_7
16    SoilT_12         56    Sec1_24          96    dT_8
17    SoilT_13         57    Sec1_25          97    dT_9
18    SoilT_14         58    Sec1_26          98    dT_10
19    SoilT_15         59    Sec1_27          99    dT_11
20    SoilT_16         60    Sec1_28          100   dT_12
21    SoilT_17         61    T20s_1           101   dT_13
22    SoilT_18         62    T20s_2           102   dT_14
23    SoilT_19         63    T20s_3           103   dT_15
24    SoilT_20         64    T20s_4           104   dT_16
25    SoilT_21         65    T20s_5           105   dT_17
26    SoilT_22         66    T20s_6           106   dT_18
27    SoilT_23         67    T20s_7           107   dT_19
28    SoilT_24         68    T20s_8           108   dT_20
29    SoilT_25         69    T20s_9           109   dT_21
30    SoilT_26         70    T20s_10          110   dT_22
31    SoilT_27         71    T20s_11          111   dT_23
32    SoilT_28         72    T20s_12          112   dT_24
33    Sec1_1           73    T20s_13          113   dT_25
34    Sec1_2           74    T20s_14          114   dT_26
35    Sec1_3           75    T20s_15          115   dT_27
36    Sec1_4           76    T20s_16          116   dT_28
37    Sec1_5           77    T20s_17          117   ________
38    Sec1_6           78    T20s_18
39    Sec1_7           79    T20s_19
40    Sec1_8           80    T20s_20

-Program Security-
0000
0000
-Mode 4-
-Final Storage Area 2-
0
-CR10X ID-
0
-CR10X Power Up-
```

Appendix E (cont.)

Program for use of time domain reflectometry with Campbell Scientific CR10 and CR10X data loggers (determination of effective cable length)

Program Title: CLEMTDRD.CSI

To be able to use the Tectronix 1502C cable tester to determine volumetric soil water content, the cable tester must identify the correct wave, i.e. the wave generated by the probe and not one generated by a joint or other artefact. This is achieved by specifying the effective cable lengths in the program. The effective cable lengths are not the actual cable lengths and can only be established *in situ*. Thus it is necessary to run a program to determine the effective cable lengths before the volumetric soil water content determination program can be used. The program set out below is one used to determine the effective cable lengths so that these values can then be entered into the program used to determine the volumetric soil water content. This program was drafted to establish the effective cable lengths of 28 TDR probes so that the correct values can be entered into the TDR program to measure water content, i.e. CLEMTDRW.CSI.

The instrument settings and connections were as follows:

The SDM1502 communication interface DIP switch was set at 0000 to give the cable tester an address of 00. The first level SDMX50 coaxial multiplexer had the MSD set to 0 and the LSD set to 1 to give an address of 01. The second level of three SDMX50 multiplexers had the MSD set to 0 while the LSD was set at 2 to give an address of 02.

The first level SDMX50 had four TDR probes connected to BNC connectors 1 to 4, connector 5 was skipped and then channels 6, 7 and 8 were connected by RG-8 coax cable to level two SDMX50 multiplexes. These SDMX50 are subsequently referred to as Box 6, Box 7 and Box 8 respectively. Each of these SDMX50 had 8 TDR probes connected to their eight BNC channels.

The CR10X is powered by means of a deep cycle 12V DC battery with the positive terminal being connected to the 12V port and the negative terminal being connected to the G port of the CR10X power terminal. Note that the CR10X must have been produced after *ca* June 1999 and be able to process Instruction 100. One way to identify that the CR10X can process Instruction 100 is if the wiring panel has markings indicating where the SDM wiring can be connected.

The SDM 1502 communication interface and the CR10X are connected as follows:

SDM 1502		CR10X
12V	!	SDM 12V
GND	!	SDM G
C1 Data	!	SDM C1
C2 Clock	!	SMD C2
C3 Enable	!	SDM C3.

Simultaneously, the SDM 1502 communication interface was connected to the SDMX50's as follows:

SDM 1502		SDMX50
12V	!	12V
GND	!	GND
C1 Data	!	C1 Data
C2 Clock	!	C2 CLK

C3 Enable ! C3 Enable.

At the rear of the Tecktronix 1502C is an external power supply terminal. The positive lead from this terminal (red wire) was connected to the SDM 12V port of the CR10X while the neutral line (black wire) was connected to the SDM G port. The clear wire from the 1502C was connected to C4 of the CR10X to enable the CR10X to switch the 1502C "on and "off".

Once the program had been downloaded to the CR10X it was activated by activating Flag 1

The program was drafted and tested on 28/11/1999.

```
*Table 1 Program
  01: 10          Execution Interval (seconds)

1:  If Flag/Port (P91)
 1: 11          Do if Flag 1 is High
 2: 30          Then Do
;Instruction to manually initiate the process of measuring the
;effective ;cable lengths.

2:  Do (P86)
 1: 44          Set Port 4 High
;Instruction to switch on the Techtronix 1502C cable tester.

3:  Excitation with Delay (P22)
 1: 1           Ex Channel
 2: 0           Delay W/Ex (units = 0.01 sec)
 3: 500         Delay After Ex (units = 0.01 sec)
 4: 0           mV Excitation

4:  TDR Measurement (P100)
 1: 00          SDM1502 Address
 2: 98          Manual MUX Address Advance
 3: .3          Probe Length (meters)
 4: 0.0         Cable Length (meters)
 5: 7104        MMMP  Mux & Probe Selection
 6: 1           Loc [ W1_06_1    ]
 7: 1           Mult
 8: 0           Offset
;Measure effective cable length for probes 1 to 4 connected to
SDMX50 in ;Box 7 and enter results beginning at Loc 1 and titled
"W1_06_1".

5:  TDR Measurement (P100)
 1: 00          SDM1502 Address
 2: 98          Manual MUX Address Advance
 3: .3          Probe Length (meters)
 4: 0.0         Cable Length (meters)
 5: 6104        MMMP  Mux & Probe Selection
 6: 5           Loc [ W2_06_2    ]
 7: 1.0         Mult
 8: 0.0         Offset
;Measure effective cable length for probes 1 to 4 connected to
SDMX50 in ;Box 6 and enter results beginning at Loc 5 and titled
"W2_06_2".

6:  TDR Measurement (P100)
```

```
 1: 00        SDM1502 Address
 2: 98        Manual MUX Address Advance
 3: .3        Probe Length (meters)
 4: 0.0       Cable Length (meters)
 5: 1004      MMMP  Mux & Probe Selection
 6: 9         Loc [ W3_06_3    ]
 7: 1.0       Mult
 8: 0.0       Offset
```

;Measure effective cable length for probes 1 to 4 connected to the SDMX50 ;at the first level and enter results beginning at Loc 9 and titled ;"W3_06_3".

```
7:  TDR Measurement (P100)
 1: 00        SDM1502 Address
 2: 98        Manual MUX Address Advance
 3: .3        Probe Length (meters)
 4: 0.0       Cable Length (meters)
 5: 6504      MMMP  Mux & Probe Selection
 6: 13        Loc [ C4_06_4    ]
 7: 1.0       Mult
 8: 0.0       Offset
```

;Measure effective cable length for probes 5 to 8 connected to SDMX50 in ;Box 6 and enter results beginning at Loc 13 and titled "C4_06_4".

```
8:  TDR Measurement (P100)
 1: 00        SDM1502 Address
 2: 98        Manual MUX Address Advance
 3: .3        Probe Length (meters)
 4: 0.0       Cable Length (meters)
 5: 7504      MMMP  Mux & Probe Selection
 6: 17        Loc [ E5_06_5    ]
 7: 1.0       Mult
 8: 0.0       Offset
```

;Measure effective cable length for probes 5 to 8 connected to SDMX50 in ;Box 7 and enter results beginning at Loc 17 and titled "E5_06_5".

```
9:  TDR Measurement (P100)
 1: 00        SDM1502 Address
 2: 98        Manual MUX Address Advance
 3: .3        Probe Length (meters)
 4: 0.0       Cable Length (meters)
 5: 8104      MMMP  Mux & Probe Selection
 6: 21        Loc [ E6_06_6    ]
 7: 1.0       Mult
 8: 0.0       Offset
```

;Measure effective cable length for probes 1 to 4 connected to SDMX50 in ;Box 8 and enter results beginning at Loc 21 and titled "E6_06_6".

```
10:  TDR Measurement (P100)
 1: 00        SDM1502 Address
 2: 98        Manual MUX Address Advance
 3: .3        Probe Length (meters)
 4: 0.0       Cable Length (meters)
```

```
 5: 8504      MMMP  Mux & Probe Selection
 6: 25        Loc [ E7_06_7    ]
 7: 1.0       Mult
 8: 0.0       Offset
;Measure effective cable length for probes 5 to 8 connected to
SDMX50 in ;Box 8 and enter results beginning at Loc 25 and titled
"E7_06_7".

11:  Do (P86)
 1: 54        Set Port 4 Low
;Switch off Tecktronix.

12:  Batt Voltage (P10)
 1: 29        Loc [ V_batt     ]
;Measure battery voltage and record in Loc 29 as "V_batt".

13:  Do (P86)
 1: 10        Set Output Flag High (Flag 0)
;Instruction to record values as an output.

14:  Real Time (P77)
 1: 1220      Year,Day,Hour/Minute (midnight = 2400)
;Instruction to record Year, Day of year, and Time that measurements
were ;recorded.

15:  Sample (P70)
 1: 29        Reps
 2: 1         Loc [ W1_06_1    ]
;Instruction to identify how many results must be sampled and at
what Loc ;the records must start.

16:  Do (P86)
 1: 21        Set Flag 1 Low
;Instruction to end this series of measurements.

17:  End (P95)

*Table 2 Program
  02: 0.0000    Execution Interval (seconds)

*Table 3 Subroutines

End Program
```

```
-Input Locations-
1     W1_06_1          12    W3_96_24         23    E6_56_20
2     W1_26_8          13    C4_06_4          24    E6_86_27
3     W1_56_15         14    C4_26_11         25    E7_06_7
4     W1_96_22         15    C4_56_18         26    E7_26_14
5     W2_06_2          16    C4_86_25         27    E7_56_21
6     W2_26_9          17    E5_06_5          28    E7_86_28
7     W2_56_16         18    E5_26_12         29    V_batt
8     W2_96_23         19    E5_56_19
9     W3_06_3          20    E5_86_26
10    W3_26_10         21    E6_06_6
11    W3_56_17         22    E6_26_13

-Program Security-
0000
0000
0000
-Mode 4-
-Final Storage Area 2-
0
-CR10X ID-
0
-CR10X Power Up-
```

Appendix E (cont.)

Program for use of time domain reflectometry with Campbell Scientific CR10 and CR10X data loggers (measurement of volumetric soil water content)

Program Title: CLEMTDRW.CSI

This program was drafted to measure soil volumetric water content at 28 positions using TDR probes having different cable lengths. For this program to work the cable tester must identify the correct wave, i.e. the wave generated by the probe and not one generated by a joint or other artefact. This is achieved by specifying the effective cable lengths in the program. The effective cable lengths are not the actual cable lengths and can only be established *in situ*. Thus it is necessary to run a program to determine the effective cable lengths (Program CLEMTDRD.CSI described in the previous section) before the volumetric soil water content determination program can be used. Once the effective cable length values have been determined, these values are then entered into the program used to determine the volumetric soil water content.

The system set-up is the same as program CLEMTDR.CSI described in the previous section

```
*Table 1 Program
  01: 10          Execution Interval (seconds)

1:  If time is (P92)
 1: 0           Minutes (Seconds --) into a
 2: 120         Interval (same units as above)
 3: 11          Set Flag 1 High
;Instruction to set the time interval to carry out the measurements
at 120 ;minutes as well as giving the option to manually set flag 1
high to ;initiate the program when required.

2:  If Flag/Port (P91)
 1: 11          Do if Flag 1 is High
 2: 30          Then Do
;If flag 1 is high then the program will initiate.

3:  Do (P86)
 1: 44          Set Port 4 High
;Instruction to switch on the Techtronix 1502C cable tester.

4:  Excitation with Delay (P22)
 1: 1           Ex Channel
 2: 0           Delay W/Ex (units = 0.01 sec)
 3: 500         Delay After Ex (units = 0.01 sec)
 4: 0           mV Excitation

5:  TDR Measurement (P100)
 1: 00          SDM1502 Address
 2: 4080        La/L with Probe Correction in mm
 3: .3          Probe Length (meters)
 4: 19.0        Cable Length (meters)
 5: 7104        MMMP  Mux & Probe Selection
 6: 1           Loc [ W1_06_1    ]
 7: 0.1138      Mult
```

```
 8: -0.1758  Offset
;Measure volumetric water content for probes 1 to 4 connected to
SDMX50 in ;Box 7 and enter results beginning at Loc 1 and titled
"W1_06_1".

6:  TDR Measurement (P100)
 1: 00       SDM1502 Address
 2: 4080     La/L with Probe Correction in mm
 3: .3       Probe Length (meters)
 4: 18.1     Cable Length (meters)
 5: 6104     MMMP  Mux & Probe Selection
 6: 5        Loc [ W2_06_2    ]
 7: 0.1138   Mult
 8: -0.1758  Offset
;Measure volumetric water content for probes 1 to 4 connected to
SDMX50 in ;Box 6 and enter results beginning at Loc 1 and titled
"W2_06_2".

7:  TDR Measurement (P100)
 1: 00       SDM1502 Address
 2: 4080     La/L with Probe Correction in mm
 3: .3       Probe Length (meters)
 4: 10.1     Cable Length (meters)
 5: 1004     MMMP  Mux & Probe Selection
 6: 9        Loc [ W3_06_3    ]
 7: 0.1138   Mult
 8: -0.1758  Offset
;Measure volumetric water content for probes 1 to 4 connected to the
SDMX50 ;at the first level and enter results beginning at Loc 9 and
titled ;"W3_06_3".

8:  TDR Measurement (P100)
 1: 00       SDM1502 Address
 2: 4080     La/L with Probe Correction in mm
 3: .3       Probe Length (meters)
 4: 18.1     Cable Length (meters)
 5: 6504     MMMP  Mux & Probe Selection
 6: 13       Loc [ C4_06_4    ]
 7: 0.1138   Mult
 8: -0.1758  Offset
;Measure volumetric water content for probes 5 to 8 connected to
SDMX50 in ;Box 6 and enter results beginning at Loc 13 and titled
"C4_06_4".

9:  TDR Measurement (P100)
 1: 00       SDM1502 Address
 2: 4080     La/L with Probe Correction in mm
 3: .3       Probe Length (meters)
 4: 19.0     Cable Length (meters)
 5: 7504     MMMP  Mux & Probe Selection
 6: 17       Loc [ E5_06_5    ]
 7: 0.1138   Mult
 8: -0.1758  Offset
;Measure volumetric water content for probes 5 to 8 connected to
SDMX50 in ;Box 7 and enter results beginning at Loc 17 and titled
"E5_06_6".
```

```
10:  TDR Measurement (P100)
 1: 00        SDM1502 Address
 2: 4080      La/L with Probe Correction in mm
 3: .3        Probe Length (meters)
 4: 21.1      Cable Length (meters)
 5: 8104      MMMP  Mux & Probe Selection
 6: 21        Loc [ E6_06_6    ]
 7: 0.1138    Mult
 8: -0.1758   Offset
;Measure volumetric water content for probes 1 to 4 connected to
SDMX50 in ;Box 8 and enter results beginning at Loc 21 and titled
"E6_06_6".

11:  TDR Measurement (P100)
 1: 00        SDM1502 Address
 2: 4080      La/L with Probe Correction in mm
 3: .3        Probe Length (meters)
 4: 21.1      Cable Length (meters)
 5: 8504      MMMP  Mux & Probe Selection
 6: 25        Loc [ E7_06_7    ]
 7: 0.1138    Mult
 8: -0.1758   Offset

;Measure volumetric water content for probes 5 to 8 connected to
SDMX50 in ;Box 8 and enter results beginning at Loc 25 and titled
"E7_06_7".

12:  Do (P86)
 1: 54        Set Port 4 Low
;Switch off Tecktronix.

13:  Batt Voltage (P10)
 1: 29        Loc [ V_batt     ]
;Measure battery voltage and record in Loc 29 as "V_batt".

14:  Do (P86)
 1: 10        Set Output Flag High (Flag 0)
;Instruction to record values as an output.

15:  Real Time (P77)
 1: 1220      Year,Day,Hour/Minute (midnight = 2400)
;Instruction to record Year, Day of year, and Time that measurements
were ;recorded.

16:  Sample (P70)
 1: 29        Reps
 2: 1         Loc [ W1_06_1    ]
;Instruction to identify how many results must be sampled and at
what Loc ;the records must start.

17:  Do (P86)
 1: 21        Set Flag 1 Low
;Instruction to end this series of measurements.

18:  End (P95)
```

```
*Table 2 Program
  02: 0.0000    Execution Interval (seconds)

*Table 3 Subroutines

End Program

-Input Locations-
1     W1_06_1          11    W3_56_17         21    E6_06_6
2     W1_26_8          12    W3_96_24         22    E6_26_13
3     W1_56_15         13    C4_06_4          23    E6_56_20
4     W1_96_22         14    C4_26_11         24    E6_86_27
5     W2_06_2          15    C4_56_18         25    E7_06_7
6     W2_26_9          16    C4_86_25         26    E7_26_14
7     W2_56_16         17    E5_06_5          27    E7_56_21
8     W2_96_23         18    E5_26_12         28    E7_86_28
9     W3_06_3          19    E5_56_19         29    V_batt
10    W3_26_10         20    E5_86_26         30    _________

-Program Security-
0000
0000
0000
-Mode 4-
-Final Storage Area 2-
0
-CR10X ID-
0
-CR10X Power Up-
3
```

Other related WRC reports available:

Facilitating irrigation scheduling by means of the soil water balance model

JG Annandale, N Benadé, NZ Jovanovic, JM Steyn and N du Sautoy

The interest in scheduling irrigations with crop growth computer models is rapidly increasing, particularly since personal computers have become accessible to crop producers. The soil water balance (SWB) model is a mechanistic, real-time, generic crop, soil water balance, irrigation scheduling model. SWB gives a detailed description of the soil-plant-atmosphere continuum, making use of weather, soil and crop management data. It thus largely overcomes the problems of other models for irrigation scheduling as indicated above. However, since SWB is a generic crop growth model, parameters specific for each crop have to be determined.

Calibration and validation of SWB with independent data sets of relevance for irrigation scheduling were required in order to establish the reliability of the model in representing the real-world system. Data sets for the validation of SWB were therefore sought for two types of models:

Crop growth and SWB model making use of specific crop growth parameters
FAO-based model making use of FAO crop factors.

The user-friendly interface, on-line help tool, range and error checking, as well as comprehensive output graphs should allow the user to easily make real-time use of the output results. The context-sensitive help tool describes how to operate the model (enter input data, run simulations, and print or create results and recommendations) and most of the technical procedures used by SWB to estimate crop growth and calculate the soil water balance. Recommended ranges for input data and general information are also given.

Report Number: 753/1/99 **ISBN 1 86845 559 9**

TO ORDER: Contact **Rina** or **Judas** - Telephone No: 012 330 0340
Fax Number: 012 331 2565
E-mail: publications@wrc.org.za

Water Research Commission
Private Bag X03, Gezina, 0031, South Africa
Tel: +27 12 330 0340, Fax: +27 12 331 2565
Web: http://www.wrc.org.za